ADSORPTION CHARACTERISTICS AND SURFACE STRUCTURAL CHANGES OF TRANSITION METAL SULPHATES BY HEAT TREATMENT

MUKUT B. RAJPAI


CENTRE FOR NFLD. STUDIES
OCT 6 1975
MEMORIAL UNIVERSITY
OF NEWFOUNDLAND

ADSORPTION CHARACTERISTICS AND SURFACE STRUCTURAL CHANGES OF TRANSITION METAL SULPHATES BY HEAT TREATMENT

by

Mukut B. Bajpai, M.Sc.

A thesis submitted in partial fulfillment of the requirements for the degree of Doctor of Philosophy.

June, 1974

Chemistry Department
Memorial University of Newfoundland
St. John's
Newfoundland
Canada

Acknowledgements

I wish to express my sincere appreciation and indebtedness to Dr. W.D. Machin for his guidance and encouragement during this investigation.

Thanks are due to Dr. F.A. Aldrich, Dean of graduate studies and Dr. E. Bullock, Dr. J.M.W. Scott and Dr. M.K. Newlands, Chairman, Chemistry Department for assisting me in many ways during the period of study. I am grateful to Dr. D. Barton for reading the manuscript and for the discussions, I had with him.

I also thank the Head, Chemical Engineering Division, Bhabha Atomic Research Centre, Trombay, India for my leave of absence during the period of this study.

Thanks are also due to technical service personnel for their cooperation and help.

I also wish to thank Miss Judy Sheppard for patiently typing this thesis and Mrs. S. Banfield and Mr. P. King for tracing the diagrams.

To Asha and our Family

ABSTRACT

The adsorption and desorption of trichlorofluoromethane ($CFCl_3$) was studied by using a microbalance on the sulphates of calcium, manganese, cobalt, nickel, copper and zinc. The effect of annealing the samples at 200, 300, 400 and 500°C on their adsorption characteristics and the heat of solution has been measured. The surface structure of the annealed adsorbents is considered from crystal field effects. Thermodynamic parameters such as the heat of adsorption and entropy of adsorption have been derived from the various isotherms at 20.0, 6.0 and -10.0°C. These quantities have been used to discuss the surface structures. The heat of solution data are analyzed and the work of previous workers is considered in terms of the present scheme. The construction of a vacuum microbalance and the twin calorimeters is also described.

Surface cobalt (II) is found to be in a tetrahedral environment at an annealing temperature of (200°C). On adsorption, the surface structure possibly changes to a trigonal bipyramidal structure. However, on annealing at higher temperatures, the surface of the anhydrous cobalt sulphate provides an octahedral environment for the cation which goes to Hush's intermediate symmetry and finally to the most stable pentagonal bipyramidal structure. Nickel sulphate manifests pentagonal bipyramidal structure on adsorption on trigonal bipyramidal surface structure. Copper sulphate most probably pro-

vides trigonal environment to the metal ion at the surface which transforms to trigonal bipyramidal structure on adsorption. Physical adsorption measurements are found to be a useful tool in analyzing possible surface structures.

INDEX

Section	Subject	Page
0.00	Acknowledgements	1
1.00	Abstract	3
2.00	Index	5
3.00	Introduction	7
4.00	Experimental	17
4.10	Materials	18
4.20	Adsorption measurements	20
4.30	Experimental methods for adsorption measurements	38
4.40	Apparatus for calorimetric measurements	50
5.00	Discussion of experimental results	61
5.10	Experimental data	62
5.20	Surface area determination	64
5.30	Thermodynamic quantities of adsorption	67
5.40	Heat of adsorption	71
5.50	Entropies of adsorption	78
5.60	Selection of the model	87
5.70	Effect of annealing on surface area	88
6.00	Discussion of crystal field effects	89
6.10	Crystal field effect and physical adsorption	90
6.20	Determination of excess heats	101
6.30	Calculation of crystal field stabilization energy	102

Section	Subject	Page
6.40	Surface structures and CFSE	104
6.50	Importance of surface structure studies	114
6.60	Conclusions	116
7.00	References'	118
8.00	Appendix A - Adsorption data	130
8.10	Gravimetric adsorption data	130
8.20	Volumetric adsorption data	157
9.00	Appendix B - Tables	159
10.00	Appendix C - Figures	188
10.10	Legend for Figures	192

3.00 INTRODUCTION

The importance of the transition metal compounds is well known and has been the subject of numerous investigations by many workers and many publications have been devoted to this area. The 3d transition metal oxides have been intensively studied in connection with their use as catalysts. Attempts to correlate semiconductivity with the catalytic activity of these oxides has been the focus of much of this work. However, Cimino, Shiavello and Stone[1] found that the p-type semiconductivity, due to the drift of charge across an array of (Ni(II)/ Ni(III)) ions, has lesser relevance for the catalysis of N_2O decomposition than has the nature of the configuration of nickel ions due to a change in crystal field stabilization resulting from chemisorbed oxygen. Sulphates of the transition metal elements have also been utilized as catalysts for various reactions[2,3,4]. Tanabe et al[5] have given a number of references to reactions catalyzed by these metal sulphates. They have tried to correlate the activity of nickel sulphate with the concentration of acid sites of the catalyst. The structure of these acid sites with respect to the coordination number of the surface cations capable of forming intermediate structures has been discussed in some detail.

Many surface phenomena can be explained if the heterogenous distribution and nature of sites on a solid surface are known. The knowledge of the interactions occurring at surface heterogeneities has been applied in such apparently diverse fields as corrosion, lubrication, catalysis and heterogeneous reactions.[6]

Several theories have been proposed to explain catalysis

by transition metal salts. Many surface reactions can be explained on the basis of the interaction of lattice defects with the reacting molecules.

Wolkenstein[7] has emphasized the importance of localized levels in catalysis. These localized interactions refer to the interactions which do not involve free electrons or holes, but involve the interactions between the adsorbate molecules and the point defects on the catalyst surface, such as anion and cation vacancies, interstitial ions, F-centers, V-centers, ad-ions and foreign impurities. Interaction between a lattice ion and adsorbed molecule without the participation of the free electrons of the conduction band or holes of the valence band is another example of localized interactions. A band formed due to such interactions may extend to near neighbors as quantum mechanical calculations imply[8]. The interactions involving local symmetry such as crystal field effects in chemisorption and catalysis, are also taken as direct evidence for the existence of localized interactions of importance in catalysis[7].

Dowden and Wells[9] have suggested the correlation between local symmetry of crystal surfaces, chemisorption and catalysis. They showed a correlation between the catalytic activity and crystal field stabilization energy (CFSE) for several first series (3d) transition metal oxides. Their argument is based on the fact that the symmetry around the transition metal ion, as well as the strength of the crystal field is altered due to chemisorption of oxide ions.

De et al[10] investigated hydrogen deuterium equilibrium,

$$H_2 + D_2 \rightleftharpoons 2HD$$

on titanium, vanadium, and chromium oxide. Magnetic susceptibility

measurements showed that catalytic activity was determined by the availability of d electrons for covalent bond formation when hydrogen was chemisorbed. Dowden and coworkers[11] showed a twin peaked activity pattern across the first period of transition metal oxides with maxima at Cr_2O_3 and Co_3O_4. Low activity was shown by the more stable $3d^0$, $3d^5$ and $3d^{10}$ configurations, whereas high activity was associated with $3d^3$, $3d^6$, $3d^7$ and $3d^8$ electronic configurations. Richardson and Rossington[12] studied the dehydrogenation of cyclohexane on a number of oxide catalysts and found that the highest activity was associated with the d^3, d^2 and d^1 configurations.

The local symmetry of a transition metal salt depends on the effect of electrostatic potential on a 'free ion' as the electron distribution in the outer shell of the transition ion is remarkably affected if the ion is subjected to the electric field of an ionic or dipolar matrix. Bethe[13] described this effect when the ion is situated in an electric field of prescribed symmetry. Van Vleck[14] extended and developed the mathematical basis of Bethe's crystal field theory.

Haber and Stone[15] were among the first workers to carry out an experimental study on the solid gas interface considering CFSE as a major factor. They reported that illumination (at 650 mμ) of a nearly stochiometric nickel oxide surface carrying adsorbed oxygen gives rise to oxygen desorption. They proposed a mechanism based on a relaxation process from octahedrally coordinated nickel ion to a tetrahedral structure ($^3A_{2g} \rightarrow {}^3T_{1g}$). Jogenpier and Schuit[16] criticized this interpretation and recommended that a more complete theory based on a molecular orbital treatment be developed, but did not do so themselves. Dunning[17] has discussed the importance of crystal field effects which

may contribute substantially to the surface energy.

Dunn et al[18] pointed out that crystal field effects are usually small and may be masked by other factors. The only way to separate the factors is by a thorough comparison of several members of a transition series including those which have zero CFSE.

The aim of the present study is to investigate the possible coordination symmetries of cations on the surface before and after adsorption, by evaluating the contribution of crystal field effects on heat of adsorption and comparing the experimental CFSE effects with the calculated CFSE effects for various models of surface structure. Such a calculation is discussed later (section 6.30). Heats of solution have been used to estimate surface structures. Crystal field effects associated with various models are discussed in detail in section 6.00 and compared with experimental results.

Whenever a gas comes in contact with a solid surface the gas molecules are concentrated near the solid surface due to adsorption forces. At equilibrium, the concentration of gas molecules is greater at the surface than in the bulk gas phase. These adsorption interactions originate from the electrical interaction of the nuclei and electrons comprising the system. In principle, these interactions can be calculated using quantum mechanics. However such a calculation requires the knowledge of exact positions and orientations of the molecules relative to the surface. In other words, the adsorption energies can be evaluated from electrical, magnetic and geometrical properties of the adsorbate and the solid adsorbent. These calculations have also to account for the effect of lateral interactions of adsorbed molecules on the adsor-

bent field and the entropy change during the adsorption process.

Dubinin et al[19] have reviewed the excellent work of Kiselev and coworkers, Crowell and coworkers, Pierotti, Graham and many other authors regarding calculations of the energy of adsorption of simple molecules. From their work it seems possible to make approximate estimates on the basis of a general theory of intermolecular forces for very simple systems involving monoatomic gas molecules and uniform, nearly ideal surfaces. However, for most real surfaces the crystal planes are not geometric planes intersecting an ideal crystal. Moreover, there are difficulties of determining the effect, due to forces of adsorption, on various internal degrees of freedom of real polyatomic adsorbate molecules. This effect will be discussed later. In view of such difficulties it becomes necessary to introduce a variety of simplifications and approximations. The example of one such simplification is to divide adsorption into physical adsorption (weak interaction) and chemisorption (strong interaction). In addition adsorbents may be calssified as ionic, covalent or metallic.

Physical adsorption is considered to arise from van der Waal's forces[20,21]. The physical and chemical properties of the molecules are not drastically altered but somewhat modified. In chemisorption, actual bonds (covalent or ionic) between admolecules and the surface are formed as in a normal chemical reaction. Physical adsorption processes occur in gas-solid interactions such as chemisorption, catalysis or heterogeneous chemical reaction.

In the absence of precise knowledge of the exact state of the system, quantum mechanical calculations become impossible. Direct experiments still remain the only practical source of our knowledge of

adsorption interactions. Thermodynamic quantities have been evaluated from the adsorption isotherms determined under various conditions and these quantities have been used to interpret the state of the systems of interest.

Trichlorofluoromethane, $CFCl_3$, the adsorbate used in this study, has 3N degrees of freedom. Ideally we should account for the transformation (alteration or restriction) of three translational, three rotational and $3N-6$ vibrational degrees of freedom during the adsorption process. A polyatomic molecule may lose all translational and rotational degrees of freedom in the extreme case of immobile localized adsorption. The three translational degrees will be transferred into three vibrational degrees. The rotational degrees of freedom will also be transformed into vibrations of various modes e.g. bending, rocking, torsional about an axis or internal rotation. In the other extreme possibility, a molecule may lose only one translational degree of freedom and retain all of its rotational and vibrational degrees of freedom. The translational degree of freedom is replaced by a vibration normal to the adsorbent surface. Adsorption of such a kind is more probable when weak physical adsorption forces are involved. However hindered rotation or translation, due to the nonuniformity of surface resulting in uneven potential barriers is much more likely to be present. Rotational motion may even be completely transformed into vibrational motion on adsorption. The selection of a model of adsorption is a very difficult problem. Entropy determinations alone are not sufficient and independent methods such as spectral or magnetic investigations are useful to confirm the model. A comparison of entropy changes as a function of surface coverage for a particular model, with the

experimentally observed entropy of adsorption data may help to visualize the state of an adsorbed layer on the surface.

Machin[22] observed that the isosteric heat of adsorption at zero surface coverage was maximum with those adsorbents having the largest crystal field stabilization energy. Accordingly the adsorbents used for the present study were the sulphates of the first series of transition metal elements from manganese to zinc and calcium. The crystal field perturbations are two orders of magnitude greater for d electrons of first series than for f electrons of the lanthanide series[23]. The f electrons of the lanthanide ions are shielded by s and p electrons which lie outside f electrons and screen them from the ligand environment. No such protection is available for the d electrons of the ions of the first transitional series. In the ions of the actinide series, it appears that crystal field effects are of an importance intermediate between those for the first transition series and for the lanthanide ions[23]. Dunn et al[14] have shown that if the spectroscopically obtained CFSE for the aqueous ions in the series calcium through zinc is subtracted from their hydration energies and the resultant plotted against the atomic number of the corresponding elements a better straight line relationship is obtained than for the corresponding trivalent ions of the series. This observation shows that the properties other than those altered by crystal field effects vary more uniformly for the divalent ions of the series than for the trivalent ions.

The aforesaid considerations led to the choice of divalent ions of the 3d series for the present study. In the case of anions, oxides were avoided due to semiconductivity complications. Furthermore, stoichiometric oxides are difficult to prepare. The other factors con-

sidered were firstly, the ease of preparation and secondly, the stability of the compounds at high temperature. Sulfates of Ca(II), Mn(II) and Zn(II) ions with empty, half-filled and completely-filled d orbitals and having zero CFSE and Co(II), Ni(II) and Cu(II) ions having d^7, d^8 and d^9 orbitals, were selected for this investigation. Ferrous sulfate was omitted because of the difficulties involved in preparing the salt without partial decomposition[22,24,25].

The choice of the method of measurement of extent of adsorption at different conditions is discussed in detail in section 4.20. The microgravimetric method has been selected and a suitable vacuum microbalance has been constructed. For determining the heats of solution necessary for the calculations of CFSE, a twin calorimeter was designed and a volumetric BET apparatus* has been used to check surface areas of the adsorbents before measuring heats of solution.

The thermodynamic analysis of adsorption is useful for the determination of the adsorptive characteristics of real adsorbents. Infrared, field ion microscopy, low energy electron diffraction etc. describe the adsorption phenomena on the atomic scale but the interpretation of the results of these methods is still only possible for simple systems eg. single crystals.

The preparation and annealing of the adsorbents is described in detail in section 4.34. The stability of the compounds and surface areas of the samples were the main considerations for adopting the method described. Ideally it would be desirable to prepare substrates consisting of single planes of specific crystallographic orientation to extend Machin's qualitative treatment. In order to minimize the uncertainties in surface structure characterization, the anhydrous

---

*The famous Brunauer, Emmett and Teller apparatus[28].

transition metal sulphates used as the adsorbents in the present work were annealed at 200, 300, 400 and 500^{o}C. The surface structure of the adsorbent may change at elevated temperature as the lattice ions should have enhanced mobility and the tendency of the ions will be to move to more stable situations. The possibility of decomposition of sulphates at the surface at higher temperature limited annealing temperature to 500^{o}C. Even at this temperature in some cases partial surface decomposition may start at reduced pressures. For these reasons and others to reduce the effects of sintering, the heat treatment for cobalt, nickel and copper sulphates was done in an argon atmosphere.

The effect of heat treatment was assessed by measuring the adsorption isotherms at three temperatures between -10^{o} and 20^{o}C, from which the isosteric heats and differential entropies of adsorption were determined. The correlation of the annealing effect on heats of adsorption has been used to give insight into the surface structure before adsorption by comparison with suitable models (section 6.30).

In the discussion the word 'model' has been used in two different ways. One refers to the state of the adsorbate on the surface and the other to the configuration around surface cations. The entropy considerations refer to the model for the adsorbate state, and the crystal field effect considerations refer to the latter surface structure model.

The choice of trichlorofluromethane ($CFCl_3$) as the adsorbate is due to several properties described below:

Firstly, freon 11 ($CFCl_3$) is a heavy molecule suitable for the gravimetric method ofadsorption studies. Secondly, the molecule is quasi-spherical and has a small dipole moment[26]. Thirdly, the vapour pressure at the temperature of isotherm measurement is convenient and

finally the purification of the adsorbate is easy.

Trichlorofluoromethane is also a suitable vapour from the point of view of thermal transpiration effect (see section 4.27). Carbon tetrachloride also fulfills the above requirements except that molecule has no dipole moment and has a lower vapour pressure. Moreover, a large variation of molecular area of CCl_4 on different adsorbents was found by Machin[27], whereas the molecular area of $CFCl_3$ was found to be almost invariant.

4.00 EXPERIMENTAL

4.10 Materials

- 4.11 Materials used in adsorption measurements
- 4.12 Materials used in calorimetric measurements

4.20 Adsorption measurements

- 4.21 Types of vacuum microbalances
- 4.22 Balance design
- 4.23 Balance sensibility
- 4.24 Outline of operating procedure
- 4.25 Calibration of the balance
- 4.26 Experimental error in weighing
- 4.27 Thermal effects of the gas phase
- 4.28 Buoyancy effects

4.30 Experimental methods for adsorption measurements

- 4.31 Vacuum requirements and vacuum rack
- 4.32 Pressure measurements
- 4.33 Temperature control
- 4.34 Sample preparation
- 4.35 Adsorbate purification

4.40 Apparatus for calorimetric measurements

- 4.41 Description
- 4.42 Calibration of the calorimeter
- 4.43 Heat of solution measurements
- 4.44 Surface area measurements

4.10 MATERIALS

4.11 Materials used in adsorption measurements:

The various adsorbents used in the investigation were the anhydrous sulphates of calcium, manganese, cobalt, nickel, copper and zinc. The anhydrous salts were prepared from the corresponding hydrated salts (Fisher certified reagent grade) by vacuum dehydration *in situ*. Sample preparation is further discussed in section 4.34.

Trichlorofluoromethane (Matheson, 99.5 mole percent) was distilled twice under vacuum using the middle fraction each time. The purification procedure is given in section 4.35.

Argon was used as a streaming gas over the sample during the annealing process. Purified grade argon (99.995%) was supplied by Matheson Co.

4.12 Materials used in calorimetric measurements:

The anhydrous sulphates used for heat of solution measurements were prepared in a similar way as for adsorption measurements. However a slightly different procedure was adopted for streaming argon over the samples while annealing. The preparation of sulphates will be discussed in section 4.41. The materials used were the same as in adsorption measurements.

Helium was used for line volume calibration in the volumetric BET apparatus. Spectral grade helium was supplied by AIRCO in one

litre bulbs equipped with break seals.

Potassium sulphate solution (0.5 M) was prepared by dissolving K_2SO_4 (Analar, B.D.H.) in distilled water.

Potassium Chloride used for the calibration of the calorimeter was supplied by Shawinigan Chemicals (ACS grade).

4.20 Adsorption measurements:

Adsorption measurements may be carried out using three types of method[28], volumetric, gravimetric or dynamic. The main considerations when selecting a method are the adsorbent surface area, the nature of the adsorbate, and the required precision.

In the present study the adsorbate used, $CFCl_3$, is a condensible vapour and any nonequilibrium method for example those based on thermal conductivity measurements[29-32] would not be suitable.

The volumetric method[29,33-36] utilizing the change in pressure of a gas at constant volume and temperature as a measure of the amount of gas adsorbed has the advantage of simplicity of apparatus and procedure. The method has disadvantages arising from the fact the equilibrium gas pressure is also used to calculate the amount adsorbed. Cumulative errors in the quantity of gas adsorbed become progressively greater as the total pressure of adsorbate increases. Errors also arise if parts of the apparatus, other than the sample, adsorb gases, or are the source of any other gases. Greased stopcocks obviously could not be used in this study since $CFCl_3$ dissolves in the stopcock grease. An apparatus with all metal valves could be used for surface area measurements, but it is not suitable for the measurement of isotherms. In this study the volumetric method was used for the measurement of surface areas of the sample which were to be used for the calorimetric measurements. The procedure is further

described in section 4.44.

Gravimetric methods, while requiring more sophisticated apparatus, can give more precise measurements of quantities adsorbed. The advantage of the gravimetric method is particularly marked when the surface area of the adsorbent is small, in fact, the method has been applied to samples having surface area less than a few hundred square centimeters[28,37]. Furthermore, pressure and amount adsorbed are measured independently thus avoiding the problem in measurements due to adsorption of the gas by other parts of the apparatus. A further advantage over volumetric method is that any amount of dead-space can be tolerated. The method is unique in that it enables one to make a series of precise measurements of high sensitivity under controlled conditions over a wide range of experimental conditions. With samples having low surface area (a few cm^2) volumetric methods lose their sensitivity as the pressure increases. If thermal effects and buoyancy corrections (sections 4.27 & 4.28) are applied, the gravimetric technique remains unchanged over a large range of pressures (10^{-10} torr to one atmosphere[36]). Czanderna[38] and others[39-41] have described the versatility of the gravimetric method for studying various adsorption characteristics and mass determination problems.

Since surface areas in the present study were expected to be small, as low as 10 m^2/g, and in view of the points discussed, a gravimetric method was chosen for adsorption measurements.

4.21 Types of vacuum microbalances:

Thomas and Williams[37] and others[35,36,42-45] have described a large variety of microbalance types that can be adopted for adsorption studies. Honig[46] has classified various types of microbalance according to their design and on the basis of the method used for monitoring mass changes. Comments on the different categories, according to their principles of operation, follow.

Cantilever type:

This type of balance is simple to construct and operates in high vacuum. It consists of a fiber with one end fixed and other supporting the sample. The deflection of the fiber is linear with weight over a limited range. It suffers from the disadvantage of being prone to errors from temperature differences and requires buoyancy corrections. The sensitivity of such balances is dependent on the capacity.

Spring type:

McBain[47] and others have used helical silica springs for a variety of adsorption studies. Tungsten[48] or copper-berylium alloys[49] have also been used to replace the fragile silica for the construction of springs. The extension is proportional to the load. Obviously, increased sensitivity can only be attained at the expense of reduced capacity. Effects of vibrations, convection currents and buoyancy unless eliminated or corrected for may reduce the sensitivity attainable.

Beam type:

These balances incorporate a symmetrical beam supported in the centre by a torsion fiber, knife edge or a very thin tungsten wire. Accordingly, these are divided into three subcategories:

(a) Pivotal type: Czanderna[38,50-52] has constructed very sensitive and sophisticated types of pivotal microbalances. The pivots were constructed of sharp pointed tungsten, resting in quartz cups. The possible errors in such balances may be due to irregularities in the pivot surfaces or from friction between the suspension point of the beam and the pivots.

(b) Torsional type: Torsional balances[53] utilize the torsional moment of the wire constituting the primary fulcrum to restore the balance to an original setting. The torsional fiber system suffers from several inherent disadvantages. Chief among these is their tendency to yaw. The load capacity of the sensitive models is limited though not as severely as in the case of spiral balances. These balances are rather delicate.

(c) Gravity type: A sufficiently thin tungsten wire support results in a simple gravity operated beam type of balance. The torsional contribution of the suspension wire that acts as primary fulcrum is made negligibly small compared with the gravity moment exerted by the sample and the counterweights which are suspended from the two secondary fulcrums. Gulbransen[54], Thomas and Williams[37,56] and Wolsky and Zdanuk[57] have described such balances in detail.

The main advantage of such a balance is that, owing to its symmetry disturbances arising from temperature and pressure gradients are minimised, and buoyancy corrections need not be applied if the counterweight is so chosen that its density matches that of the sample. Furthermore, it can be readily converted to a null-point instrument[58]. Simple gravity type of balances are more stable and less sensitive to temperature changes than the torsional balances.

The limiting value of sensibility, the smallest mass change which this type of balance can measure is $\sim 10^{-2}$ µg[37]. To a large extent the sensibility is not dependent on load[59].

Two different types of balance, namely the vertically suspended balance[37] and the quartz resonant balance[60-62], have been developed recently.

The vertically suspended balance is essentially a torsion balance. The beam rotates about a vertical axis rather than conventional horizontal axis. Such a balance is especially employed to measure vapour pressure of solids.

The quartz resonance balance is based on the effect of added mass on piezoelectric crystal frequency. A very high degree of precision is possible with such balances as frequency changes equivalent to 1×10^{-6} µg/cm^2 can be measured[37]. However the usefulness of such a balance is limited to those materials which can be uniformly bonded to the quartz plate and which will not unduly lower the amplitude of vibration of the resonator[63].

4.22 Balance design:

The apparatus design was based upon the considerations listed below:

The sensitivity, capacity and the range of the instrument must be properly coordinated in the balance design. The nature of the adsorbent and adsorbate and the method of preparation of the sample are other design considerations. Furthermore, the material of the balance and the accoutrements must be bakeable in vacuum and in an argon stream.

For the present work a gravity type beam balance, similar to that of the Gulbransen balance[54], was developed. Features of Pettersen's[55] balance were employed. The balance assembly was symmetrical in detail, except for the difference between the sample and the reference bulb. The housing was also symmetrical. Sample and counterweight were hung deep in glass tube wells which could be maintained at the same temperature. The counterweight was so designed that the density of the reference side could be made same as the sample side, thus minimizing any buoyancy corrections. This was achieved by sealing a calculated amount of mercury within the counterweight bulb capillary (Fig. 1).

The balance housing was slightly modified on the sample side in order to permit the flow of argon over the sample while annealing. The overall assembly of the balance is shown in Figure 2 & 3. The

argon inlet into the balance is shown as legend 12 in Fig. 3.

The balance beam is constructed of 1 mm quartz rods. A full size diagram of the various aspects of the balance beam is shown in Figures 4 and 5. The figures being the side view and the top view respectively. A complete sketch of the balance beam and supporting frame is shown in Figure 6.

An electromagnetic compensation method was used to restore the balance beam to a null position. The balance beam contains a magnet as shown in Fig. 6 (legend 21) and a solenoid is wound directly around outside the balance case (Fig. 2, legend 1). The solenoid windings were cemented to the tube to eliminate the possibility of slipping and consequent change in calibration of the balance. The mass change of the sample due to adsorption of the gas resulted in tilting the beam of balance to the sample side. Current was passed through the balance solenoid to restore the balance beam back to its null position as monitored by the photocurrent balance in the galvanometer of an optical electronic system. The current through the balance solenoid is the measure of the mass change. The current flow through the solenoid was measured as a potential drop across a standard resistance in series with the solenoid (Fig. 7). The advantage of using the balance as a null instrument is that errors due to the deformation of the beam, irregularities in the supporting wire and asymmetry of the beam are minimized. The magnet also serves to damp the balance vibrations and oscillations.

The optical electronic system, utilized to determine the beam position, used light sources and sensing devices. The mounting of these devices on the support is shown in Figure 2 and 3. Two matched phototransistors (Phillips OCP 71) were mounted in an aluminum block. In order to keep the phototransistors at constant temperature, water was circulated within the aluminum block from a thermostatically controlled bath at 25°C. The phototransistor circuit is shown in Figure 8. The complete circuit was mounted in an aluminum box which was attached to the phototransistor mounting block. The box was wrapped with styrofoam for thermal insulation. The response time of the system was a few seconds.

The beam assembly was mounted on a frame of 2 mm quartz rods. The beam was cemented to the thin tungsten wire by a silver chloride seal[64]. Similar seals were used to cement the wire to the mounting frame. The entire frame was cemented in the required position in the balance case at four points using epoxy resin.

The reference bulb and the sample were suspended from the beam with chains made of short thin quartz rods. This minimizes vibrations in the hangdowns[65] and also reduces the thermomolecular flow along the hangdown relative to metal wire suspensions.

4.23 Balance sensibility:

The balance sensibility[37] is defined as the smallest mass change that can be reproducibly measured with a given accuracy.

The monolayer capacity, M_m, is related to the cross-sectional molecular area, β, and the sample surface area, A, by the relation:

$$M_m = \frac{A}{\beta N} \qquad \text{mole/g} \qquad (1)$$

where N is the Avogadro's number.

To have a balance with a precision of $\pm$ 0.1% of the monolayer capacity, then the required sensibility is given by:

$$S = 10^6 \, M_m \, . \, M \, . \, x \qquad \text{micrograms} \qquad (2)$$

where x is the precision fraction factor and is equal to 0.001 of M_m in this case. M is the molecular weight of the adsorbate.

For $CFCl_3$ on a surface of area 5 m^2 the required sensibility is $\pm$ 4 microgram.

4.24 Outline of operating procedure:

The details of sample preparation of a particular surface is given in section 4.34.

1. The samples were outgassed for at least 24 hours in vacuum at 120°C before each isotherm run was started.

2. The constant current supply units and the electronic circuit were put on at least 12 hours before the run to get constant response.

3. The constant temperature bath was brought to the required temperature and allowed to equilibrate for at least two hours before starting a run. To facilitate temperature equilibrium

helium was introduced (about 4 torr) in the equilibrium manifold and evacuated before starting the experiment. A constant current reading corresponding to null of the balance was always obtained before starting a run. This zero reading was always checked at the end of the run to verify the reversibility of the balance behaviour. Whenever an appreciable deviation in the zero reading was noticed, despite evacuation, the entire isotherm run was rejected.

4. The adsorption points were obtained by taking a small dose of adsorbate vapour from the absorbent storage bulb and equilibrating until the sample weight became constant. The weight reading was taken only after constant weight was observed. Desorption points were then obtained by condensing the vapours into the adsorbate recovery flask cooled by liquid nitrogen. The $CFCl_3$ thus recovered was always discarded at end of the run.

5. The measurement of mass adsorbed has been discussed in sections 4.22 and 4.25. The pressure measurements are discussed in section 4.32.

4.25 Calibration of the balance:

The balance was calibrated by Archimedes principle of buoyancy[66].

The volume of a small glass buoyancy bulb was calibrated by weighing the displaced water using a pycnometer. The buoyancy bulb was suspended replacing the sample bulb and its apparent mass change was determined as a function of gas pressure. The

buoyancy bulb was then replaced with a solid glass bead of equivalent mass and known volume (about one-tenth that of the larger bulb). Potential and pressure readings were again recorded as in the case of buoyancy bulb.

In both of the experiments, the plots (Fig. 9) of mV (the potential drop across the standard resistor; section 4.22) versus pressure gave a straight line. Slope of these plots was calculated using the method of least squares.

The balance sensitivity is calculated by the following relation[66]:

$$S = \frac{10^6 M (V_1 - V_2)}{(S_1 - S_2) Z P V} \qquad (3)$$

Where S - balance sensitivity in μg per mV potential difference across the standard resistor;

M - molecular weight of the ambient gas in g/mole;

V_1 - volume of the buoyancy bulb in cm^3;

V_2 - volume of the glass bead in cm^3;

S_1 - slope of the plot using buoyancy bulb mV/torr;

S_2 - slope of the plot using the glass bead;

P - 760 torr;

V - 22,415 ml per mole;

and Z - temperature correction factor to operating temperature.

The data for the weight and volume of the bulbs used are:

Buoyancy bulb: Weight: 1.0011 g;

Volume: 4.643 ml;

Glass bead: Weight: 1.0010 g;

Volume: 0.425 ml.

The slopes obtained at 20°C were:

S_1: 3.29 mV/torr;

S_2: 0.03 mV/torr.

The sensitivity of the balance from the above data was calculated to be 9.72 µg/mV across a 100 ohm standard resistor.

The calibration of the balance was repeated from time to time periodically and all measurements gave a sensitivity in agreement with the above value within 1.5%. This change in sensitivity can not be attributed entirely to errors in measurement, as a few changes were made in the balance such as changing the hangdowns, sample or reference bulb, the light bulbs and the photo-transistors. Every time any such change was made, the balance sensitivity was redetermined. However, the change in sensitivity never exceeded the limit mentioned above.

The plot of E.M.F. (mV) versus the pressure (torr) is shown in figure 9. These points were taken while increasing the pressure as well as while decreasing the pressure. The plot corresponds to the data used above for the sensitivity calculation and is the typical of the measurements taken at other times. Table 1 (see appendix B) contains the pressure and mV readings.

4.26 Experimental error in weighing:

The potentiometer used, could read to the lower limit of

$\pm$ 0.05 mV. The difference between two readings of potential drop would have an error of 0.1 mV, corresponding to an error in weight of $\pm$ 0.97 µg. For $CFCl_3$ this is equivalent to an error of $\pm$ 0.007 µ moles and for a surface area of 5 m^2, the error will be $\pm$ 0.25 X 10^{-3} M_m, where M_m is the monolayer capacity.

4.27 Thermal effects of the gas phase on apparent mass:

Solid-gas equilibria, when measured using a vacuum microbalance are subject to error in mass measurements due to temperature dependent effects on the adsorbate gas. Two types of effects can cause disturbances in weighing: Brownian motion, and thermal gas flow. An enormous amount of work has been done, both theoretical as well as experimental investigating these effects. A short review is included here. Thermal gas flow includes thermomolecular flow, slip flow and convection[67]. The discussion and the figures quoted below are for a typical balance design of the type used in this work.

Brownian motion: This is a completely unavoidable and natural limitation to the sensibility of a balance. The effect arises due to the irregular bombardment of the moving parts of the balance from the random motion of gas molecules causing fluctuations. Thomas and Williams[37] and Robens[67] have given a review of the work in this field. Poulis and Thomas[68] have assessed the spurious mass arising from Brownian motion to lie in the range of 10^{-4} to 10^{-2} microgram.

Thermomolecular flow and slip flow: These effects are most important when the mean free path of gas molecules is greater than or equal to the diameter of the tubes crossing the region of temperature gradient. Consequently the particles arriving at a unit surface from the region of higher temperature provide more momentum than those coming from cooler regions. This gives rise to a net force on the hangdown wire in the direction of decreasing temperature. This phenomena is known as a thermomolecular effect, or a thermal transpiration effect. Katz and Gulbransen[69] have described it as pressure effect. The pressure is an important factor as at very low pressures the number of molecules become insignificant resulting in fewer collisions with the apparatus and the thermal transpiration effect is not noticable. At higher pressures, where the mean free path of molecules is restricted convection[67] becomes more important.

Czanderna and Honig[50,70] observed a spurious mass change when the temperature of the sample was different from that of the remainder of the balance in the pressure range of 10^{-3} to 20 torr. They attributed this effect to thermomolecular flow. Czanderna[71] separated this effect for the sample and the hangdown and found that the maximum mass change occurs over a pressure range of 10^{-2} to 10^{-1} torr. Thomas and Poulis[72] have shown by extension of Knudsen's theory[73] that the magnitude of the spurious mass change can be calculated theoretically. They have calculated the force along the hangdown wire and recommended methods to minimize

the extent of the mass changes. Massen and Poulis[74] calculated the spurious mass changes arising due to temperature inhomogeneties along the balance case to be 0.1 µg/deg. C. Czanderna[75] recommended the use of an inert gas carrier for the active gas to measure the adsorption isotherm with precision (0.2 µg) at pressures in the thermomolecular flow region (10^{-3} to 20 torr).

Thomas and Poulis[76] extended these calculations of Knudsen forces in the intermediate pressure range and suggested that it is better to avoid these errors by practical methods[77,78] rather than by correcting using theoretical calculations.

Streensland and Forland[79] found good agreement between experimental and calculated error using slip flow theory. They showed that both Knudsen and slip forces depend on the geometry of the sample and the fiber, and on the temperature gradient over these. Behrndt et al[80] quickly analysed both these theories and found them equivalent. However, the experimental results were found to be different because of the uncertainty in the exact temperature above and below the sample.

Culting[81] has emphasized that it is better to choose vapours at room temperature rather than the gases at low or high temperatures to avoid these corrections. He recommended use of CCl_4 as an adsorbate.

Effect due to convection: Convection is observed at relatively high pressures (> 100 torr) and results due to gas density differences caused by temperature differences and the action of

the gravitational field.

In the present work, it was decided to design the system so as to prevent the disturbances by thermal gas flow effects. The following points were considered in the choice of the system.

1. The temperature of the isotherms should be as close to room temperature as possible.

2. The adsorbate gas has to be a vapour near room temperature.

3. The choice of the adsorbate should be such that the pressures below 10^{-1} torr should be avoided.

4. Symmetry of reference and sample side of the balance: the entire balance assembly should be constructed and operated in a manner that enables the inherent symmetry of the system to counteract these potential sources of error.

Three temperatures for the isotherm measurements were selected: 20°, 6°, and -10°C. The adsorbate used was $CFCl_3$, which is a vapour in the range of the experimental conditions and has other advantages mentioned in section 3.00. Machin[43] calculated the thermal transpiration correction (thermomolecular flow) at equilibrium pressure for $CFCl_3$. According to his conclusions the correction need only be applied below 0.02 torr. In the present study the pressure was kept within the range of 0.1 torr to 300 torr.

4.28 Buoyancy corrections:

As already mentioned in section 4.22, the balance was

designed to minimize the undesirable influence of buoyancy forces. The densities of the reference counterweight bulb and the sample bulb were made nearly the same and both limbs of the balance including housing and hangdown wires were cooled to the same extent during the measurements.

The symmetry of the sample side and reference side was further checked by placing a representative sample in the balance and admitting dry air into the equilibrium manifold to a pressure up to 500 torr. No apparent mass change was detected.

Pierotti[82] has described another buoyancy effect due to gas-solid interactions. The density of the medium in the vicinity of the solid will be different and is dependent upon the nature of the gas-solid interaction, the temperature and the pressure. The perturbation in intermolecular potential between gas molecules is caused by the presence of the solid. The resultant change in density of the gaseous medium in the vicinity of the solid causes the mass defect and is dependent on the surface area of the solid. However such a mass defect is appreciable only at extreme temperatures. In the example given[82] for helium on carbon black the mass defect Δm is zero at $300^{\circ}K$. However it is +100 μg at $78^{\circ}K$ and -3 μg at $1000^{\circ}K$.

In the present study no consideration has been taken of this factor. However, Δm is not expected to be appreciable in the conditions of our experiment. Moreover, the error will be more or less uniform throughout the series of the anhydrous

sulphates as the nature and surface area of the samples are similar and no relative error will be caused in our comparitive isotherm treatment.

4.30 Experimental methods for adsorption measurements:

The microbalance with complete equilibrium manifold, vacuum system, constant temperature bath are the essential parts of the apparatus used for the adsorption studies. The microbalance has already been described in sections 4.21, 4.22. The description of the rest of the apparatus will be discussed in the following section.

4.31 Vacuum requirements and vacuum line:

The actual number of residual gas molecules which is potentially capable of being adsorbed by the surface may be estimated by kinetic theory[36,83]. In a vacuum of 10^{-6} torr, there are roughly 3×10^{10} molecules per cm^3 at room temperature. If a fresh surface, say of 100 cm^2 surface area, is generated in a closed system at this pressure, the extent of contamination of the surface will be less than 0.03% of the surface area, if all of the residual molecules from the gas phase[84] are finally adsorbed on the surface. It follows that our adsorption studies, a vacuum of 10^{-6} torr is adequate and there is no necessity to utilize ultra high vacuum techniques.

The vacuum system and the equilibrium manifold are illustrated in Fig. 10. Kollen and Czanderna[84] have given a theory for the design of a specific microbalance vacuum system. Wolsky and Zdanuk[57], Rhodin[85] and Cadenhead & Wagner[86] have given the experimental set up used in their micrograviметric

studies.

The vacuum rack consists of Mcleod gauges of two different ranges for low pressure measurements and a mercury manometer. Three small bulbs (6, 7 and 8 in Figure 10) are provided for purification and storage of liquid $CFCl_3$. The purification and storage of liquid $CFCl_3$ is described in Section 4.35. During the desorption runs one of the bulbs was used for condensing the $CFCl_3$ vapour. This condensate was discarded after each such run. The $CFCl_3$ was always stored at $-78^{o}C$ between runs to reduce its uptake by grease.

A pressure of 10^{-6} torr was always ensured before the run was started. The fore pumps and mercury diffusion pump were continuously in operation. A Pirani gauge and a Mcleod gauge were used to measure the low pressures.

4.32 Pressure measurements:

For the measurement of the pressure of a readily condensible vapour a conventional mercury manometer with the aid of a cathetometer could give a precision of about 0.01 torr. For pressures below 1 torr, a Mcleod gauge[87] could be readily used. Various types of pressure gauges, for example Pirani gauge[88,89], spoon gauge[89,44], thermistor gauge[90] or an automatic balancing capacitance manometer[91,92] have been used by others. Each type of gauge has its own limitations for the range and the properties of the gas used in the system. Utterback and Griffith[91] and others[92 94] have raised objections to the use of a Mcleod gauge

as a universal gauge. Errors such as mercury pumping and thermal transpiration[95] arise due to presence of a cold trap in the system, no cold trap was used in our equilibrium manifold. However, the errors in measurement are significant only for gas pressures below 10^{-3} torr[87]. Unnecessarily long contact with $CFCl_3$ vapours and the mercury surface were avoided as far as possible. Mercury diffusion to the equilibrium manifold was kept to a minimum by maintaining the flow of gas stream towards the gauge rather than away from it.

4.33 Temperature control:

The constant temperature bath consisted of an insulated stainless steel tank of about 1.5 cubic feet capacity. Water was used as coolant and for filling the tank at 20.0°C and 6.0°C. To achieve the temperature at -10°C a methanol-water solution was used as the bath liquid. The arrangement used to obtain a temperature of -10°C is shown schematically in Figure 11. Methanol at -15°C was circulated in the cooling coil immersed in the constant temperature bath (C). To cool the methanol at -15°C in the tank (B) a manually adjusted circulation of methanol solution in a copper coil was maintained by passing the methanol through a slush of dry ice and methanol kept in Dewar (A). A pump was used to circulate methanol from tank (B) to (A) and (C) as shown in the Figure 11. The flow rate was adjusted by means of pinchcocks

as indicated.

A heater coil connected through a Variac and relay provided the source of heat for the bath. A thermistor operated relay ('Thermistemp' model 63 RB, Yellow Springs Instrument Co., Maryland) was used to control the heater. Temperature variation was normally $\pm$ 0.05°C but never exceeded $\pm$ 0.10°C.

Cold tap water was used to cool the bath at 20°C and 6°C. However, whenever the tap water was above 5°C the system described above was also used for thermostating at 6°C.

4.34 Sample preparation:

Hydrated sulphates of calcium, manganese, cobalt, nickel, copper and zinc were evacuated at room temperature and the temperature was increased in steps to 50°, 100°, 125°, 150° and 200°C. At each step the pumping was carried on until constant weight was obtained. This general method was used for the following: $CaSO_4 \cdot 2H_2O$, $MnSO_4 \cdot H_2O$, $CoSO_4 \cdot 7H_2O$, $NiSO_4 \cdot 6H_2O$, $CuSO_4 \cdot 5H_2O$ and $ZnSO_4 \cdot 7H_2O$. Preparation of anhydrous $FeSO_4$ was not successful as on dehydration, the salt yields a partially decomposed and oxidized product[22,24,25].

The anhydrous products were all prepared directly in the sample bulb on the balance and the surface areas were determined. Specific details on the preparation of each adsorbent will be presented below.

Calcium Sulphate: The product on dehydration by the general proce-

dure yielded a surface area of about 12 m^2/g and the sample was used for adsorption studies.

Many workers[96-104] have carried out studies on dehydration and rehydration of calcium sulphate. Malony, Bectka, and Ridge[99] have studied the kinetics of dehydration in vacuum, finding that dehydration takes place in two steps:

$$CaSO_4 \cdot 2H_2O \rightarrow CaSO_4 \cdot \tfrac{1}{2}H_2O \rightarrow CaSO_4$$

(Monoclinic) (rhombohedral) (hexagonal, soluble anhydrite)

The 2nd step was carried out by heating at 85°C for 24 hours. They have further mentioned that on heating above 200°C the hexagonal form transforms to the orthorhombic form. The crystal structure of anhydrite is given by Wyckoff[105], Cheng et al[106] and Bokii et al[107]. Calcium sulphate has a rhombic unit cell structure and each calcium ion is surrounded by eight oxygen atoms. Betoluzza et al[103] studied infrared spectra of thermally dehydrated calcium sulphate and found that the product on heating up to 600°C is either the hexagonal or the orthorhombic.

Following dehydration, the samples were annealed in vacuum at 300° and 400° and isotherms were determined.

Manganese Sulphate: Anhydrous manganese sulphate was prepared following the general method described earlier for calcium sulphate and was found to have a specific surface area of about 8 m^2/g. This sample was used for adsorption measurements.

Tanabe *et al* [101] have heated manganese sulphate in air and vacuum and found that the acidity of the surface increased on heating. This acidity presumably arises from chemisorbed water. D.T.A. studies on $MnSO_4$ in air have been carried by Bendor and Margalith[108] . According to them $MnSO_4$ dehydrates completely at 260°C in air.

On annealing the sample to 300°C in vacuum a slight weight loss (0.7%) was observed. Slight zero shifts in the balance over long periods of time may produce apparent weight changes as well. However, this phenomenon has been observed with the other salts up to *ca* 300°, and the effect is much less important at higher temperatures which suggests that it may be due to chemisorbed water. Annealing at 400°C was also done in vacuum. An attempt to anneal the salt at 500°C in vacuum was not successful because the Pyrex balance limb was softened and deformed at this temperature.

The crystal structure of anhydrous manganese sulphate has been reported by Wyckoff [105], Rentzperis [109], Coing-Boyat [110], Pistorius [111], Will [112] and Bokii *et al* [107]. Manganese sulphate is isomorphic with $NiSO_4$ and the low temperature ($<$500°C) modification of cobalt sulphate. It has orthorhombic unit cell structure. The sulphur atoms lie at the centre of an almost regular tetrahedron of oxygen atoms. The manganese ions lie at the centre of a distorted octahedron of oxygen atoms.

Zinc Sulphate: Zinc sulphate was partially dehydrated at room temperature outside the balance assembly and then a suitable amount was placed on the balance pan (sample bulb). This sample was heated by the general procedure up to 200°C, giving a satisfactory surface area, approximately 7 m^2/g. The sample was annealed in vacuum at 200°, 300° and 400°C in vacuum and the isotherms were determined each time. An attempt to anneal at 500°C was not successful for the reasons explained above. The weight loss observed on annealing between 200°C and 300°C was <0.2% which corresponds to approximately one monolayer of water.

Dehydration studies of zinc sulphate were done by Kohler and Zäske[113] and more recently by Ball and Norwood[114], Manewa[115] and Sara Sarig[116]. According to Manewa[115] zinc sulphate is free from water within 24 hours at 140°C in high vacuum.

The crystal structure of zinc sulphate has been described by Kokkoros and Reutzeperis[117]; Pannetier and Bregeault[118] and Bokki et al[107]. Zinc sulphate, copper sulphate and the high temperature modification of cobalt sulphate (7500°C) are isomorphous The zinc ions lie at the centre of a distorted octahedron of oxygen atoms in an orthorhombic cell.

Cobalt Sulphate: Cobalt sulphate did not yield enough surface area when dehydrated by the general procedure described earlier. In order to obtain a reasonable surface area, heating in vacuum was restricted to temperatures below 125°C until dehydration was stabilized. After constant weight was obtained heating at 200°C

and further annealing at 300°C, 400°C and 500°C was done in an argon stream. By using this method, a surface area of about 7 m^2/g was obtained for the sample heated to 200°C. However, when this salt was heated to 300°C in argon, a large weight loss corresponding to one mole of water was observed. This indicates that the constant weight obtained on heating at 125°C could have been due to formation of the relatively stable monohydrate of cobalt sulphate. Simmons and Wendlandt[119] have reported that one mole of water is bonded differently in $CoSO_4$ and the correct formula for the 1-hydrate is COH_2SO_5 as previously given by Lendormy[120,121]. Kohler and Zäske[122] dehydrated $CoSO_4 \cdot 7H_2O$ at 20 torr and found the composition to be $CoSO_4 \cdot H_2O$ between 190°C and 210°C and the dehydrated product was obtained by them at 260°C.

Demassieux and Mallard[123], Guenot et al[124] Bendor and Margalith[108] and Tanabe et al[125] have reported their studies on dehydration of $CoSO_4$. Bendor and Margalith[108] have stated that "The temperature of dehydration of the monohydrates studied, except for cupric sulphate follows the same trend i.e. starting from Mn^{2+} there is a continual rise until Zn^{2+} where there is a drop in the dehydration temperature". This explains why cobalt sulphate could not be completely dehydrated at 125°C in vacuum or 200°C in an argon stream.

It is argued, on the basis of the foregoing, that the adsorbent prepared at 200°C is $CoSO_4 \cdot H_2O$ whereas at higher temper-

atures, the adsorbent is anhydrous $CoSO_4$.

The crystal structure of anhydrous cobalt sulphate has been presented by Wyckoff[105], Coing-Boyat[110], Pistorius[125], Rentzeperis[126], Dunitz[127] and Pannetier & Bregeault[118]. The low temperature modification (<500°C) is isomorphous with nickel sulphate and manganese sulphate. High temperature modification (or modifications[127]) is isostructural with copper sulphate and zinc sulphate.

Nickel Sulphate: A procedure very similar to that described in the case of the dehydration of cobalt sulphate was followed for nickel sulphate. However, in this case the argon flow at 200°C had to be maintained for 15 days in order to obtain a constant weight.

Fruchart & Michel[180], Thomas and Renshaw[127A], Tanabe & Katayama[101] and Ball & Norwood[114] have conducted studies on various aspects of dehydration of nickel sulphate. Tanabe et al[2-5,128], and Bendor & Margalith[108] have extensively studied the dehydration of cobalt sulphate[108,128] and nickel sulphate[108,2-5,128]. Tanabe et al have correlated the acid property of anhydrous salts with the structure of solid metal sulphates. Bendor et al[108] have summarized the available studies of X-ray and neutron diffraction and discussed I.R. and D.T.A* studies of the hydrates of the metal sulphates and have interpreted the acidic properties of the monohydrates on the basis of the special linkage of water molecule to the central metal ion.

* Differential thermal analysis

However, the heating procedure of Tanabe et al[2-5,128] varies from ours. They have directly heated the hydrated salts in an electric furnace for three hours at various temperatures ranging from 150 to 600°C, and cooled them in an evacuated desicator.

A weight loss amounting to about 0.5 moles of water was observed when $NiSO_4$ (300)* was heated to 400°C. Heating at 300°C also resulted in a smaller weight loss, equivalent to only about 0.2 moles of water per sample weight.

The crystal structure of anhydrous nickel sulphate has been described by Wyckoff[105], Dimaras[129], Poljack[130] and Bokii et al[107]. Nickel sulphate is isomorphous with $MnSO_4$ and the low temperature form of $CoSO_4$.

Copper Sulphate: Copper sulphate was originally dehydrated following the general procedure mentioned for the dehydration of calcium sulphate. This sample was annealed at 200°, 300° and 400°C in vacuum. Isotherms were determined. Although a good surface area was obtained following the general procedure, the method described for the nickel and cobalt sulphate was adopted for the present study. The latter method enables one to heat up to 500°C, consistent with nickel and cobalt sulphate, and yielded a reasonably good surface area (8.5 m^2/g) after heating at 200°C. In the case of copper sulphate alone the surface area decreased rapidly with increasing annealing temperature. It was also observed that a rapid increase in temperature up to 200°C results

* The notation M SO_4 (200) etc. indicates the adsorbent annealed a particular temperature, in parantheses.

in a sample with a low surface area ($\sim$2 m^2/g) which goes to nearly zero on annealing at 300°C.

Kohler and Zaske[122] have reported that on heating $CuSO_4 \cdot 5H_2O$ at 20 torr vacuum, anhydrous sulphate is obtained at 192°C. Many authors[116,122,131-137] have reported various studies concerning the dehydration of this salt.

The crystal structure of anhydrous $CuSO_4$ has been given by Kokkoros & Rentzperis[117], Wyckoff[105], Rama Rao[138] and Bokii et al[107]. It is isomorphous with zinc sulphate.

The surface areas for the adsorbents are listed in Tables 4 to 9* and discussion of change of surface area with annealing temperature is given on section 5.80.

4.35 Adsorbate purification:

The adsorbate, $CFCl_3$, was purified in the equilibrium manifold (Figure 10). The system was evacuated to 10^{-6} torr and stopcock 4 was closed. Liquid $CFCl_3$ was placed in bulb 6 and attached to the manifold. It was slowly dipped in liquid nitrogen and after all of the liquid had solidified the cylinder was opened to the pumps and evacuated. The process of solidification and liquefaction by allowing the bulb to warm up to room temperature was repeated several times to degas the $CFCl_3$. The liquid was distilled into three fractions by vacuum distillation. The middle fraction was collected in the bulb 8. The last fraction and the first fraction were collected in the bulb 6 and discarded.

*See Appendix B.

The whole procedure was repeated on the initial middle fraction in bulb 8 and again the middle fraction was collected in previously evacuated bulb 7. This liquid was used for adsorption studies. During the desorption process the vapours were condensed in bulb 6 and the collected liquid was discarded after the run.

In between the runs the adsorbate was stored in bulb 7 at dry ice temperature and the bulb stopcock was kept closed. Vapour was always removed from the bulb to prevent mercury vapours from the gauges condensing in the bulb.

4.40 Calorimetric measurements:

The present work was concerned with the effect of heat treatment of the anhydrous transition metal sulphates on their heats of solution. Accounts of calorimetric principles and apparatus have been given by several authors[28,33,139,140]. Based on the general principles, a design was developed and the twin calorimeters were constructed.

The surface areas of the samples were measured volumetrically prior to calorimetric measurements. The volumetric B.E.T. apparatus is described in section 4.44.

Different designs of calorimeters have been adopted for various types of studies. Morrison, Drain and coworkers[141-143] have studied phase transitions and other thermodynamic properties of the adsorbate on adsorption. Holmes and coworkers[144,145] have conducted heat of immersion studies. Motooka et al[146] have described the effect of grinding on the heat of solution. Tsau and Gilson[147] have studied solid phase transitions and fusion by this method. Lang[148], Readnour et al[149], Eatough and coworkers[150] and more recently Larson[151] and Hedwig et al[152] have studied the association and dissociation of ion pairs of metal sulphates from heat of dilution measurements.

Pace[153], Holmes[154] and Zettlemoyer and Narayan[155] have reviewed the various aspects of adsorption calorimetry. The application of calorimetry in the measurement of laser energy has been described by Gunn[156].

4.41 Description of calorimeters:

A twin or differential calorimeter consists of two identical cells. The cells are made of Dewar flasks of 250 ml capacity each. These were placed symmetrically in a constant temperature bath*constructed from a 7.5 cubic feet (approximately) stainless steel tank, insulated with styrofoam. A temperature controller, stirrer, cooling coil and a heating coil maintained the bath at $25.0 \pm 0.01^{\circ}C$.

The solution process is carried out in one of the cells, the second serving as reference. A single motor has been used to drive the two identical stirrers in the cells. As both the calorimeter cells are in the same environment, and the temperature was recorded differentially, any errors due to fluctuations in the environment or due to stirring heat cancelled out.

The cells: The cell assembly is shown in Figure 12. A plexiglass flange around the Dewar was sealed with a plexiglass top block using an 'O' ring on the flask between the flange and top. It was fastened with stainless steel bolts. A stirring shaft extended down to the bottom of the flask. Holes through the block let out the leads of the heating elements, the thermopile wires and the stainless steel rod which was attached to a sample breaking device in the calorimeters.

The stirring shaft was kept in position by two 'O' rings sitting on the groves on the shaft close to the two ends of

*Figure (12A)

the block hole. Thin teflon washers on the shafts and the block holes facilitated the shaft motion with minimum friction and sealed the solution chamber.

The sample breaking device consisted of a stainless steal plate with a sharp point in the centre supported by a plexiglass cylinder held by three stainless steel bolts. A threaded rod went through the block and rested on the sealed stem of the thin walled sample bulb. The bulb could be easily broken by pressing the steel rod.

The heating element, for the electrical calibration was made by a bifilar winding of enamel insulated constantan wire (30 gauge, supplied by Leeds and Northrup company) wound on a polyethylene sheet. This sheet was pressed between two thin hollow brass cylinders. The ends of the cylinders were sealed by soldering, after the leads of the heating coil along with a ground wire connected to brass cylinder were taken out through copper tubing which was then compressed to the size of the opening between the two cylinders. This made the heating coil leak proof and well protected from the silica pieces moving around in the cell after the sample bulb was broken. Either of the cells could be used as the active or reference cell.

The thermopile: A twenty five junction copper constantan thermopile, supplied by Science Products Corporation, New Jersey, U.S.A., was used differentially to measure the temperature changes in the active cell with respect to the temperature in the reference

cell. The order of temperature change detectable by the thermopile was one degree per mV.

4.42 Calibration of the calorimeters:

The temperature rise within the cell during solution process was monitored by the thermopile connected to a recorder (Type LER-12 A, Yokogaw Electric Works). The heat capacity of the cells was measured by electric calibration of the calorimeters. After the initial thermal equilibrium has been established as indicated by the baseline of the recorder, the solution was heated by known current and for a known time and the temperature rise recorded. The heats of solution calculated from these data are described later.

The calorimeters were also calibrated by determining the heat of solution of potassium chloride.

Electrical calibration circuit:

The heating current circuit for the calorimeters is shown in Figure 13. The current was measured by monitoring the potential across a standard one ohm resistor in series with the heating coil. The thermopile leads were connected to the recorder. All the leads were shielded and grounded along with the recorder and power supply to a common ground terminal. The DPDT switch* in the heating current circuit also actuated an electrically operated stopwatch.

Electrical calibration of the calorimeters:

In order to compare the stirring heat or the heat changes

*double pole double throw switch

due to the environmental fluctuations in the reference cell and the active cell, the heat capacities of the two calorimeter cells must be known. This was determined by supplying a known amount of heat to both heaters connected in series. From the measurement of temperature, current and time it was observed that both the cells had the same heat capacities. In the present study the cell in which the heat of solution was measured was calibrated for its heat capacity after each measurement, when the temperature of the cell returned to the original temperature.

Chemical calibration:

A known weight of dried potassium chloride (heated at 100°C for 24 hours and cooled at room temperature in a dessicator) was placed in a sample bulb with a glass wool plug and sealed. The twin calorimeters were assembled with 200.0 grams of distilled water in each cell. The calorimeters were left in the constant temperature bath for at least 16 hours and the sample was broken when a steady base line was obtained in the recorder in its most sensitive range (one mV or one degree full span) for about one half hour or more. The change in temperature was automatically recorded. Heat capacity was measured by supplying electric power as described earlier.

The heats of solution were calculated from the following relation:

$$\Delta H = - \frac{I^2 R t M x}{4.184 y w} \quad \text{Cal/mole} \qquad (4)$$

where,

I = heater current in amperes (stability 0.1%),

R = heater resistance in ohms (± 0.01 ohms),

t = heating time in seconds (± 0.05 seconds),

x = temperature change during dissolution (± 0.001°C),

y = temperature change due to electrical heating (± 0.001°C),

w = weight of the sample (± 0.0001 g),

M = molecular weight of the solute.

For potassium chloride the measured data were,

I = 0.1256 amp.

R = 63.55 ohm

t = 264.85 seconds

x = 0.200°C

y = 0.231°C

w = 1.0048 g

M = 74.56 g

These data for potassium chloride give a ΔH value of 4077 cal/mole at 25°C. This value of heat of solution is for the dilution up to 0.067 molal solution. The reported[157] heat of solution for KCl is 4115 cal/mole at 25°C for infinite dilution. The heat of solution of potassium chloride at various dilutions derived from the heat of formation data[158] are given in Table 10.

4.43 Heat of solution measurements:

The quantities of hydrated metal sulphates which have been calculated to give the required amount of anhydrous sulphates were weighed. These weights were such that on dissolving in 200.0 grams of solvent the solution had a similar metal ion concentration (approximately 0.01 molal). This avoided the correction due to ionic strength effects. Dehydration and the determination of surface area of samples were done using a BET apparatus as described in section 4.44. The samples were outgassed and sealed in argon at one atmospheric pressure. The sample was then placed in the calorimeter. The solvent used was 0.5 molar potassium sulphate solution to minimize the dilution effects[148,159] on the heat of solution of different metal sulphates. Another advantage of potassium sulphate solution was that the condensation of solvent on the upper part of the calorimeter was eliminated.

The procedure which was followed was the same as that described for the chemical calibration in which the heat of solution for the potassium chloride sample was measured.

The results of calorimetric studies are given in Table 2.* A typical plot obtained by the recorder for heat of solution measurement along with the electrical calibration curve for heat capacity is given in Figure 14.

4.44 Surface area measurements:

Apparatus: An apparatus was constructed for the volumetric measure-

---

*There is no trend observed in the measured heat of solution data with respect to annealing temperature. The variations are presumably due to changes in bulk and surface structures, and unfortunately it is not possible to separate the two contributions.

ment of surface area of the various samples used for calorimetric measurements. It was necessary that the surfaces of the samples used for heat of solution measurements be prepared by a method similar to that used in preparing the adsorbents used in the gravimetric adsorption studies. The apparatus is sketched in Figure 15. The principles involved in the construction are general and well known [28,29,33,35,36]. The amount adsorbed is determined as the difference between the amount of gas in the vapour phase within the free volume of the apparatus before and after adsorption. For the sake of accuracy, the free volume and the sample surface area should be such that the adsorbed amount should be insignificant as compared to the amount of gas in the entire free volume of the apparatus. As stated before, the assumption used in this method is that no part in the apparatus, other than sample and adsorbate reservoir, may either adsorb gases or be the source of any gas.

Pressure measurement: Pressure was measured by a capacitance manometer as an absolute gauge by using the high vacuum side as a reference. Capacitor manometers utilize the principle that the capacitance of any capacitor is directly proportional to the dielectric constant of the medium relative to air and to a geometric factor [160]. Capacitance gauges available commercially are excellent universal pressure sensors [91,92]. A pressure difference between two chambers separated by a metallic diaphragm, moves the diaphragm, increasing the capacitance between the diaphragm and electrode on one side,

while decreasing the capacitance on the other side. The change in capacitance is measured by a bridge circuit. There is no electrical feedback to null the diaphragm position which may alter the pressure reading. The capacitance gauge used can read the pressure with reliability to a few percent at 10^{-4} torr [95].

A MKS Baratron TM type 77 capacitance manometer using 0-100 torr range head, was incorporated in the volumetric apparatus(see 7 in Figure 15). The manometer could read to $\pm$ 0.1 torr on the 100 torr range.

Vacuum requirements: The vacuum requirement of this method is similar to that of the gravimetric method (section 4.31). There is an additional consideration in volumetric method regarding evacuation is that 'over evacuation' may leave the surfaces of the metal parts such as valves, gauges etc. in an 'active' state which may adsorb gases during the experiment. In practice, a compromise between the vacuum requirement and 'over evacuation effect' has to be made. However, if the sample surface area is large enough (a few cm^2) the adsorption by other parts of the apparatus would be insignificant. A vacuum of the order of 10^{-6} torr was obtained using a two stage oil diffusion pump backed by a fore pump. The low pressure measurement was done using a Pirani gauge and an ionization gauge.

Procedure for sample preparation: A hydrated metal sulphate sample was weighed in a thin walled silica bulb and was joined below the Pyrex-silica seal as shown at point 17 in Figure 15. The sample was evacuated, heated or annealed before adsorption as in

the case of gravimetric measurements (section 4.34). However, a slightly different arrangement was used to stream argon gas over the sample while annealing. A capillary was introduced into the sample bulb and argon was admitted through the capillary (see Figure 15) and vented to the atmosphere through the equilibrium manifold. To observe the flow of argon and to prevent back diffusion an oil bubbler was introduced near the exit of the gas. After annealing, the system was degassed at 125°C, at least 24 hours before measurements.

Volume calibration: The volume of the bulb V_c was determined before the apparatus was assembled. This was done by filling the bulb with deionized water and weighing it several times, and from the average weight the volume was calculated. The other volumes used in the calculation are: the volume between the valves* no. 1, 2, 3, 4, 5, 6 and capacitance gauge 7 equals V_1; the volume included by valves 3 and 8 equals V_2; V_2 does not include the volume of the sample or the outer jacket around the sample bulb.

V_1 and V_2 were calculated following the ideal gas law using expansion of helium gas. At constant room temperature T_R, V_1 can be calculated as

$$V_1 = V_c \, [p_2/(p_1-p_2)] \qquad (5)$$

where, p_1 and p_2 are the pressures in volume V_1 before expansion and after expansion into volume V_c respectively;

* See Figure 15

and $$V_2 = V_1 \left[p_{eq}/(p_2 - p_{eq})\right] \quad (6)$$

where, p_{eq} is the equilibrium pressure after expanding the gas to sample side.

The volume V_2 so obtained has to be corrected for the temperature difference between the thermostat and rest of the system. The volume of the bulb immersed in the thermostat is say V_B; this volume was measured at temperature T_R before joining the bulb with the apparatus. The corrected volume of the sample side, generally known as dead space V_d is given by,

$$V_d = (V_2 - V_B) + V_B \frac{T_R}{T} \quad (7)$$

Helium was used for volume calibration owing to its low critical temperature.

Isotherm measurements: During the experiment the volume V_c was not used. The rest of the apparatus was evacuated. Purified $CFCl_3$ vapour (see section 4.35) was introduced from the liquid reservoir to the volume V_1 and the dose volume was calculated. The sample was then exposed to the adsorbate and the pressure was recorded. The amount of adsorbate adsorbed per sample weight can be evaluated by using ideal gas laws. The isotherms were constructed for all the samples and surface area was calculated as discussed in section 5.20. These are tabulated in Table 2.

A typical isotherm measured volumetrically is shown along with the isotherm measured gravimetrically in Figure 16.

5.00 DISCUSSION OF EXPERIMENTAL RESULTS

5.10 Experimental data

5.11 Isotherms

5.20 Surface area determination

5.21 The BET equation

5.30 Thermodynamic quantities and adsorption

5.40 The heats of adsorption

5.50 Entropies of adsorption

5.51 Theoretical calculation of entropy for localized films

5.52 Theoretical entropy of two dimensional gas

5.60 Selection of the model

5.70 Effect of annealing on surface area

5.10 Experimental data:

The pressure and mass change data obtained from gravimetric adsorption experiments are tabulated in Appendix A (Section 8.10).

The heats of solution data are tabulated in Table 2 (Section 9.00). Volumetric adsorption data are tabulated in Appendix B (Section 8.20). An isotherm measured volumetrically as compared with one measured gravimetrically is shown in Figure 16.

The saturation vapour pressures of $CFCl_3$, (p_o), were measured at each temperature. The results are shown in Table 3 and a plot of log p_o against 1/T is shown in Figure 17.

The error in weighing is discussed in Section 4.26. The error in pressure measurement is $\pm$ 0.01 torr. In the volumetric method the error in measurement is difficult to assess. The main source of error in this method occurs in the calibration of the volumes and the temperature changes in the bath or other parts of the equilibration manifold during the course of a run. The probable error[216] in volumetric surface area measurements is estimated as between 5 to 10%.

5.11 Isotherms:

The isotherms obtained from the gravimetric data are plotted in Figures 18 to 38 (section 10.00).

Dubinin et al[19] have reviewed the theoretical basis of adsorption isotherms. The theoretical treatment involves determining the properties of adsorbent and adsorbate independently and following three operations:

1) Calculation of the potential energy of an isolated molecule in the adsorption field of a given adsorbent;

2) Calculation of the interaction energy between adsorbate molecules;

3) Calculation of the entropy of the adsorbed molecules.

The statistical thermodynamic approach is used to deduce the adsorption isotherm from the above data. However insufficient

knowledge of intermolecular interactions at intermediate distances, the nature of the surface of a real adsorbent, the realistic model for entropy calculations and finally the exact adsorbate-adsorbate interactions, do not allow one to deduce the isotherm. In a few simple cases[19,161-163] success has been achieved in correlating the theoretical and experimental isotherms. Numerous empirical and semiempical adsorption isotherm equations have also been proposed from time to time[33,164].

5.20 Surface area determination:

The literature[165] contains a number of comparisons of the various methods that have been used to determine surface area. The methods include chromatographic experiments, radiometric methods, heat of wetting, gas permeability, small angle X-ray scattering and electron microscopy. However, analysis of adsorption isotherms remains the principal method of obtaining specific surface area.

Various equations of state have been utilized to derive adsorption isotherm equations, but the BET equation is still widely applied. The Langmuir equation[36] in the form

$$\frac{p}{M} = \frac{1}{pM_m} + \frac{p}{M_m} \qquad (8)$$

is mainly used in chemisorption studies for surface area determinations.

In equation (8) p is the vapour pressure of the adsorbate and M is amount adsorbed. M_m represents the mass of the adsorbate occupying one monolayer. From the slope and intercept of the plot p/M against p, M_m can be evaluated.

In the present studies the BET equation[166] has been applied for the determination of surface area of each adsorbent used.

5.21 The BET equation

The derivation of the BET equation is given in many references[28,33,36]. One of the forms of the equation is as follows:

$$\frac{p}{M(p_o-p)} = \frac{1}{M_m C} + \frac{C-1}{M_m C} \cdot p/p_o \qquad (9)$$

where p_o is the saturation vapour pressure of the adsorbate and C is a constant. The monolayer capacity M_m is determined from the slope "S" and intercept "i" of a plot of

$$\frac{p}{M(p_o-p)} \quad \text{versus} \quad p/p_o \quad .$$

The monolayer capacity is given by,

$$M_m = \frac{1}{S+i} \qquad (10)$$

Good straight lines were obtained for the BET plots [$\frac{p}{M(p_o-p)}$ versus p/p_o] in all the cases over the range of p/p_o-p_o from 0.05 to 0.3. Gregg and Sing[28] have discussed the applicability range for the BET equation and the BET 'C' values in terms of shape of the adsorption isotherm and heat of adsorption.

Two representative BET plots are shown for $MnSO_4$ (300) in Figure 39 and for $NiSO_4$ (400) in Figure 40.

5.22 Calculation of surface area:

The surface area corresponding to monolayer capacity is given by[33],

$$A = M_m \; B \; N \; 10^{-26}, \qquad (11)$$

where,

A = area of the surface (m^2/g)

B = Cross section molecular area ($\AA^2$)

and N = Avogadro's number.

The molecular area of $CFCl_3$ was calculated from the following equation[33,36]:

$$B = f(M/\rho N)^{2/3} 10^6, \qquad (12)$$

where

M = molecular weight of the adsorbate;

ρ = bulk density of adsorbate;

and f = packing factor.

The packing factor is 1.091 if each molecule has 12 nearest neighbors. It was assumed that the packing or configuration of the adsorbate molecules on the surface was similar to that of the bulk liquid phase of the adsorbate. The density of the adsorbate is taken as 1.623 g/cm[3(167)]. These values yield an apparent molecular area for $CFCl_3$ of 31.2 $\AA^2$. Machin[27] has compared the effective molecular area of $CFCl_3$ on anhydrous transition metal sulphates with argon (taken as 13.6 $\AA^2$) on the same adsorbents. His average value of the molecular area of 29.7 $\pm$ 0.7 $\AA^2$ is in good agreement with the above value.

The surface areas for the samples were calculated using a molecular area of $CFCl_3$ of 31.2 $\AA^2$ and are tabulated in Tables 4 to 9.

The same procedure was followed for determination of surface areas from the isotherms determined volumetrically. These surface areas are reported in Table 2. A representative BET plot is shown for $CuSO_4$ (200) in Figure 68.

5.30 Thermodynamic quantities and adsorption:

It is possible to interpret the experimental adsorption isotherms with the help of thermodynamics, in two ways. Either integral or differential molar quantities can be derived from the isotherms. Although both methods yield the same conclusions, the calculation of differential molar quantities is relatively easy. Differential heats of adsorption and differential entropies of adsorption have been derived and will be compared with the assumed models.

Clark[7] has described the localized, nonlocalized, mobile and immobile models of adsorption.

Favoured positions of minimum potential energy on a surface lead to localized adsorption. In such adsorption the molecules are held at the bottom of the potential well, the depth of which is much greater than the thermal (translational) energy of the molecule (kT). The molecules cannot escape from regularly spaced and equally deep potential wells at the surface. Three translational degrees of freedom of the gas transform to three vibrational degrees of freedom on adsorption. Two of the vibrational degrees of freedom remain in the plane of the surface and one normal to the surface.

When there are no strongly favoured positions, essentially non-localized adsorption takes place. In general a non-localized adsorption phase will be mobile except at high coverages

when caging action[181] of neighboring molecules results in the transformation of free translation to vibrations of progressively decreasing amplitude with increasing coverage.

Localized molecules may be mobile or immobile depending on the surface characteristics[7] i.e. whether there are structural irregularities or surface inhomogeneities present or surface diffusion can later take place on the surface.

An intermediate situation is possible between mobile and immobile adsorption as described by de Boer[168]. In this type of adsorption, the molecules move from site to site by "hopping".

A completely immobile system is inconsistent with the concept of the equilibrium system. The residence time of adsorbed molecules in relation to the heat of adsorption is a measure of the degree of localization and no sharp division between either type of adsorption at all coverages can be made in real systems. The life time or residence time (τ) of adsorbate molecules is dependent on the heat of adsorption (q) according to the relation[168]:

$$\tau = \tau_0 \, e^{-q/RT} \qquad (13)$$

where τ_0 is the molecular vibration time ($\sim 10^{-13}$ sec); and RT represents thermal energy.

The differential heat of adsorption at a particular surface concentration is defined as the change in heat content, per mole transferred, when an infinitesimal amount of material goes from the gas phase to the surface.

A two dimensional gas is defined as the adsorbed molecules of gas, constrained to freely move parallel to the surface. Movement normal to the surface is prohibited. Everett[169] has derived equations for the heat of adsorption and the entropy loss of the surface phase of an ideal two dimentional gas. He has also formulated, from thermodynamic considerations, the various conditions to be satisfied if the adsorbed phase is an ideal two dimensional gas. The conditions are:

1) the adsorption isotherm must be linear;

2) the heat of adsorption must be independent of the surface coverage;

3) the differential entropy of adsorption $\Delta\bar{S}$ must be a linear function of surface concentration with a slope R;

4) the magnitude of $\Delta\bar{S}$ (θ) must be equal to the expected value for adsorption of a two dimensional gas.

It is only rarely that any gas-solid system obeys all the above criteria. However, the procedure followed here is to compare the $\Delta\bar{S}$ (θ) curves with the theoretical ideal two dimensional gas entropy changes as a function of θ (coverage) and interpret the deviation from ideal behaviour to improve the real model. Deviations from the model may be due to:

1) motion normal to the surface;

2) the effect of the finite size of the adsorbed molecules on the surface entropy particularly at higher coverages;

3) variations of heat of adsorption with coverage due to

molecular interactions (a cohesion term, if included in the equation of state, leads to a linear variation of heat of adsorption with coverage);

and 4) entropy changes due to structural changes in the adsorbent itself. However, this last consideration is relatively unimportant in physical adsorption. Scholten and Kruyer[170], however, have expressed their doubt about change in surface structure affecting even chemisorption entropies significantly. According to them, the bonds between the surface and subsurface layer are still so strong that the changes in adsorbent vibrations have almost no effect on the entropy of the adsorbent.

5.40 The heats of adsorption:

As mentioned in section 5.11 it is possible to make theoretical estimations of adsorption energies, based on the theory of intermolecular forces, only in a few simple cases. The various adsorption forces and theoretical calculation of adsorption energies have been given by Young & Crowell[33], Dubinin[19] and Kiselev[163]. As a result, direct experiments for measuring adsorption isotherms must still be the source for heats of adsorption. Adsorption heats can be calculated either by direct calorimetric studies as described by Morrison and coworkers[171-173] or by determining the temperature dependence of adsorption. The calculation of adsorption heats from gas chromatographic data[174] is similar in principle to that from isosteric heats of adsorption. A knowledge of adsorption heats allows one to determine entropy changes accompanying the adsorption process.

Various relationships between the heats of adsorption, measured from isosteres, or calorimetry, both adiabatic as well as isothermal and the heat of immersion, have been derived in details by Young & Crowell[33], Clark[7], Adamson[164] and more recently by Letoquart et al[175].

The isosteric heat, q_{st}, is given by,

$$q_{st} = RT^2 \left(\frac{\partial \ln p}{\partial T}\right)_{\Gamma} \quad . \qquad (14)$$

Where Γ refers to the number of moles adsorbed per unit area (n_s/a). The approach followed by Young and Crowell emphasizes

that q_{st} is also a calorimetric heat of adsorption for a suitably operated calorimeter. The differential heat of adsorption, q_d, is related to q_{st} by the following relation:

$$q_d = q_{st} - RT \qquad (15)$$

A plot of ln p against 1/T at constant coverage should yield a straight line. The slope of this line when multiplied by R yields the isosteric heat. The isosteric heats determined in this work are tabulated in appendix B (Tables 17-19). Good straight lines were obtained from the ln p plots against 1/T at three temperatures 20.0°, 6.0° and -10.0°C.

Heats of adsorption have been plotted (Figure 41-46) and straight line plots for low values of θ extrapolated to $\theta = 0$ to obtain q_{st} ($\theta = 0$) which are taken to be the isosteric heats pertaining to the high energy sites of the bare surface.

The error in isosteric heat of adsorption is estimated from the method of least squares as approximately $\pm$300 cal/mole at lower coverages. However, in the region of higher coverages, the error decreases to about $\pm$ 100 cal/mole.

An excellent review on heat of adsorption investigations for specific systems is given by Holmes [176], who has reviewed much experimental work especially that from the laboratories of Beebe, Kiselev, Morrison, Kington and their co-workers.

The form of the dependence of differential heat of adsorption (or isosteric heats) with coverage is strongly affected

by the properties of the specific adsorbents and adsorbates under study, although there is a general trend which remains more or less the same. At low coverages, differential heats of adsorption are higher due to initial surface heterogeneity. The next region is where adsorbate-adsorbate interactions are still relatively unimportant and the surface is more or less uniform. Further adsorption redutes the distance between adsorbed molecules and adsorbate-adsorbate interactions become more important. These attractive forces may increase the heat of adsorption (q_{st}). Finally, q_{st} decreases due to repulsive forces when the distance between adsorbed molecules becomes reduced, decreasing until the monolayer is complete and p approaches p_o, and q_{st} approaches the heat of condensation (6.44 kcal/mole for $CFCl_3$).

The following analysis of the heat curves obtained for individual samples will now be discussed.

Manganese Sulphate: The heat curve (Figure 41) for $MnSO_4$ (200) gradually decreases, with θ increasing up to 0.5 and then remains more or less constant suggesting an initial minor inhomogeneity of the surface. The isosteric heat curve, $q_{st}(\theta)$, of $MnSO_4$ (300) follows the same trend except that it reaches more or less constant level at θ=0.3 suggesting a smaller heterogeneous surface. Both these heat curves fall close to the heat of condensation of the adsorbate at θ=1. However, the heat of adsorption of $MnSO_4$ (400) is less than that of the other two at low coverage signifying a smaller heterogeneity. It then passes through a shallow minimum at

θ=0.5 and increases again until θ=0.7 and remains constant to θ=1. At θ=1 the q_{st} is ~7.7 kcal/mole about 1.3 kcal/mole higher than heat of condensation which probably indicates that there is some effect of the forces of the solid beyond the first layer[176].

That annealing should give a more uniform surface, is to be expected and can be seen for $MnSO_4$ (400) initial heat curve from a comparison of these heat curves.

Cobalt Sulphate: The $CoSO_4$ (200) heat curve seems to be quite different from the surfaces annealed at 300 and 400°C. The cobalt sulphate (500) shows different behaviour at low coverages, but shows similar behaviour to that of $CoSO_4$ (200) at higher coverages. There is similarity between heat curves of $CoSO_4$ (300) and $CoSO_4$ (400) except that the adsorption at low coverages seems to be more energetic with $CoSO_4$ (400) than with $CoSO_4$ (300). Adsorption at low coverages on $CoSO_4$ (200) is much less than on $CoSO_4$ (300) and $CoSO_4$ (400). This is understandable in view of the discussion of sample preparation which suggests that $CoSO_4$ (200) is probably in monohydrate form rather than the anhydrous salt. Initial heat trends in $CoSO_4$ (300), $CoSO_4$ (400) and $CoSO_4$ (500) decreases with increasing coverage. The decrease is more gradual for $CoSO_4$ (400) than for $CoSO_4$ (300) or $CoSO_4$ (500). The cobalt sulphate annealed at 500°C ($CoSO_4$ (500)) follows the general trend of a surface which is less heterogeneous compared to $CoSO_4$ (300) and $CoSO_4$ (400). This may be expected due to the

effect of treatment at a higher temperature.

Nickel Sulphate: All the $NiSO_4$ surfaces follow the same general heat curve trend with respect to coverage with the possible exceptions of $NiSO_4$ (400) which may have some scatter at low coverages. There also seems to be another trend in that the initial heat at $\theta=0$ increases with annealing temperature. The initial heterogeneity may be due to a particular surface structure which increases with increasing annealing temperature. The nickel sulphate annealed at 500°C follows the general trend predicted by the previously described model better than the other samples.

Copper Sulphate: The curves for $CuSO_4$ (200), $CuSO_4$ (300) and $CuSO_4$ (400) start off more or less the same but diverge at intermediate coverages and rejoin at $\theta=1$. In the case of $CuSO_4$ (500) the initial surface heterogeneity as indicated by a higher heat of adsorption at $\theta=0$ suggests the increasing of a particular type of surface structure. This curve also follows the general heat curve trend decreasing very close to the heat of condensation of $CFCl_3$, whereas $CuSO_4$ (200), $CuSO_4$ (300) and $CuSO_4$ (400) have q_{st} about 0.8 k cal/mole greater than that of heat of condensation at $\theta=1$.

Zinc Sulphate: With $ZnSO_4$, all the different heat treatments show more or less the same trend. The heat of adsorption decreases to $\theta=0.5$ and then remains constant. However, the initial heat

(at $\theta=0$) constantly increases with respect to annealing temperature. This may be due to the creation of more energetic sites due to removal of chemisorbed water.

Calcium Sulphate: By examining the heat curves of calcium sulphate the following references can be obtained:

In the region $\theta=0$ to $\theta=0.4$ the isosteric heat increases with increasing coverage for all three surfaces investigated, that of $CaSO_4$ (200), $CaSO_4$ (300) and $CaSO_4$ (400). However, the slope of the line joining the initial points is lesser for $CaSO_4$ (400) than for $CaSO_4$ (200) and $CaSO_4$ (300). The heat curves do not decrease to the heat of condensation at $\theta=1$. The difference is about 1 kCal/mole.

One of the possibilities is that the adsorption takes place in two different types of sites, one type being preferable to the other. Competition of the adsorbate molecules for the preferred sites brings them closer on such sites where dispersion forces come into play, and due to these attractive forces, the heat of adsorption increases with increasing coverage until all such sites are filled.

Anhydrous calcium sulphate has two crystalline forms, hexagonal and orthorhombic as discussed in section 4.34. The orthorhombic form is a high temperature form. Presumably most of the surface has the hexagonal form with patches of the other form. The surface having the orthorhombic form should increase with annealing of the sample at higher temperature and consequently

the competition of adsorbate molecules at low coverages should decrease. The slope of the initial points for the $CaSo_4$ (400) heat curve is less than that for the others.

No definite conclusion can be drawn for lack of independent adsorption data for the two forms of $CaSO_4$ and assessment of adsorbate-adsorbate interaction by independent means.

The occurrence of a minimum in the heat curve much before $\theta=1$ is presumably the result of the two opposing effects of heterogeneity and adsorbate interactions. As the higher energy sites are occupied on a nonuniform surface, q_{st} decreases with increasing θ. Some of the higher energy sites may be adjacent on the surface and a cooperative effect may take place. This effect can make an increased contribution to the heat of adsorption. Similarly interplay of lateral interaction and heterogeneity effects may also produce a maximum in the heat curves[177].

The criteria, that q_{st} must be linear with respect to coverage for either the localized or mobile model to be applicable[33], is not satisfied unless the variation of q_{st} is understood in terms of surface heterogeneity and lateral interactions. Surface heterogeneity usually plays the more important role[169].

5.50 Entropies of adsorption:

A knowledge of differential adsorption heats or isosteric heat (q_{st}) and changes in free energy as derived from the adsorption isotherm permits us to determine the entropy of adsorption. As already mentioned in section 5.30, the knowledge of the entropy of adsorption is of great importance in deriving a model for the adsorbed layer.

Young and Crowell[17] have deduced the following relationship:

$$RT \left(\frac{\partial}{\partial T} \ln p\right)_{\Gamma} = S_g - \bar{S}_s \quad , \qquad (16)$$

where,

S_g = molar entropy of the gas;

$\bar{S}_s$ = differential molar entropy of the adsorbed gas;

and

$$\Gamma = n_s/A \qquad (17)$$

where n_s is the number of moles adsorbed and A is the area of the adsorbent.

On comparing equation (14) with equation (16) we get,

$$S_g - \bar{S}_s = \frac{q_{st}}{T} \qquad (18)$$

which is the difference between molar gas entropy and differential entropy of the adsorbed gas at a particular temperature and pressure and amounts to the entropy loss during adsorption. If,

S'_g is the molar entropy of a gas at unit pressure and 6 ^{o}C, then

$$S'_g - \bar{S}_s = (S_g - \bar{S}_s) + R \ln p \qquad (19)$$

where p is pressure in atmospheres.

$$S'_g - \bar{S}_s = \frac{q_{st}}{T} + R \ln p_{torr} - R \ln 760 \qquad (20)$$

which yields,

$$\bar{S}_s = S'_g - \frac{q_{st}}{T} - R \ln p_{torr} + 6.633\ R. \qquad (21)$$

The differential entropy for the various surfaces were calculated as a function of θ (coverage). The results are tabulated in Appendix B (Tables 20-22). The differential entropy for the various surfaces have been plotted as a function of θ in Figures 47 to 52.

As mentioned earlier (section 5.30), the experimental results will be compared with two models, (i) a localized film (ii) a two dimensional freely moving adsorbed layer.

5.51 Theoretical calculation of the change of entropy on adsorption for localized film:

The Langmuir model consists of localized adsorption on a two dimensional array of active sites having the same adsorptive properties. The assumptions involved in this model are that an adsorbed molecule does not affect the properties of any other neighboring sites and that there is no adsorbate-adsorbate interactions. As per this model, from a residence time point of view, at any instant, most of the molecules will be in the vicinity of adsorption sites and only a few will be in intermediate positions.

The model also requires that the vibrational and rotational

degrees of freedom of the adsorbed molecules remain unchanged and independent of coverage and temperature.

The entropy of a localized phase can be conveniently separated into thermal entropy and configurational entropy[169]. The thermal entropy originates from excitation of rotational, vibrational and electronic states, the zero-point contribution to the entropy of adsorption usually being assumed to be negligible. The configurational entropy arises from the number of distinguishable arrangements among sites of equal energy and can be evaluated by the Boltzmann equation[164]:

$$S_{confg.} = K \ln \Omega \tag{22}$$

where Ω is the number of distinguishable arrangements of M adsorbed molecules on the N adsorption sites or,

$$\Omega = \frac{N!}{M!\ (N-M)!} \tag{23}$$

or

$$S_{confg.} = K \ln \frac{N!}{M!\ (N-M)!}\ . \tag{24}$$

On substituting $M/N = \theta$ (the fractional degree of coverage) and also using Stirlings approximation for factorials

$$x! = (x/e)^x, \tag{25}$$

(24) can be simplified to

$$S_{confg.} = -KN\ [\theta \ln \theta + (1-\theta) \ln (1-\theta)] \tag{26}$$

On differentiating (26) with respect to M and multiplying by Avagodro's number, we obtain the differential molar configurational entropy $\bar{S}_{confg.}$:

$$\bar{S}_{confg.} = -R \ln \frac{\theta}{1-\theta} \tag{27}$$

Hence,

$$\bar{S}_{local} = \bar{S}_{thermal} - R \ln \frac{\theta}{1-\theta} \tag{28}$$

The change of entropy on transferring one mole from the gas at unit pressure to the surface is:

$$\Delta\bar{S}_{local} = \bar{S}_{local} - S_{gas} \tag{29}$$

or,

$$\Delta\bar{S}_{local} = \bar{S}_{thermal} - S_{gas} - R \ln \frac{\theta}{1-\theta} \tag{30}$$

or,

$$\Delta\bar{S}_{local} = \Delta\bar{S} - R \ln \frac{\theta}{1-\theta} \tag{31}$$

The term $\Delta\bar{S}$ is a negative quantity and represents the loss in translational entropy of adsorption. This is equivalent to the complete loss of the translational entropy of the molecule in the gas phase, $S^{og}_{trans.}$. No rotational or vibrational entropy changes are involved according to this model. Equation (31) can then be rewritten as,

$$\Delta\bar{S}_{local} = -R \ln \left(\frac{\theta}{1-\theta}\right) - \bar{S}^{o,g}_{trans.} \qquad (32)$$

$\Delta\bar{S}_{local}$ is plotted as a function of θ in Figure 53*. This curve can be compared with the curves derived from the experimental data for $\bar{S}_s$ (Figures 47 to 52). Alternatively, the theoretical value of the differential configurational entropy $\bar{S}_{confg.}$ is zero at $\theta = 0.5$, the experimentally observed $\bar{S}_s$ at $\theta = 0.5$ should be the differential thermal entropy of the system, $\bar{S}_{therm.}$ Thus on adding this value of $\bar{S}_{thermal}$ to the theoretical value of $\bar{S}_{confg.}$, the experimental curve should be reproduced, if a simple localized model is valid.

The translational entropy loss $\bar{S}^{o,g}_{trans.}$ is given by[164],

$$\bar{S}^{o,g}_{trans.} = R \ln (T^{5/2} M^{3/2}) - 2.30 \qquad (33)$$

For $\theta = 0.5$, M (molecular Weight) for $CFCl_3$ = 137.37, T = 6°C, we get,

$$\Delta\bar{S}_{local} = -\bar{S}^{o,g}_{trans.} = -40.35 \text{ E.U.}$$

5.52 Theoretical entropy of mobile adsorbed layer:

Adamson[164] has derived the following relation for the mobile model:

$$\Delta\bar{S}_{mobile} = -R \ln \theta + S^{s}_{\substack{trans. \\ \sigma^{o}box}} + 63.8 \qquad (34)$$

where $S^{s}_{\substack{trans. \\ \sigma^{o}box}}$ is the translational entropy of the adsorbed layer considering the site as a two dimensional potential box. The value of the translational entropy is given by,

* These values are also tabulated in Table 11.

$$S^{s}_{\substack{trans. \\ \sigma^{o}box}} = R \ln (MT\sigma^{o}) + 63.8 \qquad (35)$$

where σ^{o} is the molecular area of adsorbate. At $\theta=0.5$ and substituting $\sigma^{o}=31.2$ A^{o2} at $T=279^{o}K$, we get,

$$S^{s}_{\substack{trans. \\ \sigma^{o}box}} = 18.40 \text{ E.U.}$$

and

$$\Delta\bar{S}^{o}_{mobile} = -20.55 \text{ E.U.} \qquad \text{from} \quad (34)$$

The experimental differential entropies for all the surfaces studied calculated at $6^{o}C$ at $\theta=0.5$ (see Appendix B)* compare reasonably well with the theoretical entropy for a mobile adsorbed layer. This suggests that the adsorbed layer is better represented by a mobile model rather than a localized model.

The differential molar entropies as a function of coverage for the model, a two dimensional van der Waal's gas having no interactions, is derived below. The differential entropies of adsorption thus calculated were compared with that of the experimental entropies in the coverage range up to $\theta=1$.

The adsorbed state of any adsorbate may be a two dimensional gas in a submonolayer region.

The translational partition function for a three dimensional gas is[178]

$$Q_3 = \frac{(2\pi mkT)^{3/2} V}{h^3} \qquad (36)$$

---

* Tables 20-22.

where V is the volume available to the molecules and the remaining symbols are well known. For a two dimensional gas the translational partition function is given by

$$Q_2 = \frac{(2\pi mkT)\ (A-b)}{h^2} \qquad (37)$$

where A is the area available per molecule and b is the area of the molecules (A-b) represents the area accessible to the molecules.

The statistical translational entropy of any two dimensional or three dimensional gas is given by[179]

$$S = RT\ \left(\frac{\partial \ln Q}{\partial T}\right)_{V,\ (A-b)} + R \ln Q - K \ln N! \qquad (38)$$

The change in entropy associated with a transition from a three-dimensional gas to a two dimensional gas will be,

(note S_g = entropy of 3d gas, S_s = entropy of 2d gas)

$$S_g - S_s = RT\left[\frac{\partial}{\partial T} \ln \frac{Q_3}{Q_2}\right]_{V,\ A-b} + R \ln \frac{Q_3}{Q_2} \qquad (39)$$

But

$$\frac{Q_3}{Q_2} = \frac{(2\pi mkT)^{3/2} V}{h^3} \cdot \frac{h^2}{(2\pi mkT)\ (A-b)} \qquad (40)$$

Or,

$$\ln \frac{Q_3}{Q_2} = \tfrac{1}{2} \ln (2\pi mkT) + \ln V - \ln h\ (A-b) \qquad (41)$$

on substitution in (40),

$$S_g - S_s = RT\ \left[\frac{\partial}{\partial T}\ (\tfrac{1}{2})\ \ln\ (2\pi mkT)\right] + RT\ \ \frac{\partial}{\partial T}\ (\ln V - \ln h\ (A-b))$$
$$+ R\ [\tfrac{1}{2} \ln (2\pi mkT) + \ln V - \ln h\ (A-b)] \qquad (42)$$

$$S_g - S_s = R/2 + R/2 \ln (2\pi mkT) + R \ln V/h (A-b) \quad (43)$$

According to Young and Crowell[33]

$$S_s = \bar{S}_s + \frac{R}{1+\Gamma b} \quad (44)$$

where $\bar{S}_s$ is the differential molar entropy and Γ is the surface concentration i.e. the number of moles of adsorbed gas per unit surface area of adsorbent.

Equation (44) can also be written as

$$S_s = \bar{S}_s + \frac{R}{1-\theta} \quad (45)$$

since

$$\Gamma b = \theta$$

On substitution in (43) we get,

$$S_g - \bar{S}_s = \frac{R}{2} + \frac{R}{2} \ln (2\pi mkT) + R \ln \frac{V}{h(A-b)} + \frac{R}{1-\theta} \quad (46)$$

from the ideal gas law, PV=RT; at the standard condition of one atmosphere pressure V=RT or,

$$R \ln V = R \ln RT$$

Therefore,

$$S_g^o - \bar{S}_s = \frac{R}{2} + \frac{R}{2} \ln (2\pi mkT) + R \ln \frac{RT}{h(A-b)} + \frac{R}{1-\theta} \quad (47)$$

where S_g^o denotes the entropy of the gas at standard conditions.

By definition, $b = A\theta$

$$b/A = \theta$$

$$\frac{A-b}{A} = 1-b/A = 1-\theta$$

$$A-b = (1-\theta)\cdot b/\theta \qquad (48)$$

$$\therefore \quad \ln (A-b) = \ln b - \ln \frac{\theta}{1-\theta} \qquad (49)$$

From equation (49) and (47) we obtain,

$$S_g^o - \bar{S}_s = \frac{R}{2} + \frac{R}{2} \ln (2\pi mkT) + R \ln RT - R \ln b\, h + R \ln \frac{\theta}{1-\theta} + \frac{R}{1-\theta} \qquad (50)$$

$$S_g^o - \bar{S}_s = \frac{R}{2} \ln (2\pi mk) + \frac{3}{2} R \ln T + R \ln \frac{R\theta}{h\, b\, (1-\theta)} + \frac{R}{1-\theta} + \frac{R}{2} \qquad (51)$$

From the equation (51) the theoretical entropy $\bar{S}_s$ of the two dimensional gas has been calculated for trichlorofluromethane and is listed in Table (11). The plot of these entropies versus θ is given in Figure (54). The curve has been plotted (with solid line) along with the experimental differential entropy plots in Figures 47 to 52 (Section 10.00).

5.60 Selection of the model:

If the assumption that the entropy loss during adsorption is mainly translational is valid, then the superimposition of Figure 54 on the experimental plots of differential entropy versus θ should be satisfactory. Neglecting weak vibrations perpendicular to the surface the comparison is good up to θ=0.5 in most cases. After this coverage the experimental entropies fall off as in the theoretical calculations. No account was taken of the adsorbate-adsorbate interactions. Where the translational or rotational freedom is restricted, the experimental entropy is found to be less than the theoretical value. The inference one gets out of these comparisons is that the adsorbate phase is better described by a mobile model rather than a localized model, particularly at low coverages.

The isosteric heat of adsorption at zero coverage should thus represent an average value for the entire surface in the absence of adsorbate-adsorbate interactions. The q_{st} (θ=0) has been obtained by extrapolation to θ=0 using the data below θ=0.5. These values are tabulated in Appendix B (Tables 17 and 18). The isosteric heat of adsorption at zero coverage should represent the average q_{st} for the high energy sites of the bare surface in the absence of adsorbate-adsorbate interactions.

5.70 Effect of annealing on surface area:

The thermal decomposition of various metal sulphates has been studied in inert atmospheres [180-184] and at low pressures [185,186]. As previously described (section 4.34) the preparation of the adsorbents involved dehydration at temperatures up to 400° either in vacuum or in argon atmosphere. The particular conditions used for each adsorbent ensured that decomposition of the anhydrous salts was prevented.

Slight apparent weight changes observed up to 400°C may be due to loss of chemisorbed water. Relatively greater weight changes of the $CoSO_4$ sample between 200 and 300°C correspond to about one mole of water. This probably accounts for the increase in surface area for this sample between 200 and 300°, in contrast to most of the other adsorbents which generally show a decrease in surface area as the annealing temperature is increased (Figure 62). Heat of adsorption q_{st} (θ) curves also clearly indicate different behaviour for the $CoSO_4$ (200) surface. Similar behaviour was also shown when nickel sulphate was heated to 400°C from 300°C.

As can be seen from Figure 62, the trend to decreasing surface area with increased annealing temperature is, apart from the above exception, quite uniform. The curves have been extrapolated to zero surface area. The annealing temperature corresponding to zero surface area on plotting against the melting point or decomposition point [215] (Figure 63) of the adsorbent (manganese sulphate through zinc sulphate) yield a straight line. The behaviour may be explained as being due to greater mobility of the ions at elevated temperature approaching the melting point. Calcium sulphate does not fall in the straight line probably because of its very high melting point.

6.0 DISCUSSION OF CRYSTAL FIELD EFFECTS

6.10 Crystal field effect and physical adsorption

- 6.11 The crystal field effect (CFE)
- 6.12 The CFE and surface energy
- 6.13 The CFE on adsorptive properties
- 6.14 The CFE on isosteric heats

6.20 Determination of excess heats

6.30 Calculation of crystal field stabilization energy (CFSE)

6.40 Surface structures and CFSE

- 6.41 Cobalt sulphate
- 6.42 Nickel sulphate
- 6.43 Copper sulphate
- 6.44 Effect of annealing and surface structures

6.50 Importance of surface structure studies

6.60 Conclusions

6.10 Crystal field effect and physical adsorption:

The study of physical adsorption at gas-solid interfaces is important in various fields such as chemisorption, catalysis, corrosion, dissolution and heterogeneous chemical reactions, as at some stage physical adsorption of a gas on a solid surface is involved.

It is well known that the method of preparation or pretreatment has a great effect on the nature of the surface produced. Certain types of crystal faces, due to geometric factors, have greater or lesser catalytic activity. Thus, a knowledge of surface structure is very important in catalysis and adsorption as well as for studying crystal growth, sintering, adhesion and mechanical strength. The surface structure of a solid may also be modified significantly by the presence of adsorbed substances. For transition metal salts with partially filled orbitals, the crystal field effects have an important role to play in the modification of surface structures.

6.11 The crystal field effect:

The cation in a transion metal salt or a complex experiences an electrostatic field due to surrounding ligands. In hydrated ions of the transition metals $M(H_2O)_6^{2+}$, the metal ion is surrounded octahedrally by six water molecules with the negative end of the water dipole nearest to the cation. The anhydrous metal sulphates of cobalt, nickel and copper have an orthorhombic crystal structure with the metal ions coordinated by oxygens from ions arranged in a

slightly distorted octahedron about the metal ion. Many authors have studied the crystal structures of the anhydrous sulphates as referred to in Section 4.34. Three theories have been used to account for the properties of the complexes of transition metals: molecular orbital[187], Valence bond[188] and the crystal field theory[18].

Crystal field theory provides a relatively simple model for the discussion of absorption spectra and electric and magnetic properties of the salts and complexes. This theory is described below. The five degenerate 3d orbitals of the cations of the transition elements have directional properties. When the cations are placed in an electric field, the 3d orbitals lose the degeneracy. Hush[189] has discussed the effect of crystal field stabilization on interatomic separations for crystals containing ions of the transition elements with partially filled d shells. For such ions, Stark splitting of electronic levels of the central ion results in an additional stabilization energy. The essential physical idea of the crystal field theory is that the electrons of a central ion avoid those regions where the field due to the attached negative ions and dipoles is largest. This tendency results in the removal of the degeneracy of the ground state of certain transition metal ions. It can be easily demonstrated that the d orbitals of the central ion, in an octahedral crystal field, are all affected, the d_{z^2} and $d_{x^2-y^2}$ orbitals more so than the d_{xy}, d_{yz} and d_{xz} orbitals. In a tetrahedral crystal field the d_{xy}, d_{yz} and d_{xz} orbitals are more affected than d_{z^2} and $d_{x^2-y^2}$. Similarly for a trigonal field the splitting produces two sets of doubly degenerate orbitals and a single orbital. Figure 64 shows the splitting of the five d orbitals in various symmetries of the crystal field.

Crystal field splitting in octahedral field:

When a transition metal ion is coordinated with six identical ligands situated on the cartesian axes as shown in Figure 65A, the electrons in all five d orbitals are repelled by the negatively charged ligands and the baricentre of the degenerate energy levels is raised. As shown in the Figure 65B, the lobes of the e_g orbitals ($d_{x^2-y^2}$ and d_{z^2}) point towards the ligands. Electrons in these orbitals are repelled to a greater extent than those in the t_{2g} orbitals (d_{xy}, d_{yz} and d_{xz}), the lobes of which point between the ligands. This results in an energy separation between the t_{2g} and e_g orbital energy levels and is termed the crystal field splitting and is denoted by Δ_o. An important rule regarding the splitting of these levels is that their centre of gravity in energy is not affected by the perturbation.* That is,

$$3\,E_{t_{2g}} + 2\,E_{e_g} = 0 \qquad (52)$$

Each electron in a t_{2g} orbital stabilizes a transition metal ion by $2/5\,\Delta_o$. The energy scale is considered in such a way that the energy is zero at the ground state of the free ion at the baricentre and 10 Dq is defined as the energy difference between the two levels after the degeneracy is removed[190]. This resultant net stabilization energy is known as crystal field stabilization energy (CFSE).

The crystal field splitting in coordinations other than octahedral symmetry can be determined by electrostatic arguments and

---

* This rule is applicable for the salts used in this study; however, this rule does not apply if the spin-orbit or configurational interactions become significant, especially in high crystal fields[18].

by group theory relative to octahedral coordination. For example the crystal field splitting in the case of tetrahedral coordination is given by [191],

$$\Delta_t = -4/9\ \Delta_o \qquad (53)$$

The distribution of d electrons utilize another rule, apart from Hund's rule of parallel spins, that the electrons will favour orbitals with the lowest energy. This leads to high spin or low spin configurations in certain transition metal ions. The strength of the field due to particular ligands decides the configuration. Sulphate ion which coordinates through oxygen might be expected to favour high spin complexes, as does water. The distinction between these two states can be assessed by magnetic susceptibility and by interatomic distances. A series which contains the ligands in order of increasing crystal field splitting (Δ) is known as a spectrochemical series. Various factors which affect the Δ_o values are discussed by Orgel [191] and Burns [192]. If the ground state or lowest energy level of the molecule is degenerate, it will distort spontaneously to remove the degeneracy. This effect is known as Jahn-Teller effect [191] and gives further stabilization to the configuration.

An approximate value is given for crystal field stabilization energy (CFSE), 10 Dq, by perturbation calculations [193,194];

$$10\ Dq = \frac{5\ e\ q\ r^4}{3R^5} \qquad (54)$$

where e is the charge on the electron,

q is the charge of one ligand,

r is the mean value of the radius of d orbital,

and R is the distance between the transition metal and surrounding ligands.

6.12 The crystal field effect and surface energy:

The crystal field decreases the electronic energy of the ion in a crystal relative to that of the gaseous ion. This change in the electronic energy decreases the potential energy of the crystal and this results in the relaxation of the surface ions[195]. On cleaving a crystal of NiO along a (001) plane, the surface energy change can be calculated following Dunning[17].

A cation in a site on the (001) face of a NiO surface is surrounded by five negative ions disposed at the corners of a square pyramid. When the relaxation of surface ions occurs, the metal ions move (relatively) towards the center of gravity of the pyramid and the symmetry of the electrostatic field would then still be that of a tetragonal pyramid. In this field, three degenerate orbitals would be split up. With the weak field approximation[191], the resultant electronic energy of the ion in the (001) face will be different than that of the ion in an octahedral environment. The CFSE in the two symmetries can be calculated by using the energy levels given by Dunn, Mclure and Pearson[18].

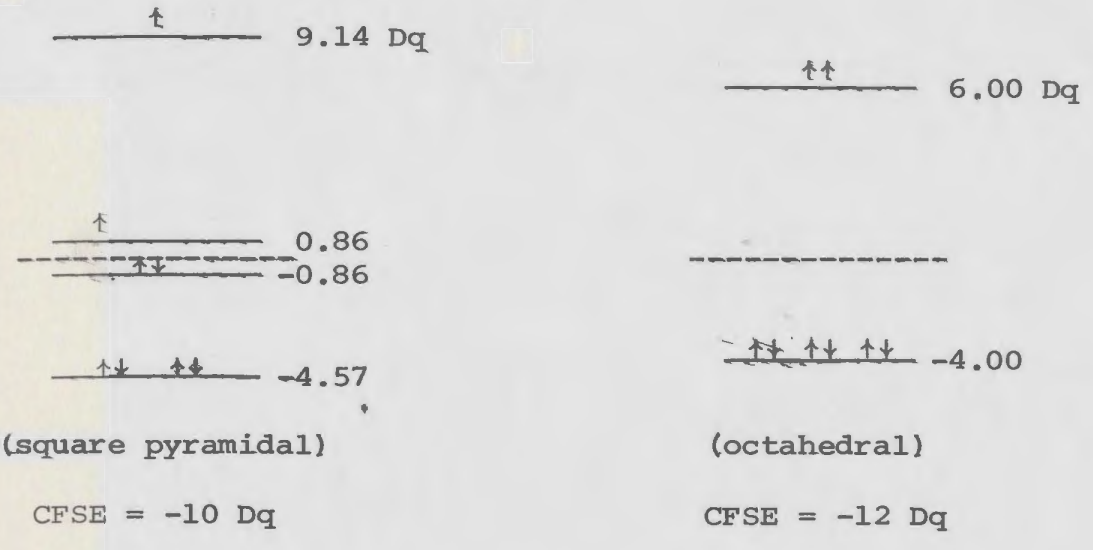

(square pyramidal)

CFSE = -10 Dq

(octahedral)

CFSE = -12 Dq

The nickel (II) ion has eight electrons in the 3d shell. When these are assigned to various levels, keeping a maximum number of parallel spins (the weak field approximation), there are two unpaired electrons in each of doubly degenerate orbitals. The electronic energy of the nickel ion in the crystal is 12 Dq less relative to that of the gaseous ion.

Thus on cleaving a crystal along (001) plane, cations in the new surfaces have electronic energies that are higher by 2 Dq compared with the electronic energies of those in the interior. The surface potential energy is increased by 2 Dq/$2a_o^2$ per unit area and assuming a value of 4600 cal/mole for this amounts to about 370 ergs/cm^2 [17]. Despite the assumptions involved in these calculations, it can be concluded that the crystal field splitting may, in many cases, make a substantial contribution to the surface energy. Furthermore, Dunning[196] has calculated the line energy of 01 step on a (001)

surface of NiO. His results indicate that the change in CFSE resulting due to change in surface structure is enough to form a kink on a step. Kollrack[197] calculated a CFSE as high as 70 K. Cal/mole for certain geometric arrangements of the transition metal oxides.

Morrin[198] has used crystal field effects to explain the conduction mechanism in transition metal oxides. Houten[199] has explained conduction in NiO by utilizing the difference in crystal field stabilization between Ni^{+}, Ni^{2+} and Ni^{3+} ions. Eggerton and Stone[200] have considered crystal field stabilization as one of the factors in determining the site preference of cations in zeolite Y.

6.13 Crystal field effects on adsorptive properties:

Kollrack[197] has shown that the crystal field affects the metal ion and also the chemisorbed reactant. Klier[201] has incorporated the concept of crystal field stabilization in a discussion of the activity of various transition metal oxide catalysts for oxidation reduction reactions. According to Dowden[202] and coworkers[9,11] the rate controlling steps in certain chemisorption and catalytic reactions which involve highly polarized species may contribute to higher energies of activation and lower activities on the cation electron configurations d^{0}, d^{5} and d^{10}, which are the configurations possessing zero stabilization energy. A twin peaked CFSE pattern, is found for the activity of hydrogen exchange reactions

$$H_2 + D_2 \rightleftharpoons 2HD$$

as a function of the number of electrons in the d orbitals of the first

transition series. The maxima was found between d^0 and d^5, and d^{10} and d^{10} configurations and minima at d^0, d^5 and d^{10} configurations.

Harrison et al[203] have studied the hydrogenation of ethylene over oxides of the 3d transition metals. They also found a twin peaked activity pattern as described by Dowden et al[9,11] for hydrogen-deuterium exchange reaction. Dixon et al[204] noted similar behaviour for the disproportionation of cyclohexane to benzene catalyzed by the same oxides. Two peaks of activity were found, the first at Cr_2O_3 ($Cr^{3+} = 3d^3$) and the second at Co_3O_4 ($Co^{3+} = 3d^6$; $Co^{2+} = 3d^7$). These two peaks of activity were separated by those oxides whose cations possess the stable $3d^5$ configuration (MnO, Fe_2O_3).

The models of Haber and Stone[205] depict clearly, as seen from Figure 66, the effect of CFSE and adsorption of oxide ions (O^{2-}) on the three principal planes (100), (110) and (111) of a NiO crystal. On cleavage, the surface may relax in such a way that the nickel ion enters the pyramid as shown to the left in the Figure 66 A. Oxygen ions also move but it is simpler to show the relative movement of the nickel ion only. Chemisorption of an oxygen ion completes the octahedron about the nickel ion as shown to the right in Figure 66 A. The change in CFSE is deduced by the change from square pyramidal to octahedral configuration. Table 12 shows the CFSE changes due to chemisorption of oxygen on different planes of nickel oxide.

The CFSE is largest for the (110) plane and this plane should be preferentially covered. Haber and Stone[205] desorbed the chemisorbed oxygen by illuminating the surface of the oxide with light of an appropriate wavelength. They suggested a model to explain the structural change after observing the desorption of oxygen as a function of the wavelength of the incident light. According to this model a surface nickel ion forms an octahedral complex after adsorbing two oxygen atoms and when irradiated, these two oxygen atoms are desorbed as an oxygen molecule and the configuration returns to the tetrahedral state when irradiated with the wavelength corresponding to the transition $^3A_{2g} \rightarrow {}^3T_{1g}$.

Cimino et al[1] have studied the decomposition of N_2O on NiO on the basis of localized interactions. They suggested that reversibly adsorbed oxygen, which correlates with the catalytic activity, is present as O^-. The strongly adsorbed oxygen is present as O^{2-} which acts as a poison in this process. O^- can be formed preferentially on (110) planes as a result of decomposition of N_2O molecules. Desorption of this oxygen is relatively easy permitting further decomposition of N_2O. The mechanism suggested for this process is also based on the transition from tetrahedral to octahedral symmetry on adsorption of two oxygen atoms on this plane. The difference between the models of Haber and Stone[205] and that of Cimino et al[1] are that the central metal ion is trivalent in Cimino's model instead of divalent and the oxygen ions are singly charged. The oxygen is doubly charged in the model of Haber and Stone. The preferential adsorption on the (110) plane at low

coverage can be similarly explained using the model proposed by Cimino.

It is evident that the anomalous properties of ions with unfilled d orbitals affect their surface chemistry. The relationships between coordination chemistry, solid state chemistry and surface chemistry reviewed so far suggest that crystal field effects should influence the adsorptive properties of appropriate solids.

6.14 The crystal field effect on the isosteric heat of adsorption:

It is well known that the CFSE contributes to heats of hydration and heats of ligation. CFSE also shows up in other thermodynamic properties such as lattice energies and stability constants. The effect on chemisorption and adsorptive properties has been discussed in previous sections. The heat of adsorption of an adsorbed molecule should also be similarly increased by the crystal field. This effect on heat of chemisorption has been discussed by Dowden[202]. Machin[22] has found that the heat of adsorption of $CFCl_3$ at zero coverage is related to the adsorbent CFSE; the adsorbent having the greatest CFSE showed the largest heats of adsorption.

Isosteric heats extrapolated to zero coverage $q_{st}(0)$ represent the heat of adsorption without any mutual interactions between adsorbed molecules (see section 5.60).

6.20 Excess heat of adsorption:

The $q_{st}(\theta=0)$ values for the surfaces annealed at 200°C were plotted as a function of atomic number of the cations. A straight line was drawn joining $q_{st}(0)$ of Mn^{+2} and Zn^{2+} both of which have zero CFSE. The perpendicular distance from this line to the $q_{st}(0)$ points of Co^{2+}, Ni^{2+} and Cu^{2+} are defined as the excess heat of adsorption. The same method was used to calculate the excess heats of adsorption on the surfaces of cobalt, nickel and copper sulphates annealed at higher temperatures. These plots are shown in Figure 55-58 and the values of the excess heats of adsorption are included in Table (16). The excess heat of adsorption will be correlated with CFSE in determining the surface structures.

Excess heat of solution:

A similar procedure was followed for the calculation of the excess heats of solution which are shown in Figures 59-61 and values included in Table (13).

6.30 Calculation of CFSE:

The following cycle[22] was used to derive the CFSE of adsorbents from the measured heats of solution:

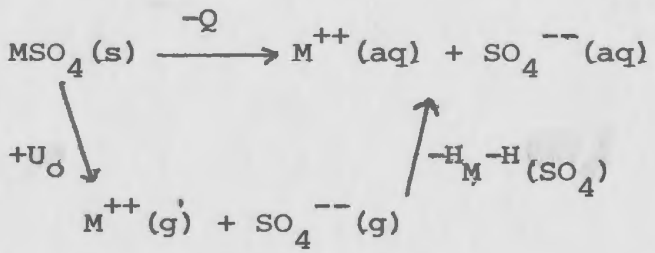

where,

Q = heat of solution,

U_o = lattice energy of the solid,

and ΔH_M and $\Delta H_{(SO_4)}$ = heats of hydration of the gaseous ions.

We derive from the energy balance

$$-Q = U_o - \Delta H_M - \Delta H_{(SO_4)} \qquad (56)$$

Both U_o and ΔH_M for transition metal ions have CFSE contributions such that,

$$U_o = U'_o + X \quad , \qquad (57)$$

and

$$-\Delta H_M = -\Delta H'_M - S \quad , \qquad (58)$$

where X is the CFSE in the solid anhydride and S is the CFSE in the aqueous solution. Hence,

$$U'_o - \Delta H'_M - \Delta H_{(SO_4)} + (X-S) = -Q \qquad (59)$$

Since manganese (II) and zinc (II) have zero CFSE in the solid and in solution, and since it is generally assumed that the properties which are not dependent on crystal field effects vary linearly or nearly so with the atomic number, we may obtain the quantity (X-S), as the difference between the experimental heat of solution and the heat of solution derived from a linear interpolation between the $MnSO_4$ and $ZnSO_4$. The quantity S has been calculated from the reported spectroscopic values[191]. The magnitude of the difference between S and X-S gives the value of the adsorbent CFSE X. These values are tabulated in Table 13.

To obtain the value of unit Dq, the CFSE X as obtained above is compared with the CFSE calculated from the energy levels[18] of the octahedral structure of the adsorbent. For example, Co (II) has seven electrons in its d orbits as shown below:

e_g $\underline{\uparrow\ \uparrow}$ 6 Dq

t_{2g} $\underline{\uparrow\downarrow\ \uparrow\downarrow\ \uparrow}$ -4 Dq

(High spin octahedral structure of Co II)

CFSE = (2x6) - (5x4)

= -8 Dq

For $CoSO_4$(200) CFSE (X) = 17.11 kCal/mole from Table 13 (this is also a negative quantity).

On comparing we get,

8 Dq = 17.11 or Dq = 2.14 kcal/mole

The Dq values so calculated are included in Table 13 for each adsorbent.

6.40 Surface structures and CFSE:

The crystal structures (bulk structures) of the adsorbents have already been discussed in sections 4.34 and 6.11.

The cations in $MnSO_4$, $CoSO_4$, $CuSO_4$ and $ZnSO_4$ are surrounded by six oxygens from six sulphate ions coordinated to the metal ion in octahedral symmetry. However the octahedra may terminate at the surface in a number of different ways depending on the surface energy and other factors such as lattice defects, effect of impurities, the rate and conditions of dehydration of salts.

If conditions are such that one surface plane is preferred during sample preparation, a layer type or a parallel plate type of structure might result. This has been suggested for nickel sulphate[206] and the sensitivity of surface CFSE to the type of crystal face exposed should be an important factor in determining the dominant crystal faces in all of the adsorbents considered here. Figure 29 shows the isotherm of $CuSO_4$ (200) which has a shape similar to that of the $NiSO_4$ isotherm, obtained by Kinloch and Machin[206].

Annealing of the sample would be expected to make the proportion of the preferred plane higher at the surface, giving a more stable surface structure. The large pores resulting from the loss of water during dehydration would, however, leave a very rough surface, giving rise to many possibilities of surface structures.

Dunning[196] has considered various symmetry coordinations for surfaces having steps, kinks, etc. Wells[207] has recently investigated some aspects of the geometry of octahedrons meeting at a point for rutile and corundum structures. Considering similar ideas, and the crystal structure of sulphates, the following possibilities for surface structures seem reasonable. Some of the structures, eg. tetrahedral would involve surface relaxation process, where a very large energy is not involved. We will consider the main possibilities of surface structures as a surface cation may possibly exist in an octahedral environment, one of the ligand sites may be vacant giving a square pyramidal environment, or the octahedron may be cut by a plane giving trigonal, trigonal bipyramidal or tetrahedral structures. The trigonal bipyramidal and tetrahedral structures would be possible as a result of surface relaxation or on edges, kinks and steps of the surfaces.

Preliminary calculations based on unit cell dimensions (Table 14), cation-cation distances in each plane, and the molecular area of the adsorbate molecule, suggest the possibility of half adsorbate molecule per cation to more than one adsorbate molecule per cation. Two adsorbed molecules per cation are possible on rough surfaces with steps, kinks and edges. There is no possibility of more than two adsorbate molecules per cation at the surface as is evident from the calculations considering the experimental monolayer capacity and surface area obtained for different adsorbents. Table 14 contains the results of these calculations for the various planes shown in Figure 67. The various possibilities of surface

structures obtained after adsorption are listed below:

Initial structure	No. of adsorbed molecules	Final structure
Octahedral	one	Hush's seven coordinated structure
Octahedral	one	Pentagonal bipyramidal
Tetrahedral	one	Trigonal bipyramidal
Square pyramidal	one	Octahedral
Trigonal	two	Trigonal bipyramidal
Trigonal bipyramidal	two	Pentagonal bipyramidal
Square planar	one	Square pyramidal

The structures involving very large energy changes have not been considered. Another consideration in choosing a model is that on adsorption a more stable surface structure should be obtained.

The considerations of the initial and final surface structure allows us to estimate the change in crystal field stabilization energy on adsorption. The calculated CFSE's for the various models will be compared with the experimental value of ΔCFSE derived from heats of adsorption (section 6.20).

The energy levels and the symmetry notation were used as given by Dunn et al[18] and by Orgel[191]. The notation (200), (300), (400) or (500) written after the chemical formula of the adsorbent indicates the temperature in degrees centigrade at which the corresponding adsorbent was annealed before taking the adsorption measurements.

6.41 Cobalt Sulphate:

Cobalt II has seven d electrons. Energy level diagrams for the 3d orbitals in various ligand symmetries are shown below:

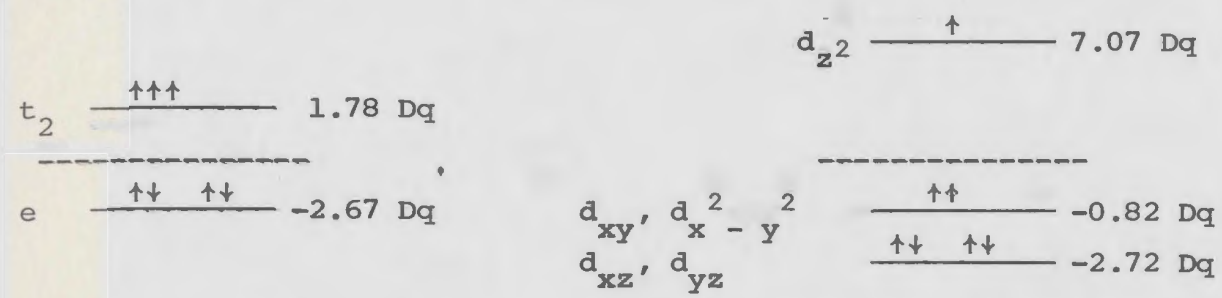

(Tetrahedral)

CFSE = (3x1.78) - (4x2.67)

= -5.34 Dq

(Trigonal bipyramidal)

CFSE = 7.07 - (2x0.82) - (2x2.72)

= -5.45 Dq

The trigonal bipyramidal structure is more stable than the tetrahedral structure by 0.11 Dq. The value of unit Dq value has already been calculated in section 6.40 and listed in Table 13.

The stabilization energy of 0.11 Dq due to adsorption on tetrahedral Co(II), giving trigonal bipyramidal structure can be expressed in kcal/mole units by substituting the unit Dq value.

for $CoSO_4$ (200): 0.11 x 2.14 = 0.24 kcal/mole,

for $CoSO_4$ (300): 0.11 x 2.70 = 0.30 kcal/mole,

and for $CoSO_4$ (400): 0.11 x 2.28 = 0.25 kcal/mole.

On comparing with the CFSE obtained from heat of adsorption (the excess heat of adsorption given in Table 16 for various surfaces of cobalt sulphate, only $CoSO_4$ (200) surface matches this model: 0.30 kcal/mole (experimental) against 0.24 kcal/mole

(calculated). The excess heat of adsorption for $CoSO_4$ (300) and $CoSO_4$ (400) are higher than the values calculated according to this particular model. Further models considered are octahedral, pentagonal bipyramidal and Hush's intermediate. The crystal field stabilization energy for these models are;

Octahedral	:	-8 Dq
Pentagonal bipyramidal	:	-10.55 Dq
Hush's intermediate	:	-8.69 Dq

Considering octahedral going to Hush's intermediate structure on adsorption, the gain in stabilization energy is 0.69 Dq and on going to pentagonal bipyramidal the gain in CFSE is 2.55 Dq. Substituting the unit Dq value from Table 13 for the various adsorbents we get,

	Octahedral ⟶ Hush's intermediate	
$CoSO_4$ (200):	0.69 x 2.14 = 1.48	kcal/mole
$CoSO_4$ (300):	0.69 x 2.70 = 1.86	kcal/mole
$CoSO_4$ (400):	0.69 x 2.28 = 1.57	kcal/mole
	Octahedral ⟶ Pentagonal bipyramidal	
$CoSO_4$ (200):	2.55 x 2.14 = 5.46	kcal/mole
$CoSO_4$ (300):	2.55 x 2.70 = 6.89	kcal/mole
$CoSO_4$ (400):	2.55 x 2.28 = 5.81	kcal/mole

The octahedral structure yielding Hush's intermediate seems to be closest for $CoSO_4$ (300) and $CoSO_4$ (400) as the CFSE (calculated) values are much higher for the model (octahedral Pentagonal bipyramidal). However, there is possibility of a mixture of some sites with pentagonal bipyramidal structure of cation environment. This will be further discussed when considering the annealing effect in section 6.44.

Considering a square planar surface model yielding square pyramidal structure on adsorption the following values of crystal field stabilization energy are obtained:

CFSE for square planar structure : -10.28 Dq

CFSE for square pyramidal structure: - 9.14 Dq

One obtains a less stable final structure, by 1.14 Dq. Such a possibility is less likely to be effective. Furthermore such structural change will result in a decreased heat of adsorption. The presence of this sort of site might contribute to the decreasing heat of adsorption as the surface coverage increases. There are other possible structures which can give less stable surface structures on adsorption, some of them have been listed in Table 16.

6.42 Nickel Sulphate:

Three models out of the eight considered yield more stable structure on adsorption. Moreover, the models, tetrahedral →

trigonal bipyramidal, and square pyramidal → octahedral involve high CFSE changes as evident from Table 16. Adsorption on a trigonal bipyramidal site yielding a pentagonal bipyramid is considered below:

CFSE for trigonal bipyramid : -6.27 Dq

CFSE for pentagonal bipyramid: -7.73 Dq

The final structure, pentagonal bipyramidal, which results when two molecules of adsorbate molecules are adsorbed on each cation, is more stable than the trigonal bipyramidal surface by 1.46 Dq. This value is calculated in kcal/mole below for different surfaces:

$NiSO_4$ (200): 1.46 x 2.05 = 2.99 kcal for two moles of adsorbed $CFCl_3$

= 1.50 kcal/mole

$NiSO_4$ (300): 1.46 x 2.13 = 3.11 kcal

= 1.56 kcal/mole

$NiSO_4$ (400): 1.46 x 2.78 = 4.06 kcal

= 2.03 kcal/mole

These values compare reasonably well with the experimental excess heats of adsorption (Table 16).

6.43 Copper Sulphate:

Comparison of the eight models summarized in Table 16 suggests the model of a trigonal environment around the cation changing to a trigonal bipyramidal symmetry on adsorption of two $CFCl_3$ molecules per cation.

The crystal field stabilization energy for a trigonal structure is -5.48 Dq and for trigonal bipyramidal structure is -7.09 Dq. The final structure, trigonal bipyramid, is more stable by 1.61 Dq, which on conversion of units yields,

$CuSO_4$ (200): 1.61 x 3.64 = 5.86 kcal for two moles of $CFCl_3$

= 2.93 kcal/mole

$CuSO_4$ (300): 1.61 x 4.82 = 7.76 kcal for two moles

= 3.88 kcal/mole

$CuSO_4$ (400): 1.61 x 2.86 = 4.61 kcal for two moles

= 2.30 kcal/mole

These values compare reasonably well with the experimental excess heat of adsorption. However, the difference between calculated change of CFSE and excess heat of adsorption for $CuSO_4$ (300) and $CuSO_4$ (400) surfaces may be accounted for if a fraction of surface possessed octahedral (more probably) or tetrahedral symmetry.

6.44 Effect of annealing on surface structures:

Annealing of the surface is expected to yield a more stable

surface structures. The mobility of the ions in the lattice is increased at elevated temperature and thus annealing should give a surface with fewer lattice defects (unless lattice defects are caused by impurities) and more stabilized surface structures.

Cobalt sulphate surface structure is discussed in section 6.41. $CoSO_4$ (200) is found to have a tetrahedral environment of ligands around the cations which changes on annealing at 300°C to an octahedral structure and which remains octahedral on annealing at higher temperatures up to 500°C. This change between the (200) & (300) surface structures may have been caused by the removal of water. The structures for $CoSO_4$ (500) could not be measured. However when the $q_{st}(o)$ for $ZnSO_4$ (200), (300) and (400) surfaces were plotted against the annealing temperatures a straight line was obtained which when extrapolated yielded a q_{st} (o) at 500°C of 2.53 kcal/mole. The excess heat of adsorption for $CoSO_4$ (400) is 2.75 kcal/mole. These excess heats of adsorption values for the (400) and (500) surfaces are higher than the calculated CFSE of 1.57 kcal/mole for $CoSO_4$ (400). This difference suggests that annealing at higher temperatures yields surface structures which have a tendency to go to more stable (pentagonal bipyramidal) structure on adsorption. Probably, by this argument, it is expected that annealing at still higher temperatures will finally yield surface structures close to the model,

Octahedral → Pentagonal bipyramidal

Most of the nickel sulphate surface seems to agree with the model trigonal bipyramidal going to pentagonal bipyramidal structure on adsorption. However the annealing effect seems to favour formation of the square pyramidal or tetrahedral sites on the stabilized surface which give larger experimental excess heats of adsorption. The extrapolation technique as discussed for $CoSO_4$ (500), yielded an excess q_{st} (o) for $NiSO_4$ (500) of 3.37 kcal/mole, consistent with the above argument. Annealing at still higher temperatures is expected to yield more stable surface structures close to the model square pyramidal → octahedral. The probability of the tetrahedral going to trigonal bipyramidal on adsorption is not ruled out. However, intitutively, this seems less likely in view of the bulk crystal structures.

The calculated CFSE's for copper sulphate (200) and (300) surfaces for the model trigonal → trigonal bipyramidal, are a bit higher than the experimental excess q_{st} (o).

Such a difference may be due to the presence of octahedral cation sites on the surface. On annealing to 400°C the calculated CFSE is decreased indicating the disappearance of such sites while annealing at 400°C. The (500°C) surface yields an excess q_{st} (o) of 2.95 kcal/mole by the extrapolation (as used for $CoSO_4$ (500)). This suggests that the surface is very sensitive to the presence of traces of chemisorbed water. However, these results indicate that the most likely model for the stable surface of $CuSO_4$ is the trigonal → trigonal bipyramidal one.

6.50 Importance of surface structure studies:

Recently Cimino, Pepe and Schiavello[208] have given a good account of the effect of symmetry of the cation at the surface on the catalytic activity of oxide solid solutions. They found that the catalytic activity of Cu^{2+} ions in tetrahedral symmetry is very low. Cobalt(II) ions and nickel(II) ions with octahedral coordination were found to be much more active. The heat treatment was found to increase the occupancy of octahedral sites by Co^{2+} and decrease the occupancy of octahedral sites by Ni^{2+}. The effect due to surface defects was not significant. The explanation for lower activity with tetrahedral structure is given by them as being due to the shorter bond lengths in tetrahedral symmetry. These bonds are stronger and more difficult to cleave. Dunning[196] explained the effect of symmetry on the catalytic activity as being due to the availability of cations near the surface or deeper in the interior depending upon the specific symmetry.

Dunning[196] has also demonstrated how different ligand symmetries around surface cations eg. a cation lying on edges, steps or kinks of a particular plane can affect catalytic activity. Erofeeve[209] et al have explained that the symmetry of the cation decides the stability of the intermediate complex formed during catalytic process. They compared their results of symmetry considerations and activity with the multiplet theory and found that both have their origin in the crystal field theory and are related.

Studies of acidity and catalytic activity of $NiSO_4$ and $CuSO_4$ have been carried out[2,3,4,114]. Tanabe and coworkers[5] studied the problem using X-ray and N.M.R. analysis and found the relation between structures of acid sites based on coordination symmetry and catalytic activity. Bendor and Margalith[108] have explained the acid properties of the monohydrates of $NiSO_4$ on the basis of the special linkage of the water molecule to the central metal ion. Wade et al[210] have found during their microcalorimetric estimation of surface acidity of hydrated $NiSO_4$ that the heat of immersion for the adsorbent differed in two ligands pyridine and 2,6-dimethylpyridine, having similar base strength. This difference may have arisen from CFSE differences due to different symmetries.

6.60 Conclusions:

The quantitative understanding of all the forces involved in physical adsorption is not yet possible. From the general quantum mechanical point of view physical adsorption, chemisorption, heterogeneous catalysis and homogeneous catalysis are all particular cases of the overall problem of intermolecular interactions. Although it is possible to make approximate estimations of adsorption energies, for very simple cases, on the basis of general theory of intermolecular forces[19,211,212], in most real cases nonadditivity of interactions, heterogeneity complications, uncertain crystal structures and more uncertain surface structures make inferences uncertain. Direct experimentation still remains the most useful means of our knowledge of adsorption phenomena.

Many powerful techniques such as LEED have been applied to studies of the surfaces of single crystals. However, polycrystalline substances are most commonly used as catalysts. Physical adsorption measurements allow us to probe the surfaces in the form in which they are used and generally it is possible to closely reproduce the actual environment which the adsorbent may meet during a catalytic process. The thermodynamic approaches coupled with band theory, crystal field theory and the general principles of organic and inorganic chemistry can give insight into the possible properties of the transition complex formed at

the surface. An attempt has been made in this work to utilize crystal field theory in assessing surface structures and it is found that the physical adsorption measurements can be used as a suitable tool, in simpler manner than other more powerful physical methods, for determining the surface structures.

There is a need to couple infrared, magnetic susceptibility and differential thermal analysis studies along with the adsorption studies, preferably in situ. These should enable one to quantitatively assess the proportion of sites having different surface structures and the number of adsorbate molecules per cation on the surface under any set of experimental conditions.

7.00

References

1. A. Cimino, M. Schiavello and F.S. Stone; Discussions Faraday Soc., 41, 350 (1966).

2. K. Tanabe and A. Aramata; J. Res. Inst. Catal., Hokkaido Univ., 8, 43 (1960).

3. K. Tanabe and R. Ohnishi; Ibid, 10, 229 (1962).

4. Y. Watanabe and K. Tanabe Ibid, 12, 56 (1964).

5. T. Takeshita, R. Ohinishi, T. Matsui and K. Tanabe; J. Phys. Chem., 69, 4077 (1965).

6. W.E. Garner; International Symposium on Reactivity of Solids, 3d, Madrid, 1956, p 73; R.M. Barrer; Ibid, p 127; I.N. Stranski; Ibid, p 657.

7. A. Clark; 'The Theory of Adsorption and Catalysis', Academic Press Inc., New York, N.Y., 1970.

8. N.B. Hannay; 'Solid State Chemistry'. Prentice Hall Inc., Englewood Cliffs, N.J., 1967.

9. D.A. Dowden and D. Wells; Actes 2^{e} Congr. Intern. Catalyse Technip, Paris, 1961, p 1499.

10. K.S. De, M.J. Rossister and F.S. Stone; Proceedings of International Congress on Catalysis, 3rd, Amsterdam, 1964, 1, 512 (1965).

11. D.A. Dowden, N. McKenzie and B.M.W. Trapnell; Proc. Roy. Soc. London, A. 237, 245 (1956).

12. P.C. Richardson and D.R. Rossington; J. Catalysis, 14, 175 (1969).

13. H. Bethe; Ann. Physik, 3, 133 (1929).

14. J.H. Van Vleck; 'The Theory of Electric and Paramagnetic Susceptibilities', Oxford Univ. Press, London, 1932.

15. J. Haber and F.S. Stone; Proc. Chem. Soc. London, 424 (1961).

16. R. Jogenpier and G.C.A. Schuit; J. Catalysis, 3, 464 (1964).

17. W.J. Dunning; 'The Solid Gas Interface' 1, Marcel Dekker Inc., New York, N.Y., Ed. E.A. Flood, 1967.

18. T.M. Dunn, D.S. Mclure and R.G. Pearson; 'Some Aspects of Crystal Field Theory', Harper and Row, Publishers, New York, N.Y., 1965.

19. M.M. Dubinnin, B.P. Bering and V.V. Serpenskii; Recent prog. Surface Sci., Vol. 2, Academic Press Inc., New York, N.Y., 1964, p 1.

20. H. Margenau; Rev. Mod. Phys., 11, 1 (1939).

21. J.P. Hobson; Crit. Rev. Solid State Sci., 4, 221 (1974).

22. W.D. Machin; Trans. Faraday Soc., 65, 529 (1969).

23. B.N. Figgis; 'Introduction to Ligand Fields', John Wiley and Sons, Inc., New York, N.Y., 1966.

24. A.H. Kamel, Z. Swires, H. Khalifa, S.A. Saleh and M. Abdullah; J. Appl. Chem. & Biothech., 22, 591 (1972).

25. A.H. Kamel and M. Abdullah, Ibid, 22, 599 (1972).

26. A.L. McClellan; 'Tables of Experimental Dipole Moments', Ed. W.H. Freeman & Co., San Francisco, 1963, p 36.

27. W.D. Machin; J. Phys. Chem. 73, 1170 (1969).

28. S.J. Gregg and K.S.W. Sing; 'Adsorption, Surface area and Porosity', Academic Press Inc., New York, N.Y., 1962.

29. Z. Knor; Catalysis Rev., 1, 257 (1967).

30. F.M. Nelsen and F.T. Eggertsen; Anal. Chem., 30, 1387 (1958).

31. R.M. Cahen and J. Marechal, Ibid, 35, 259 (1963).

32. S.K. Ghosh, H.S. Sarkar and N.C. Saha; J. Chromatogr., 74, 171 (1972).

33. D.M. Young and A.D. Crowell; 'Physical Adsorption of gases', Butteworths and Co. Ltd., London, 1962.

34. R.A. Pierotti and H.E. Thomas; Surface & Colloid Science, 4, 93 (1971).

35. S. Ross and J.P. Oliver; 'On Physical Adsorption, Interscience, Inc., New York, N.Y., 1964.

36. J.M. Thomas and W.J. Thomas; 'Introduction to Principles of Heterogenous Catalysis', Academic Press Inc., New York, N.Y., 1967.

37. J.M. Thomas and B.R. Williams, Q. Rev., 19, 231 (1965).

38. A.W. Czanderna; J. Phys. Chem., 68, 27 (1964).

39. L.D. Scheel, C.H. Gorski, R.W. Vest, L.E. Steller, W.C. Tripp and G.P. Gray; Amer. Indust. Huyg. Assoc. J., no. 10, 673 (1971).

40. W.C. Tripp, R.W. Vest and H.C. Graham; VMBT*, 6, 107 (1967), K.M. Laing; Ibid, p 149, C.L. Angell; Ibid, p 77.

41. K.M. Dijkema and Stouthart; VMBT, 7, 79 (1970).

42. W.D. Machin; Ph.D. Thesis, Rensselaer Polytechnic Institute, 1961.

43. A.G. Foster; J. Chem. Soc., 360 (1945).

44. W.D. Machin; Can. J. Chem., 45, 1904 (1967).

45. F.S. Micale and A.C. Zettlemoyer; J. Colloid & Interface Sc., 24, 464 (1967).

46. J.M. Honig; VMBT, 1, 55 (1961).

47. J.W. McBain and A.M. Baker; J. Am. Chem. Soc., 48, 690 (1926).

48. S.L. Madorky; VMBT, 2, 47 (1962).

49. A.J. Anderson and R.F. Horlock; Trans.Faraday.Soc., 58, 1993 (1962).

50. A.W. Czanderna and J.M. Honig; Anal. Chem., 29, 1206 (1957).

51. A.W. Czanderna; VMBT, 4, 159 (1965).

52. A.W. Czanderna; Ibid, p 175.

53. H. Mayer, R. Neidermayer, W. Schroen, D. Stünkel and H. Göhre; VMBT, 3, 75 (1963).

54. E.A. Gulbransen; 'Advances in Catalysis', Vol. 5, Academic Press Inc., New York, N.Y., 1953, p 119.

---

*Note: VMBT stands for Vacuum Microbalance Technique, Plenum Press, New York, N.Y.

55. T.N. Rhodin; Ibid, p 40.

56. J.M. Thomas and B.R. Williams; VMBT, 4, 204 (1965).

57. S.P. Wolsky and E.J. Zdanuk; VMBT, 1, 35 (1961).

58. T. Gast; Chem. Ing. Tech., 29, 262 (1957).

59. R.F. Hampson and R.J. Walker; J. Res. Nat. Bur. Stand., Sect. A, 65, 289 (1961).

60. W.H. King (Jr.); VMBT, 8, 183 (1971).

61. A.W. Warner and C.D. Stockbridge; VMBT, 3, 55 (1963).

62. C.D. Stockbridge; VMBT, 5, 193 (1966).

63. A.W. Warner and C.D. Stockbridge; VMBT, 2, 71 (1962).

64. Y.C. Chiu; Rev. Sci. Instrum., 41, 639 (1970).

65. R.F. Walker; VMBT, 1, 87 (1961).

66. K.H. Behrandt; VMBT, 1, 69 (1961).

67. E. Robens; VMBT, 8, 73 (1971).

68. J.A. Poulis and J.M. Thomas; J. Sci. Instrum., 40, 95 (1963).

69. O.M. Katz and E.A. Gulbransen; VMBT, 1, 111 (1961).

70. A.W. Czanderna and J.M. Honig; J. Phys. Chem., 63, 620, (1959).

71. A.W. Czanderna; VMBT, 1, 129 (1961).

72. J.M. Thomas and J.A. Poulis; VMBT, 3, 15 (1963).

73. M. Knudsen; Ann. Phys., 31, 205 (1910).

74. C.H. Massen and J.A. Poulis; VMBT, 4, 35 (1965).

75. A.W. Czanderna; VMBT, 4, 57 (1965).

76. J.M. Thomas and J.A. Poulis; VMBT, 5, 1 (1966).

77. J.A. Poulis, C.H. Massen and B. Pelupessy; VMBT, 4, 41 (1965).

78. J.A. Poulis; Appl Sci. Res. A. 14:98 (1965).

79. T. Streensland and K.S. Forland; VMBT, 5, 17 (1966).

80. K.H. Behrndt, C.H. Massen and J.A. Poulis; VMBT, 5, 33 (1966).

81. P.A. Culting; VMBT, 7, 71 (1970).

82. R.A. Pierotti; VMBT, 6, 1 (1967).

83. G. Ehrlich; Adv. Catalysis, 14, 255 (1963).

84. W. Kollen and A.W. Czanderna; VMBT, 7, 145 (1970).

85. T.N. Rhodin; J. Am. Chem. Soc. 72, 4343 (1950).

86. D.A. Cadenhead and N.J. Wagner; J. Phy. Chem., 72, 2775 (1968).

87. J.H. Leck; 'Pressure measurement in Vacuum System', Inst. of Physics & Physical Soc., London, 3 (1964).

88. D.M. Young, R.A. Beebe and H. Biene; Trans. Faraday Soc. 49, 1086 (1953).

89. G. Kinloch; M.Sc. thesis, Memorial University of Newfoundland 1969.

90. M.L. Corrin; J. Phys. Chem., 59, 313 (1953).

91. N.G. Utterback and T. Griffith; Rev. Sci. Instrum., 37, 866 (1966).

92. C. Pierce and B. Ewing; J. Phys. Chem., 71, 3408 (1967).

93. C. Meinke and G. Reich; Vacuum, 13, 579 (1963).

94. P.H. Carr; Vacuum, 14, 37 (1964).

95. E.W. Rothe; J. Vac. Sci. Tech., 1, 66 (1964).

96. A.W. Gardner and E. Glueckauf; Trans. Faraday Soc., 66, 1081 (1970).

97. M.F.C. Ladd and W.H. Lee; J. Phys. Chem., 73, 2033 (1969).

98. B. Malony, J. Bectka and M.J. Ridge; Aust. J. Chem., 24, 449 (1971).

99. B. Malony and M.J. Ridge; Ibid, 21, 1063 (1968).

100. M. Gato, B. Malony and M.J. Ridge; J. Chem. Soc., A, 9 (1966).

101. K. Tanabe and M. Katayama; J. Res. Inst. Catal., 7, 106 (1959).

102. N.I. Savchenko, L.V. Petrova and N. Ya. Novotel'nova; Zh. Prik. Khimii, 46, 2089 (1973), translated by 1974 Consultant's Bureau.

103. A. Betoluzza, B. Righetti and P. Saporetti; Att. Acad. Naz. Lincei, Cl. Sci. Fis. Mat. Natur., Rend. 53, 1 (1973), Chem. Abs. 79, 118882y, (1973).

104. S. Vladir and S. Joroslov; Anal. Chem., 45, 154 (1973).

105. R.W.G. Wyckoff; 'Crystal Structures' Vol. 3, 2nd ed., Interscience Publishers Inc., New York, N.Y., 1951.

106. G.C.H. Cheng and J. Zussman; Acta. Cryst., 16, 757 (1963).

107. G.B. Bokii and L.I. Gorogotskaya; J. Struckl. Chem., 8, 590 (1967).

108. L. Bendor and R. Margalith; Inorg. Chimica Acta. 1, 49 (1967).

109. P.J. Rentzperis; Neues Jalule. Mineral. Monatsh. 211 (1958).

110. J. Coing-Boyat; C.R. Acad. Sci., Paris, 248, 2109 (1959).

111. C.W.F.T. Pistorius; J. Chem. U.A.R., 3, 79 (1960).

112. G. Will; Acta. Cryst., 19, 854 (1965).

113. V.K. Kohler and P. Zäske; Z. Anorg. Allg. Chemie, Bd., 331, 1 (1964).

114. M.C. Ball and L.S. Norwood; J. Chem. Soc. Faraday Trans. 1, 169 (1973).

115. M. Manewa; Monatsh. Chem., 104, 814 (1973).

116. Sara Sarig; Thermochimica Acta, 7, 297 (1973).

117. P.A. Kokkoros and P.J. Rentzeperis; Acta. Cryst., 11, 361 (1958).

118. G. Pannetier and J.M. Bregeault; Bull. Soc. Chim. Fr., 609 (1965).

119. E.L. Simmons and W.W. Wendlandt; Thermochimica Acta., 3, 25 (1971).

120. N. Lendormy; C.R. Acad. Sci. Paris, 253, 1804 (1961).

121. N. Lendormy; Chim. Anal. (Paris), 44, 255 (1962).

122. V.K. Kohler and P. Zäske; Z. Anorg. Allg. Chemie Bd., 331, 7 (1964).

123. N. De'massieux and C. Mallard; C.R. Acad. Sci. Paris, 245, 1429 (1957).

124. J. Guenot, J. M. Manoli and J.M. Bregeault; Bull. Soc. Chim. Fr. 8, 2666 (1969).

125. C.W.F.T. Pistorius; Acta Cryst. 14, 543 (1961).

126. P.J. Rentzeperis; Acta. Cryst., 14, 1305 (1961).

127. J.D. Dunitz; Acta. Cryst. 18, 737 (1965).

127A. J.M. Thomas and G.D. Renshaw; J. Chem. Soc. A, 2077, 2753, 2756 (1969). Three papers.

128. R. Ohinishi, S. Ishikura and K. Tanabe; Nippon Kagakukai, no. 1, 183 (1973).

129. P.I. Dimaras; Acta. Cryst., 10, 313 (1957).

130. R.J. Poljack; Acta. Cryst., 11, 306 (1958).

131. M.L. Smith and B. Topley; Proc. Roy. Soc. A 134, 224 (1931).

132. C.A. Beevers and H. Lipson; Proc. Roy. Soc. A 146, 570 (1934).

133. N.F.H. Bright and W.E. Garner; J. Chem. Soc., 1872 (1934).

134. H.J. Brochardt and D. Farrington; J. Phys. Chem., 61, 917 (1957).

135. J. Paulik, F. Poulik and L. Erdey; Anal. Chim. Acta., 34, 419 (1966).

136. J. Guenot and J.M. Monoli; Bull. Soc. Chim. Fr., 8, 2663 (1969).

137. Z. Halmos and W.W. Wendlandt; Thermochimica acta, 7, 93 (1973).

138. B. Rama Rao; Acta. Cryst., 14, 321 (1961).

139. H.D. Brown; 'Biochemical Microcalorimetry', Academic Press, New York, N.Y., 1969.

140. J.M. Sturtevant; 'Techniques of Chemistry', Vol. 1 (5), Ed. Weissberger and Rossister, Interscience Publishers Inc., 1971, p 347.

141. J.A. Morrison, L.E. Drain and J.S. Dugdale; Can. J. Chem., 30, 890 (1952).

142. L.E. Drain and J.A. Morrison; Trans. Faraday Soc., 48, 316 (1952).

143. L.E. Drain and J.A. Morrison; Ibid, 49, 654 (1953).

144. H.F. Holmes, E.L. Fuller (Jr.) and C.H. Secoy; J. Phys. Chem., 72, 2095 (1968).

145. E.L. Fuller (Jr.), H.F. Holmes, C.H. Secoy and J.E. Stuckey; J. Phys. Chem., 72, 573 (1968).

146. I. Motooka, G. Hashizume and M. Kobayashi; J. Phys. Chem., 73, 3012 (1969).

147. J. Tsau and D.F.R. Gilson; J. Phys. Chem., 72, 4082 (1968).

148. E. Lang; 'The Structure of Electrolyte Solution', Ed. W.J. Hamer, John Wiley and Sons, Inc., New York, N.Y., 1959, Chapter 7.

149. J.M. Readnour and J.W. Cobble; J. Inorg. Chem., 8, 2174 (1969).

150. D.E. Ealough, J.J. Christensen and C.H. Bartholomew; J. Chem. Soc., A. 47 (1969).

151. J.W. Larson; J. Phys. Chem., 74, 3392 (1970).

152. G.R. Hedwig, H. Kipton and J. Powell; J. Chem. Soc. (Dalton), 798 (1973).

153. E.L. Pace; 'The Solid Gas Interface', ed. E.A. Flood, Marcel Dekker Inc., New York, N.Y., 1966, p 105.

154. J.M. Holmes; Ibid, p 127.

155. A.C. Zettlemoyer and K.C. Narayan; Ibid, p 145.

156. S.R. Gunn; J. Phys. (E): Sci. Instrum., 6, 105 (1973).

157. "Handbook of Chemistry and Physics", 54th ed., Chemical Rubber Publishing Co., 1973-74, p D-81.

158. F.D. Rossini, D.D. Wagman and H.E. Williams; 'Selected Values of Chemical thermodynamic properties', National Bureau of Standards (500), Washington, D.C., 1952, p 487.

159. 'Chemistry book of data', Longmans/Penguin Books, 1968.

160. D.J. Curran; J. Chem. Educ., 46, A 465 (1969).

161. L.A. Garden and G.L. Kington; Proc. Roy. Soc., A 234, 24 (1956).

162. L.A. Garden and G.L. Kington; Ibid, A 234, 35 (1956).

163. A.V. Kiselev; Quart. Rev., 99 (1967).

164. A.W. Adamson; 'Physical Chemistry of Surfaces', 2nd ed., Interscience Publishers, New York, N.Y., 1967.

165. J. Cartwright, K. Wheatley and K.S.W. Sing; J. Appl. Chem., 8, 259 (1958).

166. P.H. Emmett and S. Brunauer ; J. Am. Chem. Soc., 59, 1553 (1937).

167. 'Handbook of Chemistry and Physics', 48th ed., Chemical Rubber Publishing Co., 1968.

168. J.H. de Boer; 'The Dynamical Character of Adsorption', Oxford University Press, London, 1953.

169. D.H. Everett; Proc. Chem. Soc., 38 (1967).

170. J.J.F. Scholten and S. Kruyer; 'Physical and Chemical Aspects of adsorbents and catalysis', ed. B.G. Linsen, Academic Press Inc., New York, N.Y., 1970, p 147.

171. J.A. Morrison and J.M. Los; Discussions Faraday Soc. no. 8, 321 (1950).

172. J.A. Morrison and J.M. Los and L.E. Drain; Trans. Faraday Soc., 47, 1023 (1951).

173. L.E. Drain and J.A. Morrison; Trans. Faraday Soc., 48, 840 (1952).

174. S.A. Greene and H. Pust; J. Phys. Chem., 62, 55 (1958).

175. C. Letoquart, F. Rouquerol and J. Rouquerol; J. Chim. Phys. Physicochim. Biol. 70, 559 (1973).

176. J.M. Holmes; "The Solid Gas Interface", ed. E.A. Flood, Marcel Dekker Inc., New York, N.Y., 1967.

177. H.W. Edwards and M.L. Corrin; J. Phys. Chem., 71, 3373 (1967).

178. E.A. Molwyn-Hughes; 'Physical Chemistry' 2nd ed., 350, Pergamon Press, New York, N.Y., 1961.

179. S. Glasstone; 'A text book of Physical Chemistry', Von Nostrand Reinhold, New York, N.Y., 1957.

180. R. Fruchart and A. Michel; C.R. Acad. Sci., Paris, 246, 1222 (1958).

181. C. Duval; 'Inorganic Thermogravimetric Analysis' translated by R.E. Oesper, Elsevier Publishing Co., New York, N.Y., 1963.

182. T.R. Ingraham and P. Marier; Can. Mettall. Quart., 6, 249 (1967).

183. S. Ahmed; Pak. J. Sci. Ind. Res. 15, 146 (1972).

184. J. Krochural; Rudy i Metale Niezelazme, 17, 251 (1972).

185. J. Cueilleron and O. Hartmanshenn; Soc. Chimi. France Bull., 168 (1959).

186. P.P. Budniko and A.M. Ginstling; 'Principles of solid state chemistry', Maclaren Press, London, 1968, translated by K. Shaw, p 120.

187. J.H. Van Vleck; J. Chem. Phys. 3, 807 (1935).

188. L. Pauling; 'The nature of the chemical bond', Cornell Univ. Press, New York, N.Y.,1948.

189. N.S. Hush; Discussions Faraday Soc., 26, 145 (1958).

190. R. Krishnamurthy and W.B. Schaap; J. Chem. Educ., 46, 799 (1969).

191. L.E. Orgel; 'An introduction to transition metal chemistry', Methuen and Co., London, 1960.

192. R.G. Burns; 'Mineralogical applications of crystal field theory', Cambridge Univ. Press., London, 1970.

193. F. Basolo and R.G. Pearson; 'Mechanism of Inorganic Reactions', Wiley, New York, N.Y., 1958, p 53.

194. R. Kollrack; J. Catal. 18, 314 (1970).

195. E.J.W. Verwey; Rec. Trav. Chim. Pays-Bas., 65, 521 (1946).

196. W.J. Dunning; Proc. Brit. Ceram. Soc., 5, 59 (1965).

197. R. Kollrack; J. Catal., 12, 321 (1968).

198. F.J. Morin; Physical review, 93, 1195 and 1199 (1954).

199. Van Housten; J. Physics. Solids, 17, 7 (1960).

200. T.A. Eggerton and F.S. Stone; J. Chem. Soc. Faraday. Trans. 1, 69, 22 (1973).

201. K. Kleir; J. Catalysis, 8, 14 (1967).

202. D. Dowden; Catalysis Rev., 5, 1 (1971).

203. D.L. Harrison, D. Nicholls and H. Steiner; J. Catal., 7, 359 (1967).

204. G.H. Dixon, D. Nicholls and H. Steiner; Proc. Intern. Catalyse, 2e, Paris, 1960, 2, 1409 (1961).

205. J. Haber and F.S. Stone; Trans. Faraday Soc., 59, 192 (1963).

206. G.A. Kinloch and W.D. Machin; Can. J. Chem., 49, 1515 (1971).

207. A.F. Wells; J. Solid State Chem., 6, 469 (1973).

208. A. Cimino, F. Pepe and M. Schiavello; 'Proc. 5th Intern. Cong. Catalysis,(1972), Ed. J.W. Hightower, North Holland Publishing Co. 1973.

209. B.V. Erofeeve, E.F. Ivankevich and N.V. Nikifozova; 'Scien. Selec. Catal.', Ed. A.A. Badandin, 94-104 (1968).

210. W.H. Wade, S. Teranishi and J.L. Durham; J. Colloid. Science, 20, 838 (1965).

211. O. Sinanoglu and K.S. Pitzer; J. Chem. Phys., 32, 1279 (1960).

212. C. Mavroyannis and M.J. Stephen; Mol. Phys., 5, 629 (1962).

213. J.W.S. Jamieson, G.R. Brown, D.W. Gruener, R.V. Peiluck and R.A. LaMontagne; Can. J. Chem. 43, 2148 (1965).

214. G.B. Frost, K.A. Moon and E.H. Tompkins; Can. J. Chem., 29, 604 (1951).

215. N.A. Lange; "Handbook of Chemistry", 10th ed., McGraw Hill Book Co., New York, N.Y. (1967); J.A. Dean; "Lange's Handbook of Chemistry", 11th ed., McGraw Hill Book Co., New York, N.Y. (1973).

216. J.T. Nelson; U.S. Nat. Tech. Inform. SA. AD. Rep. 1972 AD. 741785, Washington D.C.

8.00 APPENDIX A

8.10 Adsorption Data (gravimetric)

Pressure (P) is recorded in torr and amount adsorbed is recorded as W micromoles. The temperature at which the sample was annealed is shown in parenthesis along with the various adsorbents. The start of each run is indicated by 'X'. $CFCl_3$ was used as an adsorbate in all the runs.

$CaSO_4$ (200°C)

Sample weight, 414 mg.

Temperature, 20.0°C

	P	W	P	W	P	W
'X'	1.15	4.25	20.20	18.93	236.40	43.69
	2.50	7.03	44.75	24.64	193.10	39.80
	4.30	9.83	71.25	28.63	140.75	35.59
	9.35	14.47	131.90	34.70	101.20	31.84
	15.95	18.11	172.80	38.20	54.60	26.24
	30.45	22.76	223.20	42.05	10.10	14.26
	59.60	27.83	262.30	44.17	0.360	2.02
	91.50	31.73	329.10	51.08		
'X'	0.950	3.78	289.80	47.77		

Temperature, 6.0°C

	P	W	P	W		P	W
'X'	0.590	4.55	70.95	35.32	'X'	0.530	4.41
	1.05	6.51	102.65	39.72		8.50	17.92
	1.55	8.23	152.15	47.70	'X'	14.70	21.52
	2.15	9.67	130.05	44.89		51.50	31.73
	5.90	15.78	110.70	41.98		78.55	35.99
	10.45	19.67	90.35	39.15		97.90	38.77
	20.90	24.34	61.60	34.70		121.60	42.19
	39.50	29.39	30.60	28.15			

Temperature, -10.0°C

	P	W		P	W	P	W
'X'	0.280	5.79		41.40	38.11	9.00	24.69
	0.560	8.33		50.80	40.80	37.20	36.72
	0.9000	10.61		61.10	43.62	57.05	42.16
	1.75	14.16		44.70	39.22	46.60	39.51
	4.60	20.29		25.15	32.99	34.65	35.85
	11.75	26.61		15.85	29.21	27.50	33.53
	21.10	31.24	'X'	1.90	14.58	18.00	29.71
	31.40	35.11		4.00	19.07	7.65	23.57

$CaSO_4$ (300 C)

Sample weight, 414 mg.

Temperature, 20.0°C

	P	W		P	W	P	W
'X'	0.250	1.19		203.25	32.50	299.50	38.81
	0.570	2.13		1.10	2.75	251.80	35.18
	1.25	3.52		6.15	9.00	189.60	30.86
	4.90	8.77		19.15	15.34	130.80	26.85
	14.05	14.92		39.90	19.46	88.60	23.85
	31.20	19.28		82.20	23.57	63.45	21.72
	51.40	22.04		121.95	26.35	9.40	11.09
	101.55	26.08		170.35	29.53		
	152.80	29.29		221.35	32.95		

Temperature, 6.0°C

	P	W		P	W	P	W
'X'	0.200	1.47		161.25	38.74	25.90	20.71
	0.460	2.44		119.15	33.06	44.85	24.20
	0.980	4.39		91.50	29.87	68.20	27.23
	1.80	6.56		60.95	26.05	86.60	29.40
	5.95	12.83		39.80	23.17	111.35	32.15
	14.45	17.64		19.65	19.35	95.80	30.41
	31.15	21.79		10.35	16.08	78.40	28.49
	51.40	24.65	'X'	0.36	2.30	55.50	25.63
	73.55	27.70		1.10	4.85	34.40	22.53
	102.60	31.03		2.45	7.88		
	132.15	35.88		8.40	15.17		
	182.45	41.39		17.70	18.97		

Temperature, -10.0°C

	P	W		P	W	P	W
'X'	0.270	3.77		89.95	42.75	7.60	19.00
	0.430	5.09		73.85	38.50	23.80	25.18
	1.15	8.65		55.10	33.86	43.75	30.20
	1.45	10.53		44.05	30.51	54.60	32.78
	4.30	16.28		34.65	28.07	71.05	37.10
	9.60	20.19		25.45	25.73	101.90	47.11
	21.90	24.72		15.60	22.84	80.65	40.59
	30.85	27.16	'X'	0.158	2.51	48.45	31.77
	39.00	29.15		0.46	5.23	36.65	28.66
	51.65	32.32		0.865	7.67	10.40	20.78
	60.70	34.49		2.35	12.87		

$CaSO_4$ (400°C)

Sample weight, 413 mg.

Temperature, 20.0°C

	P	W		P	W	P	W
'X'	0.950	2.89		175.70	26.19	137.80	23.78
	5.55	7.32		126.65	23.57	186.95	26.40
	19.70	13.60		74.35	20.33	230.85	28.73
	51.15	18.27		35.65	16.70	210.60	27.62
	102.70	22.11		10.90	10.67	160.25	24.79
	151.85	24.79	'X'	0.345	1.40	91.00	20.92
	198.45	27.34		0.935	2.37	59.10	18.55
	252.70	30.62		3.00	4.85	26.80	14.65
	357.10	38.01		16.75	12.17	8.50	8.89
	293.50	33.96		42.75	16.95		
	225.45	28.98		76.25	19.95		

Temperature, 6.0°C

	P	W		P	W	P	W
'X'	0.380	2.18		180.85	35.27	43.30	20.57
	0.945	3.93		150.05	31.96	66.15	22.56
	2.05	5.95		109.70	26.80	86.45	24.65
	7.30	11.95		90.00	25.02	106.95	26.54
	20.50	16.76		70.30	23.14	75.20	23.61
	40.25	19.97		49.85	21.12	55.40	21.65
	61.20	22.34		30.15	18.68	33.90	19.11
	81.30	24.15		15.00	15.50	4.75	9.87
	102.00	26.14		5.90	11.04	0.460	2.55
	130.75	28.82	'X'	2.20	6.15		
	161.50	32.42		10.00	13.53		
	202.00	38.06		25.80	17.82		

Temperature, -10.0°C

	P	W	P	W	P	W
'X'	0.735	6.21	93.60	37.56	1.45	8.09
	1.70	9.50	80.30	34.28	2.40	11.23
	5.25	15.45	59.95	29.95	6.90	15.97
	10.40	18.24	45.75	26.22	13.10	18.69
	22.25	21.41	34.25	23.96	24.15	21.60
	30.95	23.36	25.35	22.25	33.15	23.29
	39.70	25.11	15.80	19.95	43.05	25.32
	50.60	27.13	0.48	4.46	53.00	27.20
	70.50	31.45	0.80	5.93	47.55	26.15
					37.70	24.13

$MnSO_4$ (200°C)

Sample weight, 542 mg.

Temperature, 20.0°C

	P	W		P	W	P	W
'X'	21.55	3.80		239.00	27.69	13.90	3.42
	35.75	6.98		180.90	22.34	26.70	6.00
	80.10	12.90		139.95	18.68	50.75	10.30
	116.00	16.55		101.15	15.09	101.60	16.32
	158.15	20.58		57.15	9.86	153.75	21.34
	100.00	24.15	'X'	5.85	1.60	78.75	13.77

Temperature, 6.0°C

	P	W		P	W	P	W
'X'	7.65	3.59		142.40	31.07	50.35	14.17
	20.10	7.60		100.35	22.91	91.75	20.99
	40.85	12.97		60.30	16.46	122.50	25.73
	84.00	20.43	'X'	7.10	3.17	110.05	23.73
	122.55	26.29		13.80	5.54	69.05	17.44
	163.60	33.85		28.15	9.59	18.20	7.22

Temperature, -10.0°C

	P	W		P	W	P	W
'X'	0.550	0.82		31.65	17.82	51.40	24.55
	0.870	1.15		41.40	20.96	34.60	18.69
	4.95	5.06		62.75	27.83	13.50	10.43
	10.45	8.84		88.80	38.39	1.90	2.57
	20.50	13.77		72.55	32.26		

$MnSO_4$ (300°C)

Sample weight, 537 mg.

Temperature, 20.0°C

	P	W		P	W		P	W
'X'	2.80	1.81		101.40	15.44		164.10	18.06
	7.90	3.52		61.00	12.17	'X'	59.55	11.08
	18.60	6.09		29.20	7.99		119.80	15.73
	38.75	9.49		9.70	4.12		181.00	18.83
	81.05	14.23		3.55	2.19		239.75	21.34
	119.35	16.70	'X'	0.92	0.59		206.50	19.95
	161.05	18.72		49.15	10.15		148.55	17.40
	202.15	20.50		131.05	16.53		89.85	13.95
	231.10	21.62		209.75	19.86		29.55	7.04
	184.30	19.67		295.90	23.75		15.20	4.48
	141.45	17.73		250.35	21.93			

Temperature, 6.0°C

	P	W	P	W	P	W
'X'	0.78	0.66	60.40	15.41	107.70	19.33
	1.40	0.98	79.40	17.23	90.65	18.15
	2.20	1.47	101.00	18.83	69.70	16.42
	6.20	4.30	118.80	20.23	48.25	14.06
	17.20	8.23	171.40	24.04	28.80	10.67
	38.45	12.73	146.30	22.11	10.65	5.66

Temperature, -10.0°C

	P	W	P	W	P	W
'X'	0.66	1.16	41.80	17.87	16.00	12.32
	1.00	1.63	62.05	20.74	12.45	10.70
	4.75	5.45	83.10	23.82	8.15	8.19
	10.65	9.67	49.80	19.28	3.10	4.21
	19.10	13.27	35.00	16.98		
	31.50	16.26	25.25	15.00		

$MnSO_4$ (400°C)

Sample weight, 537 mg.

Temperature, 20.0°C

	P	W		P	W		P	W
'X'	0.635	0.17		152.75	13.97		50.45	7.97
	1.70	0.49		212.70	16.09		102.25	11.77
	5.55	1.33		180.70	14.98		160.15	14.30
	10.40	2.60		119.70	12.65		213.20	16.15
	21.35	4.43		65.80	9.24		189.35	15.31
	41.05	7.05	'X'	1.40	0.35		140.80	13.37
'X'	42.50	7.10		7.15	1.81		108.00	11.89
	90.30	11.10		29.80	5.44		78.55	10.22

Temperature, 6.0°C

	P	W		P	W		P	W
'X'	0.23	0.25		60.90	12.82		70.00	14.42
	0.75	0.59		80.90	14.23		50.60	11.74
	1.50	0.91		111.40	15.44		30.65	9.17
	2.10	1.24		122.55	16.57		15.35	5.96
	4.30	2.41		172.30	19.27		6.80	3.28
	10.40	4.69		137.65	17.30		3.70	2.08
	20.45	7.28		108.05	15.73			
	40.25	10.81		89.80	14.62			

Temperature, -10.0°C

	P	W		P	W		P	W
'X'	0.222	0.43		18.85	11.33		44.55	15.16
	0.455	0.74		31.25	13.40		35.50	14.05
	0.798	1.20		42.45	14.80		25.30	12.55
	1.25	1.74		51.30	15.81		15.45	10.32
	4.15	4.42		69.70	17.74		8.25	7.25
	6.20	5.71		90.15	20.25		3.40	4.14
	12.05	8.96		58.45	16.70		1.75	2.68

$CoSO_4$ (200°C)

Sample weight, 358 mg.

Temperature, 20.0°C

	P	W		P	W		P	W
'X'	0.84	0.11	'X'	0.78	0.12		2.40	0.46
	2.10	0.39		3.60	0.67	'X'	154.70	17.02
	6.05	1.17		5.20	0.86		196.35	19.75
	14.30	2.23		9.20	1.42		239.85	22.26
	27.40	3.77		15.75	2.27		289.30	24.94
	46.75	6.00		20.45	2.73		260.80	23.48
	91.60	11.08		26.95	3.51		219.15	21.10
	131.30	14.69		36.70	4.57		178.60	18.62
	171.95	17.79		59.50	7.22		142.25	15.53
	202.00	19.93		87.65	10.30		101.60	11.45
	151.40	16.28		117.25	13.16		59.30	6.56
	109.80	12.64		138.50	15.05		32.75	3.74
	68.10	8.40		126.00	13.98			
	30.95	4.14		84.85	9.96			

Temperature, 6.0°C

	P	W		P	W		P	W
'X'	4.95	1.77		69.20	14.04		56.60	11.93
	10.10	2.92		48.95	10.56		77.45	15.27
	15.45	3.65		16.75	4.04		97.60	17.95
	24.90	5.67		6.70	1.81		117.60	20.17
	38.75	8.46	'X'	0.57	0.21		143.25	22.66
	60.20	12.49		2.05	0.85		162.40	24.43
	81.15	15.80		6.50	2.01		125.90	20.96
	111.45	19.53		12.25	3.34		87.35	16.67
	150.15	23.19		19.65	4.90		49.80	10.83
	169.45	24.92		24.05	5.82		15.35	3.87
	131.30	21.51		43.20	9.74		7.45	2.09
	90.80	17.18	'X'	27.35	6.27			

Temperature, -10.0°C

	P	W		P	W	P	W
'X'	0.446	0.34		70.00	22.95	9.75	5.51
	0.750	0.52		92.10	26.94	15.55	8.13
	1.000	0.69		79.50	24.82	20.95	10.49
	2.90	1.90		59.80	21.33	28.45	13.30
	4.85	2.99		39.05	16.57	56.10	20.60
	8.55	4.74		24.70	11.86	66.75	22.66
	13.10	6.95		2.75	1.95	44.60	18.03
	17.70	9.03	'X'	0.795	0.59	33.40	14.93
	30.60	13.84		1.30	0.80	22.25	11.96
	40.85	16.95		2.25	1.59	11.55	6.36
	50.05	19.17		6.65	4.02	6.50	4.06

$CoSO_4$ (300°C)

Sample weight, 298 mg.

Temperature, 20.0°C

	P	W	P	W	P	W
'X'	0.54	0.39	81.60	19.29	192.85	28.43
	1.15	0.67	122.45	23.54	141.05	24.71
	2.00	1.17	172.10	27.22	90.10	20.07
	4.70	2.44	220.60	30.33	30.20	10.16
	8.10	3.82	271.30	33.81	15.10	5.84
	19.40	7.58	303.65	36.00		
	40.80	12.85	248.25	32.18		

Temperature, 6.0°C

	P	W		P	W	P	W
'X'	0.675	0.92		14.55	10.66	51.00	21.35
	2.45	2.62	'X'	0.294	0.46	70.10	24.53
	5.75	5.38		0.422	0.57	91.35	27.40
	10.00	7.86		0.772	0.92	125.35	31.26
	21.15	13.20		1.15	1.17	161.60	35.33
	40.50	19.19		2.45	2.45	202.35	40.64
	78.70	25.77		5.15	4.60	181.05	37.95
	115.60	30.16		7.35	6.09	141.20	33.17
	99.35	28.53		12.00	8.74	95.00	27.90
	60.90	23.40		23.95	14.23	65.40	23.97
	30.60	16.74		37.30	18.34	33.75	17.63

Temperature, -10.0°C

	P	W	P	W	P	W
'X'	0.210	0.99	9.10	13.45	59.80	31.22
	0.420	1.81	20.15	20.43	52.40	29.56
	0.635	2.44	30.70	24.25	43.45	27.54
	0.780	2.94	40.25	26.73	34.00	25.13
	2.40	6.41	50.45	29.03	24.00	22.09
	4.60	10.12	71.50	33.52	13.90	17.17
'X'	0.620	1.95	99.05	40.36	3.20	6.66
	2.45	5.42	85.10	36.78	1.70	3.89

$CoSO_4$ (400°C)

Sample weight, 293 mg.

Temperature, 20.0°C

	P	W		P	W		P	W
'X'	0.51	0.53		14.30	6.66		270.35	29.81
	1.80	1.42		6.25	3.79		216.05	26.73
	4.80	2.87	'X'	0.366	0.28		164.45	23.90
	10.00	4.99		1.80	1.13		114.50	20.53
	20.60	8.32		4.15	2.23		74.70	16.53
	40.85	13.06		9.55	4.25	'X'	0.41	0.43
	70.10	17.74		13.40	5.49		2.50	1.98
	120.45	22.48		19.20	7.15		40.40	12.43
	170.85	25.67		27.75	9.31		84.95	18.80
	222.20	28.67		50.35	13.52		125.30	22.23
	200.10	27.40		89.60	18.51		166.80	24.99
	149.75	24.60		141.65	22.48		186.90	26.16
	98.80	20.89		191.20	25.45		145.90	23.75
	61.65	16.74		241.65	28.18		94.35	19.79
	29.95	10.80		301.15	31.51		66.55	16.78

Temperature, 6.0°C

	P	W		P	W		P	W
'X'	0.22	0.35		168.25	31.29		37.80	17.17
	0.67	0.81		120.95	27.22		58.90	20.74
	1.95	2.30		100.00	25.35		78.90	23.25
	4.65	4.32		81.35	23.40		97.30	25.13
	9.50	7.08		59.60	20.82		138.35	28.82
	17.20	10.66		37.90	17.03		180.95	32.71
	25.25	13.68		28.00	14.37		157.10	30.55
	49.25	19.22		13.90	9.03		110.80	26.41
	70.65	22.23		7.50	5.49		88.40	24.39
	90.95	24.39		1.35	1.35		66.50	21.88
	110.40	26.13	'X'	0.32	0.53		46.45	18.87
	150.90	29.67		1.85	2.41		26.40	14.30
	192.75	33.74		18.20	11.51		7.60	6.37

Temperature, -10.0°C

	P	W	P	W	P	W
'X'	0.22	1.13	14.70	18.16	81.10	32.82
	0.43	1.95	20.15	20.53	60.15	29.35
	0.72	2.80	30.10	23.58	45.15	26.76
	1.25	4.32	40.70	25.95	33.80	24.53
	3.55	8.50	51.00	27.72	24.45	21.84
	5.45	10.83	72.15	31.22	6.70	12.11
	10.60	15.68	95.35	35.44		

$CoSO_4$ (500°C)

Sample weight, 288.2 mg.

Temperature, 20.0°C

	P	W	P	W	P	W
'X'	52.00	11.57	0.73	0.50	240.40	23.54
	97.55	17.06	4.05	2.23	297.80	26.23
	150.40	19.65	10.75	4.35	271.50	25.28
	201.25	21.70	14.60	5.49	220.20	23.36
	250.75	23.61	20.80	7.12	179.25	21.59
	225.75	22.73	40.75	11.12	138.95	19.75
	171.40	20.46	79.50	15.61	98.70	17.35
	120.15	17.88	120.95	18.51	60.85	14.09
	74.05	14.76	160.95	20.36	27.00	8.85
'X'	0.455	0.32	198.80	21.95	6.40	3.54

Temperature, 6.0°C

	P	W	P	W	P	W
'X'	0.30	0.35	40.60	14.51	126.45	22.66
	0.70	0.57	56.00	17.24	93.90	20.46
	2.65	2.12	79.70	18.94	69.35	18.48
	5.50	3.89	108.85	21.13	27.95	12.46
	9.80	5.95	151.10	24.07	5.80	4.39
	15.30	8.18	192.40	27.00		
	20.20	10.02	168.90	25.38		

Temperature, -10.0°C

	P	W		P	W		P	W
'X'	0.235	0.78		56.00	21.49		38.00	19.12
	0.630	1.52		86.70	25.28		47.85	20.50
	1.80	3.54		37.55	19.12		90.15	25.81
	6.10	8.18	'X'	0.65	1.70		71.15	23.47
	12.65	12.39		2.80	4.96		23.65	16.53
	22.35	15.72		9.10	10.48		5.55	8.21
	32.60	18.02		18.05	14.59		1.45	3.36
	43.55	19.82		28.60	17.31			

$NiSO_4$ (200°C)

Sample weight, 452 mg.

Temperature, 20.0°C

	P	W		P	W		P	W
'X'	5.95	0.85		39.75	9.00	'X'	0.745	0.43
	37.05	7.01		70.20	15.90		2.50	1.10
	79.00	17.70		112.30	24.35		6.30	2.37
	119.70	25.35		151.10	29.98		9.15	3.29
	160.75	30.94		192.45	34.44		16.25	5.20
	200.95	35.61		234.50	38.42		25.90	7.72
	177.20	32.92		266.50	41.77		35.15	10.02
	139.15	28.99		314.85	46.09		64.65	16.53
	98.30	22.37		289.50	43.90		96.75	22.36
	59.25	14.05		250.95	40.37		129.15	27.01
	19.60	5.17		210.30	36.43		167.75	31.95
'X'	0.405	0.18		167.85	32.16		199.30	35.19
	2.95	0.35		124.70	26.62		151.45	30.34
	4.75	0.99		88.85	20.43		111.40	24.89
	9.75	2.20		48.85	12.21		58.20	13.20
	19.50	4.18		2.95	0.67		1.65	0.885

Temperature, 6.0°C

	P	W		P	W		P	W
'X'	0.30	0.19		182.10	46.06		87.15	30.78
	0.72	0.46		208.40	50.87		74.90	28.14
	2.10	1.38		194.45	48.39		54.75	23.22
	4.30	2.55		164.90	43.61		34.35	15.72
	11.20	5.98		135.15	39.05	'X'	18.30	10.12
	20.75	10.12		105.40	34.44		39.95	18.69
	41.10	18.41		80.20	29.59		79.25	29.42
	71.15	22.98		50.80	21.77		120.05	36.85
	2.45	1.20		24.05	11.68		166.00	44.32
	14.05	6.87	'X'	3.40	1.70		144.65	40.43
	30.40	13.74		9.95	4.60		98.90	33.77
	60.70	24.32		15.65	7.51		59.95	25.13
	91.35	31.58		23.90	11.33		4.35	3.26
	122.10	36.71		45.90	19.40			
	152.40	41.75		65.55	25.38			

Temperature, -10.0°C

	P	W		P	W		P	W
'X'	3.80	5.31		3.40	5.70		19.00	20.60
	11.45	13.66		8.05	10.41		14.25	16.82
	21.35	21.38		13.05	15.01		4.50	7.04
	40.95	32.00		17.55	19.40		0.52	2.23
	71.10	41.59		25.30	24.36	'X'	1.30	2.62
	99.05	51.05		35.60	30.41		1.90	3.72
	85.85	46.30		45.90	34.30		5.25	8.25
	47.25	34.27		60.40	39.22		10.40	13.31
	28.85	26.80		53.25	36.32		20.05	21.59
	15.20	17.49		46.20	34.87		31.10	28.29
	0.45	1.56		37.90	31.93		41.30	33.17
'X'	1.30	2.62		28.50	27.01		51.20	36.29

$NiSO_4$ (300°C)

Sample weight, 441 mg.

Temperature, 20.0°C

	P	W		P	W		P	W
'X'	2.20	0.57		31.05	9.30		101.60	22.09
	7.80	1.81		61.30	16.25		152.40	28.32
	20.20	5.56		91.40	21.66		201.30	33.10
	51.10	13.06		120.45	26.02		233.30	36.32
	99.95	22.16		162.20	30.83		176.25	31.05
	150.20	28.67		142.40	28.36		126.00	25.63
	197.80	33.77		107.95	24.43		75.25	17.98
	248.60	37.91		61.20	16.53		40.00	11.29
	297.25	42.13		40.55	11.75		19.30	5.91
	275.05	40.00	'X'	3.90	1.70		5.95	2.20
	226.75	36.25		10.30	3.79		1.00	0.35
'X'	3.50	1.63		31.50	9.35			
	9.95	3.65		51.10	13.31			

Temperature, 6.0°C

	P	W	P	W	P	W
'X'	0.567	1.27	59.70	25.67	29.60	16.74
	2.55	2.51	80.65	30.23	13.90	9.24
	5.65	4.39	110.80	35.65	6.40	5.17
	9.90	6.69	95.55	33.56	3.30	3.54
	21.25	12.21	68.90	28.57	0.76	1.91
	41.15	20.21	49.65	23.12		

Temperature, -10.0°C

	P	W	P	W	P	W
'X'	1.35	2.80	0.70	1.63	64.25	37.10
	3.40	5.77	1.65	3.26	54.35	34.30
	8.85	11.54	5.40	7.86	44.35	31.15
	19.85	20.28	11.35	13.52	34.60	27.79
	30.40	26.20	25.75	23.79	14.30	15.58
	39.25	29.81	50.45	33.36	6.80	8.71
	59.60	35.99	72.20	39.40	3.90	5.52
	80.00	41.56	97.10	46.44	2.40	3.86
'X'	0.23	0.64	89.75	44.04	0.60	1.52

$NiSO_4$ (400°C)

Sample weight, 417 mg.

Temperature, 20.0°C

	P	W	P	W		P	W
'X'	19.50	12.28	5.65	4.50	'X'	1.65	1.88
	48.95	21.49	9.85	6.44		7.45	5.70
	99.25	31.15	29.20	14.59		24.80	13.74
	149.50	37.45	59.40	22.73		84.65	26.90
	196.30	42.20	86.40	28.57		160.20	37.35
	178.55	40.43	117.10	32.29		241.15	44.96
	126.30	35.12	105.20	30.73		322.80	52.89
	74.35	27.51	69.20	25.35		279.65	48.68
'X'	0.38	0.43	38.75	17.74		208.10	42.16
	3.10	3.01	14.15	8.92		121.15	32.92

Temperature, 6.0°C

	P	W	P	W		P	W
'X'	0.34	0.78	141.50	45.28	'X'	0.975	1.49
	0.56	1.20	172.45	49.78		2.90	4.25
	1.50	2.48	202.10	55.08		5.55	7.26
	3.20	4.81	186.95	52.29		8.50	9.63
	6.10	7.89	156.05	47.37		15.50	14.44
	10.55	11.33	126.65	43.40		24.85	19.53
	20.65	17.35	95.05	38.06		40.35	25.28
	49.60	28.18	64.70	32.39		50.80	28.32
	80.75	35.33	34.95	23.68		91.15	36.53
	111.05	40.71	0.665	2.30		69.85	32.60

Temperature, -10.0°C

	P	W		P	W		P	W
'X'	0.183	1.17		71.00	46.41		12.35	22.27
	0.280	1.18		96.05	53.95		22.45	29.59
	0.466	2.16		83.75	50.02		38.20	36.46
	0.685	2.41		54.55	41.70		47.85	38.75
	1.05	3.68		44.60	38.44		47.30	40.43
	2.55	7.75		33.90	34.55		58.35	43.65
	5.15	12.85		24.25	30.13		67.85	46.27
	8.00	16.60		14.70	23.68		77.45	48.36
	11.00	20.28		1.75	6.62		45.90	39.29
	19.30	27.19	'X'	0.735	3.51		25.00	31.08
	31.30	33.52		1.20	4.81		9.45	19.75
	40.15	36.92		3.40	10.55			
	50.15	40.11		7.05	16.57			

$NiSO_4$ (500°C)

Sample weight, 411 mg.

Temperature, 20.0°C

	P	W		P	W		P	W
'X'	1.15	2.12		4.65	5.49		38.85	19.399
	10.05	9.45	'X'	2.20	3.47		18.55	12.92
	30.25	18.34		7.35	7.26	'X'	0.081	0.14
	60.10	25.74		16.40	12.14		0.330	0.53
	102.80	31.44		31.05	17.52		0.965	1.42
	151.45	36.29		49.95	21.49		3.05	3.93
	200.75	40.00		98.35	28.99		5.85	6.20
	248.05	43.26		150.40	33.45		7.70	7.61
	247.05	43.01		200.15	37.35		10.65	9.31
	301.10	47.15		247.85	40.89		16.95	12.28
	276.55	45.14		309.55	45.77		27.20	16.11
	227.20	41.42		276.50	43.15		36.15	18.76
	178.05	37.89		223.15	39.65		46.50	21.20
	136.15	33.67		177.75	35.93		56.60	22.90
	75.90	27.90		125.75	31.61		67.55	24.78
	19.90	13.95		74.55	26.02		77.90	26.41

Temperature, 6.0°C

	P	W		P	W		P	W
'X'	0.555	1.59		100.85	36.07		0.872	2.90
	0.79	2.83		130.20	39.40		2.00	5.03
	2.05	5.06		160.95	43.19		4.10	8.00
	3.70	7.43		190.65	47.26		6.45	10.80
	7.85	11.86		176.50	45.14		11.50	14.94
	10.85	14.69		146.50	41.24		17.10	18.44
	15.45	17.35		115.00	37.70		25.75	22.02
	19.35	19.65		89.80	34.62		36.40	25.45
	39.55	26.30		69.20	31.68		45.40	27.51
	60.50	30.44		50.00	28.14		76.85	32.64
	81.40	33.45	'X'	0.482	1.91			

Temperature, -10°C

	P	W		P	W		P	W
'X'	0.298	2.73		90.90	45.92		26.15	30.94
	0.570	4.14		70.35	40.78		36.60	34.02
	0.850	5.27		49.35	36.11		46.70	36.60
	1.80	8.57		29.40	31.05		57.70	38.87
	4.80	15.29		14.45	24.39		53.05	37.95
	8.90	20.60	'X'	0.150	2.27		41.45	35.29
	20.25	28.00		0.400	3.89		32.40	33.06
	41.20	34.27		1.30	7.75		22.95	29.70
	60.85	38.66		5.90	18.20		11.85	23.86
	80.75	43.26		10.45	22.62		3.70	14.66
	100.95	48.85		16.75	27.05			

$CuSO_4$ (200°C)

Sample weight, 486 mg.

Temperature, 20.0°C

	P	W		P	W		P	W
'X'	1.85	7.26		1.75	6.05		273.65	121.88
	50.30	48.46		5.65	13.03		226.05	102.73
	98.35	66.84		10.80	19.47		180.70	89.39
	147.95	80.54		21.05	29.03		142.60	79.15
	199.10	94.34		39.30	41.35		100.85	67.72
	175.00	87.97		80.30	59.65		59.65	53.10
	125.85	74.87		120.25	72.22		30.90	38.06
	74.65	59.30		159.90	82.94		14.40	25.31
	24.35	34.35		201.10	94.52		7.10	17.88
	9.40	20.71		250.90	110.91			
'X'	0.79	3.61		297.35	129.39			

Temperature, 6.0°C

	P	W		P	W		P	W
'X'	0.326	3.08		180.90	147.62		291.95	259.66
	0.775	5.42		141.70	124.43		336.40	348.76
	2.15	10.27		100.50	89.39		388.25	798.55
	5.60	18.55		88.05	83.47	'X'	363.50	551.50
	8.65	24.28		69.00	74.80		316.00	362.64
	11.40	28.99		47.10	63.12		270.20	312.55
	15.05	33.77		24.40	46.55		228.50	269.71
	20.50	40.50		12.25	32.04		189.45	223.59
	31.10	50.66		2.65	14.37		153.80	158.56
	39.95	57.35	'X'	34.50	51.93	'X'	359.85	442.50
	60.65	69.28		94.45	83.40		380.25	644.46
	81.45	79.40		131.20	102.70		367.80	535.25
	121.55	95.76		171.40	130.73		346.50	438.96
	161.60	125.32		209.35	164.75		180.10	222.52
	201.05	158.59		255.80	212.37			

Temperature, -10.0°C

	P	W	P	W		P	W
'X'	0.400	6.66	21.75	63.26	'X'	0.743	9.35
	0.865	10.34	40.80	82.91		6.30	33.60
	1.65	15.01	59.50	103.40		26.50	68.46
	3.60	23.93	79.50	132.01		47.70	89.88
	5.35	30.37	48.45	91.86		69.55	116.43
	7.35	36.71	29.85	72.22		109.65	187.23
	10.55	44.57	13.45	50.76		87.75	161.18
	15.15	53.81	1.00	12.36		54.20	103.72

$CuSO_4$ (300°C)

Sample weight, 482 mg.

Temperature, 20.0°C

	P	W	P	W	P	W
'X'	0.430	0.67	262.10	25.28	71.90	14.05
	1.25	1.38	197.65	22.55	121.10	17.98
	4.85	3.15	153.30	20.50	187.15	21.49
	15.15	5.98	108.85	17.84	247.40	24.00
	40.65	10.41	62.20	13.63	164.15	20.39
	79.35	15.05	25.40	8.39	94.25	16.14
	132.65	19.01	10.20	5.20	51.40	11.72
	182.35	21.42	'X' 0.690	0.85	12.30	5.17
	231.40	23.65	2.30	1.95	6.70	3.68
	295.60	26.66	20.75	7.01		

Temperature, 6.0°C

	P	W	P	W	P	W
'X'	0.425	0.92	79.35	19.93	91.00	20.60
	0.820	1.42	105.60	21.28	69.35	18.66
	2.65	3.12	142.20	24.00	48.95	16.28
	5.70	4.96	180.70	26.73	29.05	12.67
	10.80	7.29	218.40	30.09	14.45	8.50
	20.45	10.62	192.40	27.79	7.15	5.84
	40.80	15.22	161.55	25.35		
	59.55	17.91	119.60	22.62		

Temperature, -10.0°C

	P	W	P	W	P	W
'X'	0.315	1.59	29.90	18.23	55.30	22.30
	0.900	3.08	39.30	19.97	44.75	20.89
	2.00	4.89	49.85	21.45	33.55	19.08
	4.15	7.01	69.40	23.93	24.95	17.31
	6.05	8.57	89.05	26.48	11.90	12.39
	10.10	11.29	109.80	30.13	7.60	9.70
	15.85	14.23	99.10	28.21		
	20.85	16.04	79.80	25.42		

$CuSO_4$ (400°C)

Sample weight, 480 mg.

Temperature, 20.0°C

	P	W		P	W	P	W
'X'	0.905	0.74		303.60	15.58	7.65	2.90
	3.90	1.88		272.70	14.76	12.10	3.65
	7.80	2.80		215.35	13.28	36.75	6.62
	12.05	3.47		172.45	12.21	81.15	9.66
	17.40	4.25		131.30	11.05	121.80	11.33
	21.10	4.64		89.30	9.52	161.45	12.50
	40.00	6.80		55.90	7.72	201.70	13.59
	69.15	8.85		30.00	5.31	180.90	13.10
	111.20	10.27		18.55	3.86	138.55	11.86
	151.55	11.86	'X'	0.65	0.71	90.00	10.09
	191.40	12.74		2.45	1.49	54.15	8.04
	239.70	13.88		4.45	2.12	19.50	4.78

Temperature, 6.0°C

	P	W		P	W	P	W
'X'	0.660	0.99		89.25	12.25	10.25	4.96
	1.70	1.91		109.50	13.06	29.10	8.43
	3.20	2.58		150.00	14.59	44.00	9.95
	5.20	3.33		198.90	16.25	58.20	10.83
	7.60	4.04		168.50	15.40	78.10	11.93
	10.80	4.99		128.80	13.88	99.15	13.17
	15.35	6.02		108.70	13.13	140.65	14.83
	19.30	6.83		69.70	11.47	119.15	13.98
	39.90	8.50		48.80	10.16	80.40	12.43
	50.40	10.27	'X'	0.51	0.89	41.10	10.09
	72.25	11.51		1.95	2.12		

Temperature, -10.0°C

	P	W		P	W	P	W
'X'	0.355	1.59		85.40	15.93	1.95	3.47
	0.720	2.37		60.45	14.09	4.35	5.06
	2.80	4.67		44.85	13.03	8.60	7.29
	5.15	6.09		34.00	12.14	11.95	8.50
	11.50	8.92		24.60	11.22	18.50	9.98
	19.75	10.69		14.70	9.70	30.70	11.58
	28.90	11.79		7.40	7.40	41.05	12.57
	39.65	12.67		2.85	4.67	56.35	13.74
	51.35	13.52		1.20	3.47	39.95	12.50
	69.05	14.76	'X'	0.255	1.20	32.30	11.82
	100.75	17.31		0.600	1.88	11.40	8.46

$CuSO_4$ (500°C)

Sample weight, 479.2 mg.

Temperature, 20.0°C

	P	W	P	W	P	W
'X'	0.635	0.14	152.85	4.67	169.25	4.71
	2.20	0.53	190.65	5.10	129.60	4.18
	7.90	0.99	239.90	5.66	109.40	3.89
	16.15	1.45	296.30	6.27	77.70	3.40
	30.10	2.05	257.70	5.77	43.10	2.51
	59.45	3.08	220.00	5.31	20.05	1.59

Temperature, 6.0°C

	P	W	P	W	P	W
'X'	0.44	0.28	68.10	4.35	90.45	4.74
	1.05	0.57	88.50	4.78	76.85	4.46
	4.45	1.27	110.15	5.17	58.90	4.07
	9.90	1.84	155.35	5.84	38.40	3.40
	16.40	2.37	193.60	6.58	19.75	2.51
	29.45	3.19	168.00	6.09		
	49.85	3.93	130.80	5.45		

Temperature, -10.0°C

	P	W	P	W	P	W
'X'	0.375	0.53	4.90	1.95	15.75	3.22
	0.800	0.81	6.85	2.34	20.70	3.51
	2.30	1.27	9.75	2.69	30.40	3.90

$ZnSO_4$ (200°C)

Sample weight, 530 mg.

Temperature, 20.0°C

	P	W		P	W	P	W
'X'	50.60	5.72		127.40	12.76	12.60	1.60
	112.70	11.71		91.20	9.79	23.20	2.75
	151.45	14.88		70.50	7.60	32.55	3.69
	200.30	18.68		36.80	4.22	43.00	4.81
	249.65	21.85		15.70	2.20	27.40	3.21
	220.65	19.97		0.94	0.52	7.70	1.15
	173.10	16.62	'X'	3.90	0.49	0.87	0.31

Temperature, 6.0°C

	P	W	P	W	P	W
'X'	33.25	6.48	179.60	25.72	27.70	5.68
	56.95	10.59	145.40	22.30	15.80	3.42
	91.90	15.89	112.55	18.68	5.20	1.39
	130.30	20.70	74.00	13.35	3.00	1.05
	162.35	23.98	40.20	7.81	0.70	0.56

Temperature, -10.0°C

	P	W	P	W	P	W
'X'	8.65	3.69	89.95	26.17	15.25	6.52
	20.40	8.33	107.40	29.80	4.75	2.41
	32.15	12.65	70.80	22.58	2.85	1.57
	57.90	19.97	44.60	16.62	0.91	0.63
	67.05	21.85	25.35	10.42	0.61	0.45

$ZnSO_4$ (300°C)

Sample weight, 529 mg.

Temperature, 20.0°C

	P	W		P	W	P	W
'X'	2.70	0.56		58.20	6.80	202.15	17.36
	6.10	1.01		23.50	3.19	251.00	19.83
	16.35	2.37		5.20	0.98	175.00	15.86
	28.65	3.69	'X'	22.45	2.93	125.80	12.51
	47.65	5.61		49.35	5.76	75.35	8.33
	64.80	7.32		104.75	10.87		
	81.15	8.85		151.55	14.32		

Temperature, 6.0°C

	P	W	P	W	P	W
'X'	2.65	0.96	76.50	13.91	54.85	10.87
	7.00	2.06	105.00	16.90	31.35	6.94
	12.30	3.24	131.70	19.20	15.95	3.97
	18.50	4.32	155.20	21.05	6.55	1.95
	26.10	6.06	114.15	17.63	0.81	0.45
	39.15	9.15	89.10	15.26		

Temperature, -10.0°C

	P	W	P	W	P	W
'X'	4.70	2.88	100.00	24.47	5.65	3.28
	11.10	5.68	51.85	17.25	2.10	1.50
	18.95	8.75	36.80	14.05	3.15	2.09
	42.00	15.33	26.15	11.14	0.42	0.53
	62.75	18.96	16.00	7.53		
	83.70	22.03	8.95	4.74		

$ZnSO_4$ (400°C)

Sample weight, 528 mg.

Temperature, 20.0°C

	P	W		P	W		P	W
'X'	2.85	0.38		180.40	13.70		69.55	6.39
	6.55	0.85		283.85	18.43		111.00	9.63
	20.05	2.16		219.45	15.65		141.00	11.58
	50.45	4.74		170.25	13.24		162.20	12.85
	80.20	7.18		101.65	8.92		192.85	14.48
	121.45	10.20	'X'	1.25	0.15		207.60	15.26
	150.10	12.00		22.75	2.34		261.00	17.49

Temperature, 6.0°C

	P	W		P	W		P	W
'X'	2.50	0.67		161.15	18.40		19.85	4.04
	6.85	1.67		199.45	21.12		7.95	2.00
	11.20	2.51		180.80	19.87		4.85	1.36
	42.30	7.28		140.00	17.08		0.70	0.37
	80.95	12.18		100.30	14.06			
	126.70	16.10		59.45	9.79			

Temperature, -10.0°C

	P	W		P	W		P	W
'X'	3.60	2.04		39.85	12.65		14.95	5.95
	5.25	2.72		82.20	18.84		8.30	3.69
	7.25	3.42		97.45	20.84		5.25	2.54
	10.35	4.41		60.45	16.10		3.20	1.78
	21.05	8.00		48.10	14.15		0.56	0.49

8.20 Volumetric Adsorption Data

The temperature at which the isotherms were measured was 6°C. Amount adsorbed W is expressed in micromoles of $CFCl_3$ per gram of adsorbent.

	$MnSO_4$ (200)		$MnSO_4$ (300)		$MnSO_4$ (400)	
	P	W	P	W	P	W
	16.124	12.72	10.588	5.33	15.455	3.21
	31.937	22.26	21.684	9.61	34.748	6.64
	53.068	31.80	32.912	13.52	45.275	8.76
	72.137	40.06	43.474	17.01	57.765	11.16
	93.083	47.85	53.992	20.48	73.288	14.13
			64.960	23.79	90.640	17.72
			76.156	26.94		
			87.340	29.46		

	$ZnSO_4$ (200)		$ZnSO_4$ (300)		$ZnSO_4$ (400)	
	P	W	P	W	P	W
	14.400	3.65	14.210	7.52	25.510	12.01
	32.386	7.83	35.600	13.59	32.960	15.43
	50.495	12.09	55.152	16.93	48.290	18.54
	65.342	15.28	76.926	19.89	61.878	21.21
	89.682	29.23	87.790	21.26	76.363	22.55
'X'	14.392	3.79	97.840	22.63	89.786	24.47
	52.750	11.80				
	77.390	16.66				
	94.110	20.12				

$NiSO_4$ (200)

P	W
17.924	18.52
47.444	43.31
68.974	59.56
90.872	70.34
104.810	75.35

$NiSO_4$ (300)

P	W
21.910	21.79
47.546	41.20
67.392	50.40
85.392	59.72
98.300	65.39

$NiSO_4$ (400)

P	W
15.240	29.32
40.866	51.11
55.066	58.97
71.748	65.90
90.526	72.76

$NiSO_4$ (500)

P	W
18.705	37.97
36.027	54.48
60.310	74.08
75.620	80.44
89.768	179.72

$CoSO_4$ (200)

P	W
22.064	10.75
40.820	19.25
60.624	28.11
86.673	38.22
95.466	41.85

$CoSO_4$ (300)

P	W
20.916	11.17
40.716	21.15
58.692	30.03
79.100	38.63
95.970	44.45

$CoSO_4$ (400)

P	W
18.935	11.80
36.247	18.47
55.227	23.65
72.025	26.79
93.424	30.45

$CoSO_4$ (500)

P	W
23.901	18.12
44.203	25.88
58.967	29.40
20.445	15.71
36.775	22.75
55.460	28.75
72.065	33.16
88.280	37.02

'X'

$CuSO_4$ (200)

P	W
15.292	53.30
31.255	82.41
48.865	104.60
64.105	118.93
83.035	133.32

$CuSO_4$ (300)

P	W
19.158	26.35
34.532	39.90
49.900	51.03
70.835	61.94
88.375	68.99

$CuSO_4$ (400)

P	W
18.738	27.37
33.106	34.62
49.684	39.64
68.480	42.97
89.877	45.78

$CuSO_4$ (500)

P	W
19.645	16.29
35.214	21.31
50.615	24.38
75.296	27.32
91.552	29.29

9.00 Appendix B

List of Tables:

Table no.	Title	Page
1.	Calibration data for balance calibration	
	A. using buoyancy bulb	161
	B. using glass bead	163
2.	Heat of solution and surface area of adsorbents	164
3.	Vapour pressure of $CFCl_3$	165
4.	Monolayer capacity and surface area of calcium sulphate	166
5.	Monolayer capacity and surface area of manganese sulphate	167
6.	Monolayer capacity and surface area of cobalt sulphate	168
7.	Monolayer capacity and surface area of nickel sulphate	169
8.	Monolayer capacity and surface area of copper sulphate	170
9.	Monolayer capacity and surface area of zinc sulphate	171
10.	Heat of solution of potassium chloride at various dilutions	172
11.	Differential entropy calculated for localized adsorbed layer or mobile adsorbed layer	173
12.	CFSE gain on adsorption on nickel oxide	174
13.	Crystal field properties of adsorbents	175
14.	Crystal structure parameters	176
15.	CFSE for various symmetries	180
16.	CFSE change on adsorption for various models	181

17.	Isosteric heat of adsorption, calcium sulphate, manganese sulphate and cobalt sulphate	182
18.	Isosteric heat of adsorption, nickel sulphate and copper sulphate	183
19.	Isosteric heat of adsorption	184
20.	Differential entropy, calcium sulphate and manganese sulphate	185
21.	Differential entropy, cobalt sulphate and nickel sulphate	186
22.	Differential entropy, copper sulphate and zinc sulphate	187

Table 1 A. OBSERVATION DATA FOR BALANCE CALIBRATION USING BUOYANCY BULB

RUN 1	BATH TEMP. 20°C	RUN 2	BATH TEMP. 20°C	RUN 3	BATH TEMP. 20°C
Pressure (torr)	E.M.F. (mV)	Pressure (torr)	E.M.F. (mV)	Pressure (torr)	E.M.F. (mV)
15.3	44.0	19.2	57.5	0.87	3.0
48.2	148.0	38.8	129.0	3.2	10.5
99.9	322.0	81.7	272.0	6.7	23.0
151.0	483.0	111.6	397.0	17.8	60.0
201.9	653.0	161.7	539.0	29.8	97.0
252.6	822.0	220.4	738.0	62.5	207.0
298.0	975.0	180.5	608.0	98.8	328.0
350.4	1154.0	137.7	461.0	150.0	499.0
		101.8	341.0	205.0	682.0
		59.3	204.0	250.6	835.0
		9.2	30.0	290.0	967.0
				341.4	1142.0
				372.9	1248.0
				218.8	727.0
				179.5	596.0

Table 1A (cont'd.)

RUN 3 (Contd.) Pressure (torr)	BATH TEMP. 20°C E.M.F. (mV)	RUN 4 Pressure (torr)	BATH TEMP. 10°C E.M.F. (mV)	RUN 5 Pressure (torr)	BATH TEMP. 20°C E.M.F. (mV)
118.0	390.0	50.2	167.5	50.8	175.0
17.4	59.0	81.8	270.0	118.0	404.0
		149.5	492.5	195.0	667.0
		200.8	665.0	258.0	886.0
		248.9	820.0	153.7	521.0
		301.2	1000.0	94.9	287.0
		255.5	850.0	25.0	82.0
		187.9	625.0		
		137.2	455.0		
		28.4	97.5		

Table 1 B. OBSERVATION DATA FOR BALANCE CALIBRATION USING GLASS BEAD

RUN 1	BATH TEMP. 20°C	RUN 2	BATH TEMP. 20°C	RUN 3	BATH TEMP. 10°C
Pressure (torr)	E.M.F. (mV)	Pressure (torr)	E.M.F. (mV)	Pressure (torr)	E.M.F. (mV)
99.2	3.0	50.0	1.0	106.2	2.5
199.9	6.0	151.5	5.5	151.0	4.0
295.4	10.0	277.8	8.5	201.1	6.0
249.3	9.5	297.4	11.0	264.1	8.5
149.3	5.5	202.4	7.0	172.8	5.5
		99.6	5.0	101.6	2.5
				67.4	1.5

Table 2 HEAT OF SOLUTION AND SURFACE AREA OF THE ADSORBENTS

ADSORBENT	ANNEALING TEMP. (^{o}C)	HEAT OF SOLN. (kcal/mole)	EXCESS HEAT OF SOLN. (kcal/mole) (X-S)	SURFACE AREA (Volumetric) (m^2/g)
	200	14.85	—	9.97
Manganese	300	17.52	—	6.92
Sulphate	400	13.32	—	5.75
	200	21.10	4.05	10.57
Cobalt	300	19.65	-0.42	10.56
Sulphate	400	18.83	2.95	5.23
	500	18.54	—	6.56
	200	22.50	4.40	12.10
Nickel	300	24.81	3.45	11.81
Sulphate	400	12.70	-4.40	11.79
	500	—	—	15.21
	200	18.87	-0.35	23.66
Copper	300	15.29	-7.40	13.43
Sulphate	400	22.69	4.35	6.49
	500	15.35	—	4.43
	200	20.27	—	5.22
Zinc	300	23.99	—	3.61
Sulphate	400	19.59	—	3.97

Table 3

Vapour pressure of $CFCl_3$

Temperature (^{o}C)	Vapour pressure (P_0)	$\log_{10} P_0$	1/T (T in ^{o}K)
20	666.23	2.82362	.003411
6	385.50	2.58602	.003582
-10	191.40	2.28194	.003800

Table 4

Monolayer Capacity and Surface Area of Calcium Sulphate

Annealing Temperature (°C)	Isotherm Temperature (°C)	Monolayer Capacity (μmoles/g)	Specific Surface (m^2/g)	Weight of Sample (g)
200	20.0	73.41	13.79	0.4141
	6.0	73.65	13.81	
	-10.0	73.90	13.86	
300	20.0	58.03	10.90	0.4136
	6.0	58.27	10.93	
	-10.0	58.51	10.98	
400	20.0	49.64	9.32	0.4130
	6.0	48.43	9.08	
	-10.0	49.15	9.23	

Table 5

Monolayer Capacity and Surface Area

of Manganese Sulphate

Annealing Temperature (^{o}C)	Isotherm Temperature (^{o}C)	Monolayer Capacity (μmoles/g)	Specific Surface (m^2/g)	Weight of Sample (g)
200	20.0	41.18	7.74	0.5415
	6.0	40.63	7.63	
	-10.0	41.74	7.83	
300	20.0	28.67	5.38	0.5372
	6.0	29.04	5.45	
	-10.0	29.97	5.62	
400	20.0	23.47	4.43	0.5368
	6.0	23.10	4.34	
	-10.0	23.66	4.45	

Table 6

Monolayer Capacity and Surface Area of Cobalt Sulphate

Annealing Temperature (°C)	Isotherm Temperature (°C)	Monolayer Capacity (μmoles/g)	Specific Surface (m^2/g)	Weight of Sample (g)
200	20.0	54.44	10.23	0.3582
	6.0	54.44	10.23	
	-10.0	54.99	10.33	
300	20.0	76.46	14.35	0.2982
	6.0	76.46	14.35	
	-10.0	76.46	14.35	
400	20.0	70.26	13.20	0.2932
	6.0	70.26	13.20	
	-10.0	72.31	13.59	
500	20.0	58.29	10.95	0.2882
	6.0	58.29	10.95	
	-10.0	58.29	10.95	

Table 7

Monolayer Capacity and Surface Area of Nickel Sulphate

Annealing Temperature (^{o}C)	Isotherm Temperature (^{o}C)	Monolayer Capacity (μmoles/g)	Specific Surface (m^2/g)	Weight of Sample (g)
200	20.0	74.18	13.93	0.4516
	6.0	75.07	14.08	
	-10.0	73.52	13.80	
300	20.0	69.68	13.07	0.4406
	6.0	69.68	13.07	
	-10.0	69.68	13.07	
400	20.0	80.52	15.12	0.4173
	6.0	80.52	15.12	
	-10.0	80.52	15.12	
500	20.0	69.55	13.06	0.4112
	6.0	69.55	13.06	
	-10.0	69.55	13.06	

Table 8

Monolayer Capacity and Surface Area of Copper Sulphate

Annealing Temperature (^{o}C)	Isotherm Temperature (^{o}C)	Monolayer Capacity (μmoles/g)	Specific Surface (m^2/g)	Weight of Sample (g)
200	20.0	46.12	8.65	0.4857
	6.0	44.06	8.28	
	-10.0	42.82	8.03	
300	20.0	35.88	6.74	0.4822
	6.0	35.88	6.74	
	-10.0	35.88	6.74	
400	20.0	21.66	4.06	0.4802
	6.0	22.07	4.14	
	-10.0	22.28	4.19	
500	20.0	8.35	1.57	0.4792
	6.0	8.35	1.57	
	-10.0	8.35	1.57	

Table 9

Monolayer Capacity and Surface Area of Zinc Sulphate

Annealing Temperature (^{o}C)	Isotherm Temperature (^{o}C)	Monolayer Capacity (μmoles/g)	Specific Surface (m^2/g)	Weight of Sample (g)
200	20.0	35.67	6.70	0.5298
	6.0	37.56	7.06	
	-10.0	40.77	7.66	
300	20.0	34.04	6.39	0.5288
	6.0	37.63	7.07	
	-10.0	33.28	6.25	
400	20.0	29.19	5.48	0.5276
	6.0	29.19	5.48	
	-10.0	27.86	5.23	

Table 10

Heat of solution of potassium chloride at various dilutions

Description of state and dilution	Heat of formation[158] (at 25°C) kcal/mole	Heat of solution (at 25°C) kcal/mole
Crystalline	-104.175	——
Std. state, m = 1	-100.060	4.115
in 50 H_2O	-100.105	4.070
100 H_2O	-100.015	4.160
200 H_2O	- 99.974	4.201
400 H_2O	- 99.973	4.202
800 H_2O	- 99.982	4.193
1600 H_2O	- 99.994	4.181
3200 H_2O	-100.008	4.167
6400 H_2O	-100.626	4.149
∞ H_2O	-100.060	4.115

Example of calculation of heat of solution ($\Delta H_{soln.}$) from heat of formation (ΔH_f):

$$K(s) + \tfrac{1}{2}Cl_2(g) \rightarrow KCl(s) \qquad \Delta H_8 = -104.175$$

$$KCl(s) + H_2O \rightarrow KCl(aq) \qquad \Delta H_{soln.} = x$$

$$K(s) + \tfrac{1}{2}Cl_2(g) + H_2O\ (\ell)\ (800\ H_2O) \rightarrow KCl(aq) \qquad \Delta H_f = -99.982$$

$\therefore x = 104.175 - 99.982 = 4.193$ kcal/mole

0.067 moles of KCl in 1000 gms. of water corresponds to 1 mole of KCl in 829 moles of H_2O. The heat of solution of .067 m KCl derived from above table is 4.19 kcal/mole.

Table 11

Differential entropy calculated for localized adsorbed layer or mobile adsorbed layer

θ	$S_g^o - \bar{S}_{local}$ E.U.	$\bar{S}_{local}$ E.U.	$S_g^o - \bar{S}s_{mobile}$ E.U.	$\bar{S}s_{mobile}$ E.U.
0.05	46.20	5.85	14.18	26.17
0.10	44.72	4.37	15.78	24.57
0.15	43.80	3.45	16.83	23.52
0.20	43.11	2.76	17.67	22.68
0.25	42.53	2.18	-	-
0.30	42.03	1.68	19.10	21.25
0.40	41.16	0.81	20.45	19.90
0.50	40.35	0	21.92	18.43
0.60	39.54	-0.81	23.72	16.63
0.70	38.67	-1.68	26.23	14.12
0.80	37.60	-2.75	30.63	9.72
0.90	35.98	-4.37	42.18	1.83

Table 12

Plane	Crystal field	CFSE Dq	Atoms ads.	Final field	CFSE Dq	Gain Dq	Gain per ads. atom
(100)	Sq. pyramidal	-10.0	1	octahedral	-12.0	2.0	2.0
(110)	Tetrahedral	- 3.6	2	"	-12.0	8.4	4.2
(111)	Trigonal	-10.9	3	"	-12.0	1.1	0.4

Table 13

Crystal field properties of adsorbents

Properties	$CoSO_4$			$NiSO_4$			$CuSO_4$		
	(200)	(300)	(400)	(200)	(300)	(400)	(200)	(300)	(400)
Excess heat of soln. (X-S) kcal/mole	4.05	-0.42	2.95	4.40	3.45	-4.40	-0.35	-7.40	4.35
CFSE in aqueous Soln. (S). kcal/mole $-4/5\Delta$. Δ from ref. 191		21.16			29.01			21.50	
Adsorbents CFSE (X) kcal/mole	17.11	21.58	18.21	24.61	25.56	33.41	21.85	28.90	17.15
Unit Dq value for octahedral structure see section 6.20 kcal/mole	2.14	2.70	2.28	2.05	2.13	2.78	3.64	4.82	2.86

Crystal field parameters derived from heat of solution data of Jamieson et al[213] and Frost et al[214]

$(X-S)_{max}$ (kcal/mole)	8.07	(Jamieson)	6.19	(Jamieson)	3.51 (Frost)
$(X-S)_{min}$ (kcal/mole)	6.52	"	6.04	"	-3.83 "
X_{max} (kcal/mole)	12.99	"	22.82	"	17.99 "
X_{min} (kcal/mole)	14.65	"	22.97	"	25.33 "
Unit Dq value from X_{max}	1.62	"	1.90	"	3.00 "
Unit Dq value from X_{min}	1.83	"	1.91	"	4.22 "
Dq value of $M(H_2O)^{++}$ [191] from orgel's S value in aqueous solution kcal/mole	2.65		2.42		3.58

Table 14

Crystal Parameters

(i) Unit Cell Dimensions

Parameter	$CoSO_4$ 'A'	$CoSO_4$ 'B'	$NiSO_4$	$CuSO_4$
	A^o	A^o	A^o	A^o
a	5.198 '	8.62	5.155	8.396
b	7.871	6.70	7.842	6.698
c	6.522	4.75	6.338	4.829

(ii) Area of planes and number of cations:

$CoSO_4$ 'A' is isostructural with $NiSO_4$.

$CoSO_4$ 'B' is isostructural with $CuSO_4$.

Both types of crystal structures are shown in Figure 67.

All the length units are in Angströms (A^o).

Plane	$CoSO_4$'A'	$CoSO_4$'B'	$NiSO_4$	$CuSO_4$	Number of cations/unit cell	
					Struc. A	Struc. B
(001)	40.91	57.75	40.43	56.24	2	2
(100)	51.34	31.85	49.70	32.35	2	2
(110)	61.52	51.87	59.48	51.86	4	2
(111)	28.77	31.69	27.98	31.18	1	1
(010)	33.90	40.95	32.67	40.54	2	2
(101)	65.64	65.93	64.07	55.33	2	4
(011)	53.12	70.77	51.96	69.35	2	2

Table 14 (cont'd)

(iii) Surface area and monolayer capacity of adsorbents:

	Cobalt Sulphate			
Annealing Temperature (^{o}C)	200	300	400	500
Surface area ($A^{o2} \times 10^{20}$)	3.66	4.28	3.90	3.15
Monolayer Capacity (moles $\times 10^{-6}$)	19.5	22.8	20.8	16.8
No. of moles of $CFCl_3$ @ θ=1 (moles $\times 10^{20}$)	0.117	0.137	0.125	0.101

	Nickel Sulphate			
Annealing Temperature (^{o}C)	200	300	400	500
Surface area ($A^{o2} \times 10^{20}$)	6.29	5.76	6.29	5.37
Monolayer Capacity (moles $\times 10^{-6}$)	33.5	30.7	33.53	28.6
No. of moles of $CFCl_3$ @ θ=1 (moles $\times 10^{20}$)	0.202	0.185	0.202	0.172

	Copper Sulphate			
Annealing Temperature (^{o}C)	200	300	400	500
Surface area ($A^{o2} \times 10^{20}$)	4.04	3.25	1.98	0.75
Monolayer Capacity (moles $\times 10^{-6}$)	21.53	17.30	10.57	4.00
No. of moles of $CFCl_3$ @ θ=1 (moles $\times 10^{20}$)	0.130	0.104	0.064	0.024

Table 14 (cont'd)

(iv) Area per cation:

Plane	$CoSO_4$ 'A'	$CoSO_4$ 'B'	$NiSO_4$	$CuSO_4$
(001)	20.45	28.88	20.22	28.12
(100)	25.67	15.93	24.85	16.18
(110)	15.38	25.94	14.87	25.93
(111)	28.77	31.69	27.98	31.18
(010)	16.95	20.48	16.34	20.27
(101)	32.82	16.48	32.04	13.83
(011)	26.56	35.39	25.98	34.68

(v) Number of cations on each plane (at surface annealed at $200^{\circ}C$). Each number to be multiplied by 10^{20}.

Plane	$CoSO_4$ 'A'	$CoSO_4$ 'B'	$NiSO_4$	$CuSO_4$
(001)	0.179	0.127	0.311	0.144
(100)	0.143	0.230	0.253	0.250
(110)	0.238	0.141	0.423	0.156
(111)	0.127	0.116	0.225	0.130
(010)	0.216	0.179	0.385	0.199
(101)	0.112	0.222	0.196	0.292
(011)	0.138	0.103	0.242	0.117

Table 14 (cont'd)

(vi) Number of $CFCl_3$ moles per cation:

Plane	$CoSO_4$ 'A'	$CoSO_4$ 'B'	$NiSO_4$	$CuSO_4$
(001)	0.65	0.92	0.65	0.90
(100)	0.82	0.51	0.79	0.52
(110)	0.49	0.83	0.48	0.83
(111)	0.92	1.01	0.90	1.00
(010)	0.54	0.65	0.53	0.65
(101)	1.05	0.53	1.03	0.45
(011)	0.85	1.14	0.84	1.11

Table 15

Crystal field stabilization energy for various surface environments for adosrbents.

Symmetry	coord. number	Cobalt(II)	Nickel(II)	Copper(II)
Trigonal	3	- 7.73 Dq	-10.94 Dq	- 5.48 Dq
Tetrahedral	4	- 5.34	- 3.56	- 1.78
Square planar	4	-10.28	-14.56	-12.26
Trigonal bipyramidal	5	- 5.45	- 6.27	- 7.09
Square pyramid	5	- 9.14	-10.00	- 9.14
Octahedral	6	- 8.00	-12.00	- 6.00
Pentagonal bipyramidal	7	-10.55	- 7.73	- 4.91
Hush's intermediate	7	- 8.69	-10.20	- 8.81

Table 16

CFSE change on adsorption for various models

ΔCFSE in kcal per mole of $CFCl_3$

Model (surface structures)		Cobalt Sulphate			Nickel Sulphate			Copper Sulphate		
(Before ads.)	(After ads.)	(200)	(300)	(400)	(200)	(300)	(400)	(200)	(300)	(400)
Tetrahedral	Trig. bipyr.	0.24	0.30	0.25	5.56	5.77	7.53	19.33	25.59	15.19
Sq. pyramidal	Octahedral	Fin. struc. less stable			4.10	4.26	5.56	Fin. struc. less stable		
Octahedral	Hush's inter.	1.48	1.86	1.57	Fin. struc. less stable			10.23	13.54	8.04
Octahedral	Pent. bipyr.	5.46	6.89	5.81	Fin. struc. less stable			Fin. struc. less stable		
Trigonal	Trig. bipyr.	Fin. struc. less stable			Fin. struc. less stable			2.93	3.88	2.30
Trig. bipyr.	Pent. bipyr.	10.91	13.77	11.63	1.50	1.56	2.03	Fin. struc. less stable		
Sq. planar	Sq. pyramidal	Fin. struc. less stable			Fin. struc. less stable			Fin. struc. less stable		
Sq. planar	Octahedral	Fin. struc. less stable			Fin. struc. less stable			Fin. struc. less stable		
Excess heat of ads.		0.30	1.50	2.75	1.35	1.50	1.80	2.20	2.20	2.55

Table 17

Isosteric Heat of Adsorption

θ	Calcium Sulphate			Manganese Sulphate			Cobalt Sulphate			
	200	300	400	200	300	400	200	300	400	500
0*	8.30	7.70	7.50	8.50	8.20	7.80	8.30	9.50	10.75	10.50
0.05	8.23	6.95	8.02	9.00	9.15	7.90	7.46	10.63	11.58	9.60
0.1	8.90	7.30	7.93	8.25	8.00	7.70	8.00	9.57	8.72	8.51
0.15	9.55	8.65	8.12	8.05	7.95	7.75	7.67	9.00	10.18	7.65
0.2	9.35	9.00	8.35	8.00	7.41	7.75	7.55	9.00	9.96	7.25
0.3	9.42	9.55	8.70	7.40	7.00	7.74	7.35	8.91	9.70	7.17
0.4	9.26	8.68	8.38	7.35	7.02	7.45	7.03	8.82	9.65	6.62
0.5	8.65	8.75	8.48	7.15	7.20	7.00	7.23	8.51	8.96	6.82
0.6	8.48	8.45	8.30	7.10	7.20	7.55	6.90	7.88	8.72	6.72
0.7	8.15	8.35	8.48	7.20	7.13	7.80	6.42	7.97	8.39	5.59
0.8	8.20	7.83	8.10	7.10	7.17	7.75	6.95	7.84	8.23	6.85
0.9	7.95	8.00	8.00	7.15	7.07	7.85	6.70	7.81	8.15	6.70
1.0	7.45	7.55	7.65	7.12	6.85	7.75	6.50	7.51	7.85	6.57
'Excess' heat							0.30	1.50	2.75	2.53

* q_{st} θ=0 values are extrapolated values from the q_{st} vs θ curves.

The isosteric heat has been expressed in kcal/mole in Tables 17, 18 and 19.

Table 18

Isosteric Heat of Adsorption

θ	Nickel Sulphate				Copper Sulphate			
	200	300	400	500	200	300	400	500
0*	9.15	9.45	9.90	11.60	9.80	10.05	10.50	11.70
0.05	10.72	9.93	8.12	11.96	10.30	10.12	10.22	-
0.1	8.83	8.91	8.01	10.42	9.42	9.58	9.25	10.20
0.15	8.37	8.88	8.60	9.23	7.73	8.95	9.87	9.12
0.2	8.38	8.44	8.65	8.81	9.16	8.26	8.42	8.67
0.3	8.04	8.12	8.04	8.40	8.65	7.98	9.37	8.97
0.4	7.73	7.97	7.44	8.43	8.32	8.15	8.92	8.98
0.5	7.78	7.62	7.73	8.86	7.88	7.61	8.50	8.80
0.6	7.58	7.66	7.75	8.75	7.87	7.66	8.39	8.63
0.7	7.62	7.53	7.54	8.44	7.55	7.83	8.15	7.97
0.8	7.56	7.40	7.47	8.31	7.51	7.56	8.17	7.39
0.9	7.62	7.23	7.32	7.97	7.37	7.76	8.07	6.74
1.0	7.58	7.00	7.04	7.78	7.37	7.27	7.37	6.53
'Excess' heat	1.35	1.50	1.80	3.37	2.20	2.20	2.55	2.95

* q_{st} θ=0 values are extrapolated values from the q_{st} vs θ curves.

Table 19

Isosteric Heat of Adsorption

θ	Zinc Sulphate		
	200	300	400
0*	7.35	7.75	8.30
0.05	7.80	8.50	9.20
0.1	7.20	7.54	8.20
0.15	7.00	7.50	8.40
0.2	7.15	7.48	8.30
0.3	7.00	7.17	7.78
0.4	6.80	7.39	7.50
0.5	6.81	7.40	7.52
0.6	7.00	7.20	7.35
0.7	6.85	7.30	7.30
0.8	7.09	7.15	7.30
0.9	7.30	7.00	7.07
1.0	7.30	6.95	6.95

* q_{st} θ=0 values are extrapolated values from the q_{st} vs θ curves.

Table 20

Differential Entropy

	Calcium Sulphate			Manganese Sulphate		
Annealing temp.	200	300	400	200	300	400
θ						
0.05	28.18	32.37	28.85	19.90	21.06	25.64
0.1	27.16	27.69	31.24	18.40	26.85	24.65
0.15	19.92	22.32	26.78	20.66	22.87	21.62
0.2	22.14	21.25	20.32	19.61	23.38	23.03
0.3	17.10	17.98	18.55	22.70	23.62	22.00
0.4	17.83	19.92	21.17	21.35	23.21	22.33
0.5	17.32	18.93	19.92	20.96	22.28	22.62
0.6	19.08	19.10	19.59	19.84	20.72	20.64
0.7	19.16	18.42	17.35	21.35	20.87	19.17
0.8	17.98	19.73	17.16	20.93	19.65	19.05
0.9	18.16	18.04	19.00	21.59	19.81	17.90
1.0	15.84	18.92	15.81	21.26	20.00	18.00

Differential entropies have been expressed in entropy units (kcal per mole per degree) in Tables 20, 21 and 22.

Table 21

Differential Entropy

Annealing temp.	Cobalt Sulphate				Nickel Sulphate			
	200	300	400	500	200	300	400	500
θ								
0.05	24.95	15.52	12.18	19.58	13.55	21.17	24.78	12.93
0.1	21.19	17.66	21.85	21.79	18.91	19.39	23.42	16.64
0.15	21.34	19.88	15.06	23.80	19.55	18.34	20.25	19.64
0.2	20.97	18.19	14.97	24.71	18.86	19.19	19.36	20.14
0.3	20.76	17.46	15.01	23.95	19.02	19.42	20.34	20.40
0.4	21.19	16.93	14.28	24.30	19.37	19.66	20.64	19.41
0.5	20.12	17.42	16.14	23.62	18.67	19.92	19.90	17.17
0.6	20.92	19.11	16.50	23.41	18.93	19.08	19.26	16.25
0.7	23.32	18.42	17.30	25.85	18.40	19.18	19.46	17.32
0.8	19.90	18.30	17.12	22.10	18.21	19.92	19.17	17.15
0.9	20.60	17.94	17.11	22.08	17.65	19.45	19.21	17.79
1.0	20.92	18.54	17.26	22.00	17.36	19.90	19.77	17.90

Table 22

Differential Entropy

Annealing temp.	Copper Sulphate				Zinc Sulphate		
	200	300	400	500	200	300	400
θ							
0.05	21.21	19.10	20.07	23.46	23.40	21.26	18.75
0.1	22.98	19.21	21.10	24.12	24.01	23.55	20.68
0.15	27.93	20.09	17.78	20.57	23.91	22.30	18.92
0.2	22.10	21.63	22.11	21.16	22.20	21.55	18.77
0.3	22.54	21.38	11.19	18.61	21.62	21.71	19.72
0.4	22.85	19.76	17.50	17.01	21.76	19.45	19.96
0.5	23.70	20.90	18.18	17.22	21.48	19.81	19.39
0.6	23.19	20.18	17.86	17.04	20.35	19.81	19.34
0.7	23.85	18.97	18.21	18.84	20.43	19.21	19.10
0.8	23.53	19.40	17.37	20.23	18.68	19.49	18.70
0.9	23.60	18.21	17.23	21.93	17.89	19.36	19.06
1.0	23.26	19.27	19.21	22.16	17.83	19.49	19.19

10.00

Appendix C (Figures)

List of Figures

Fig. no.	Title	Page
1.	Reference bulb	196
2.	Top view of balance assembly	196
3.	Side view of balance assembly	197
4.	Side view of the balance beam	198
5.	Top view of the balance beam	198
6.	Balance beam and support	199
7.	Electromagnetic compensation circuit	200
8.	Phototransistor circuit	200
9.	Balance calibration plots	201
10.	Vacuum line and equilibrium manifold	202
11.	Low temperature control assembly	203
12.	Calorimeter cell assembly	204
12A.	Twin calorimeter	205
13.	Electrical calibration circuit	205
14.	Calorimetric measurement [heat of solution of $CuSO_4$ (300)]	206
15.	Volumetric BET apparatus	207
16.	An isotherm plot containing gravimetric and volumetric points	208
17.	Vapour pressure plot for $CFCl_3$	209
18.	Isotherms for $MnSO_4$ (200)	210
19.	Isotherms for $MnSO_4$ (300)	211

20.	Isotherms for $MnSO_4$ (400)	212
21.	Isotherms for $CoSO_4$ (200)	213
22.	Isotherms for $CoSO_4$ (300)	214
23.	Isotherms for $CoSO_4$ (400)	215
24.	Isotherms for $CoSO_4$ (500)	216
25.	Isotherms for $NiSO_4$ (200)	217
26.	Isotherms for $NiSO_4$ (300)	218
27.	Isotherms for $NiSO_4$ (400)	219
28.	Isotherms for $NiSO_4$ (500)	220
29.	Isotherms for $CuSO_4$ (200)	221
30.	Isotherms for $CuSO_4$ (300)	222
31.	Isotherms for $CuSO_4$ (400)	223
32.	Isotherms for $CuSO_4$ (500)	224
33.	Isotherms for $ZnSO_4$ (200)	225
34.	Isotherms for $ZnSO_4$ (300)	226
35.	Isotherms for $ZnSO_4$ (400)	227
36.	Isotherms for $CaSO_4$ (200)	228
37.	Isotherms for $CaSO_4$ (300)	229
38.	Isotherms for $CaSO_4$ (400)	230
39.	BET plots for $MnSO_4$ (300)	231
40.	BET plots for $NiSO_4$ (400)	232
41.	Isosteric heat curves for $MnSO_4$	233
42.	Isosteric heat curves for $CoSO_4$	234
43.	Isosteric heat curves for $NiSO_4$	235

44.	Isosteric heat curves for $CuSO_4$	236
45.	Isosteric heat curves for $ZnSO_4$	237
46.	Isosteric heat curves for $CaSO_4$	238
47.	Differential entropy vs. coverage for $MnSO_4$	239
48.	Differential entropy vs. coverage for $CoSO_4$	240
49.	Differential entropy vs. coverage for $NiSO_4$	241
50.	Differential entropy vs. coverage for $CuSO_4$	242
51.	Differential entropy vs. coverage for $ZnSO_4$	243
52.	Differential entropy vs. coverage for $CaSO_4$	244
53.	Differential entropy of localized model vs. θ	245
54.	Differential entropy of mobile model vs. θ	246
55.	Excess heat of adsorption for adsorbents annealed at 200°C	247
56.	Excess heat of adsorption for adsorbents annealed at 300°C	248
57.	Excess heat of adsorption for adsorbents annealed at 400°C	249
58.	Excess heat of adsorption for adsorbents annealed at 500°C	250
59.	Excess heat of solution for samples annealed at 200°C	251
60.	Excess heat of solution for samples annealed at 300°C	252

61.	Excess heat of solution for samples annealed at 400°C	253
62.	Surface area change with annealing temperatures	254
63.	Melting point versus the extrapolated annealing temperature	255
64.	Crystal field splittings for various symmetries	256
65.	A. Octahedral field around a cation B. d orbitals in an octahedral field	257
66.	Changes in nickel ion coordination during chemisorption of oxygen on NiO	258
67.	Crystal structues and crystal planes	259
68.	Volumetric BET plot for $CuSO_4$ (200)	260

10.10

LEGEND FOR FIGURES

Figures 2 to 6:

1. Solenoid. 2. Solenoid connections. 3. Light bulbs (25 watts each). 4. Support. 5. Aluminium box with phototransistors circuit. 6. Balance case. 7. B.45 cone and socket. 8. B.34 cone and socket. 9. Phototransistor circuit connections. 10. Sample bulb. 11. Reference bulb. 12. Inert gas inlet stopcock. 13. Inert gas inlet. 14. Quartz rods (2 mm) supporting frame. 15. Support for the tungsten wire. 16. Thin tungsten wire. 17. Balance beam and beam arrests. 18. Aluminium foil. 19. Secondary fulcrum (tungsten wire). 20. Balance beam arrest. 21. Magnet. 22. Quartz weight to adjust centre of gravity. 23. Balance frame.

Figure 7:

1. Regulated power supply (23.3 volts technipower PC-23.3-0.100). 2. IK resistance. 3. Coarse adjust (IKΩ in ten turns, Bourns). 4. Fine adjust (100Ω in ten turns, Bourns). 5. Double pole double throw switch. 6. Standard resistor (Gen. radio 100Ω ± 0.05%). 7. Solenoid (approx. 100Ω). 8. Potentiometer.

Figure 8:

1. and 2. Matched phototransistors (Phillips OCP 71). 3. Regulated power supply unit 23.3 volts (Technipower PC-23, 3-0, 100). 4. Galvanometer (G.H. Laboratories Inc.) (Catalogue N. 570-212).

Figure 9:

1. Change in E.M.F. with pressure using glass bead. 2. Change in E.M.F. with pressure using buoyancy bulb. ◯ Points measured while increasing pressure. ◍ Points measured while decreasing pressure.

Figure 10:

1. and 2. Mcleod gauges. 3. Manometer. 4. Stopcock. 5. Cold trap. 6, 7 and 8. Bulbs. 9. Bellows.

Figure 11:

A and B. Dewars. C. Constant temperature bath. D. Pinchcocks. E. Pump. F. Copper cooling coils. T. Thermometers.

Figure 12:

1. Dewar. 2. Stirrer. 3. Heater. 4. Thermopile. 5. Sample bulb holder (plate). 6. Sample bulb. 7. Plexi-ring. 8. 'O' ring. 9. Plexi-top. 10. Bolt. 12. Thermopile leads. 13. Stainless steel rod. 14. Stirrer-shaft. 15. Motor for stirrer. 16. Teflon tubing. 17. 'O' ring on stirrer rod. 18. Heater leads.

Figure 13:

1. Electrical clock. 2. Double pole double throw switch. 3. Standard resistance (one ohm). Model 601, Ballantine laboratories. 4. Potentiometer. 5. Stabilized power

supply unit (constant voltage and constant current). Harrison 6200 B, DC, S. No. prefix 6A Hewlett Packard. H_1 and H_2. Heating coils.

Figure 15:

1 to 6. Stopcocks. 7. Capacitance manometer lower plate. 8 and 9. Stopcocks. 10. Sample bulb. 11. Capillary. 12. P.V.C. tubing. 13. Glass wool. 14. Sample. 15. Outer jacket. 16. Constant temperature bath. 17. Glass to pyrex seal.

Figure 18 to 40:

⊡ Adsorption points at -10°C. ⊙ Adsorption points at 6°C. △ Adsorption points at 20°C. Half-filled squares, circles or triangles represent desorption points.

Figure 41 to 52:

⊙ Points for adsorbents annealed at 200°C. ⊙ Points for adsorbents annealed at 300°C. ⊙ Points for adsorbents annealed at 400°C. ⊡ Points for adsorbents annealed at 500°C.

Figure 63:

The symbol of the element represents corresponding sulphate compound. e.g. Cu stands for copper sulphate.

Figure 65A:

● Cation. ○ Anion.

Figure 66:

(A) (100) plane. (B) (110) plane. (C) (111) plane.

● Nickel ion. ○ Lattice oxygen ion. ◍ Adsorbed oxygen ions. Middle column refers to a bare surface at the instant of cleavage; left column, bare surface, relaxed position; right column, after adsorption of oxygen. (After Haber & Stone[205]).

Figure 1. Reference bulb

Figure 2.

BALANCE ASSEMBLY

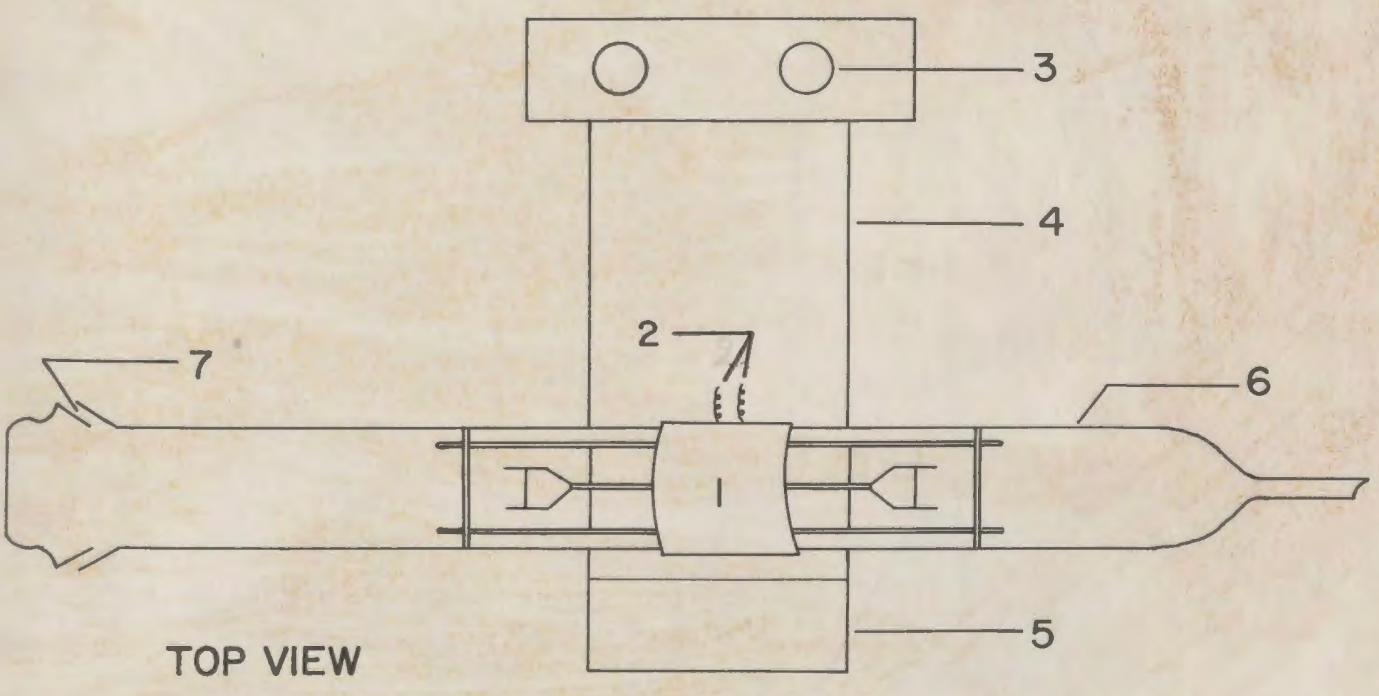

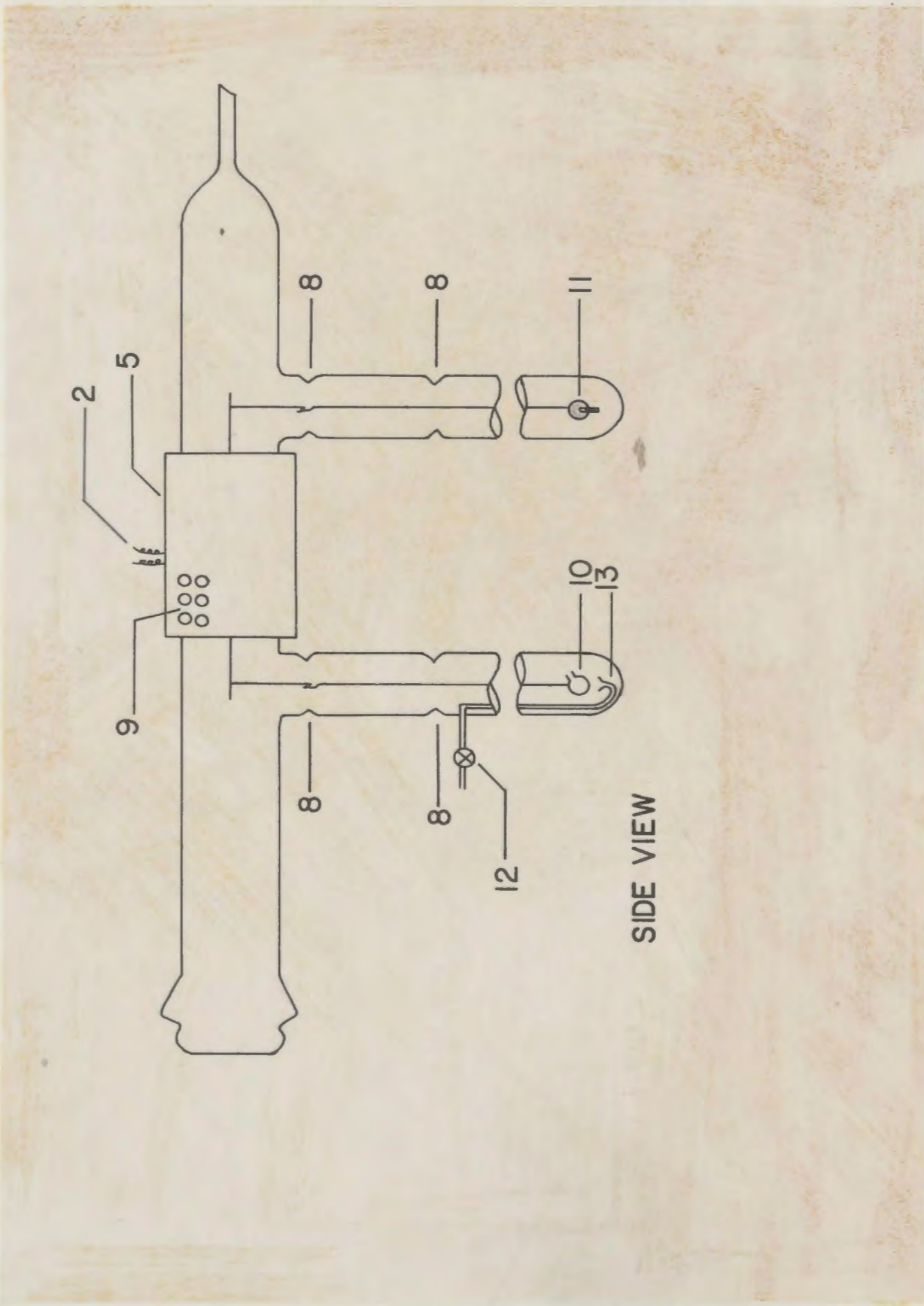

Figure 3. Balance assembly

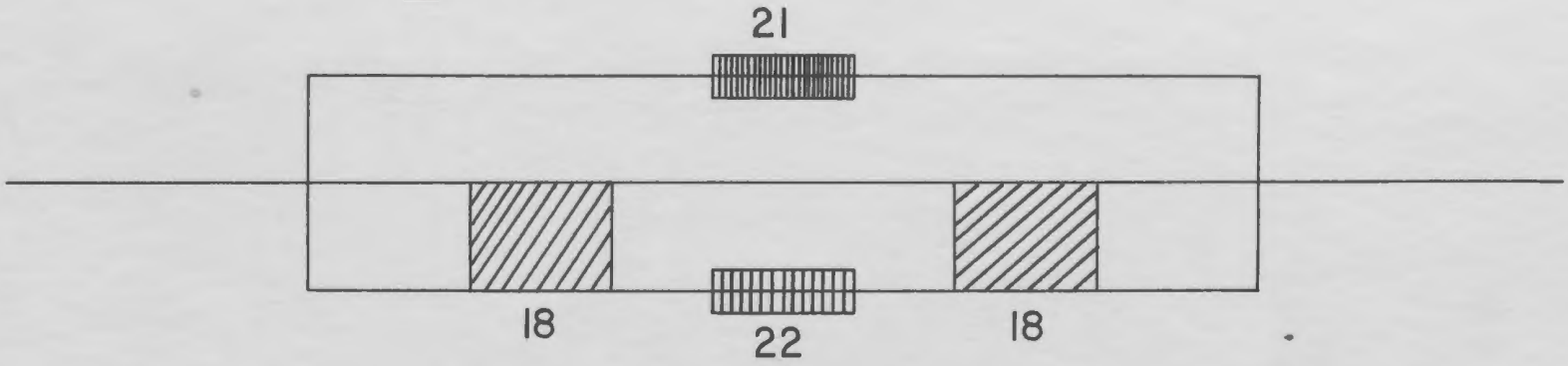

Figure 4. SIDE VIEW OF THE BEAM

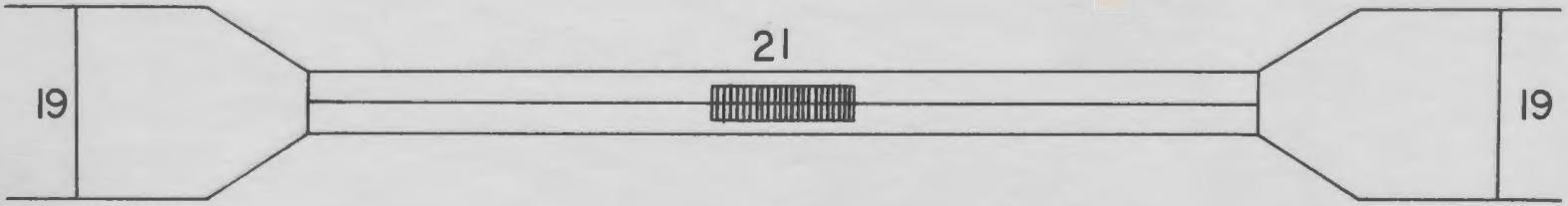

Figure 5. TOP VIEW OF THE BEAM

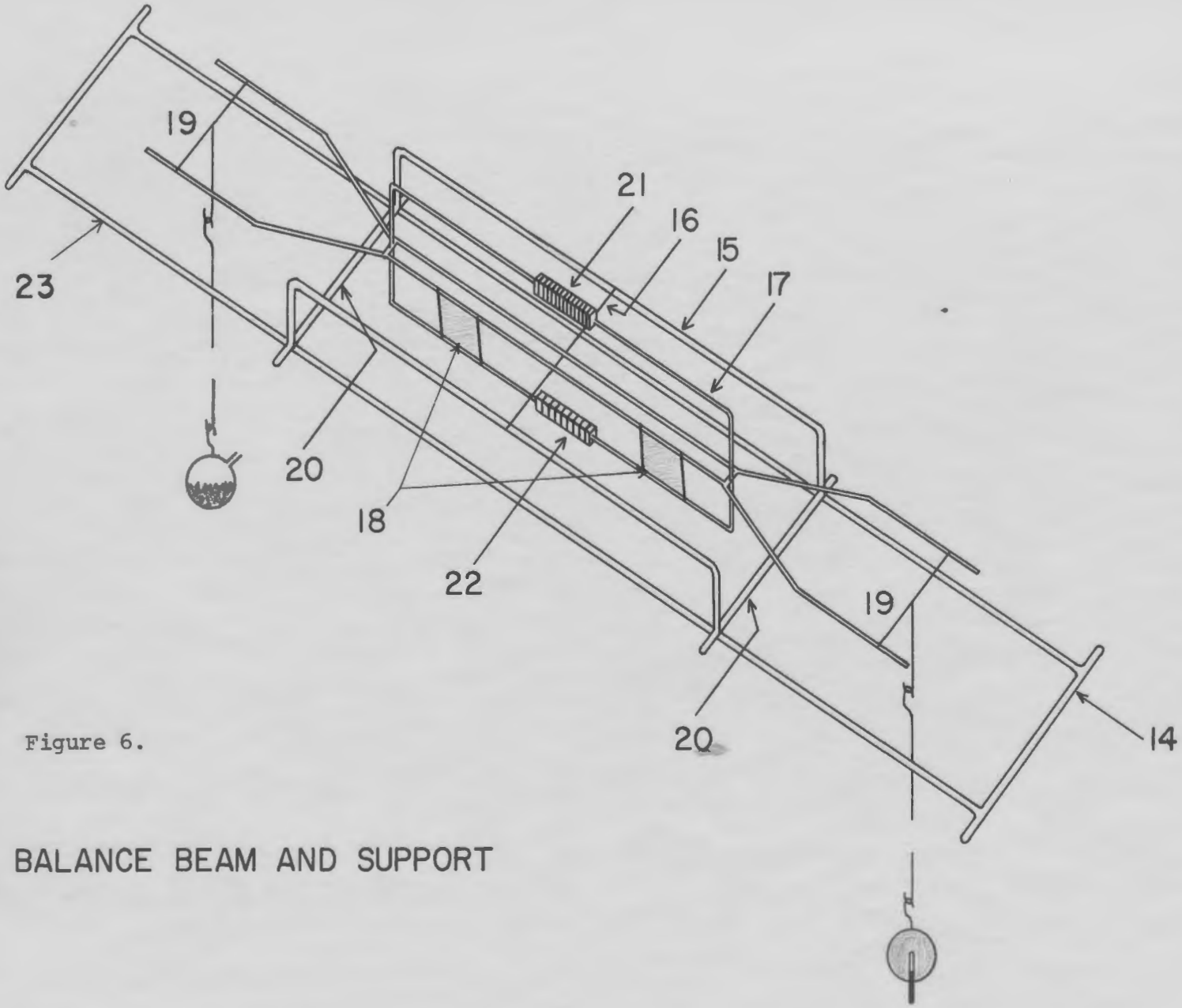

Figure 6.

BALANCE BEAM AND SUPPORT

Figure 7.

ELECTROMAGNETIC COMPENSATION CIRCUIT

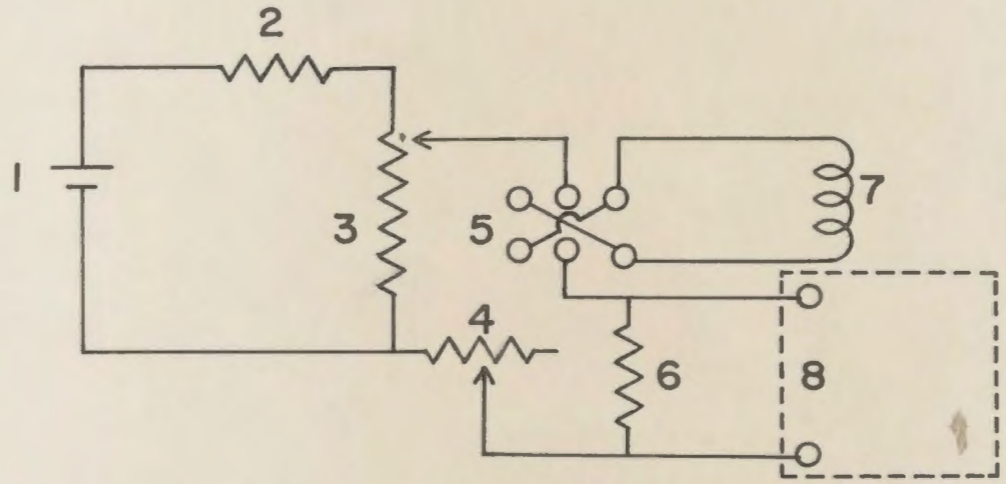

Figure 8.

PHOTOTRANSISTOR CIRCUIT

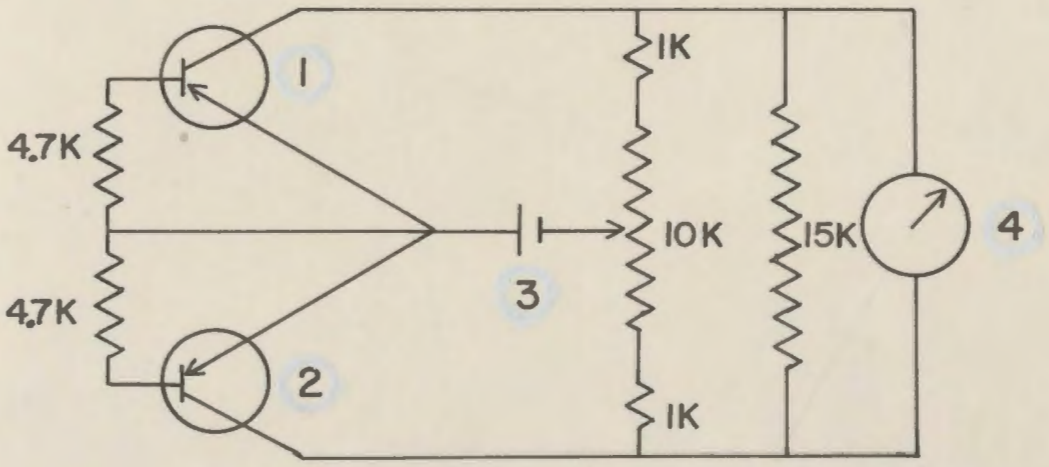

Figure 9. Balance calibration plots

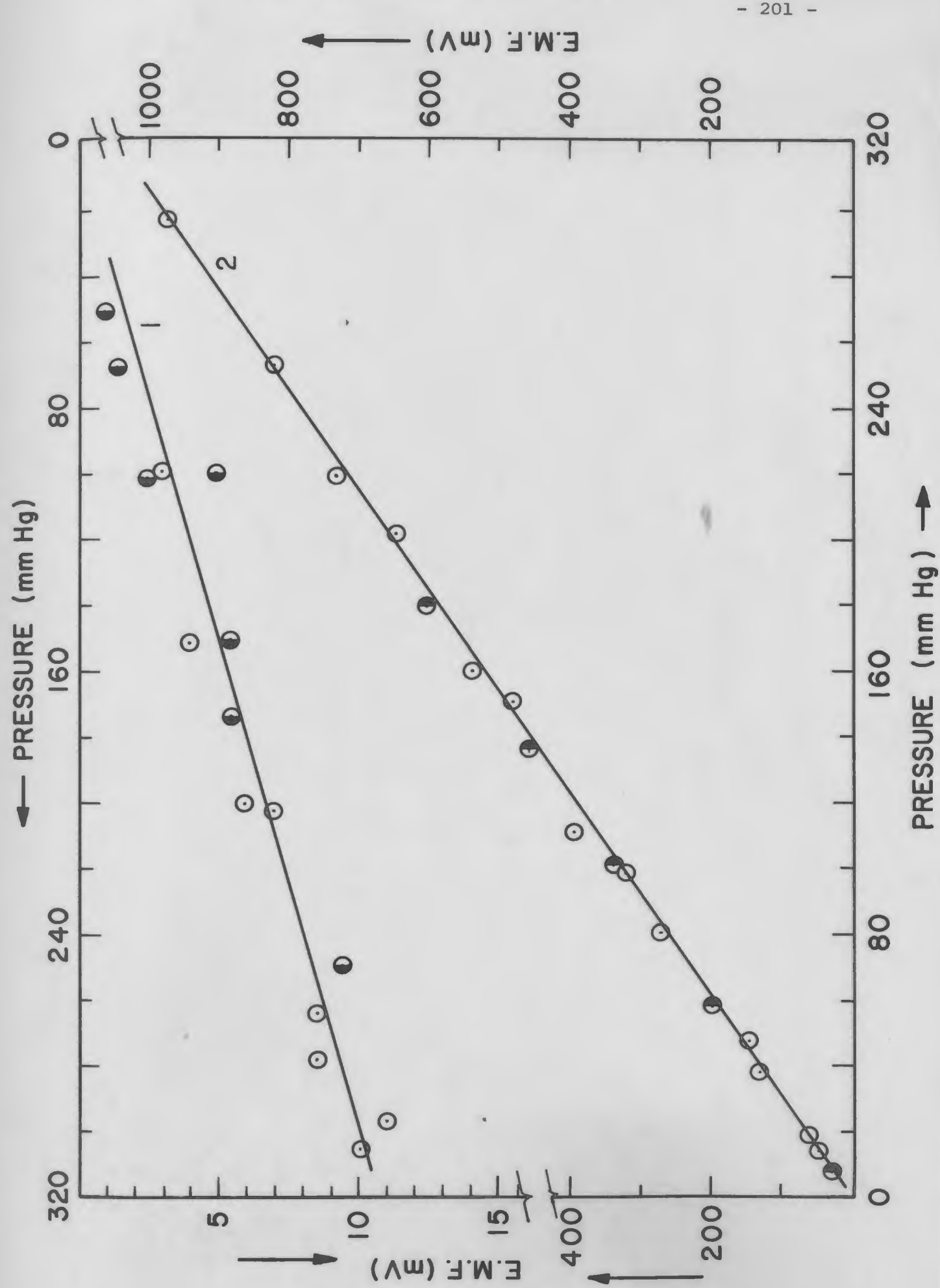

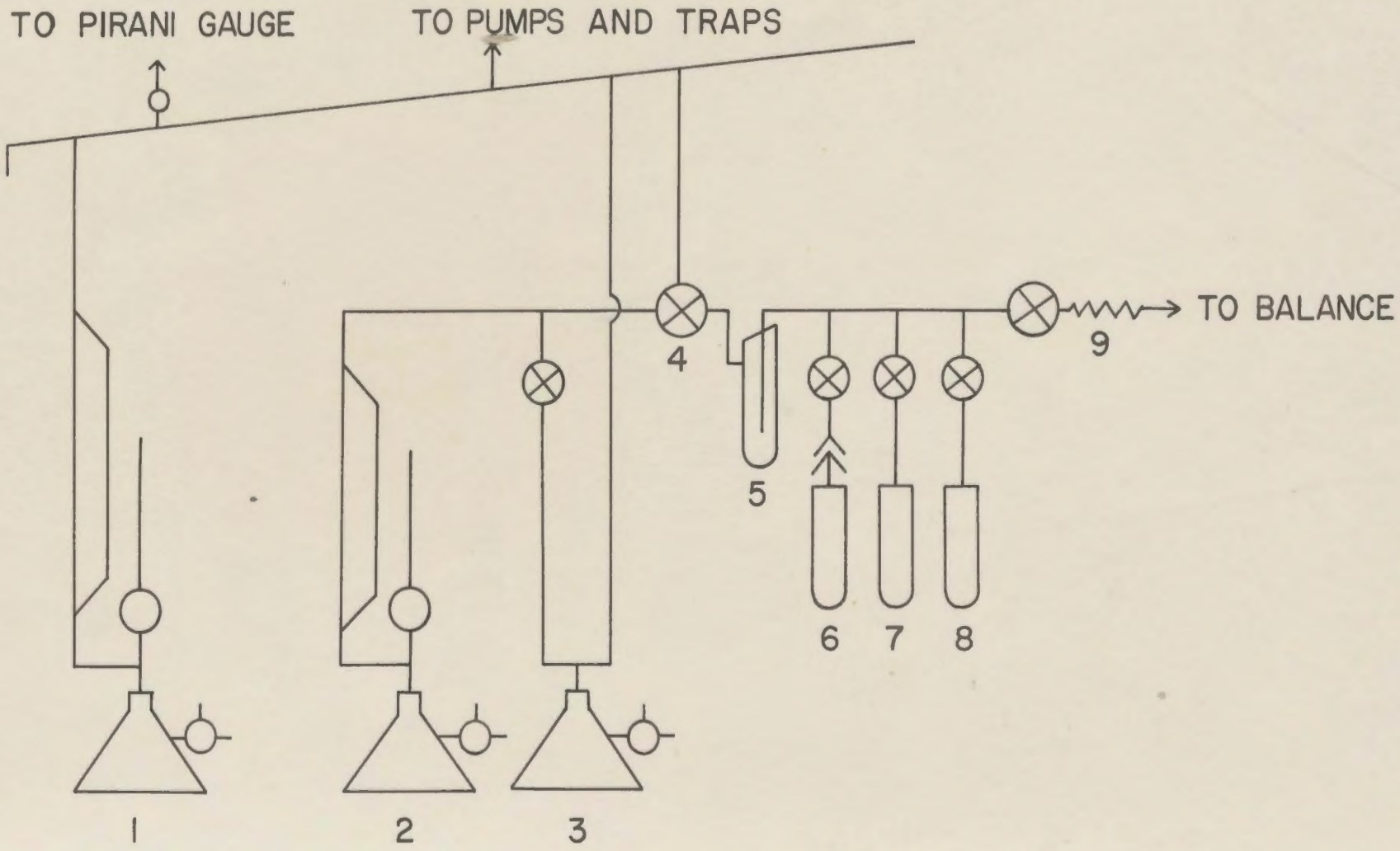

Figure 10. Vacuum line and Equilibrium manifold

Figure 11. Low temperature control assembly

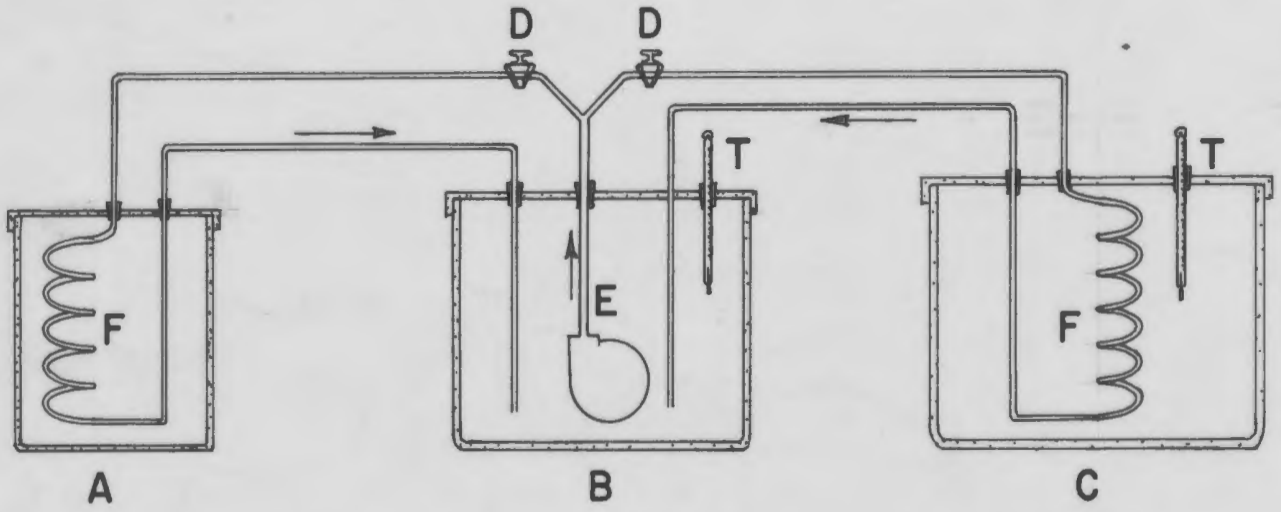

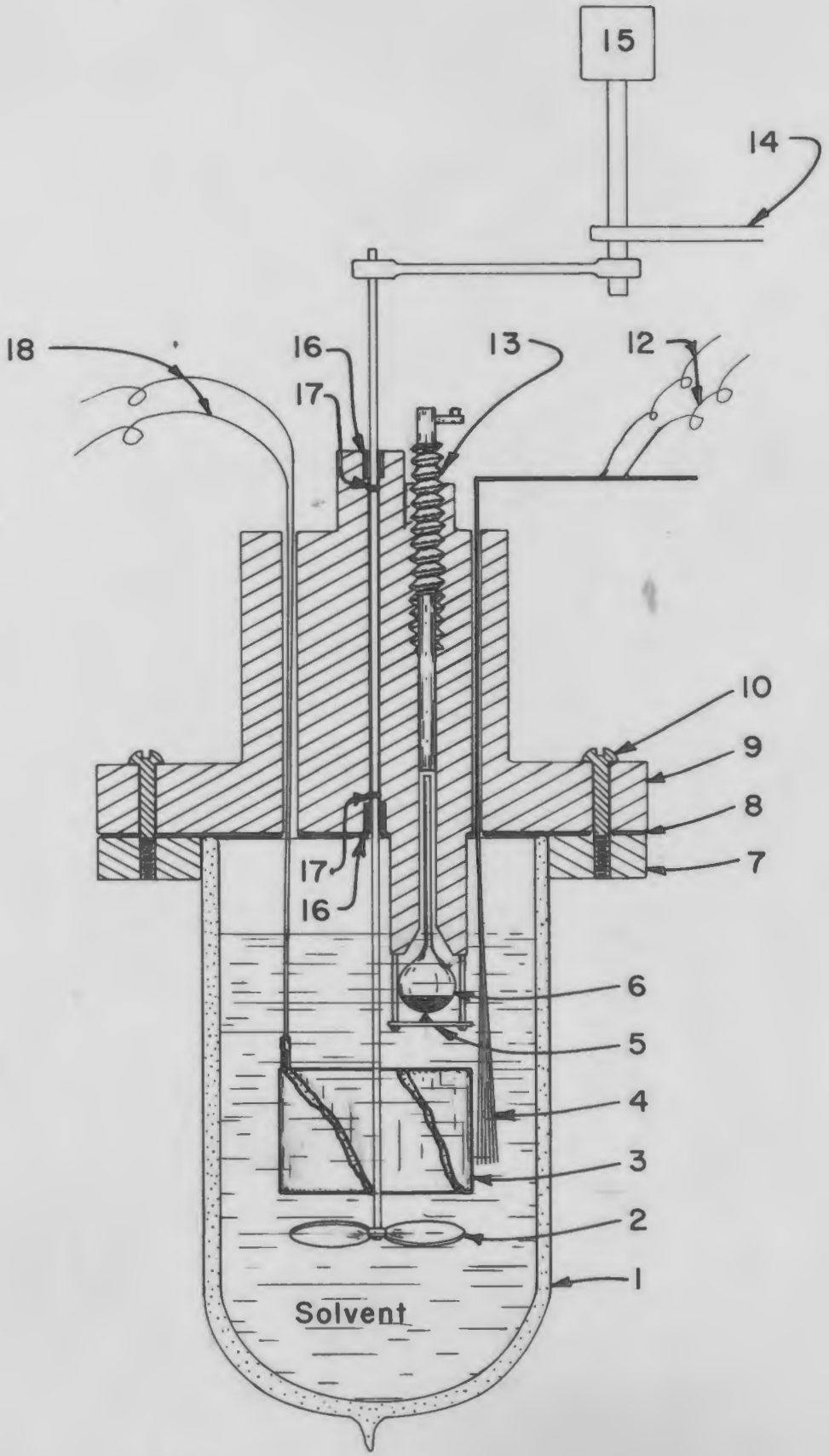

Figure 12. Calorimeter cell assembly

Figure 12A. Twin calorimeters

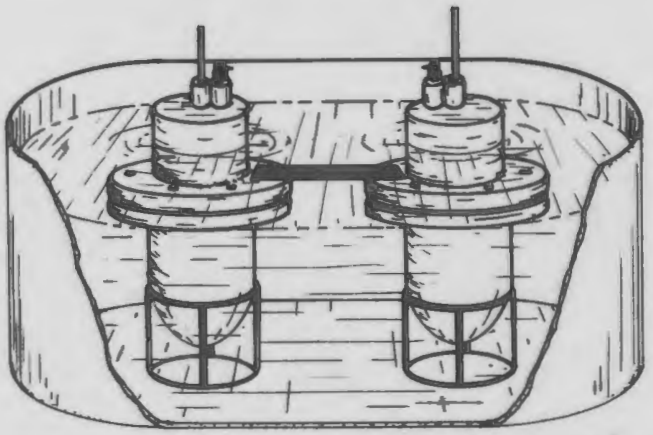

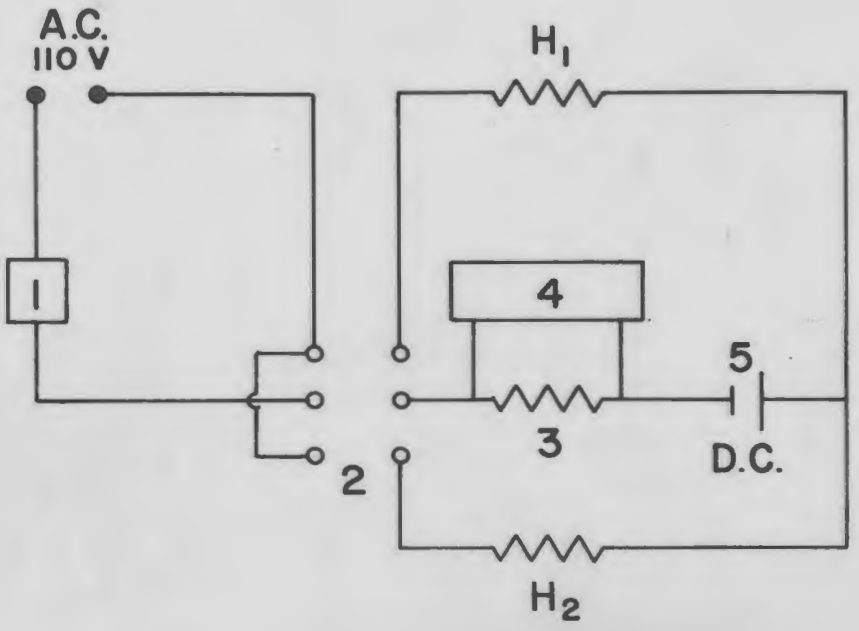

Figure 13. Electrical calibration circuit

Figure 14. Calorimetric measurement
Heat of solution of $CuSO_4$ (300)

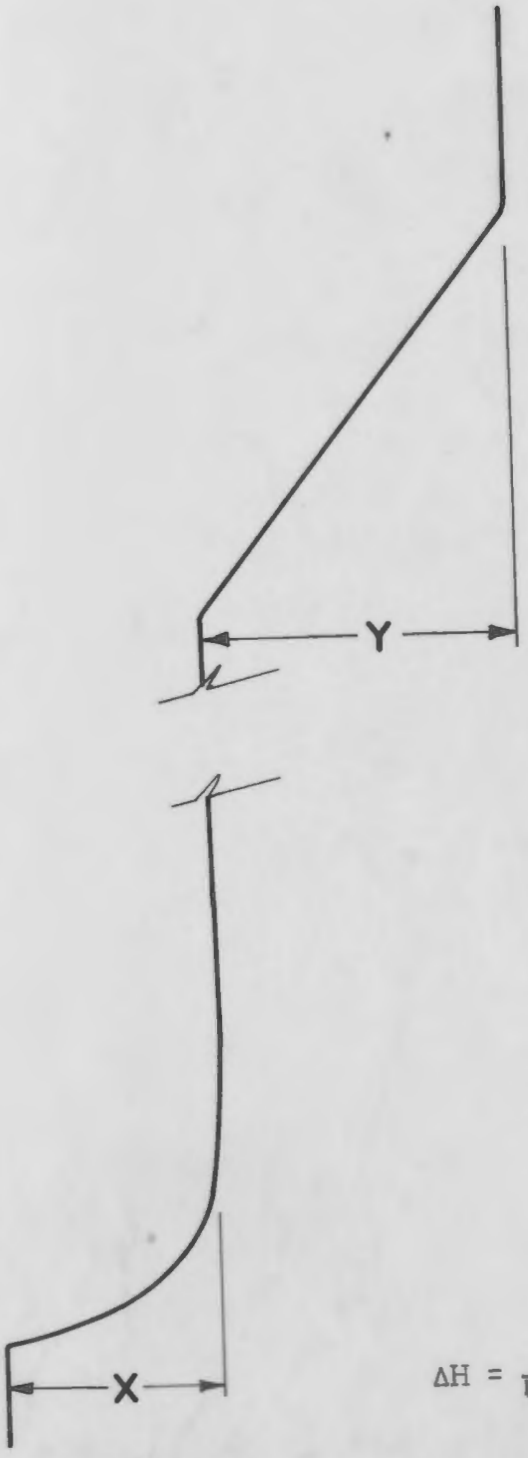

Time of heating: 150.3 sec.

Current: 0.12794 amps.

R: 70.67Ω

Y: 1.58"

W = 0.29664

M = 159.63

X = 1.08"

$$\Delta H = \frac{I^2 Rt \; X \; M}{4.184 \; Y \; W} \text{ cal/mole} = 15.285 \text{ k.cal/mole}$$

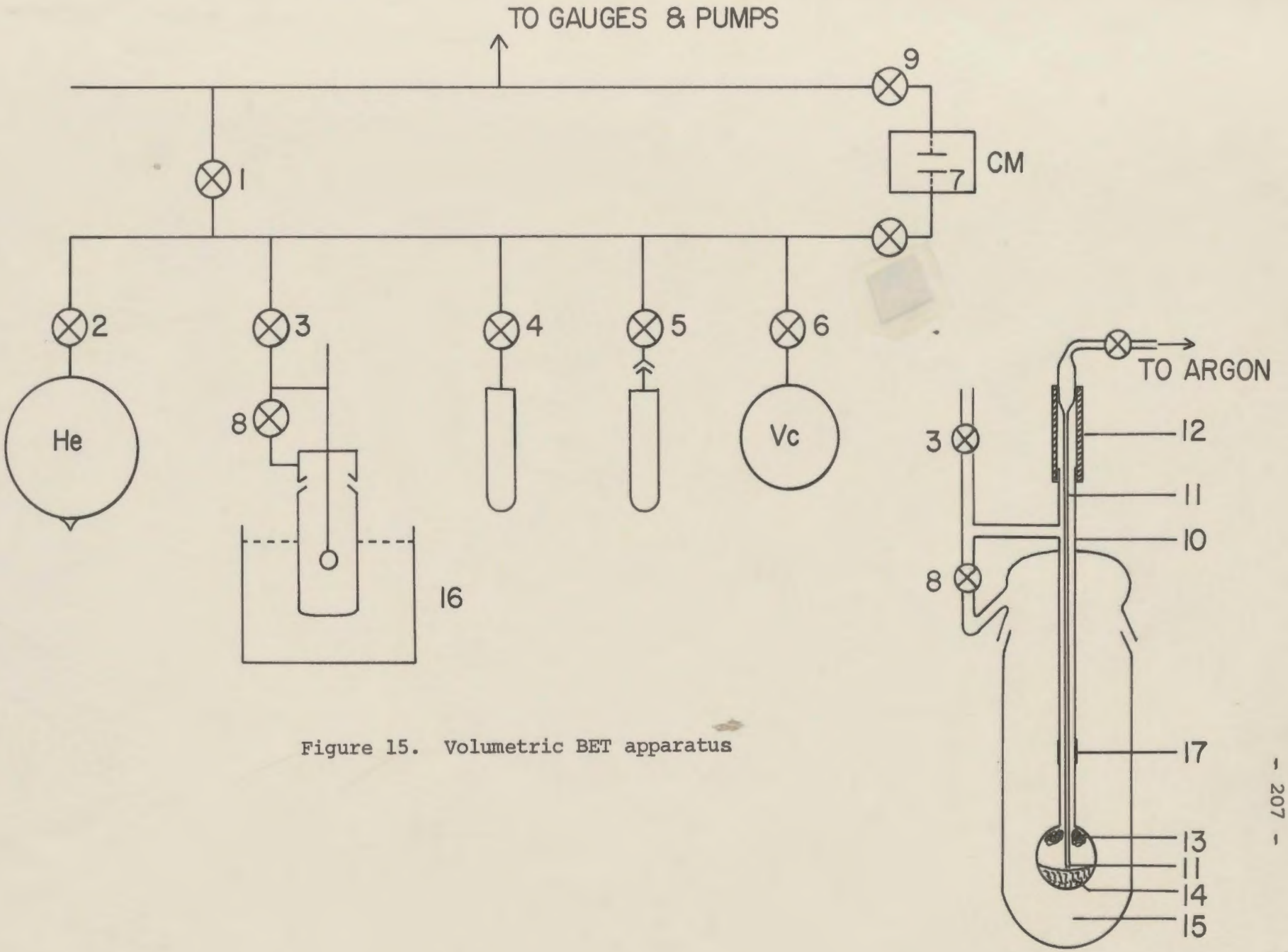

Figure 15. Volumetric BET apparatus

Figure 16. Isotherm for $NiSO_4$ (200)

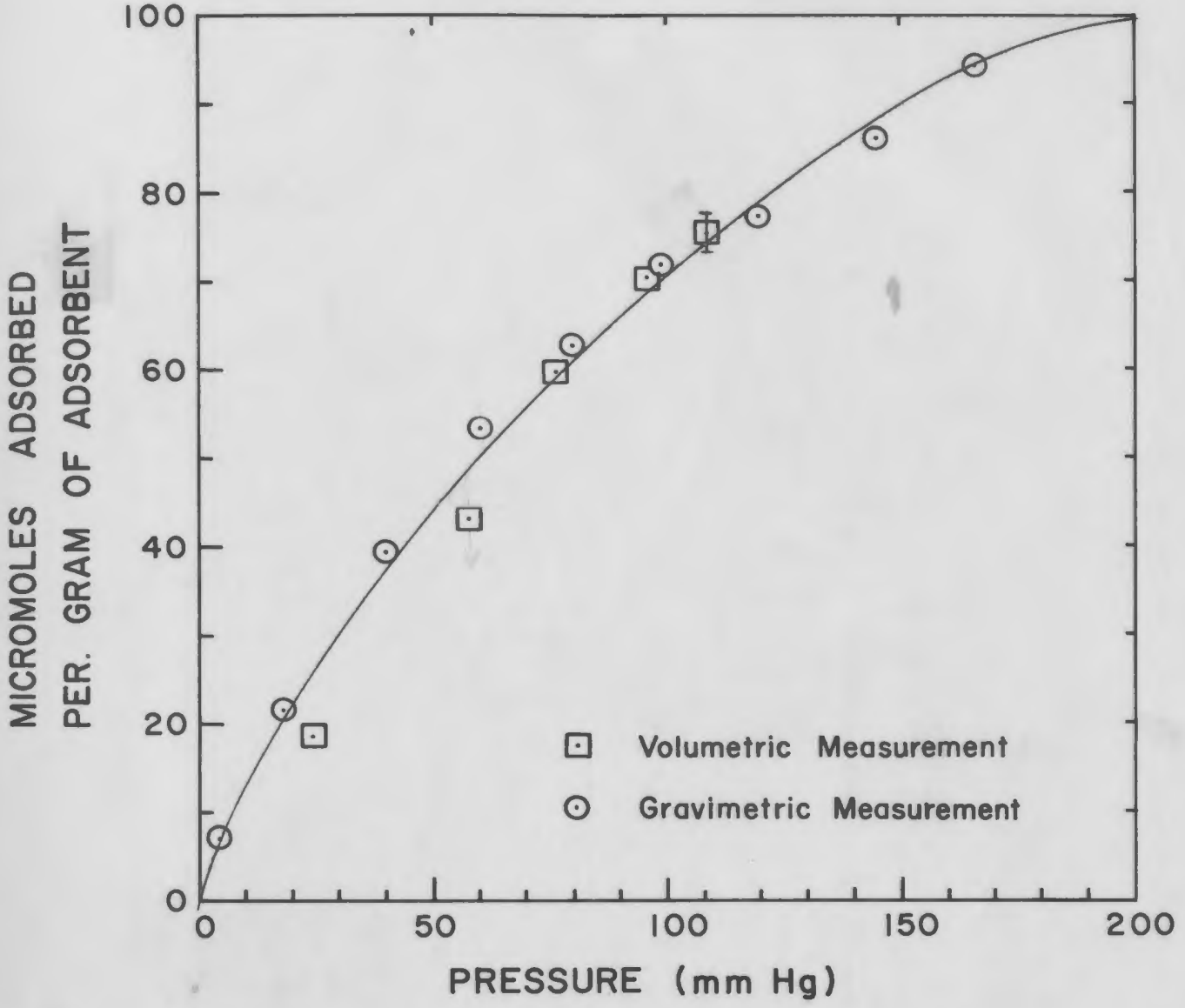

Figure 17. Vapour pressure plot for $CFCl_3$

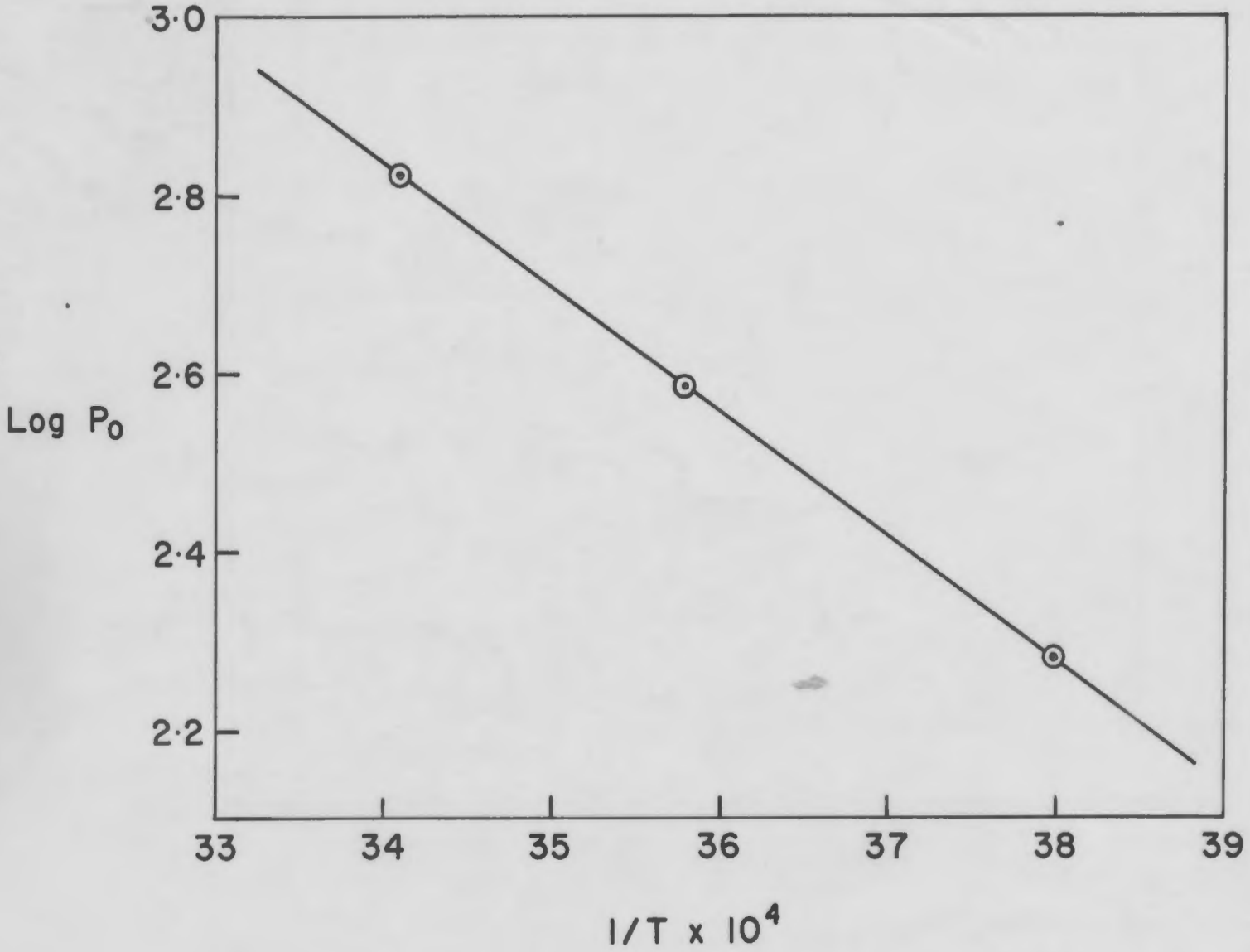

Figure 18. Isotherms for $MnSO_4$ (200)

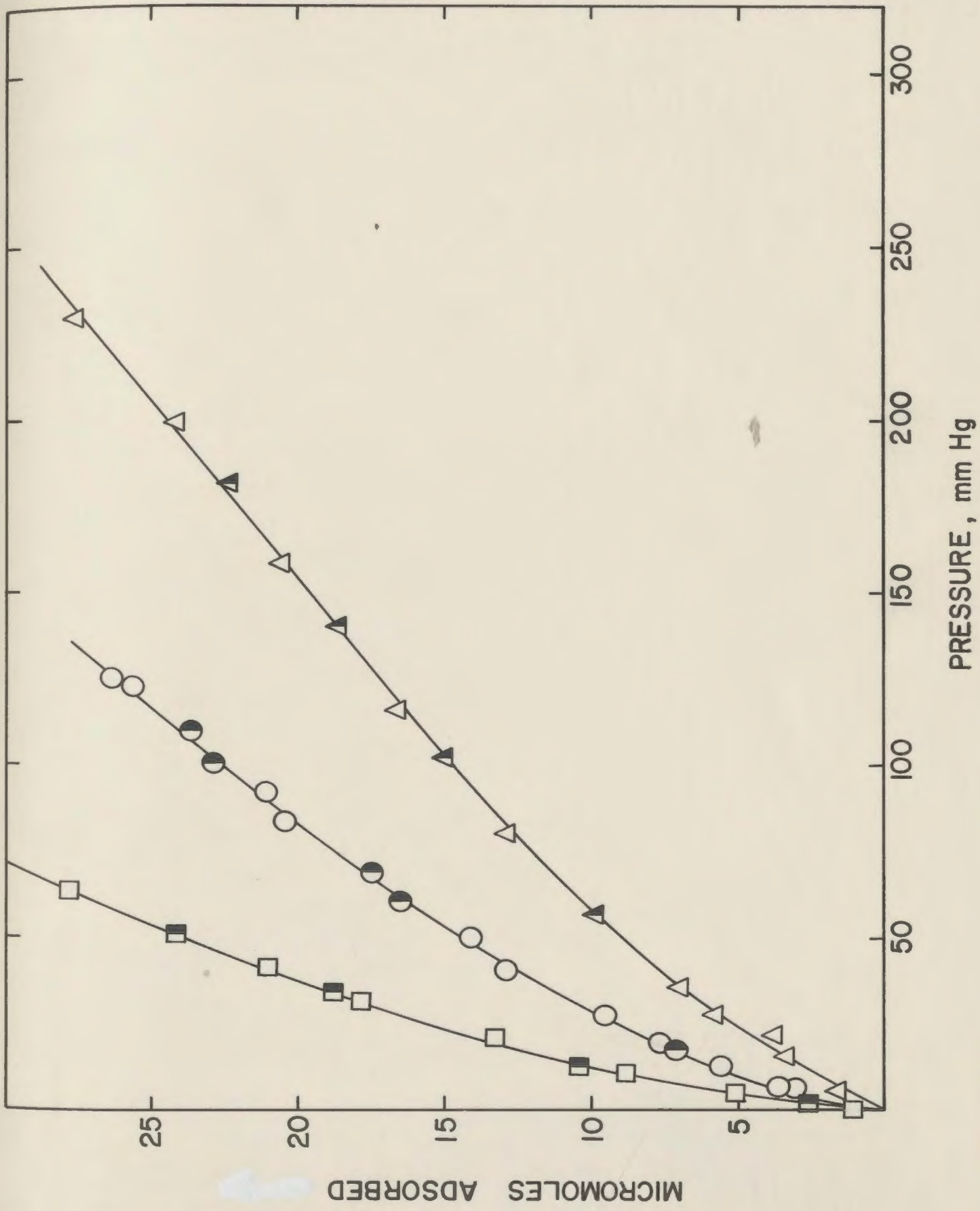

Figure 19. Isotherms for $MnSO_4$ (300)

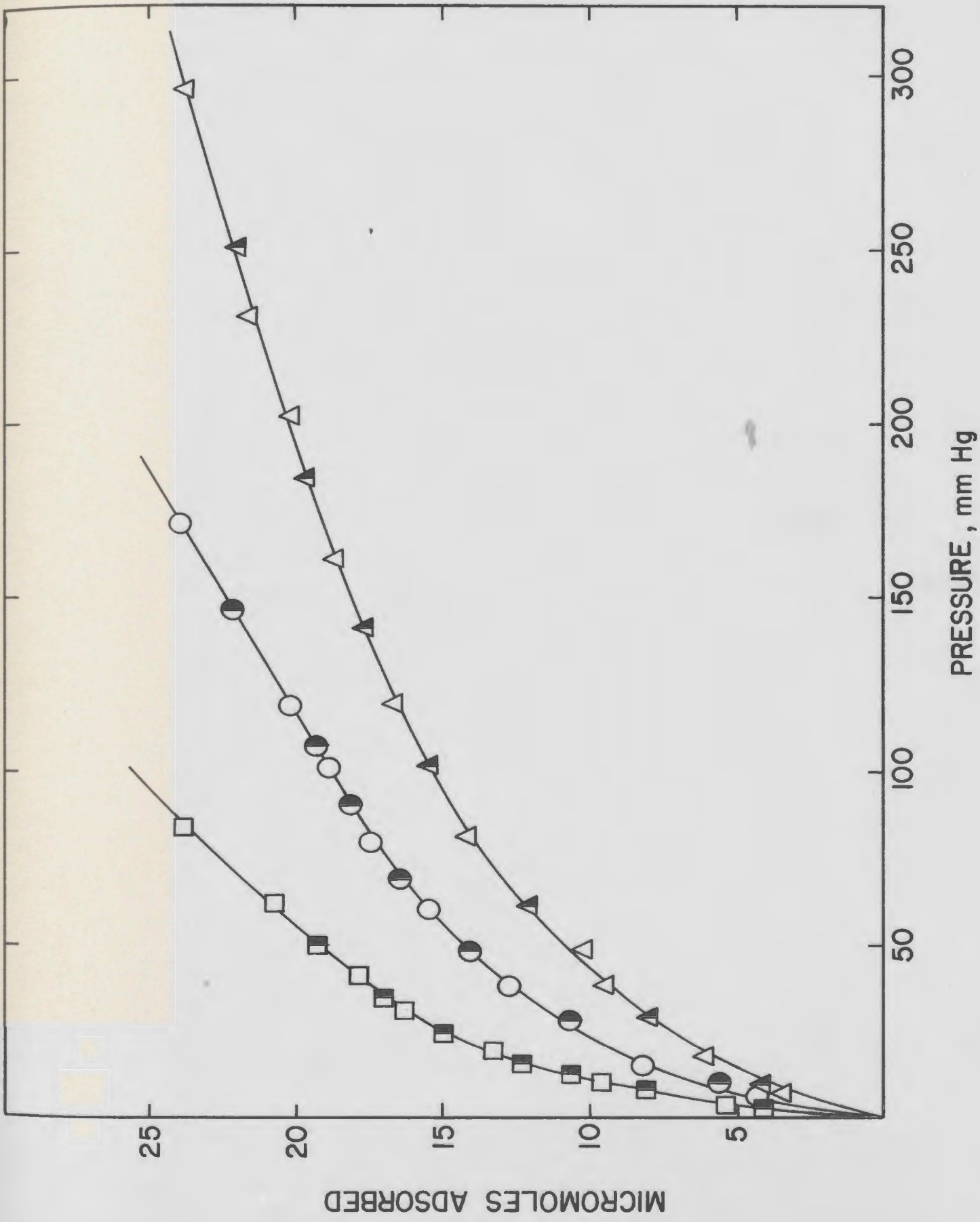

Figure 20. Isotherms for $MnSO_4$ (400)

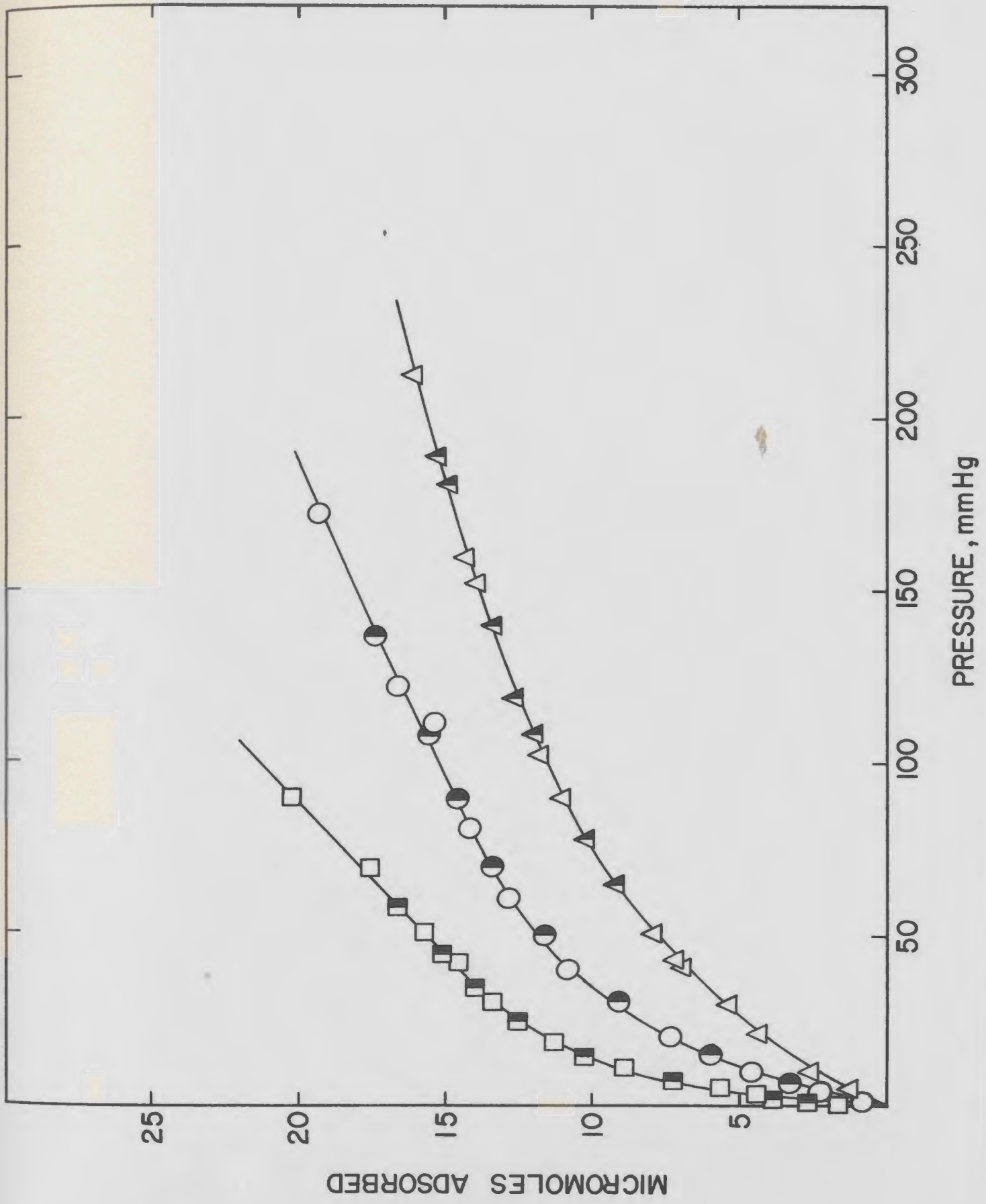

Figure 21. Isotherms for $CoSO_4$ (200)

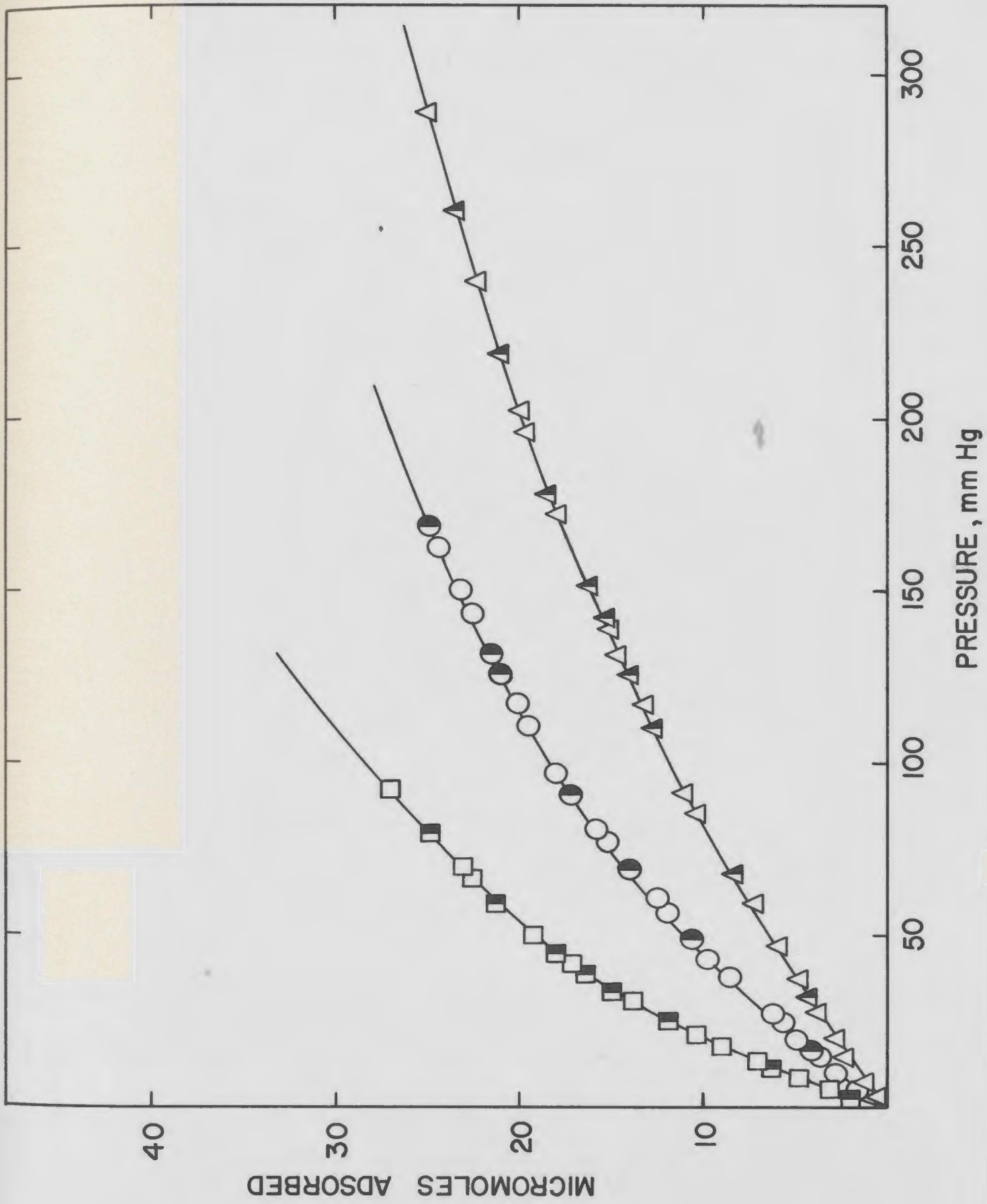

Figure 22. Isotherms for $CoSO_4$ (300)

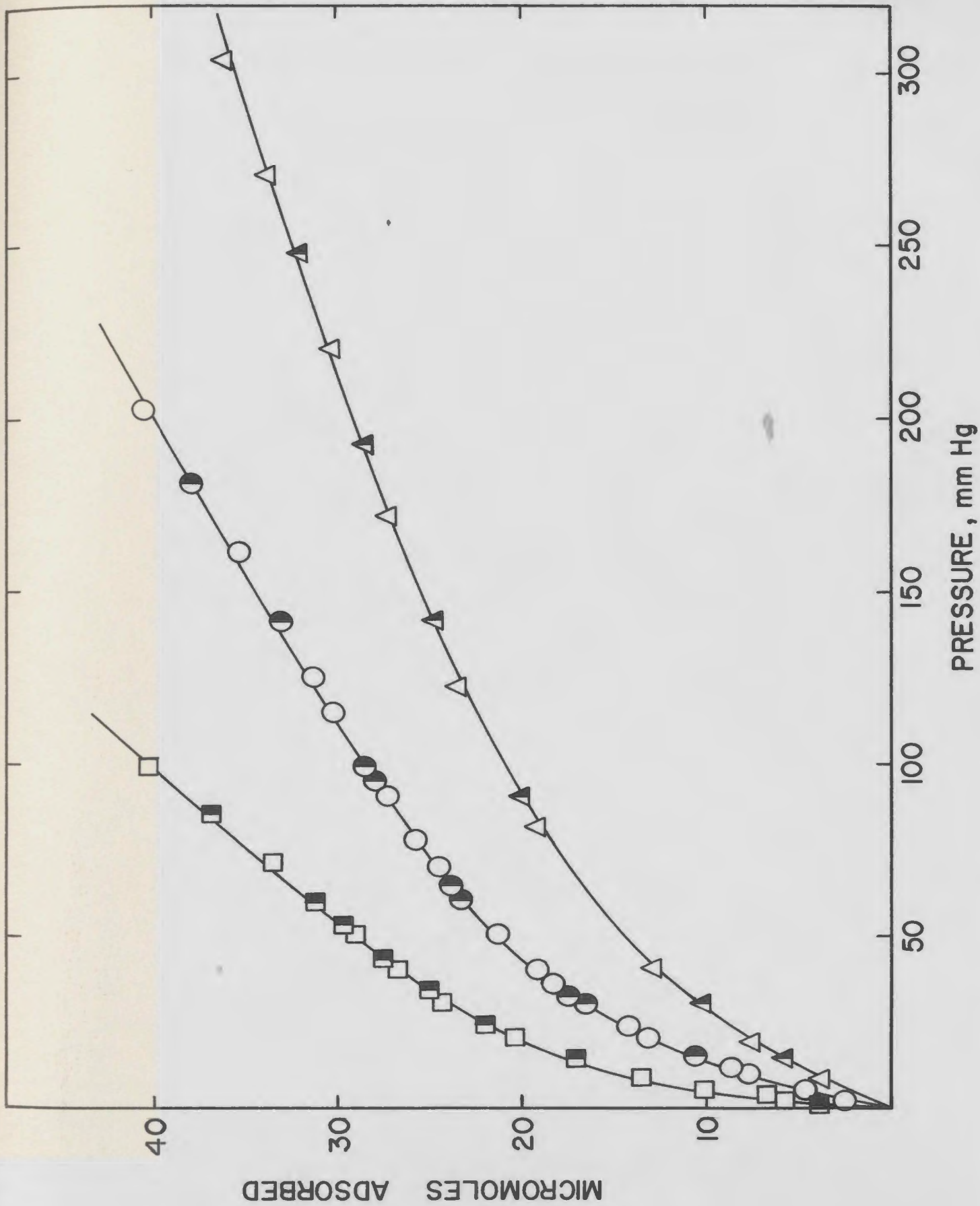

Figure 23. Isotherms for $CoSO_4$ (400)

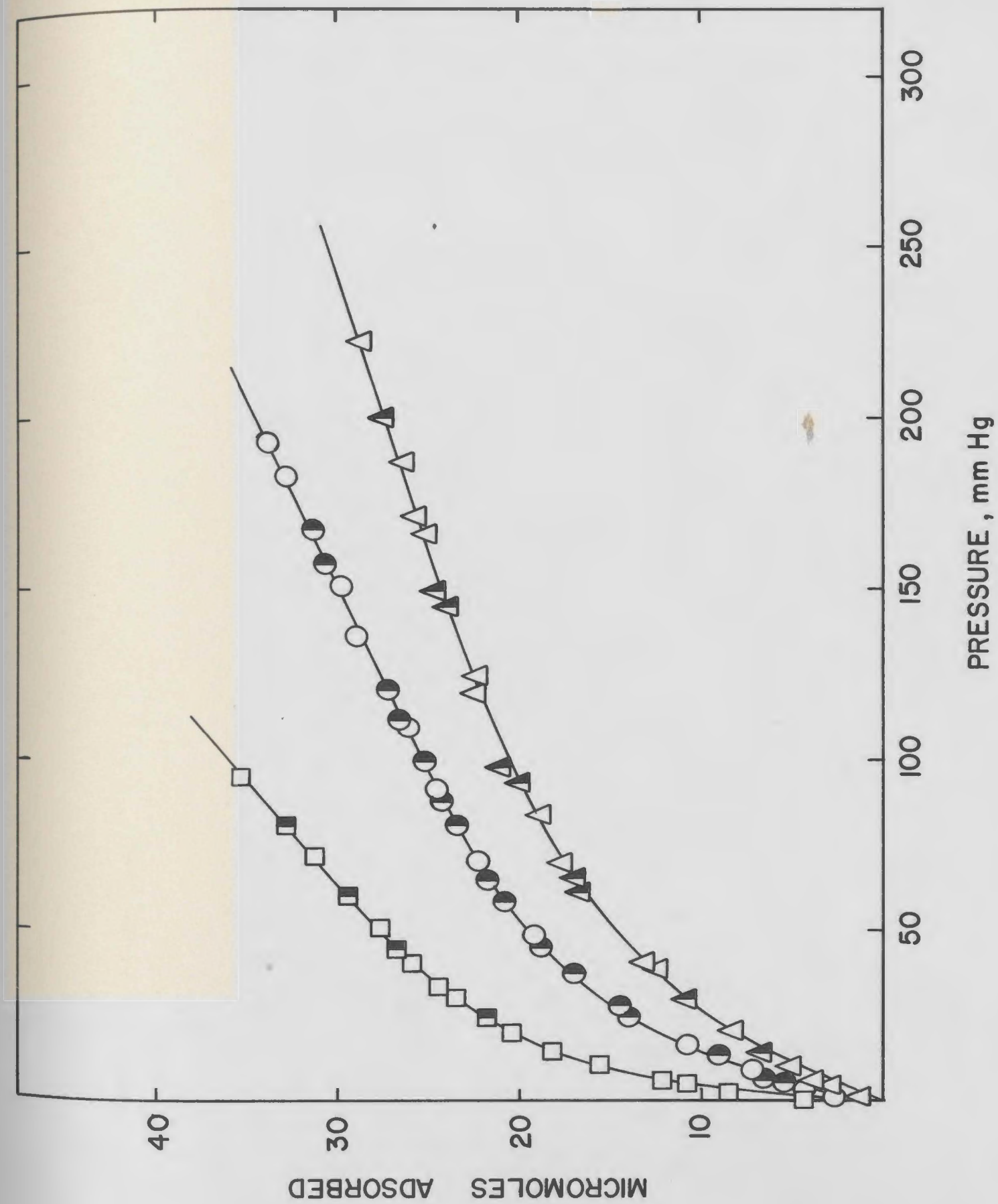

Figure 24. Isotherms for $CoSO_4$ (500)

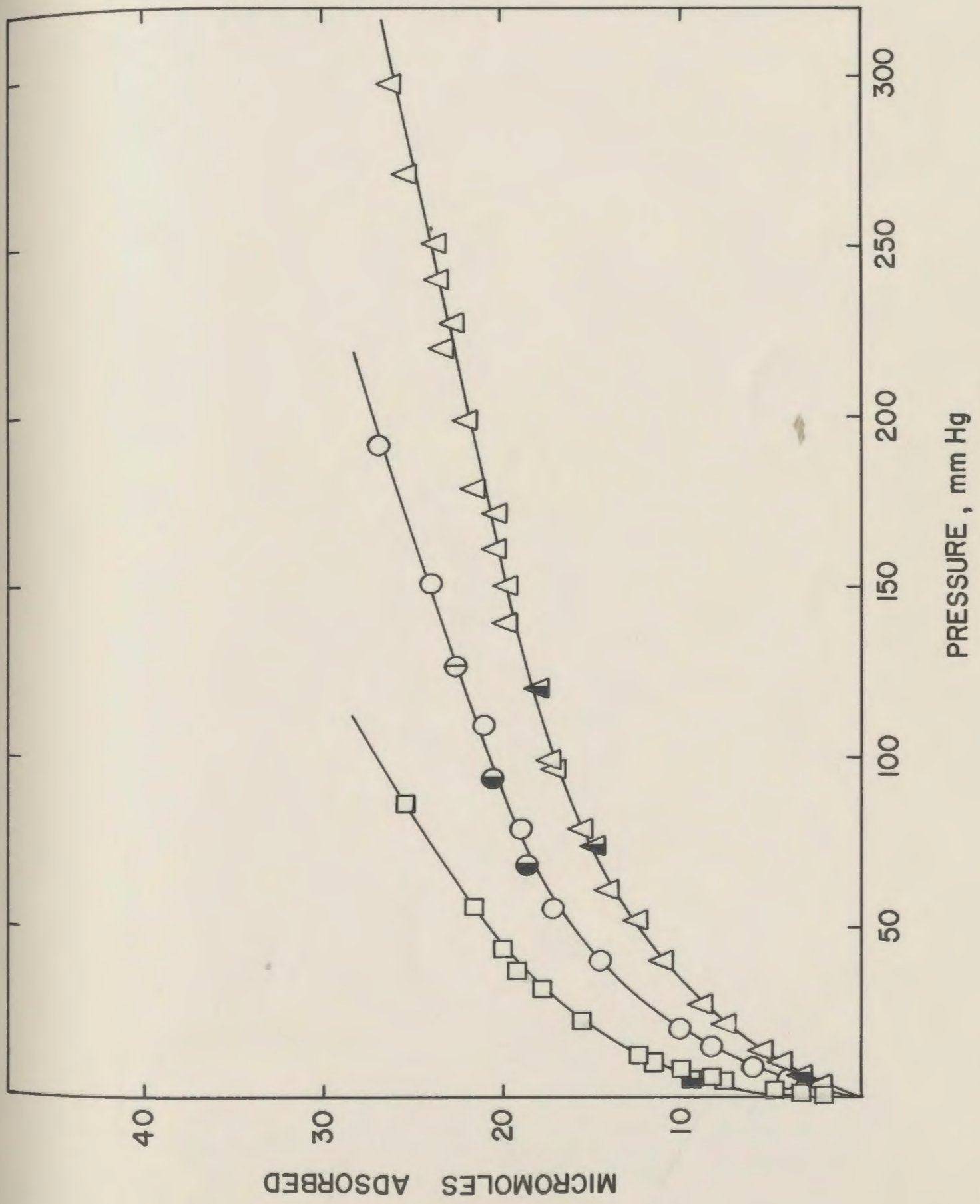

Figure 25. Isotherms for $NiSO_4$ (200)

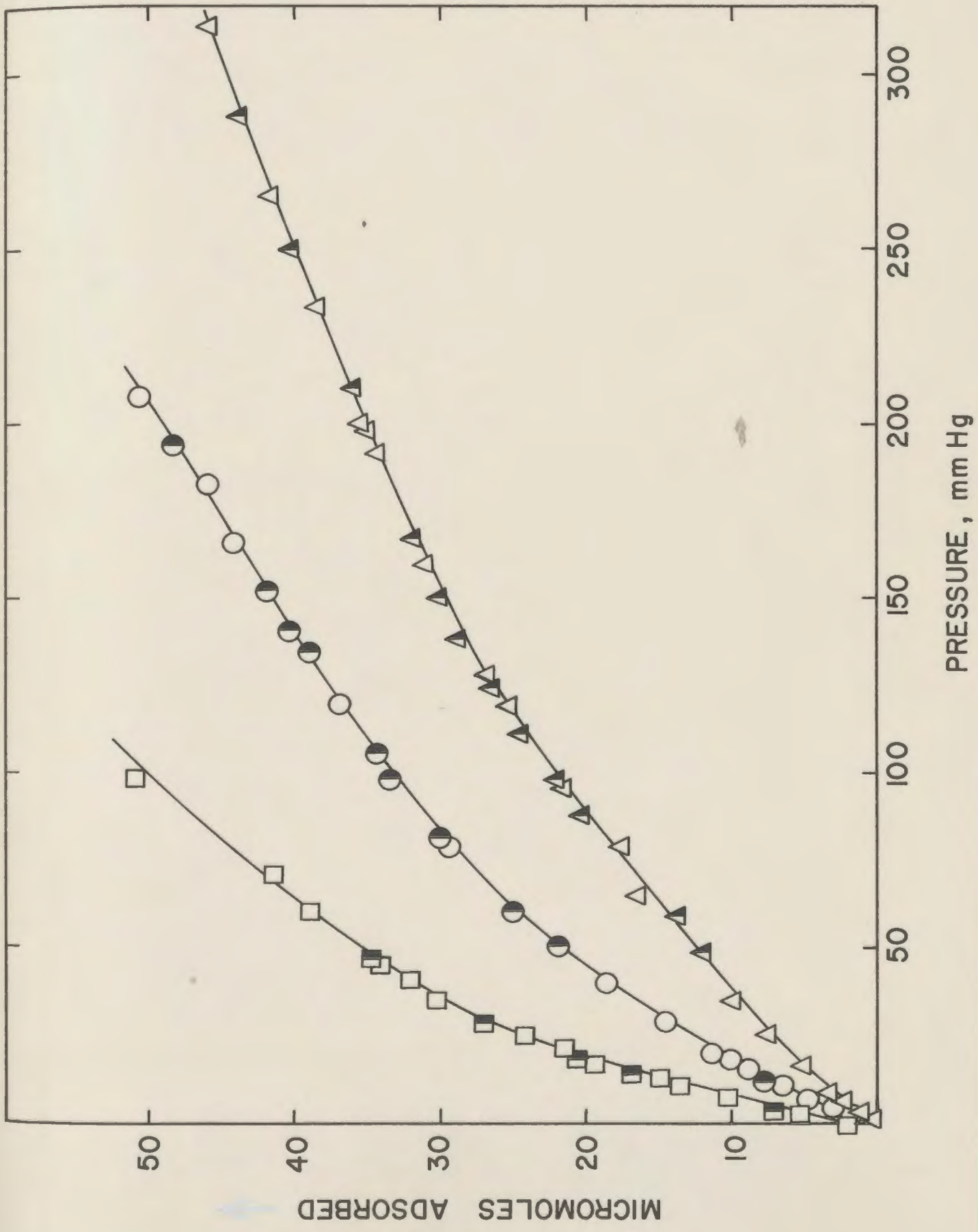

Figure 26. Isotherms for $NiSO_4$ (300)

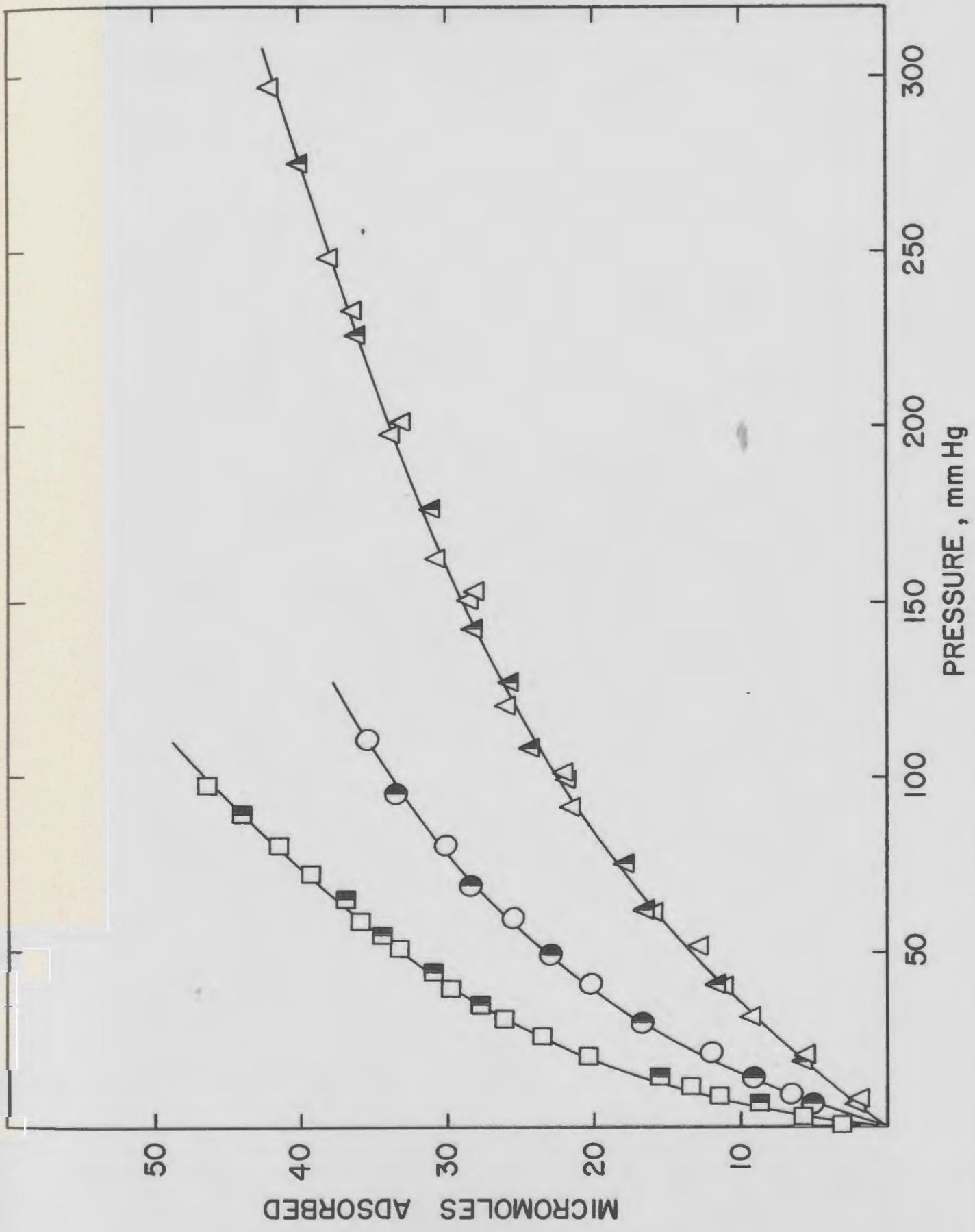

Figure 27. Isotherms for $NiSO_4$ (400)

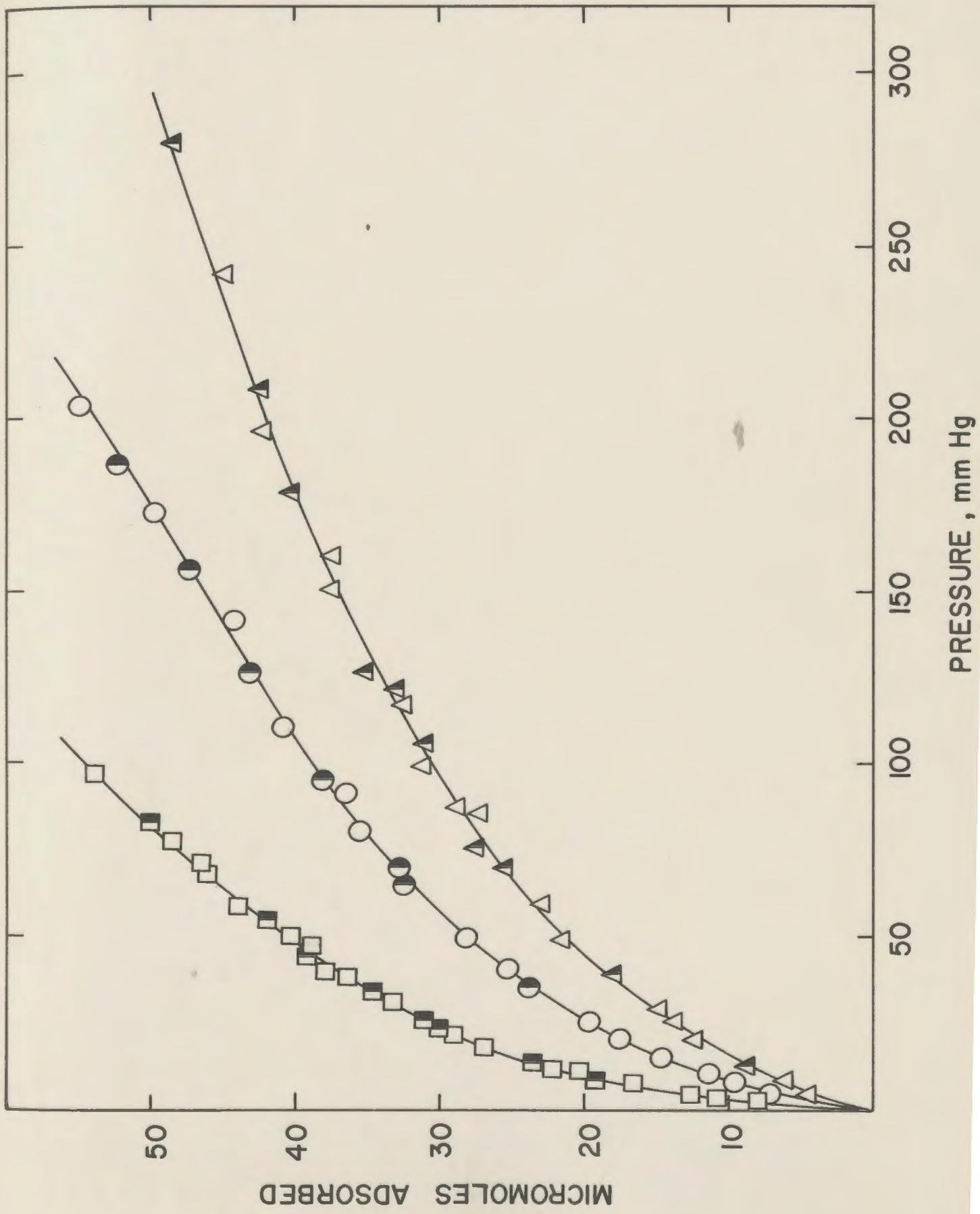

Figure 28. Isotherms for $NiSO_4$ (500)

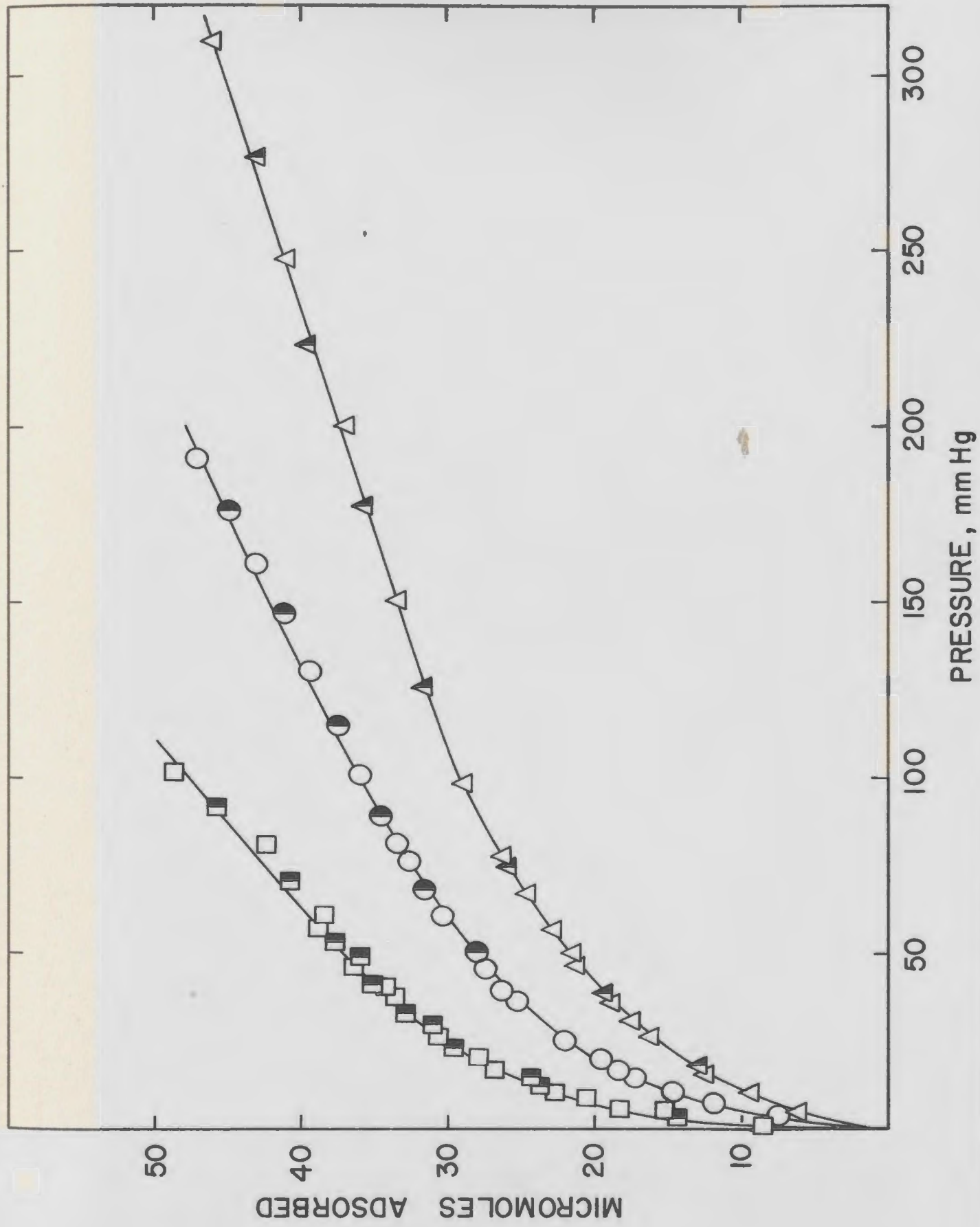

Figure 29. Isotherms for $CuSO_4$ (200)

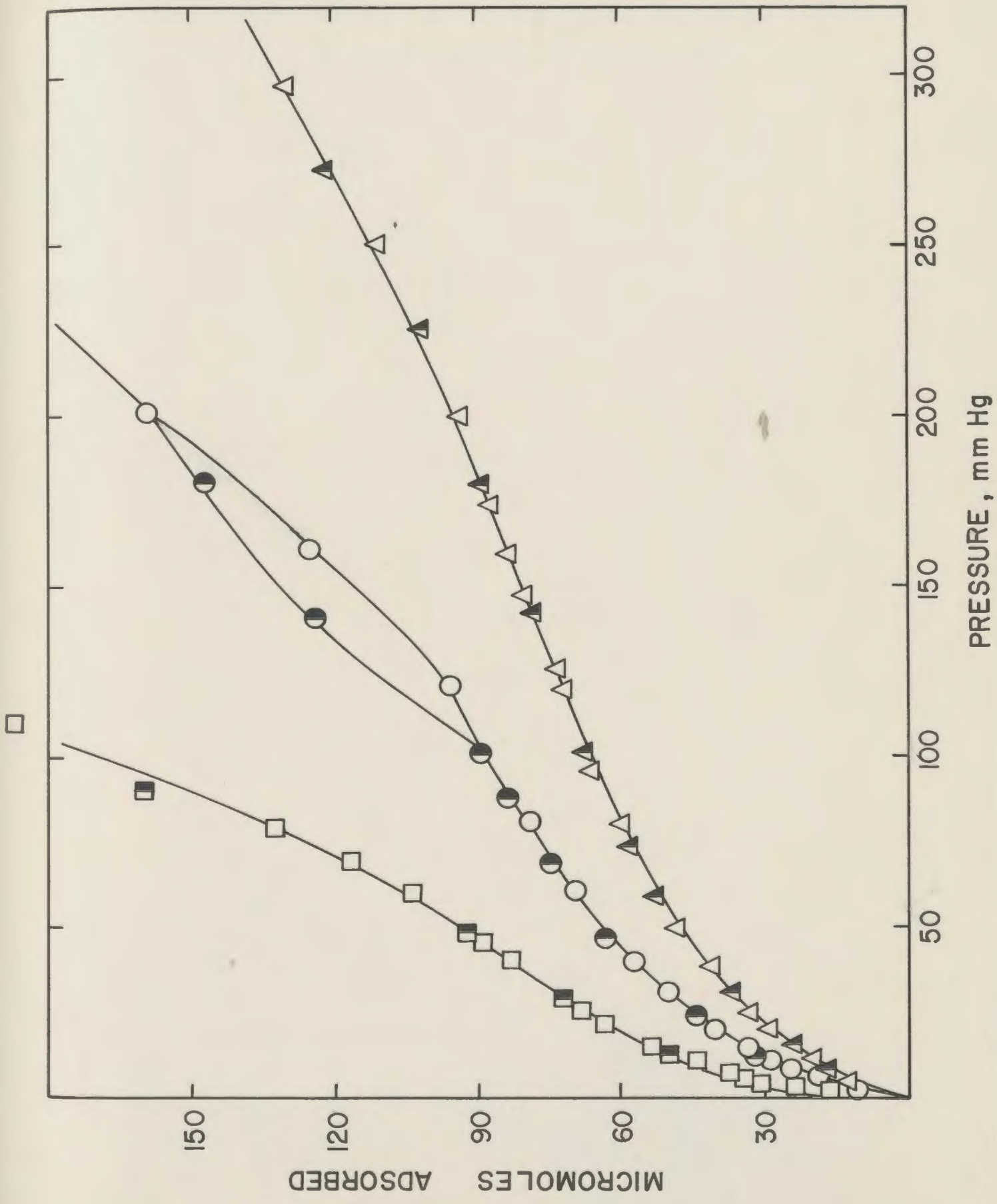

Figure 30. Isotherms for $CuSO_4$ (300)

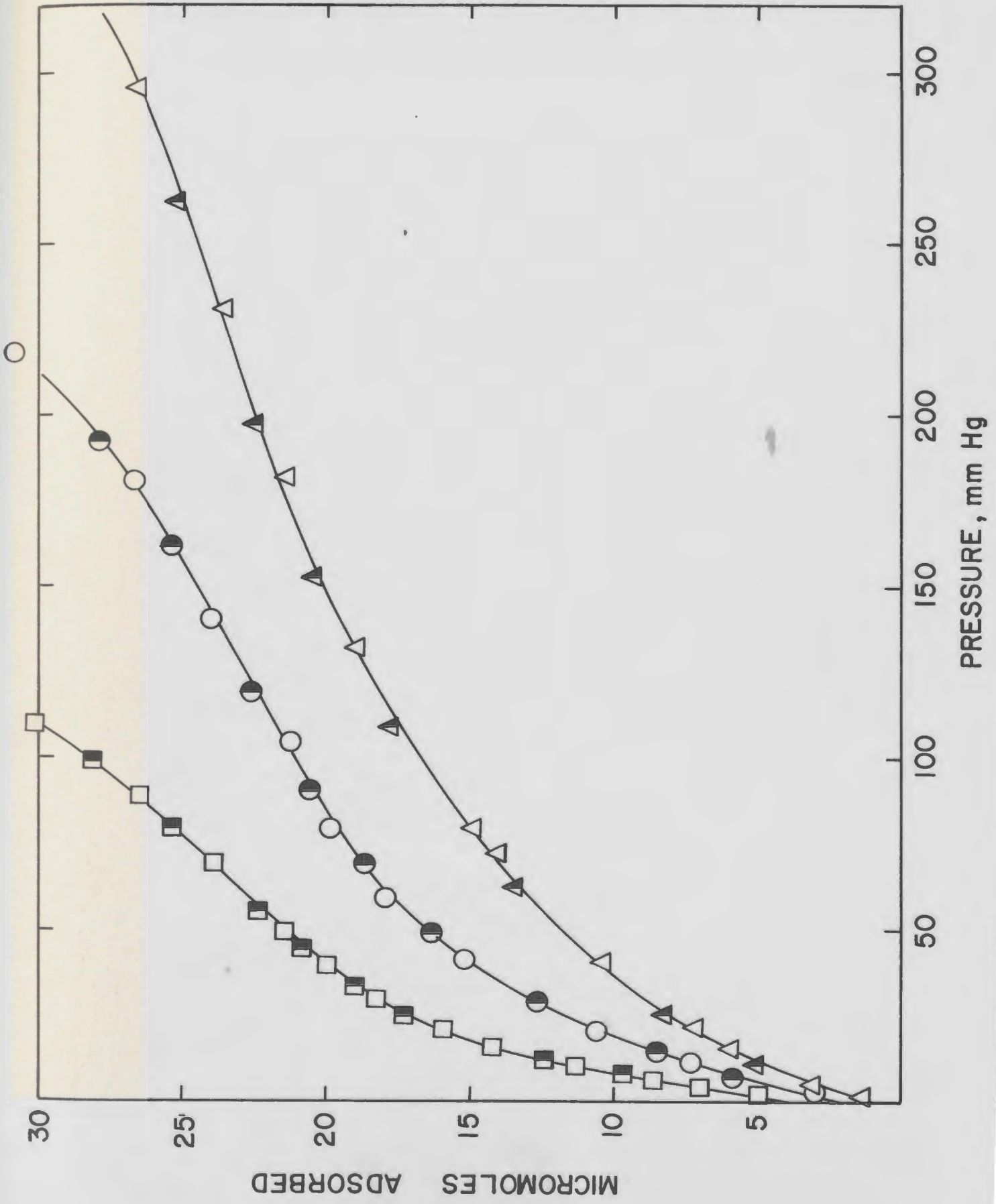

Figure 31. Isotherms for $CuSO_4$ (400)

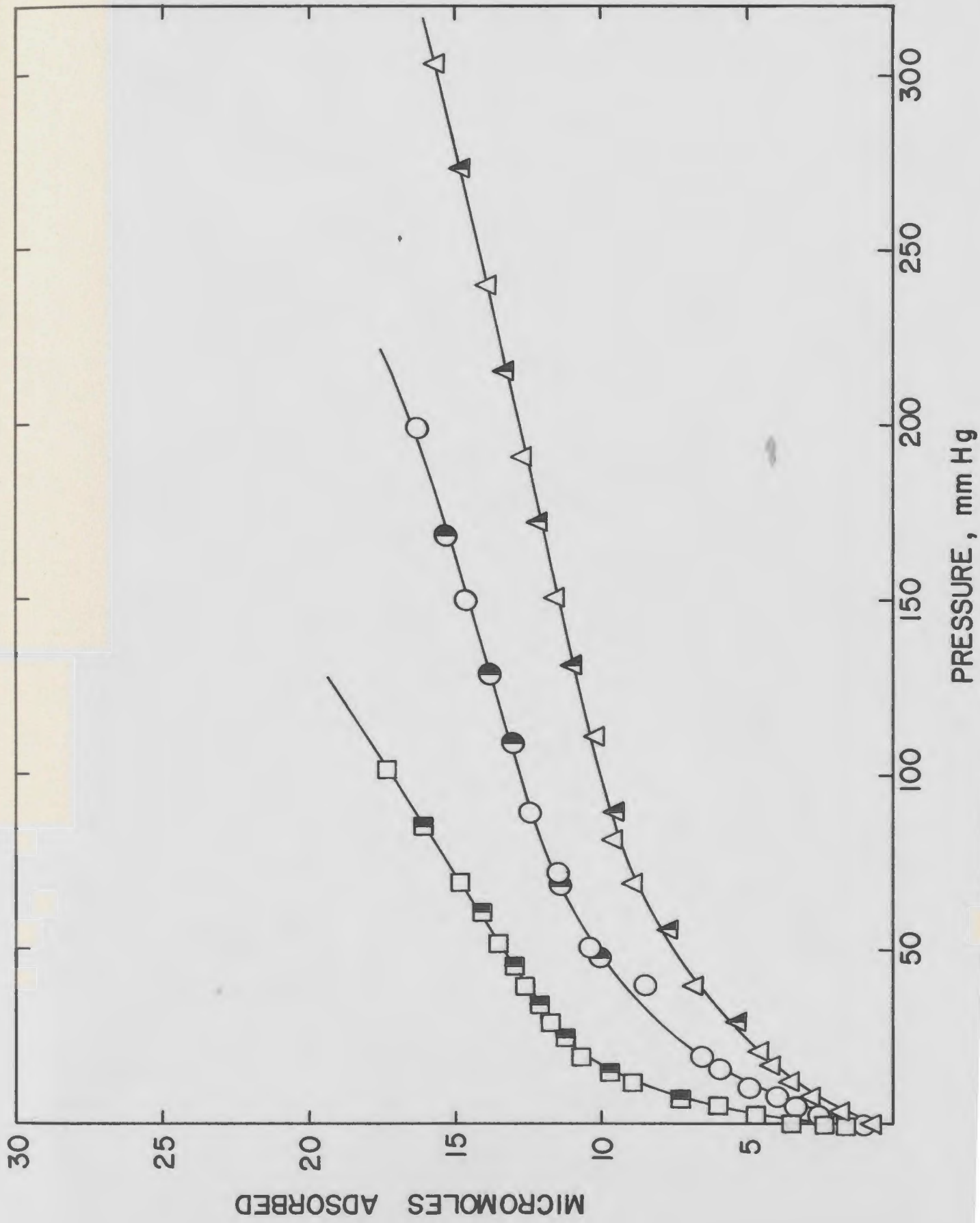

Figure 32. Isotherms for $CuSO_4$ (500)

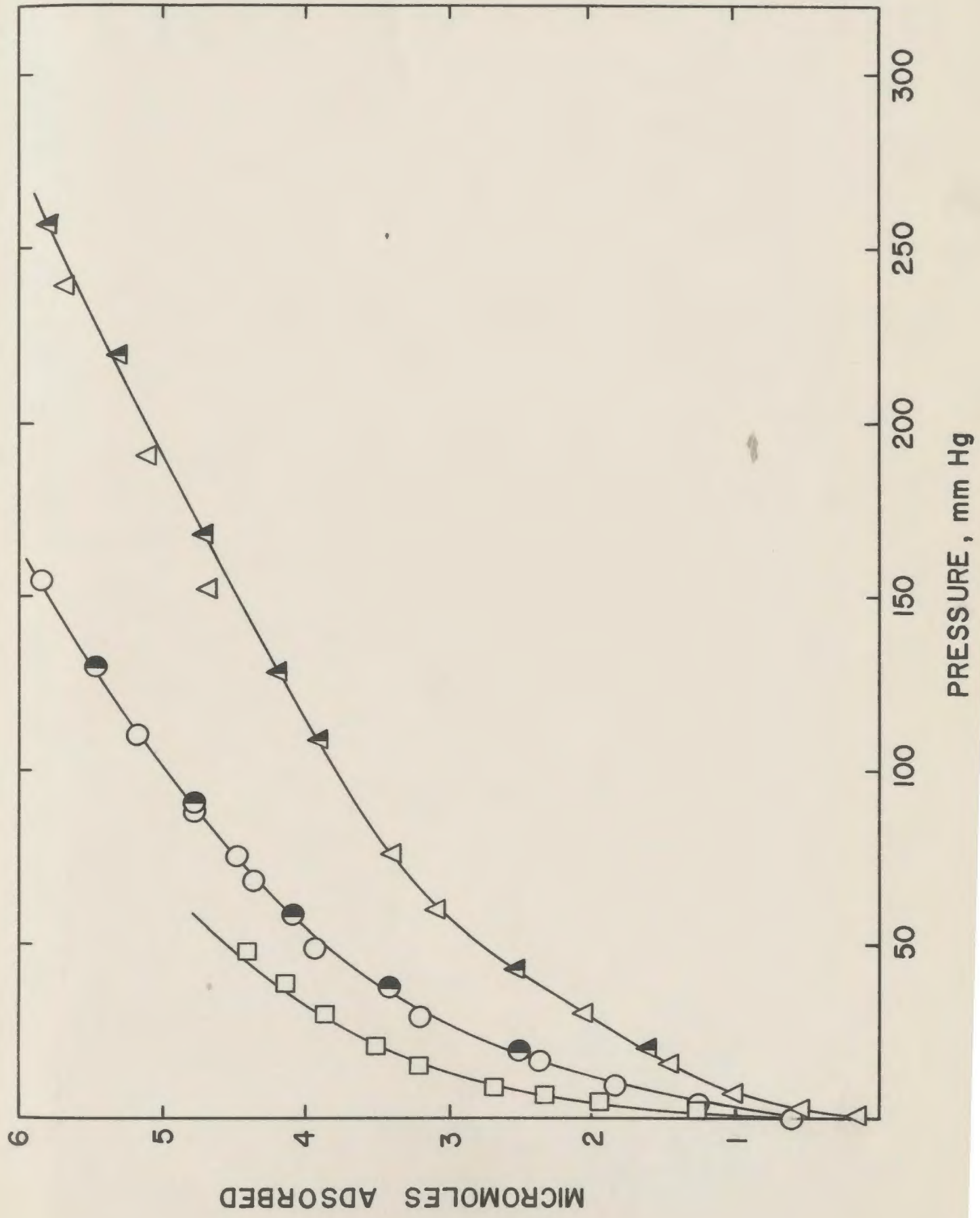

Figure 33. Isotherms for $ZnSO_4$ (200)

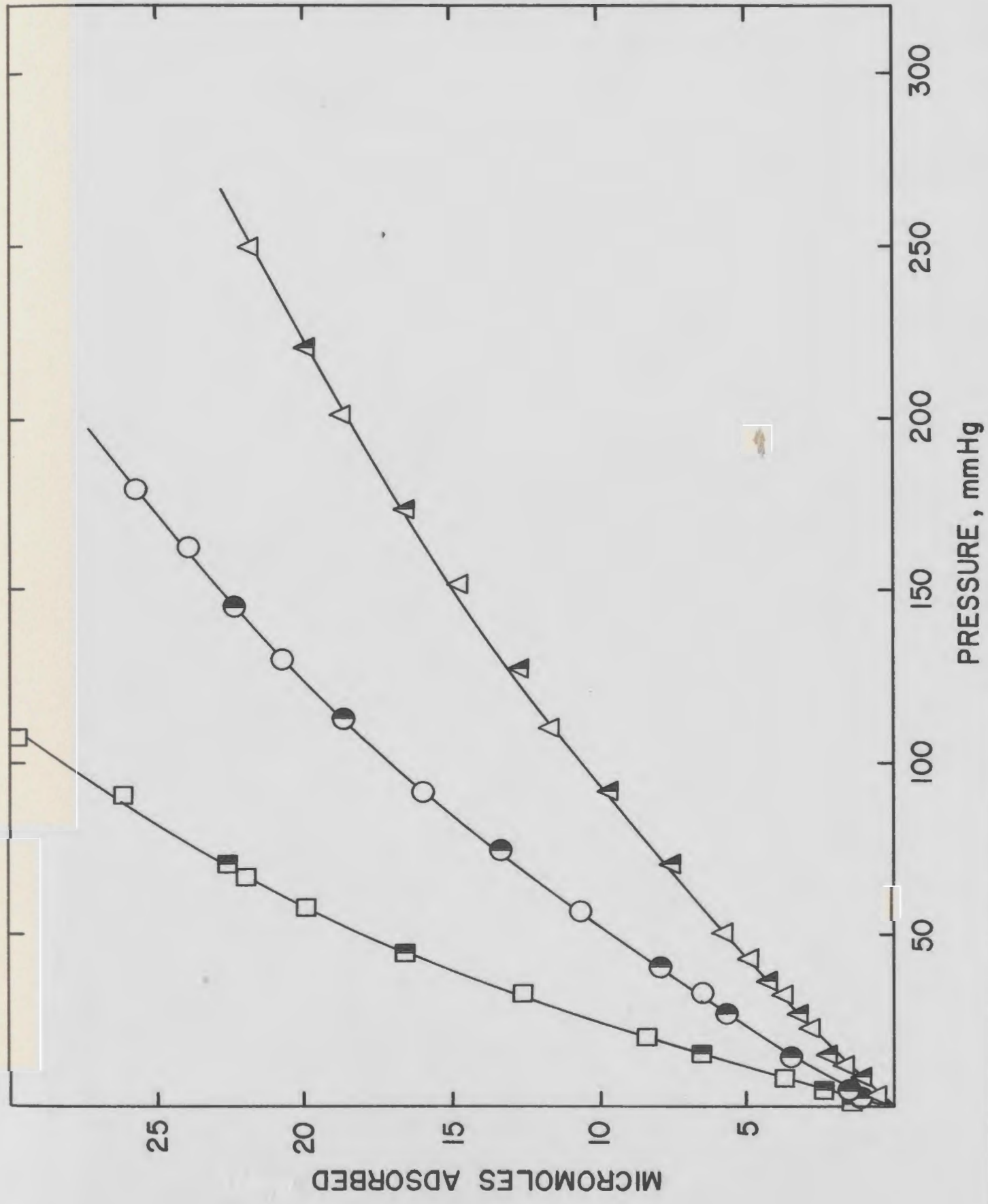

Figure 34. Isotherms for $ZnSO_4$ (300)

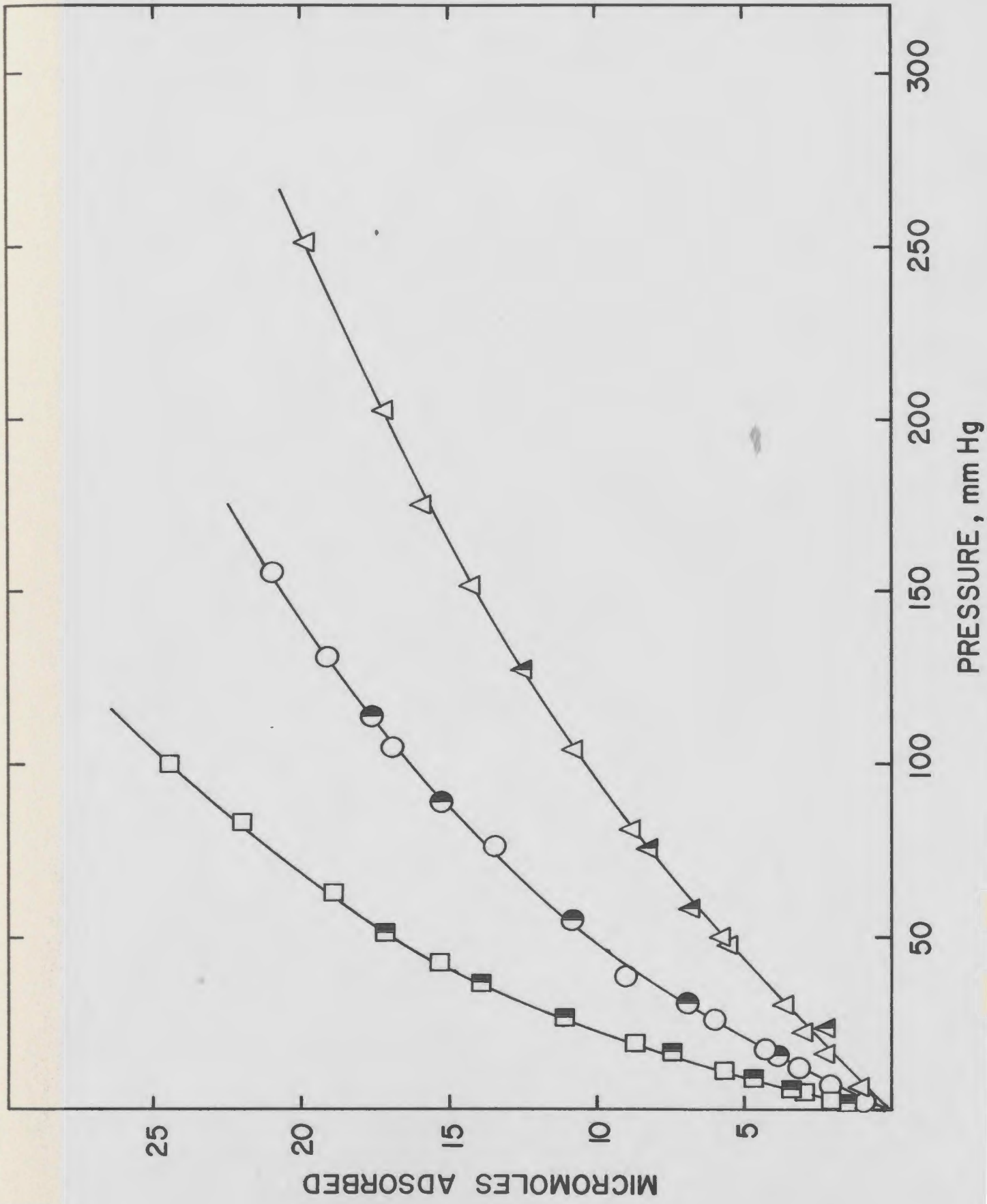

Figure 35. Isotherms for $ZnSO_4$ (400)

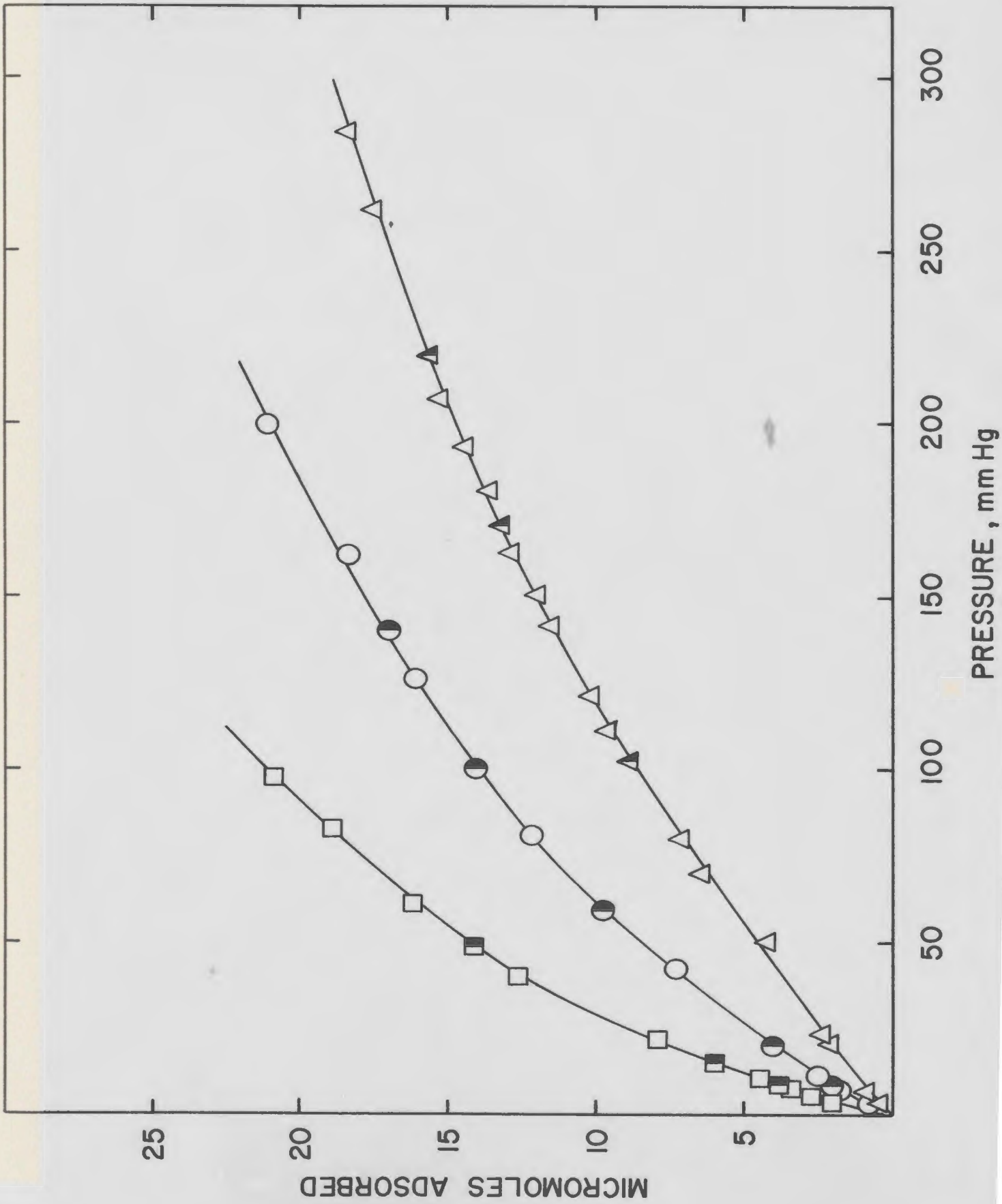

Figure 36. Isotherms for $CaSO_4$ (200)

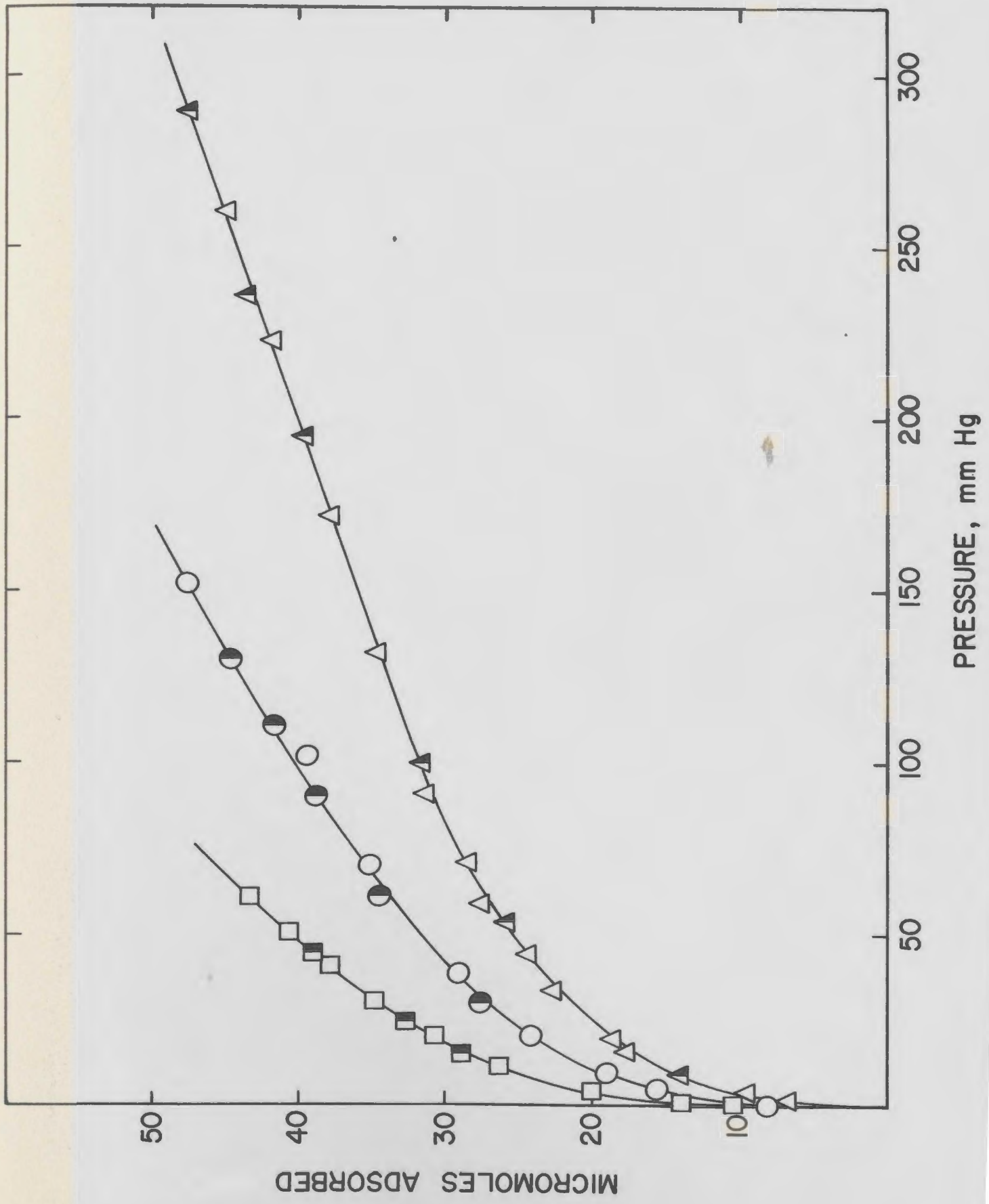

Figure 37. Isotherms for $CaSO_4$ (300)

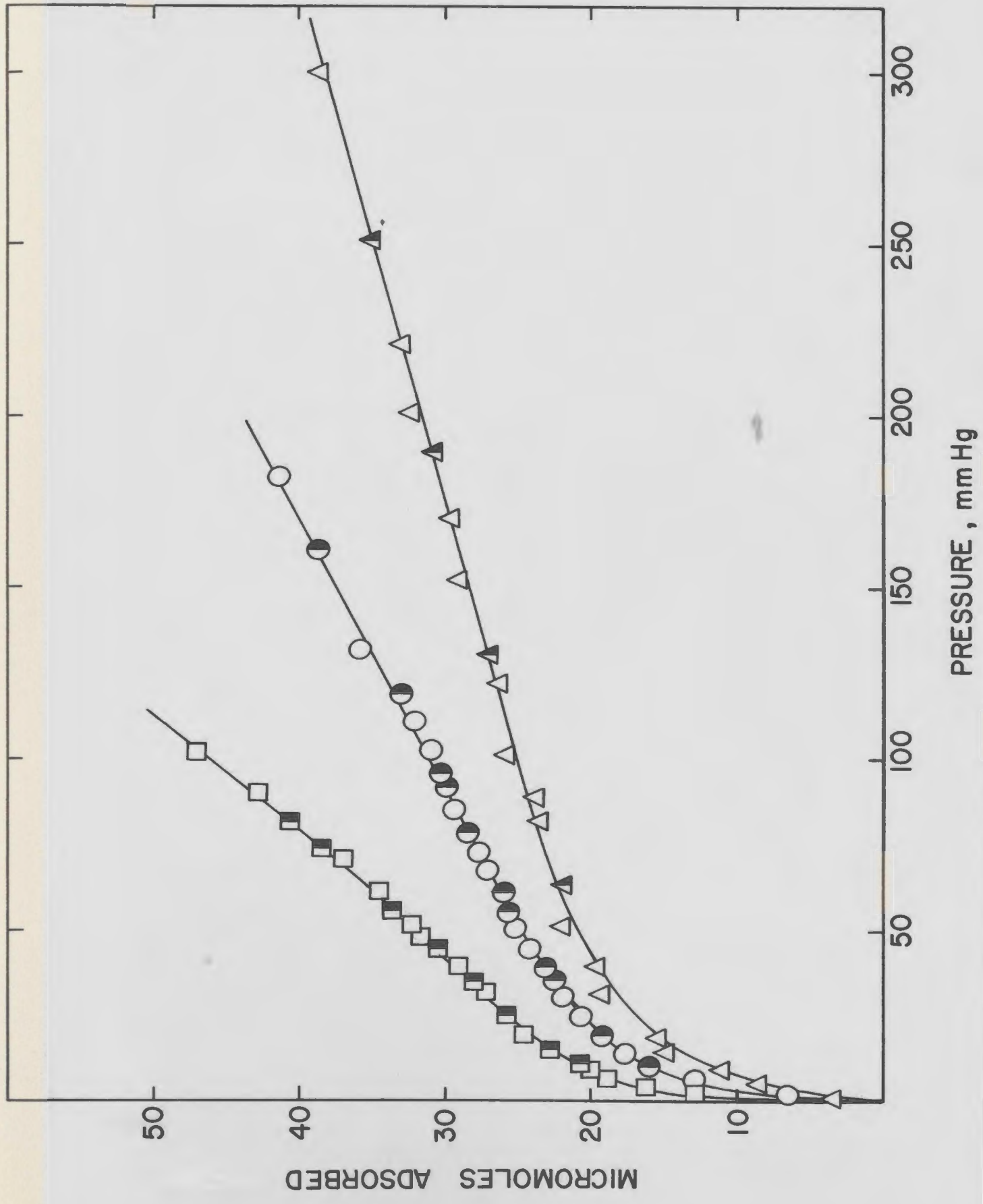

Figure 38. Isotherms for $CaSO_4$ (400)

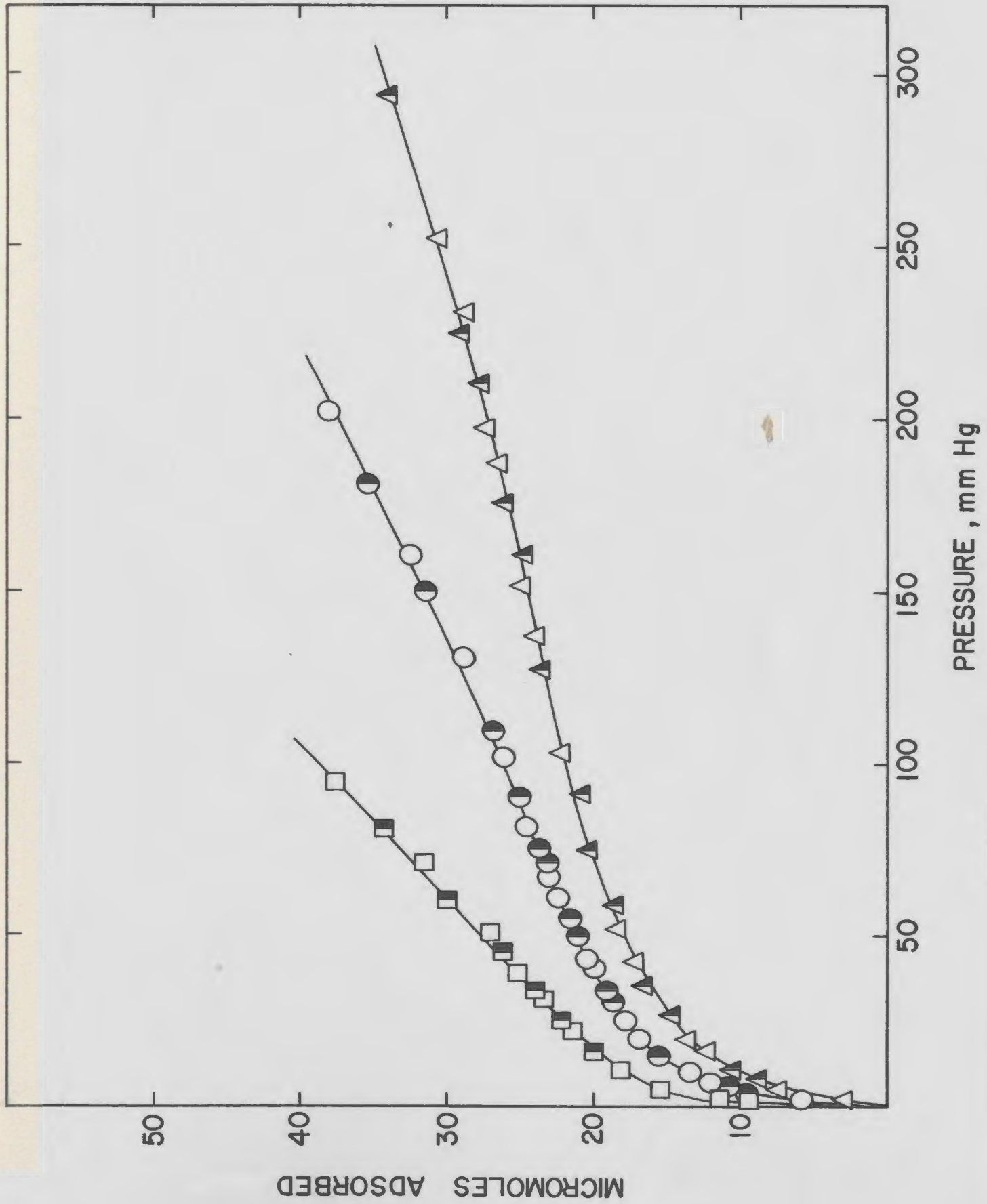

Figure 39. BET plot for $MnSO_4$ (300)

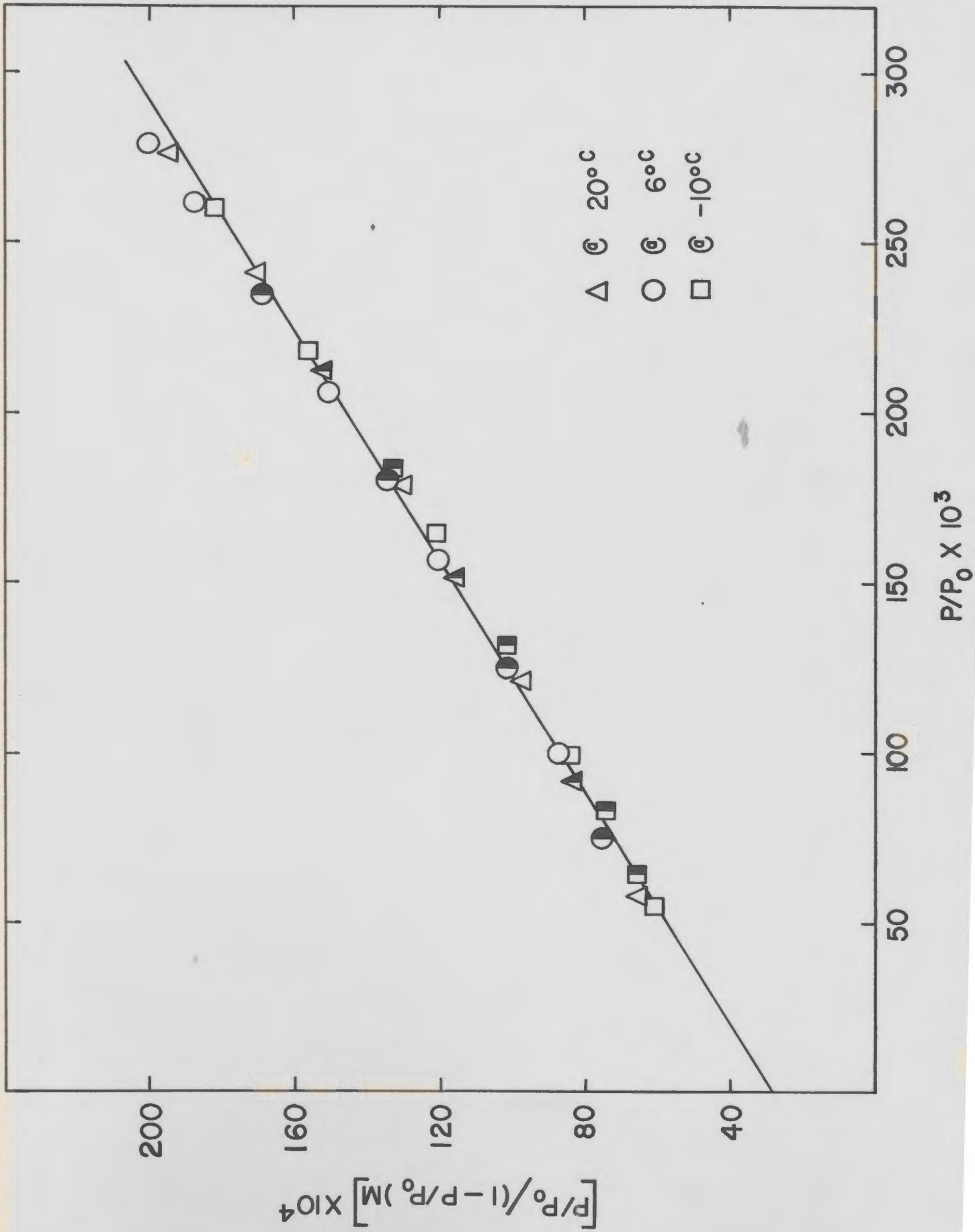

Figure 40. BET plot for $NiSO_4$ (400)

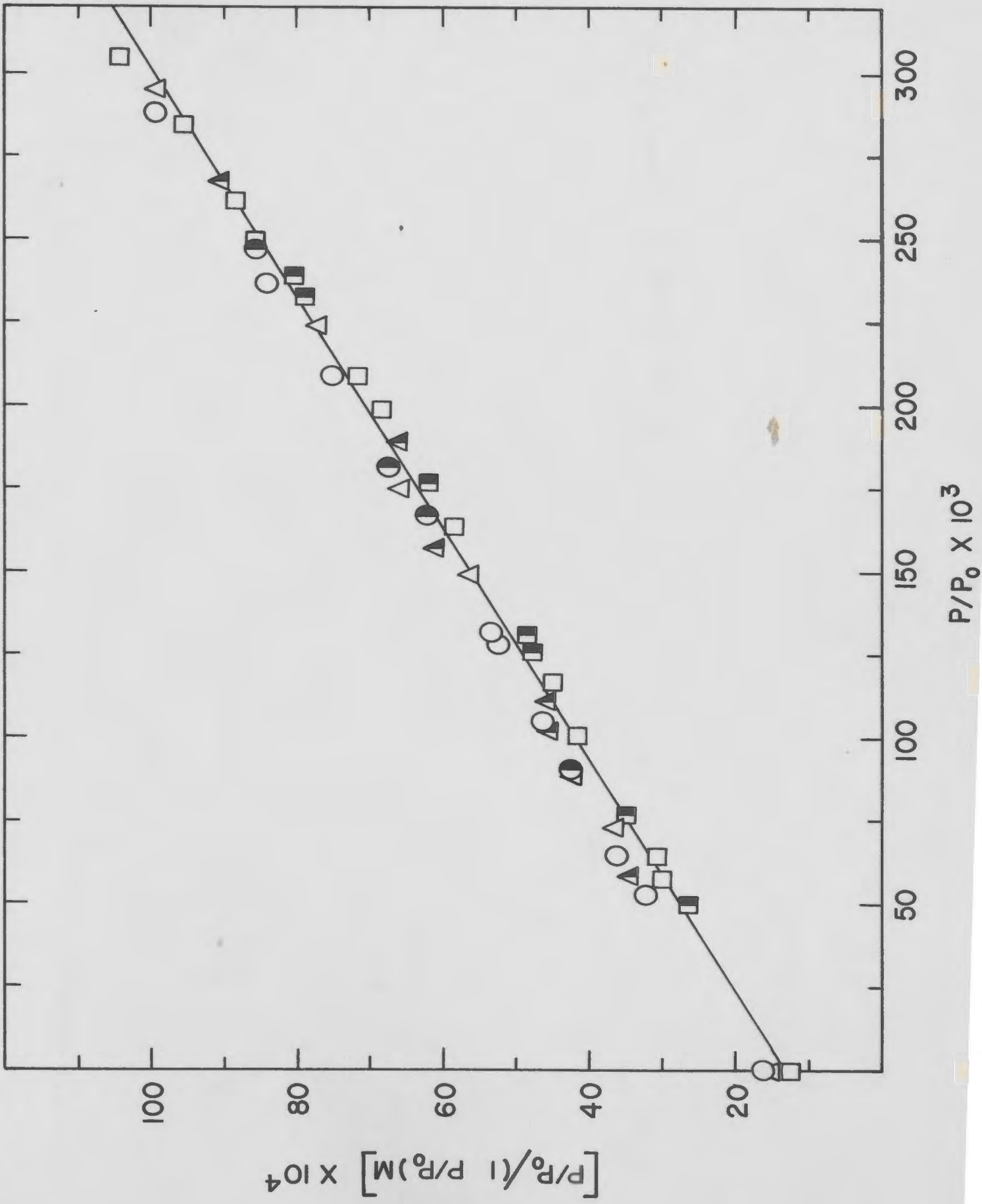

Figure 41. Isosteric heat curves for $MnSO_4$

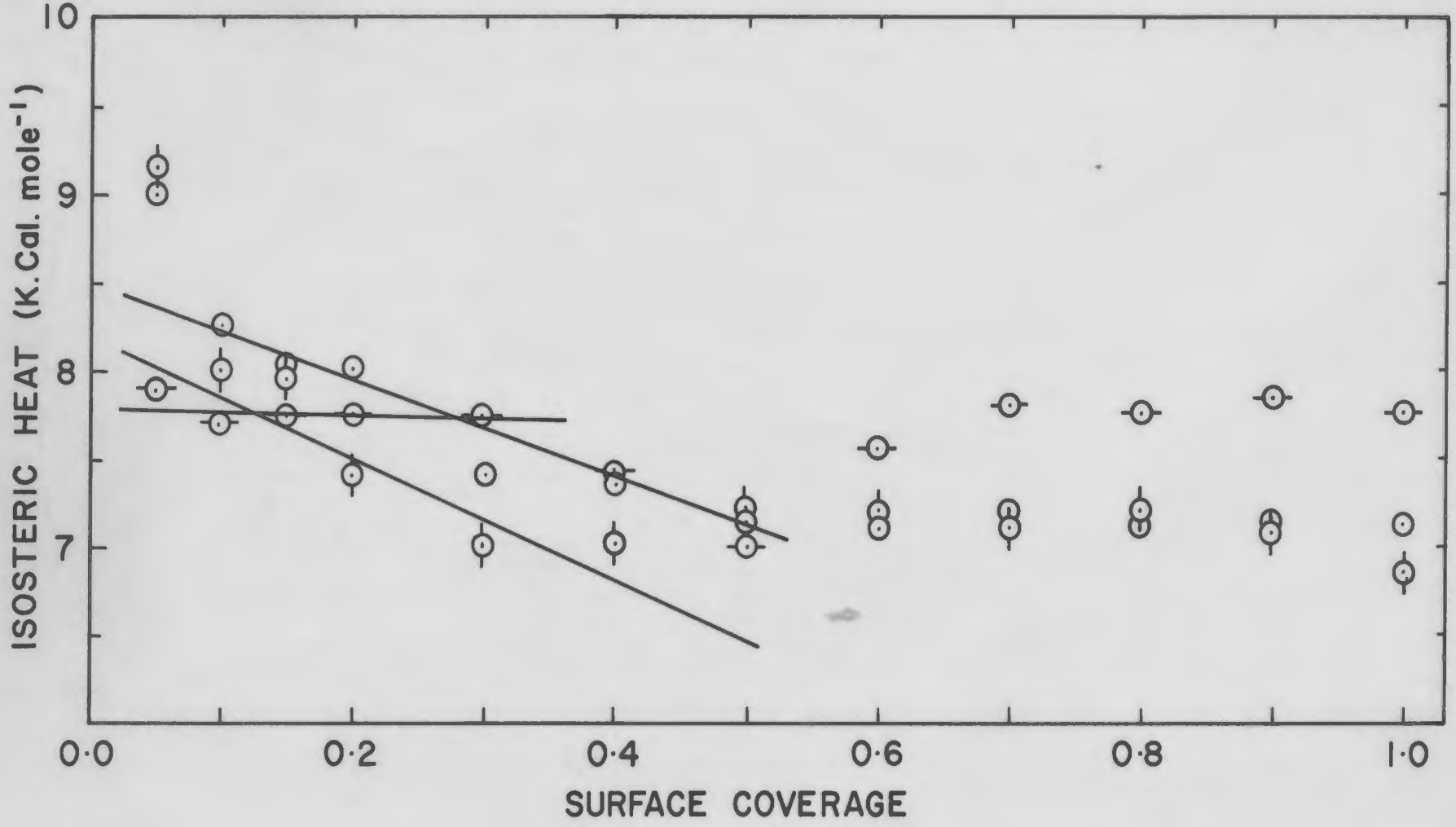

Figure 42. Isosteric heat curves for $CoSO_4$

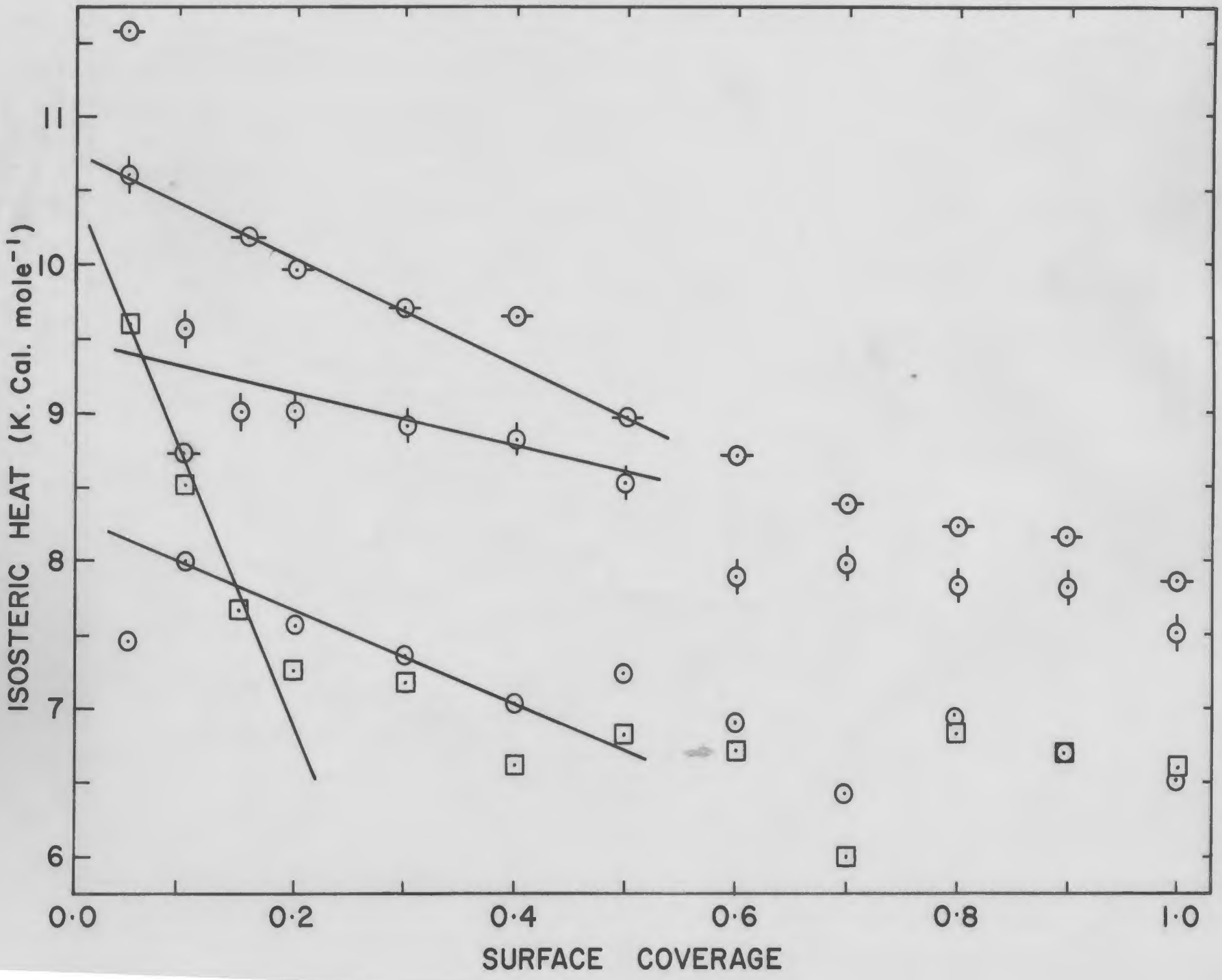

Figure 43. Isosteric heat curves for $NiSO_4$

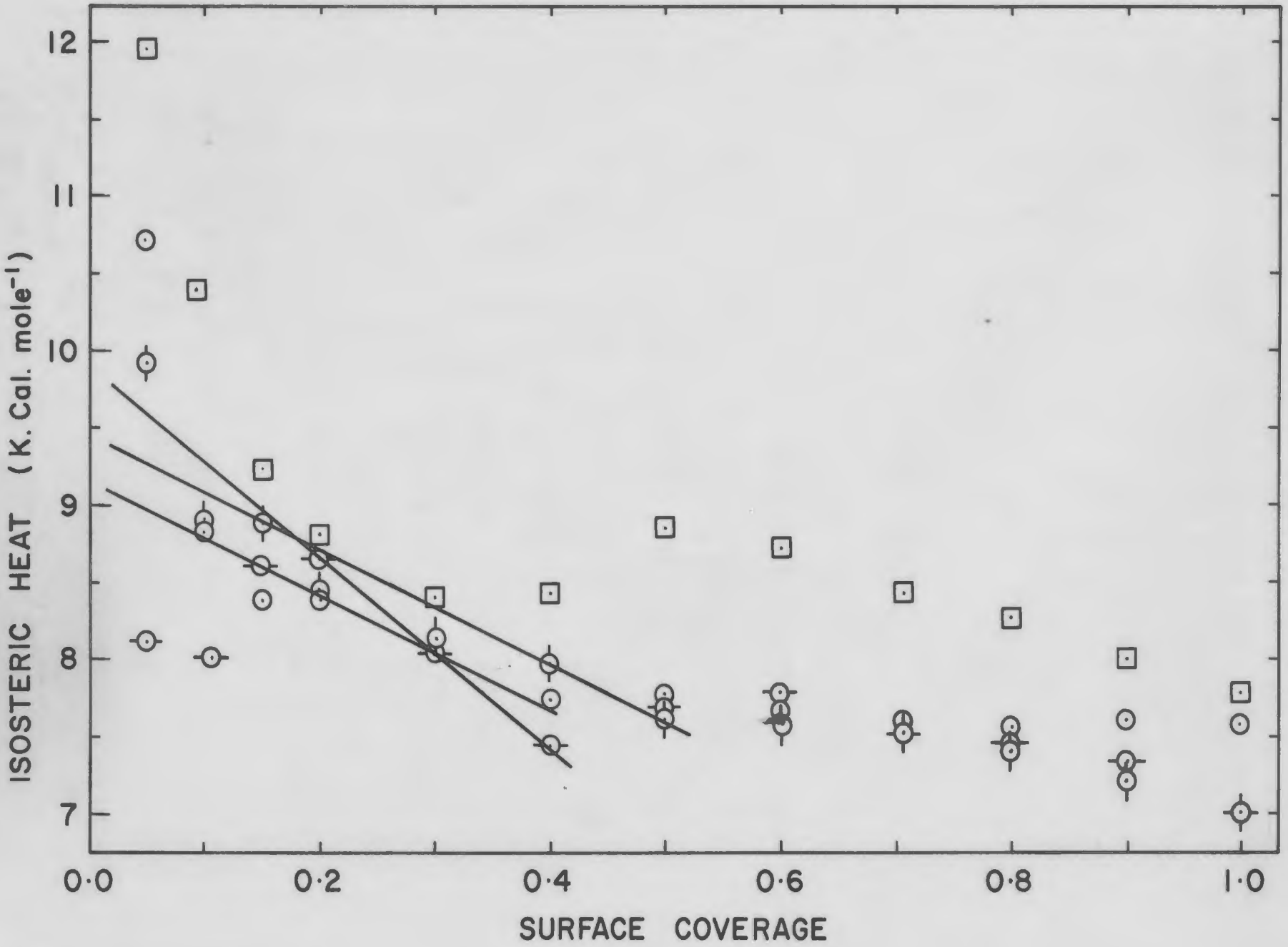

Figure 44. Isosteric heat curves for $CuSO_4$

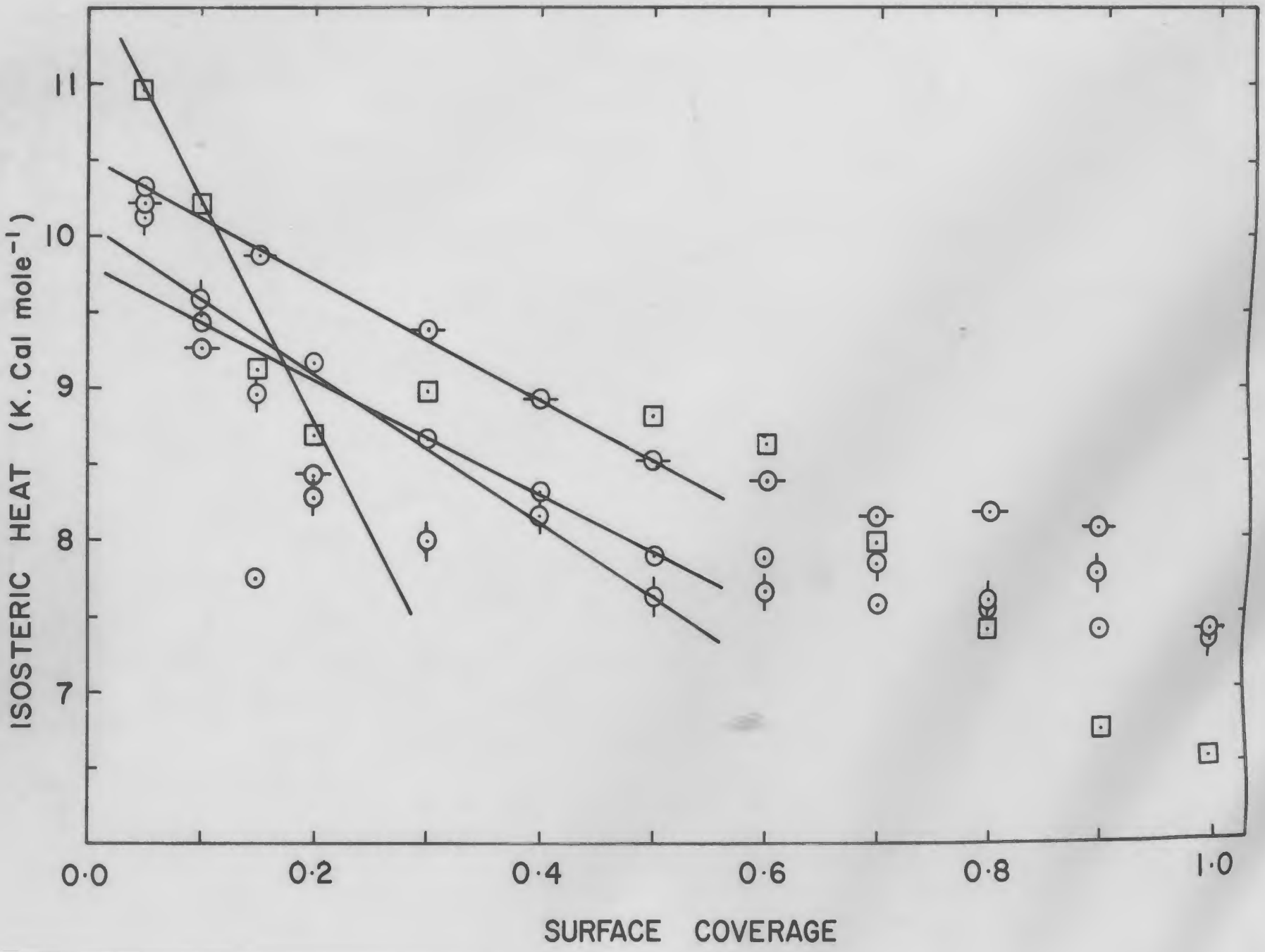

Figure 45. Isosteric heat curves for $ZnSO_4$

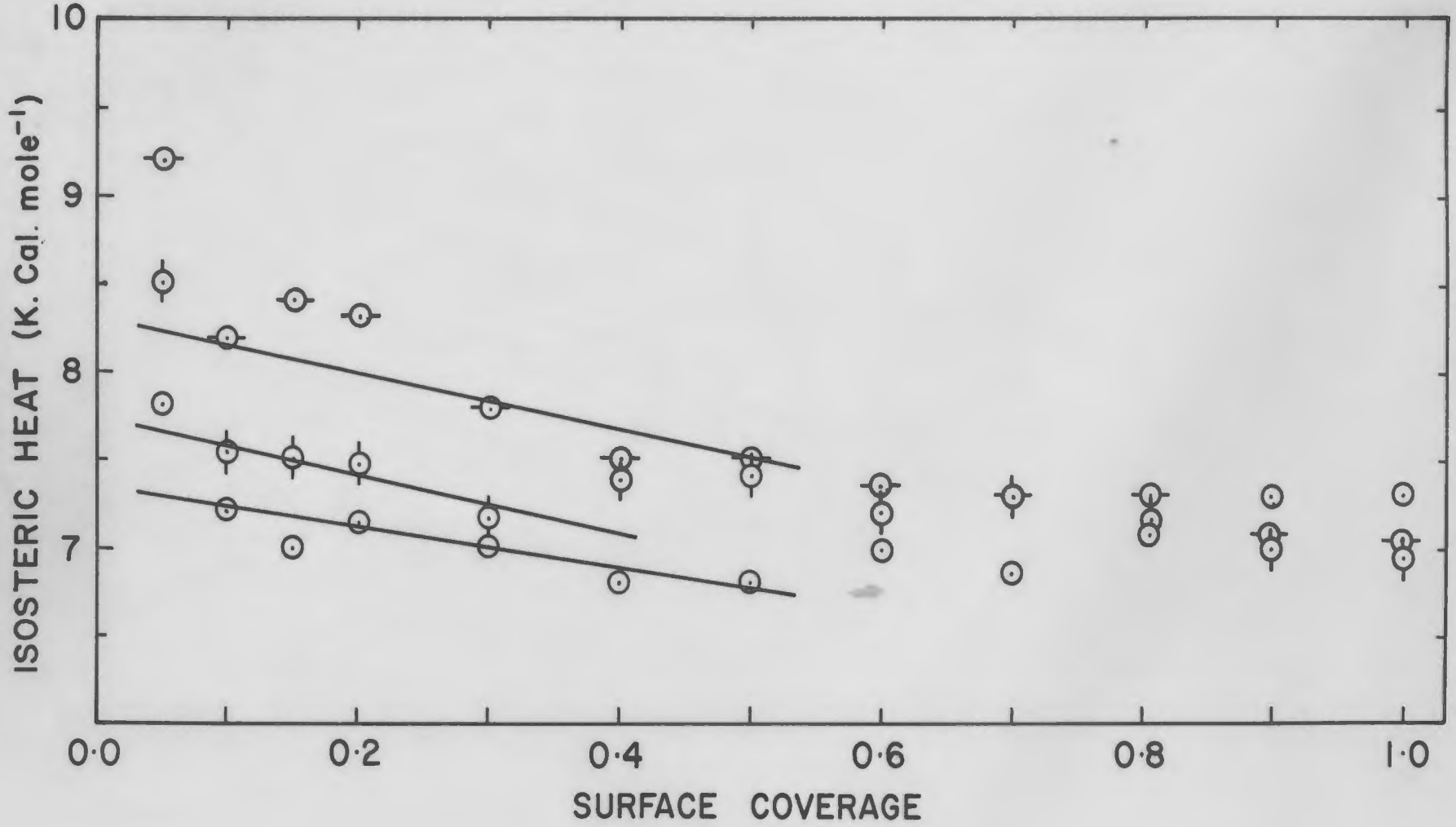

Figure 46. Isosteric heat curves for $CaSO_4$

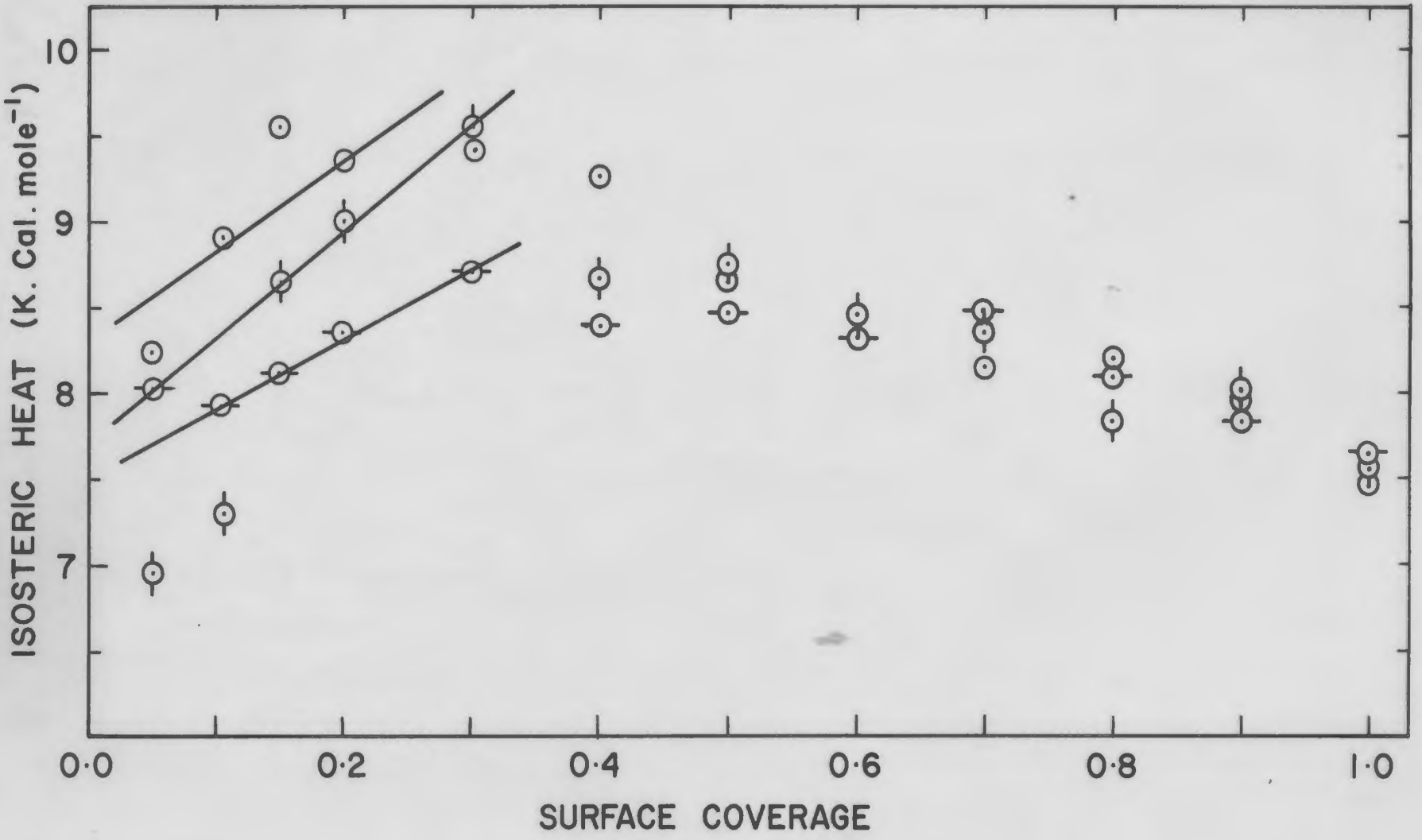

Figure 47. Differential entropy vs. coverage

($MnSO_4$)

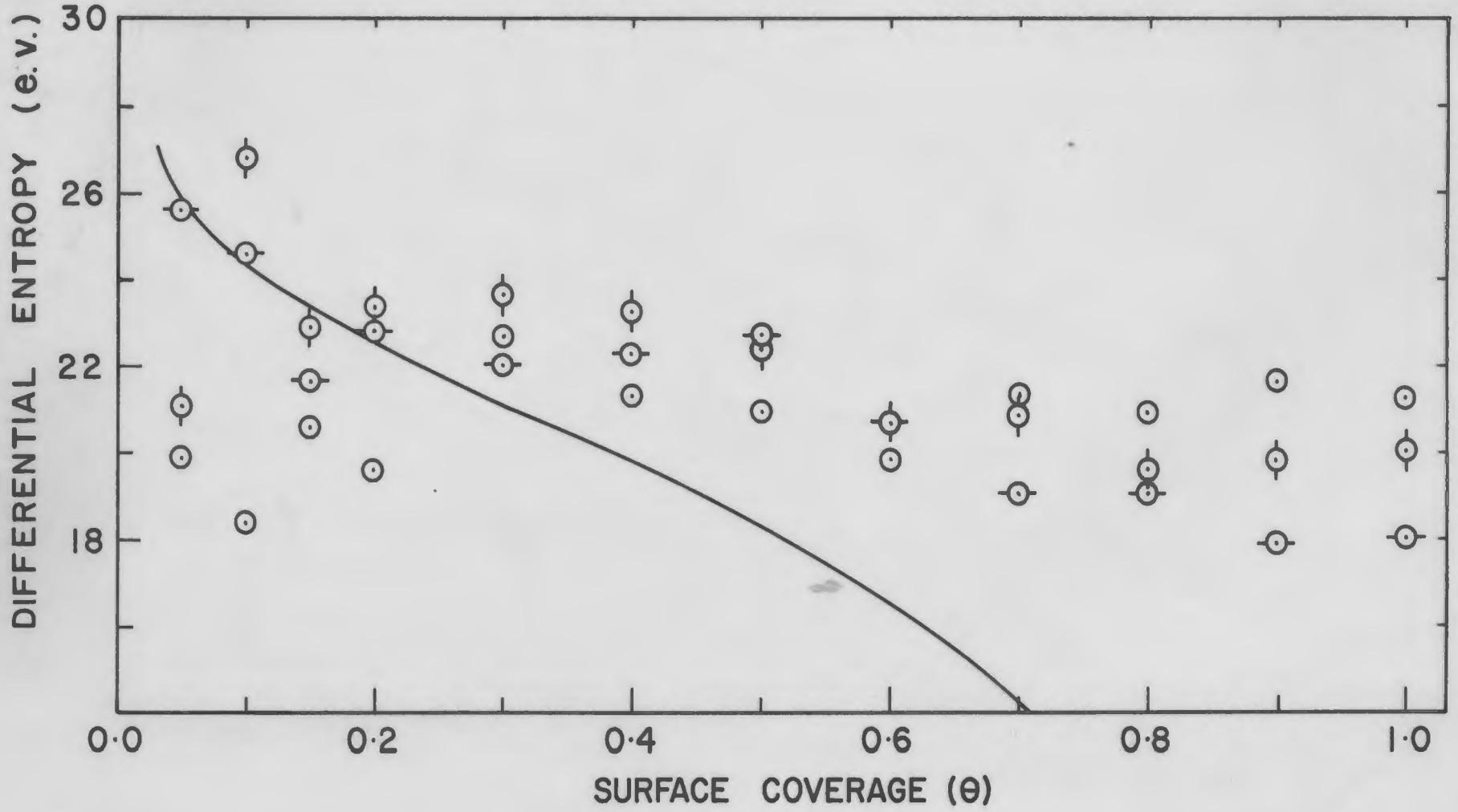

Figure 48. Differential entropy vs. coverage

($CoSO_4$)

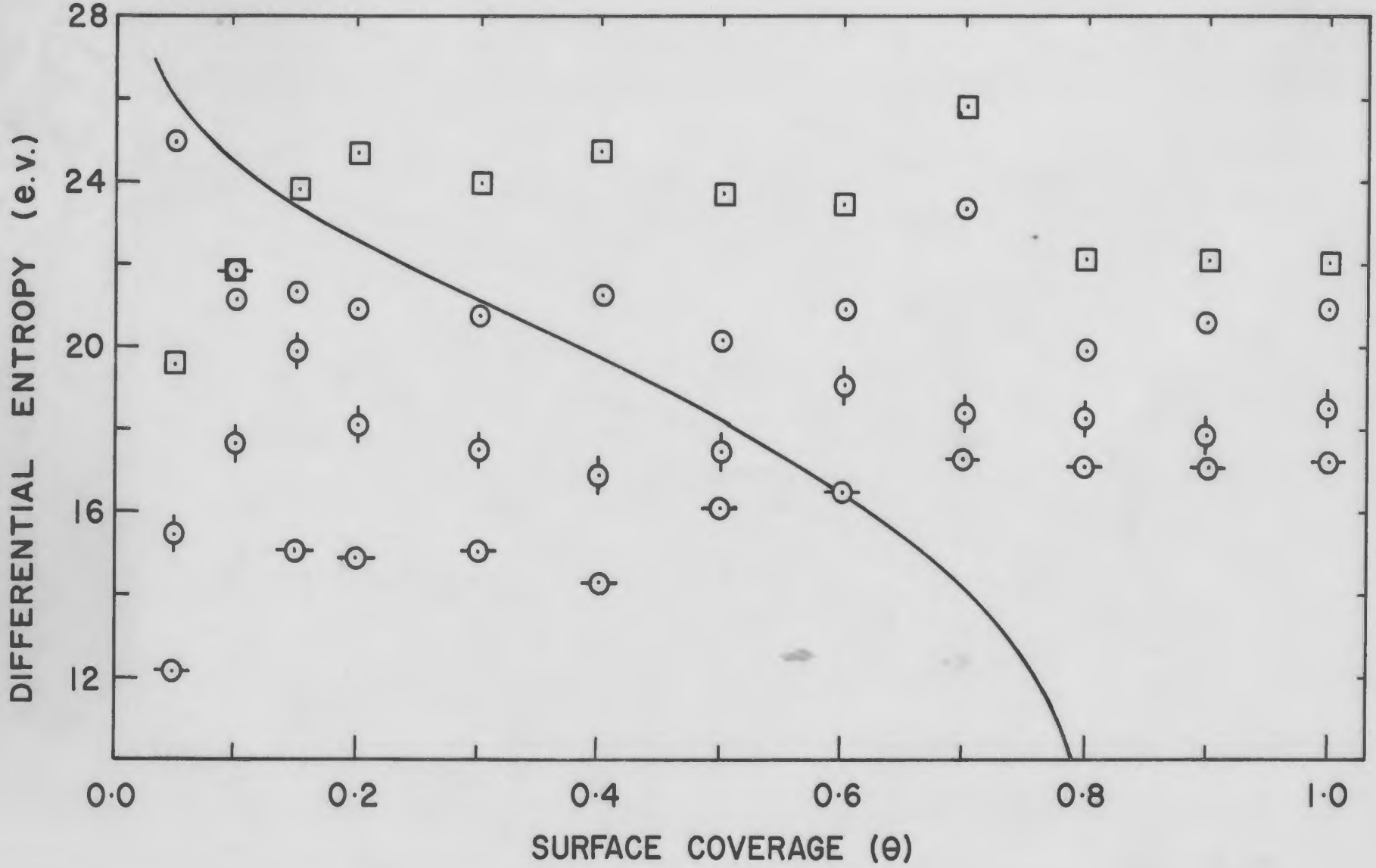

Figure 49. Differential entropy vs. coverage

($NiSO_4$)

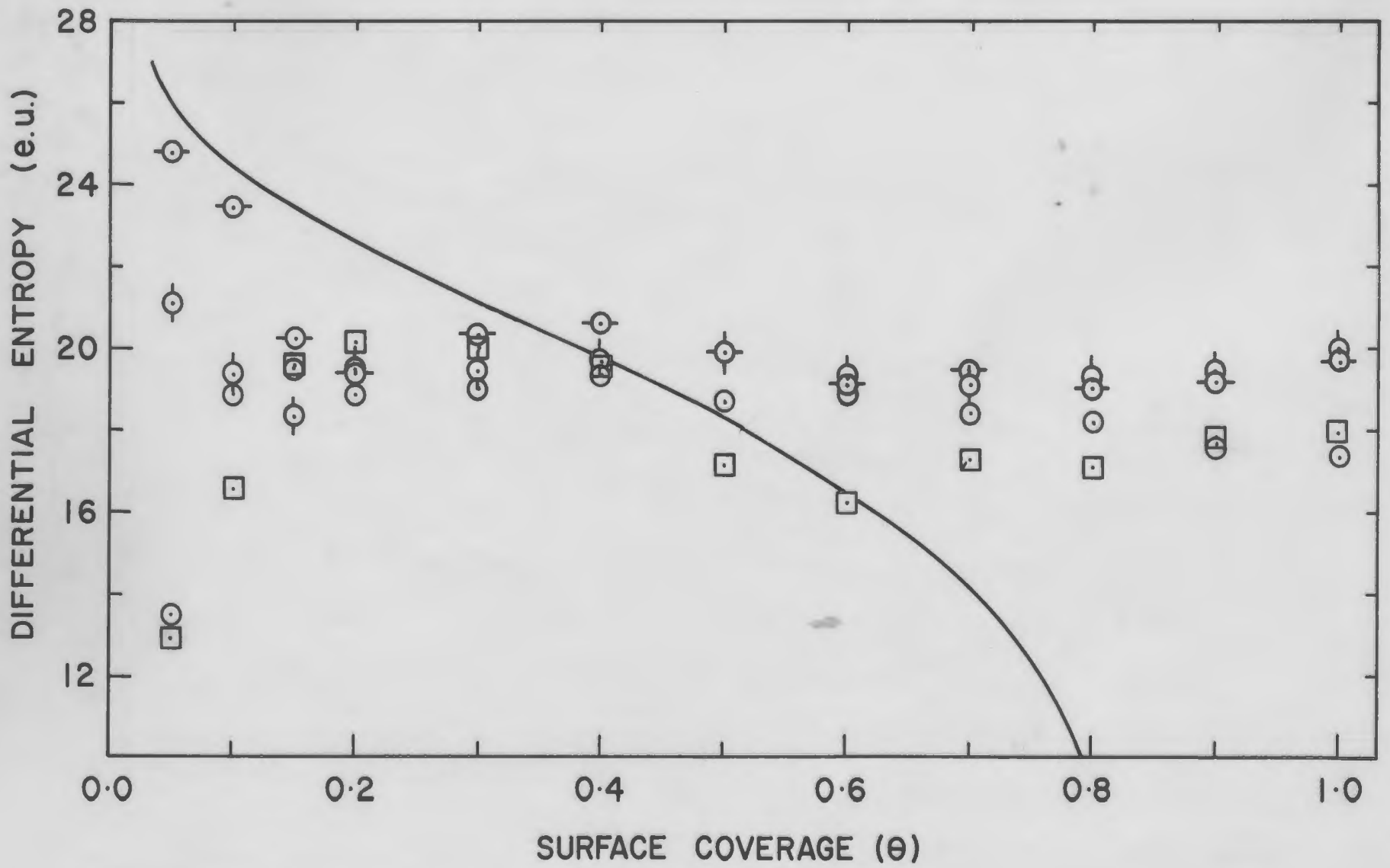

Figure 50. Differential entropy vs. coverage

($CuSO_4$)

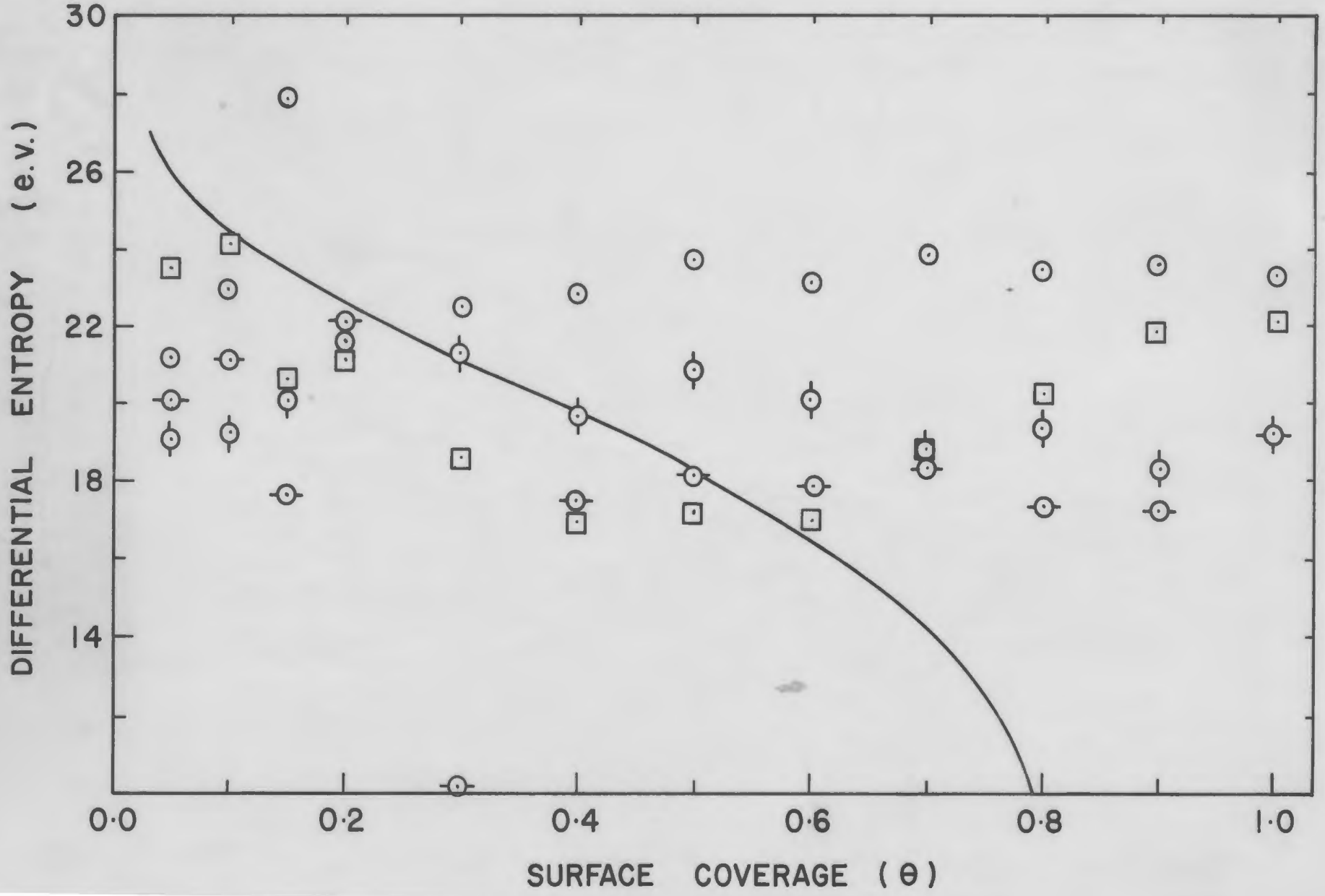

Figure 51. Differential entropy vs. coverage

($ZnSO_4$)

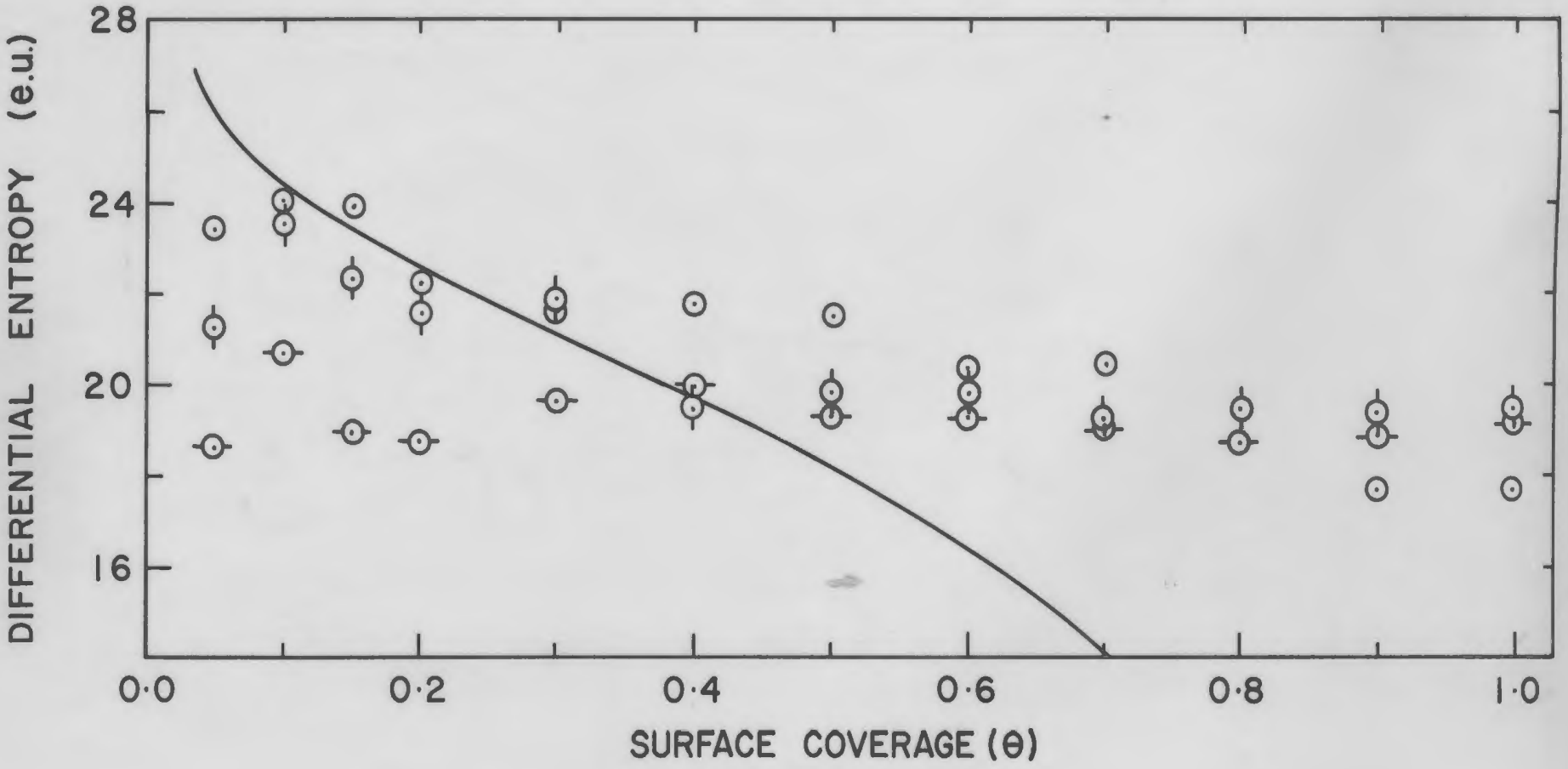

Figure 52. Differential entropy vs. coverage

($CaSO_4$)

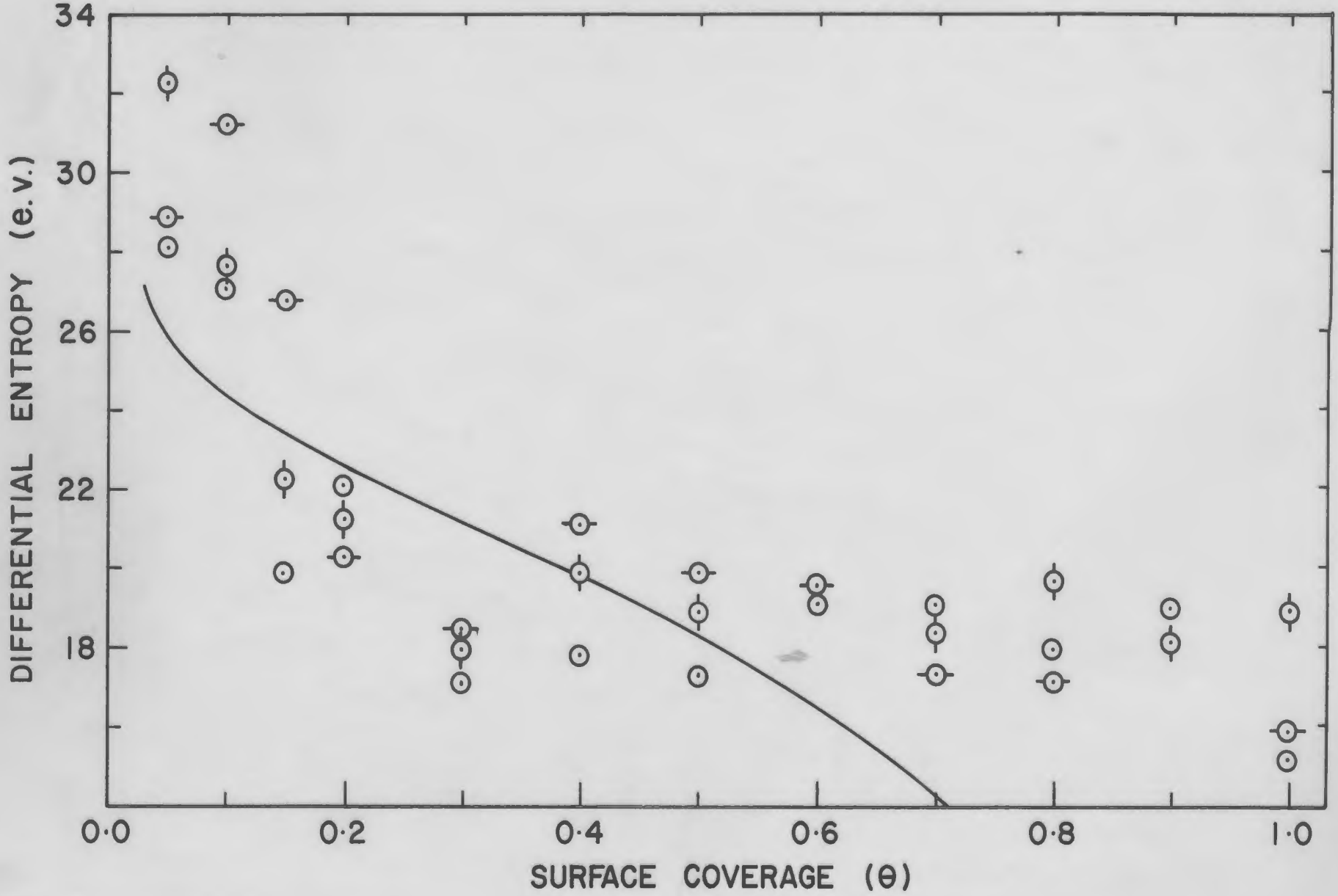

Figure 53. Theoretical entropy for localized model

Figure 54. Theoretical entropy for mobile model

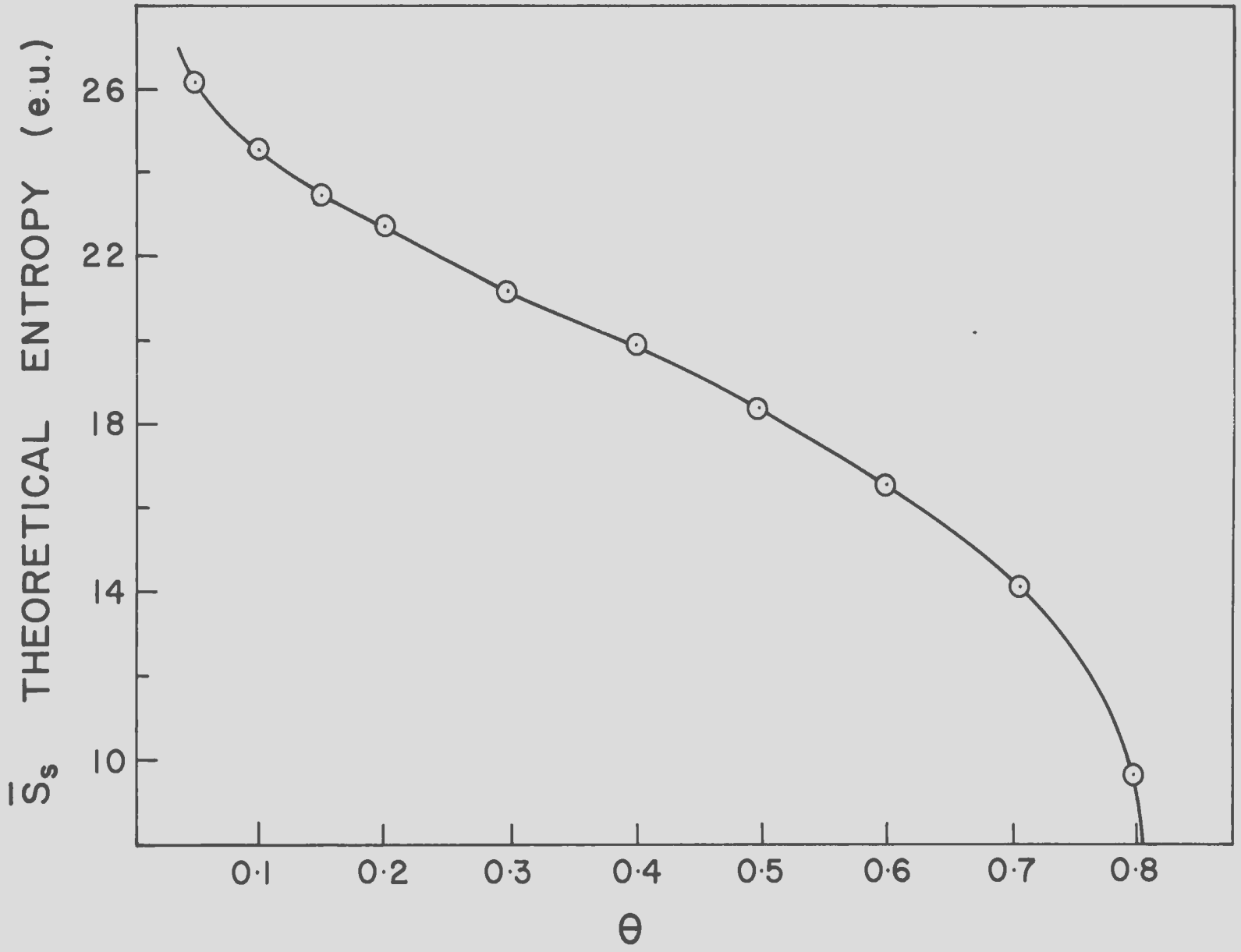

Figure 55. Excess heat of adsorption for adsorbents annealed at 200°C

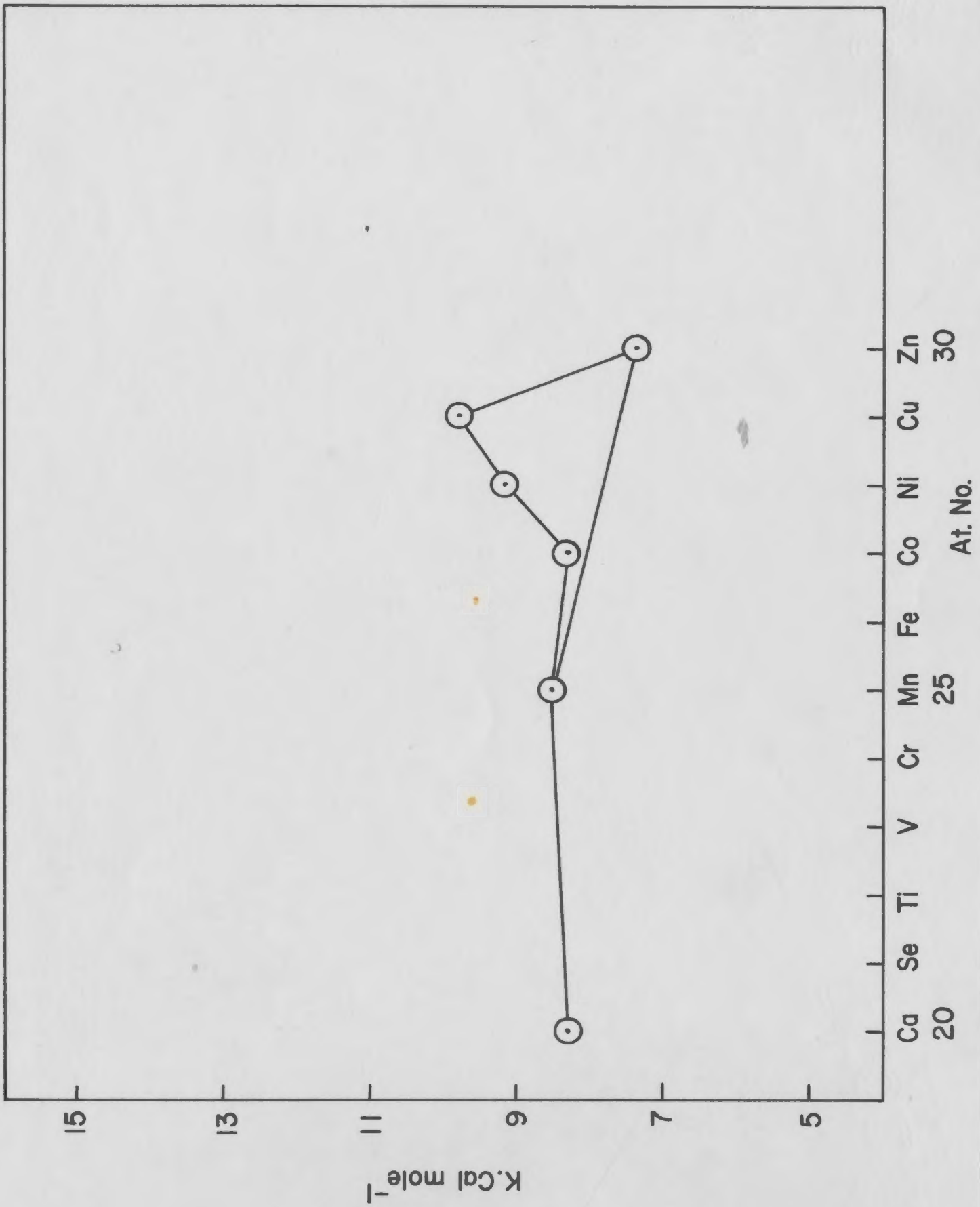

Figure 56. Excess heat of adsorption for adsorbents annealed at 300°C

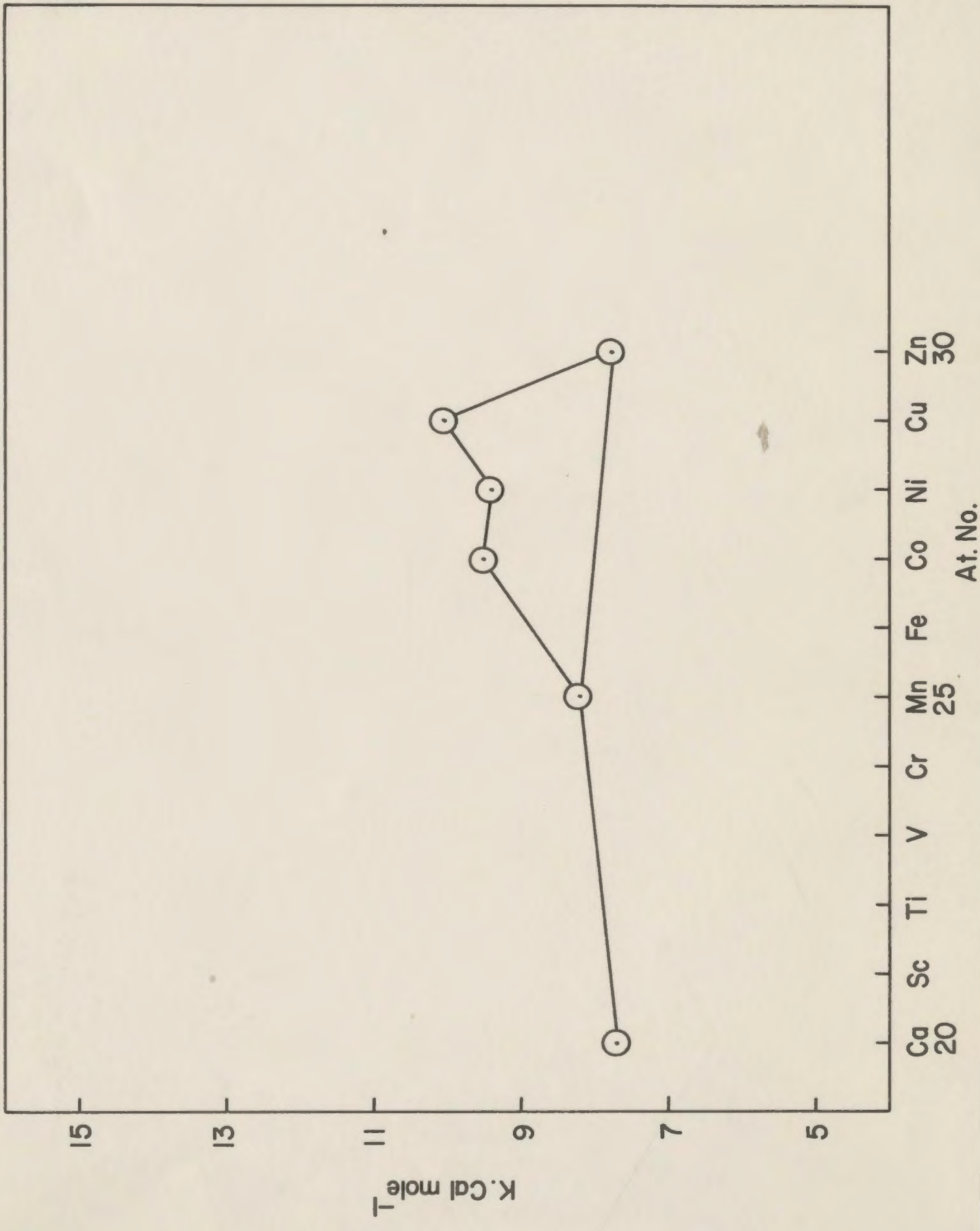

Figure 57. Excess heat of adsorption for adsorbents annealed at 400°C

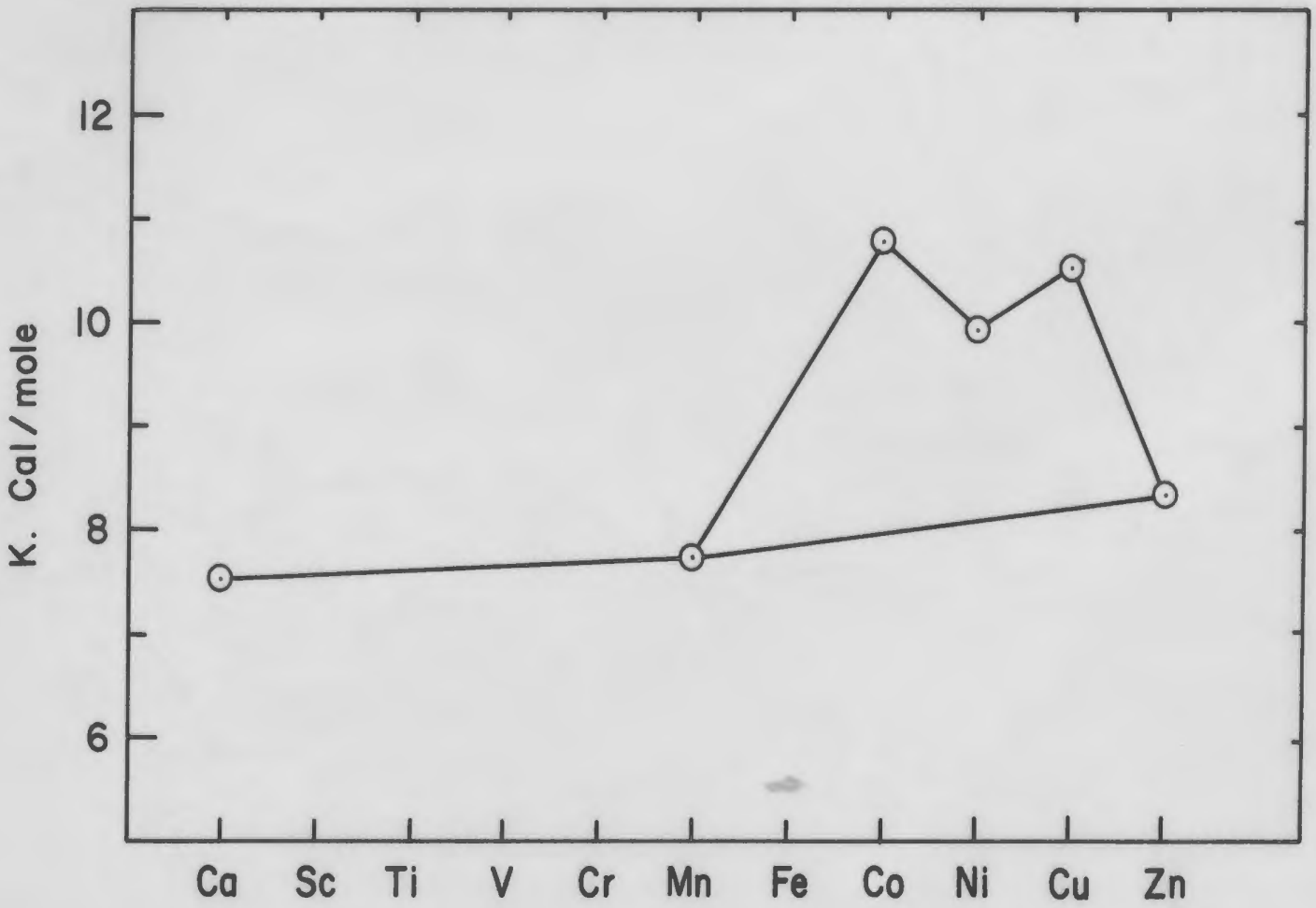

Figure 58. Excess heat of adsorption for adsorbents annealed at 500°C

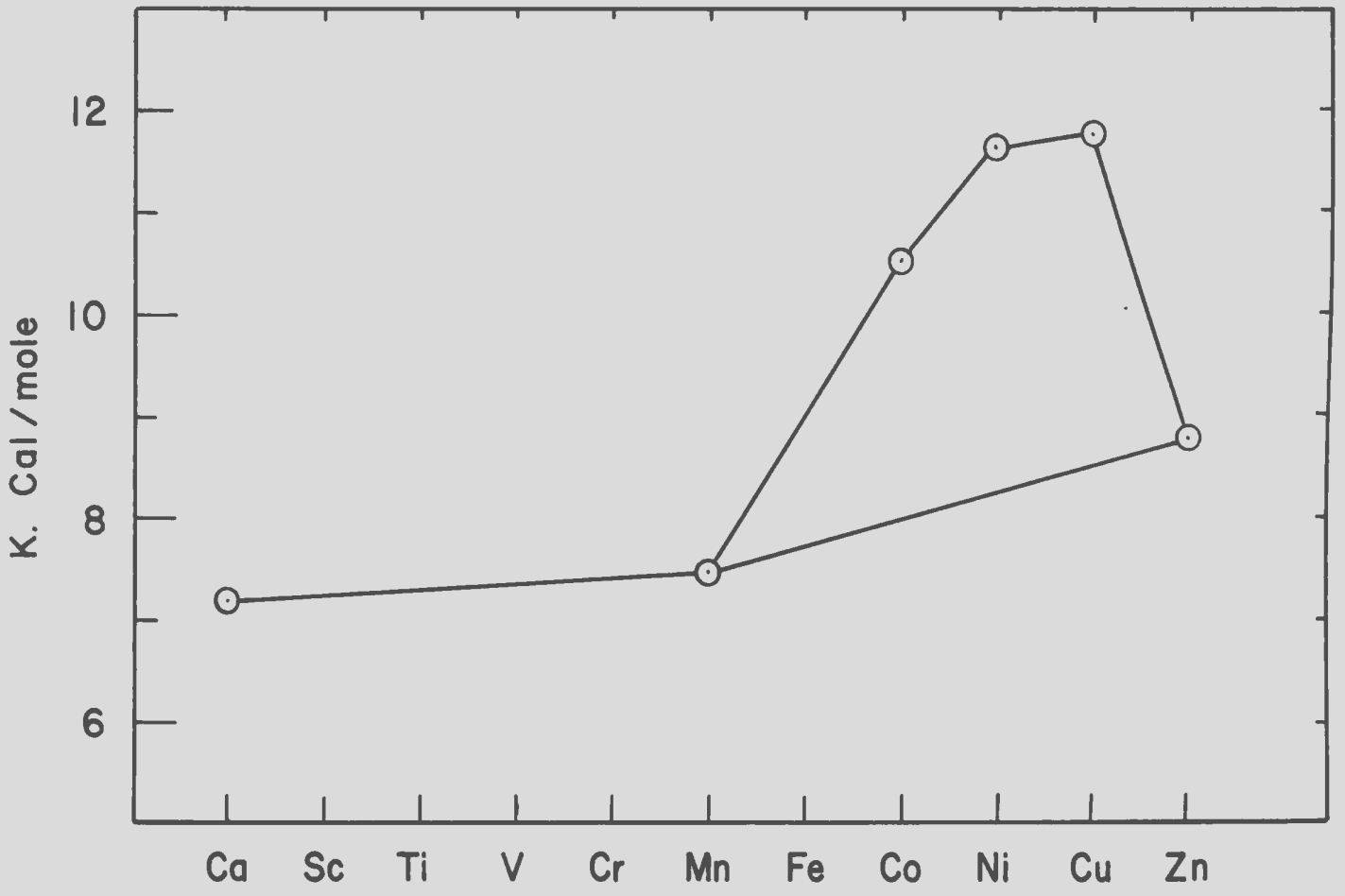

Figure 59. Excess heat of solution for (200) surfaces

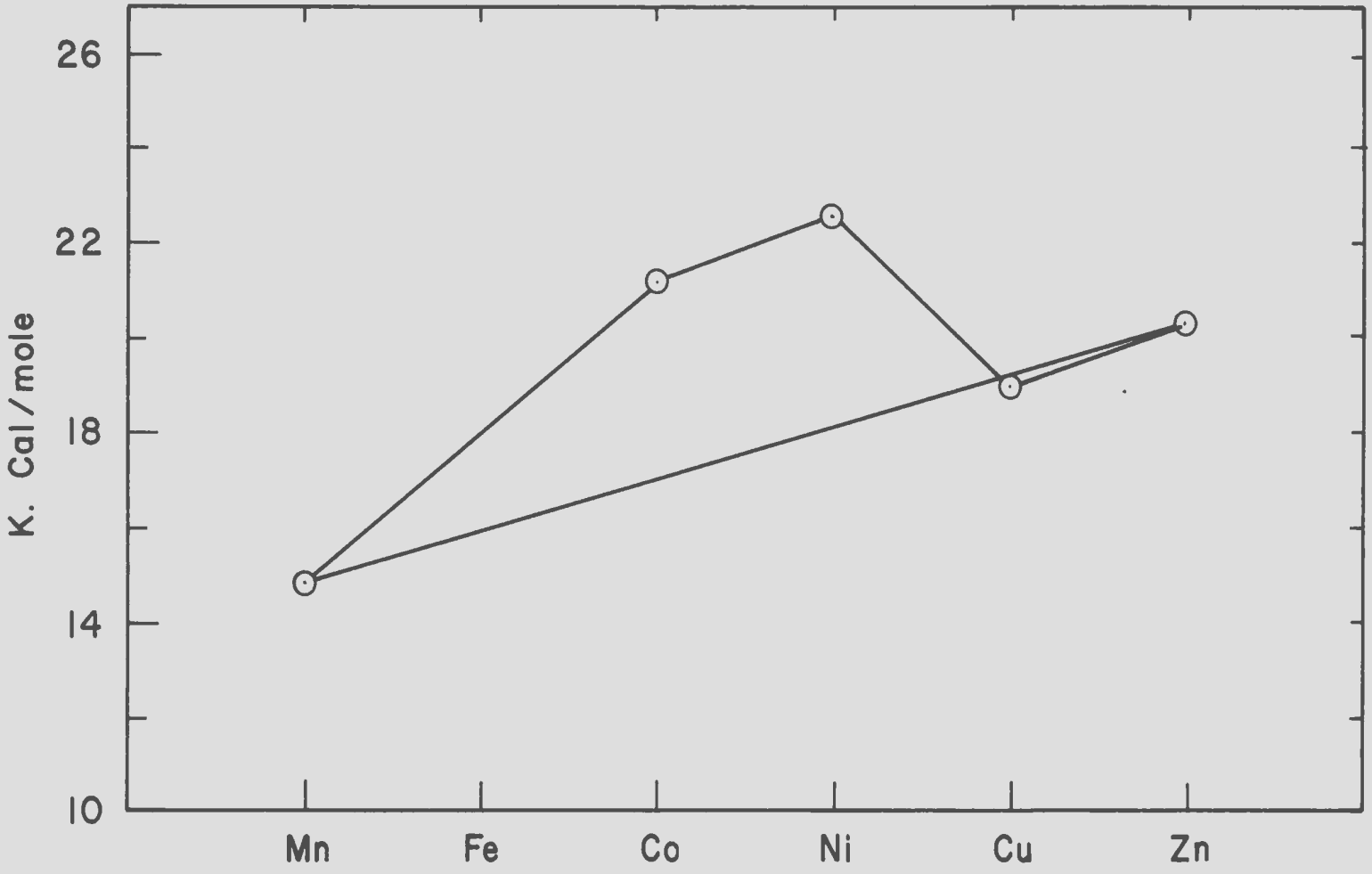

Figure 60. Excess heat of solution for (300) surfaces

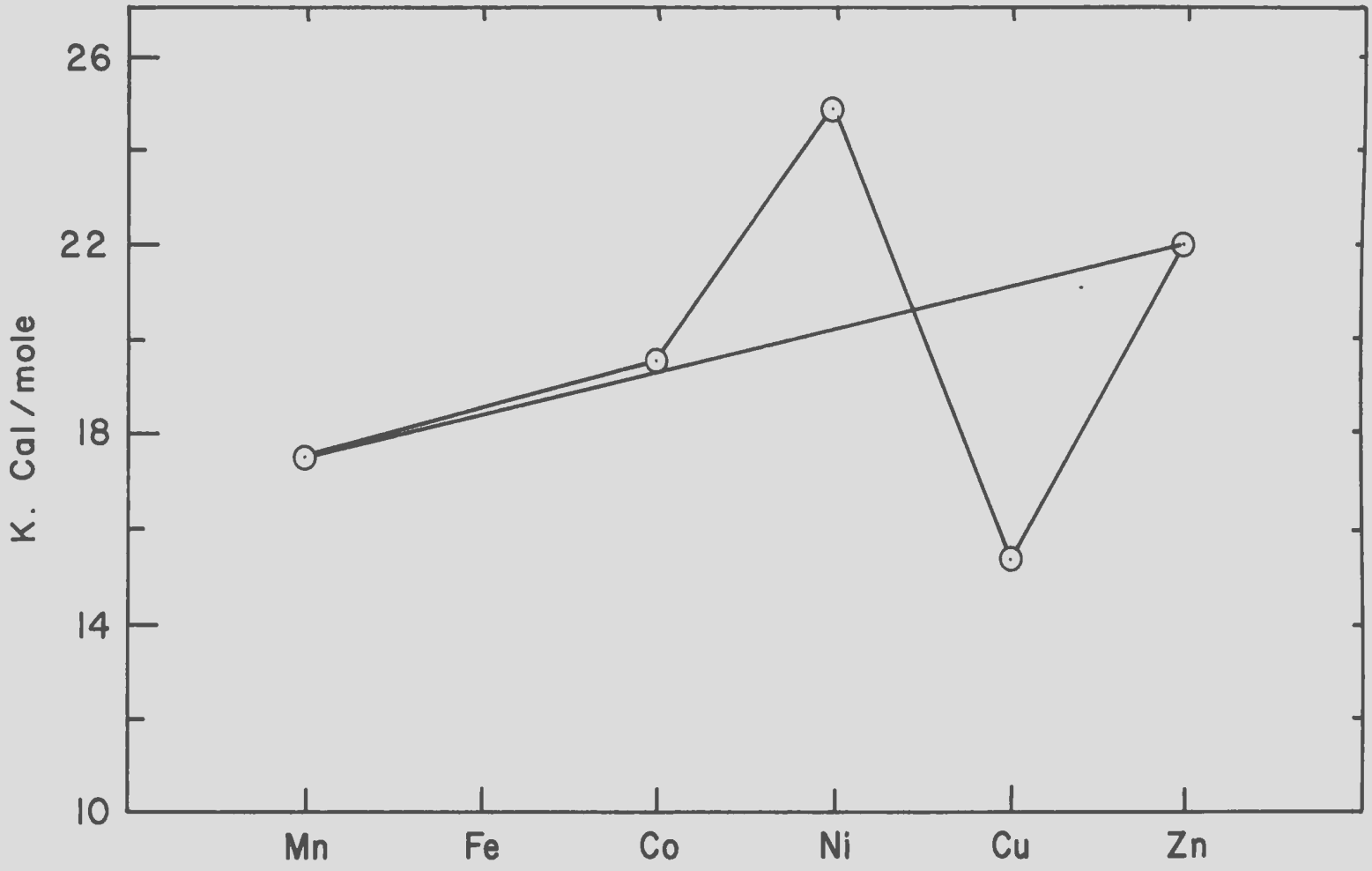

Figure 61. Excess heat of solution for (400) surfaces

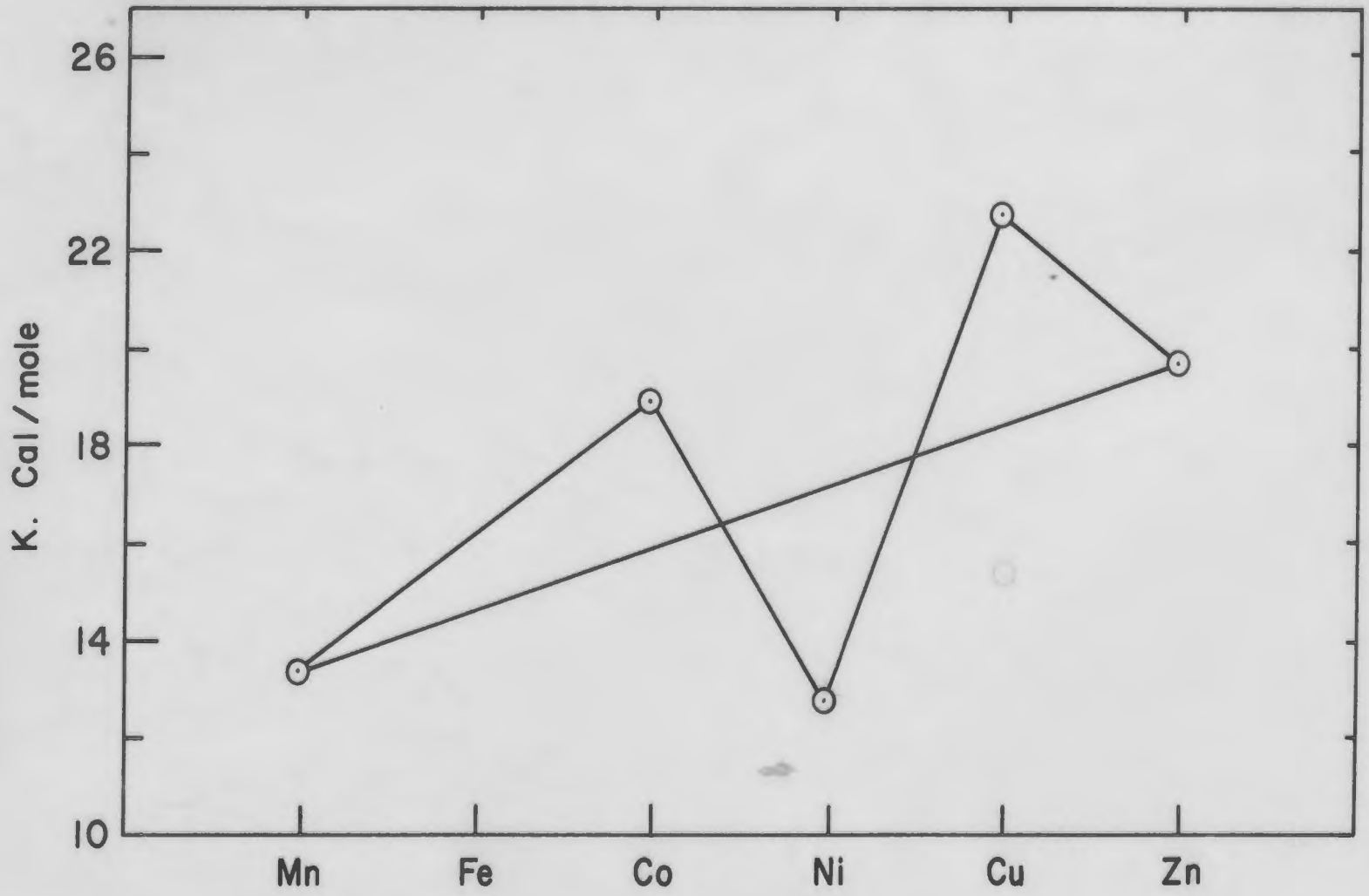

Figure 62. A surface area change with annealing temperature

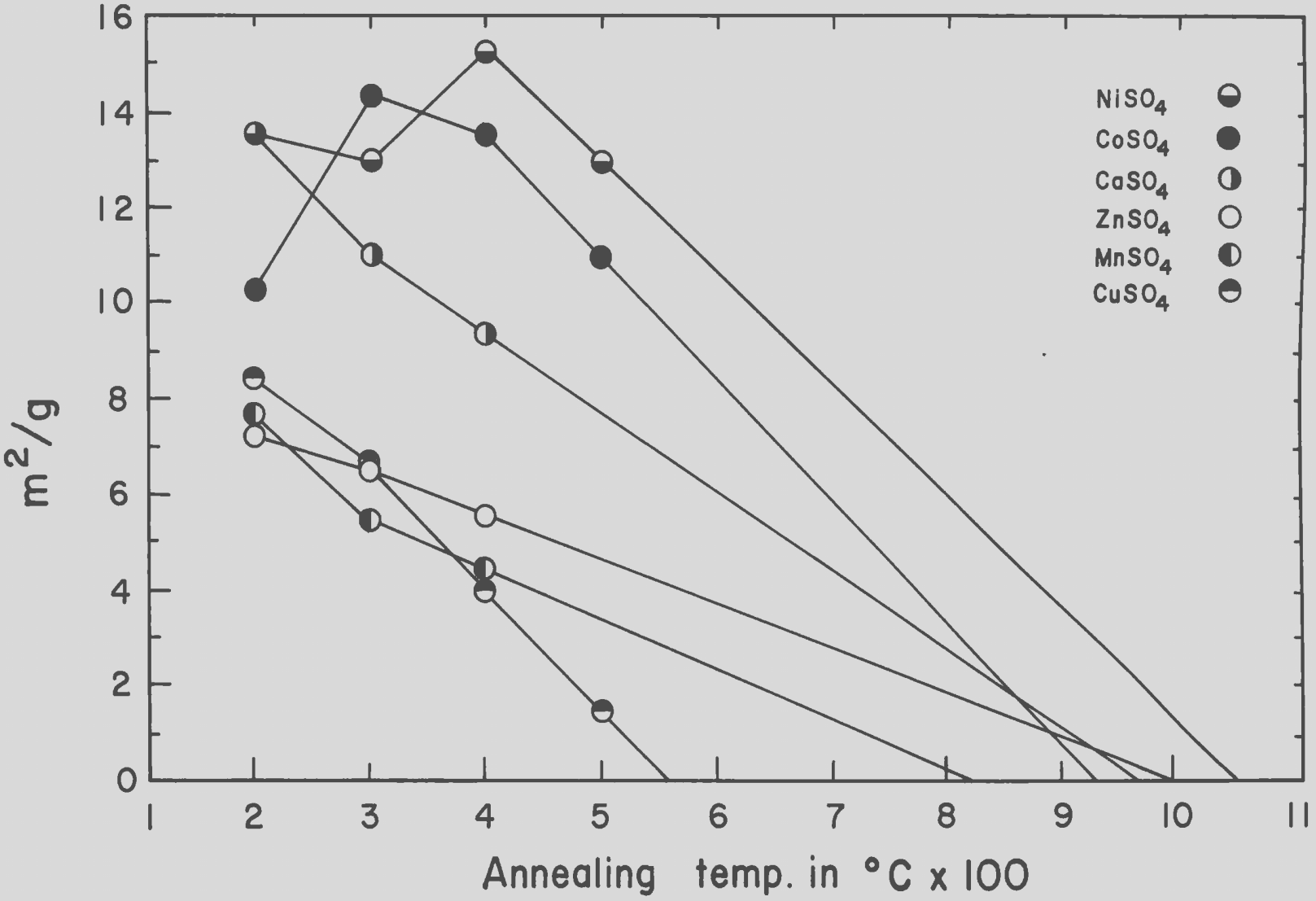

Figure 63

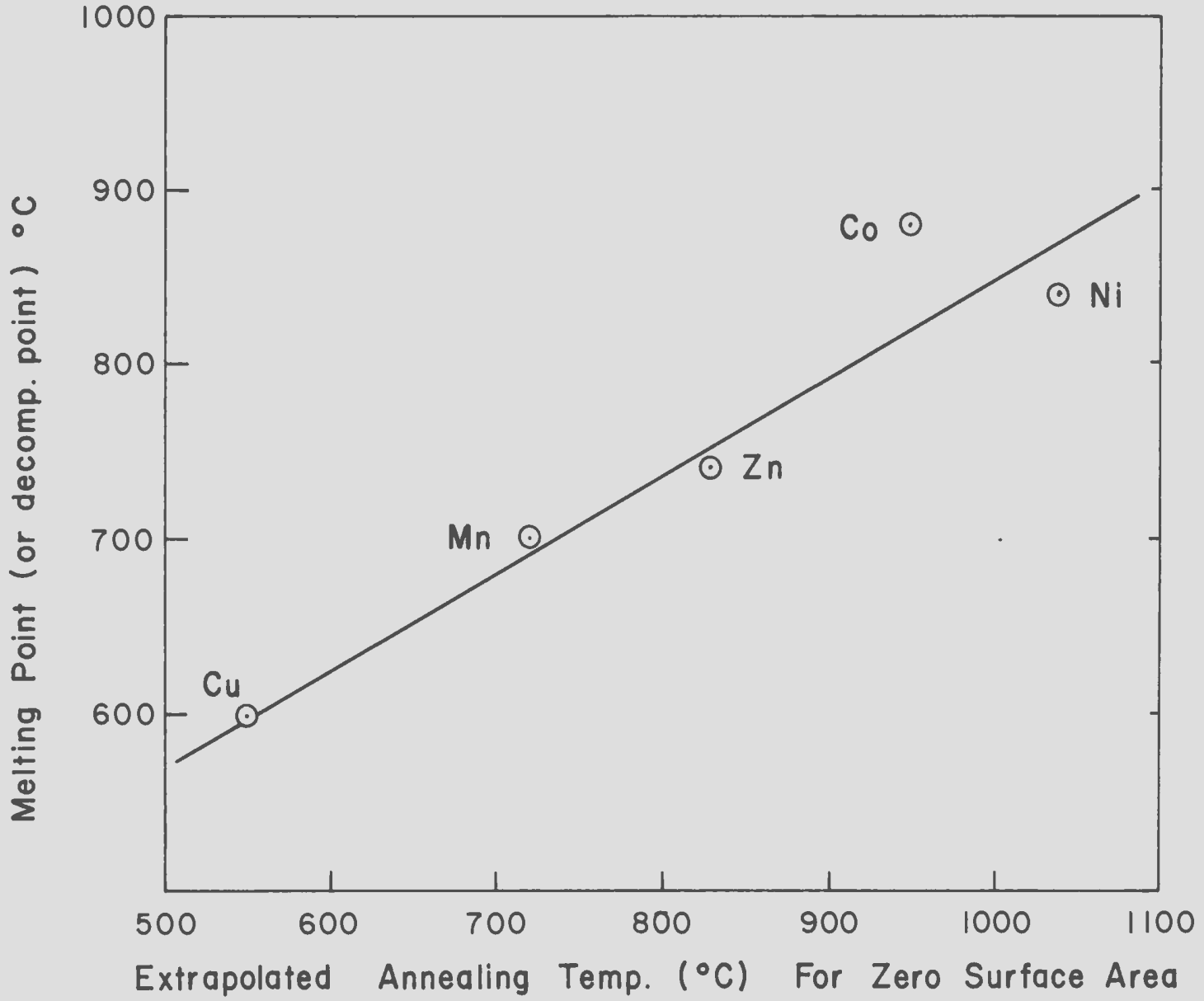
1000
900
800
700
600
Melting Point (or decomp. point) °C
Co
Ni
Zn
Mn
Cu
500
600
700
800
900
1000
1100
Extrapolated Annealing Temp. (°C) For Zero Surface Area

Figure 64. Crystal field splittings for various symmetries

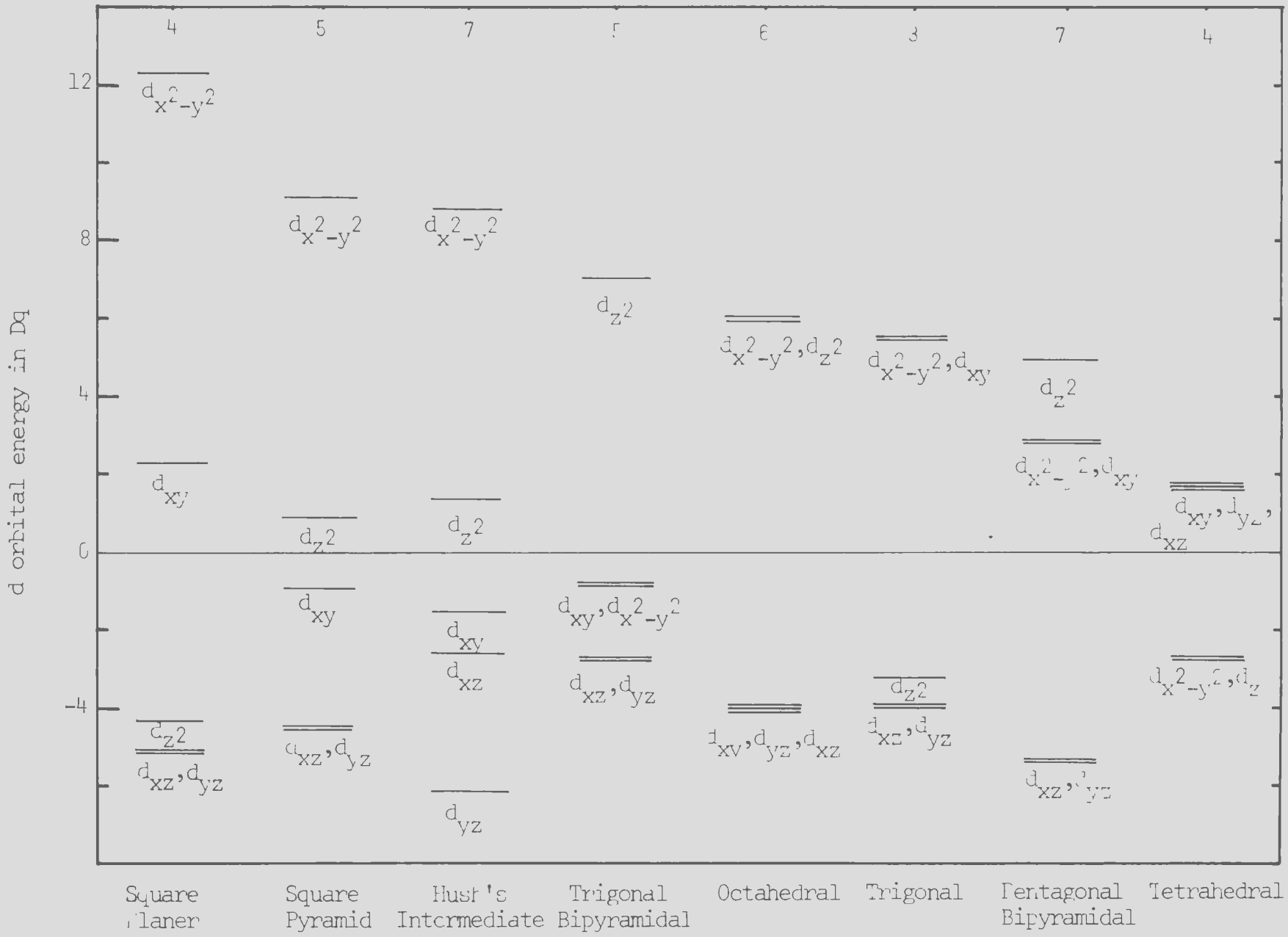

Figure 65A. Octahedral field around a cation

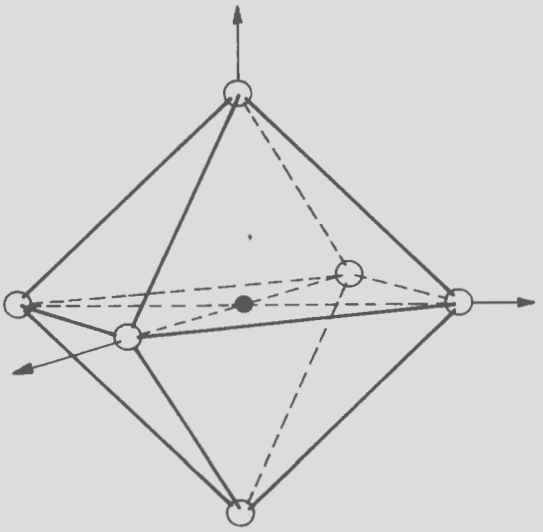

Figure 65B. d orbitals in an octahedral field

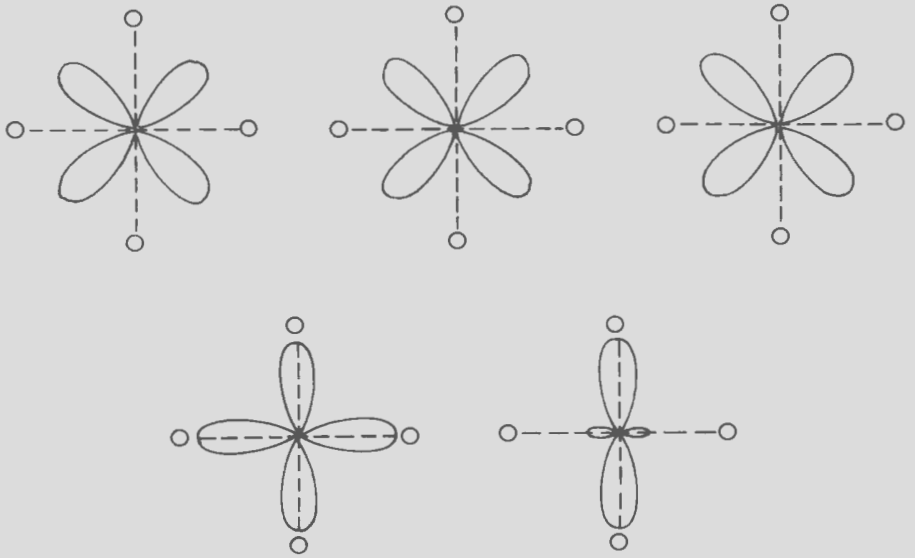

Figure 66. Changes in nickel ion coordination during chemisorption of oxygen on NiO

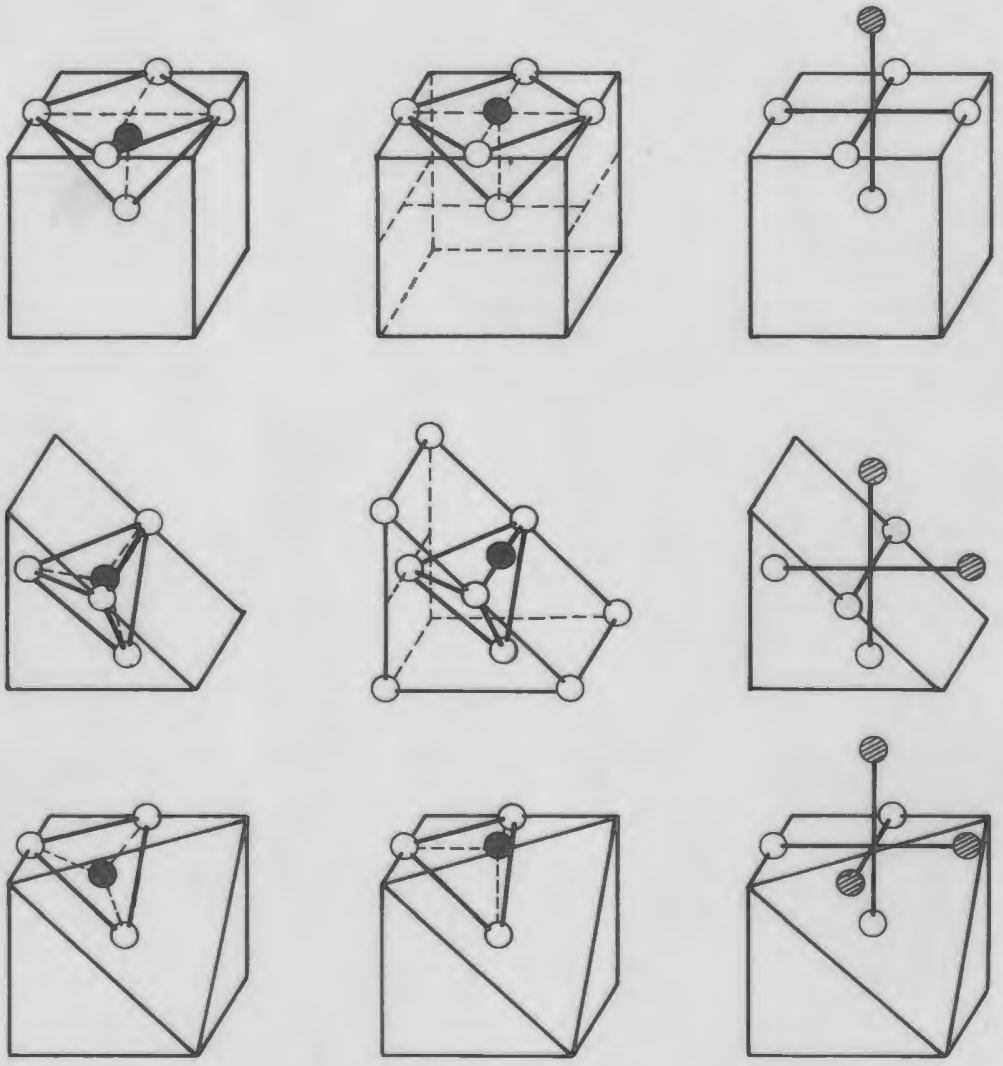

(After Haber & Stone[205])

Figure 67. Crystal structures and crystal planes

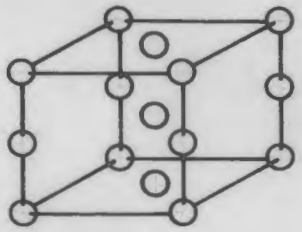

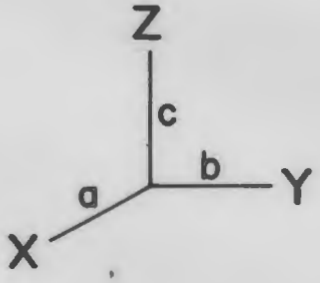

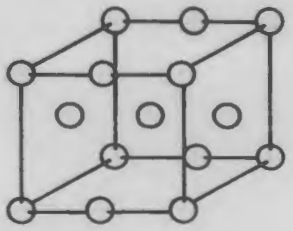

Figure 67A. $CoSO_4$ 'A' and $NiSO_4$

Figure 67B. $CoSO_4$ 'B' and $CuSO_4$

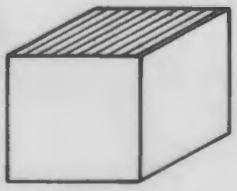

Planes

(001)

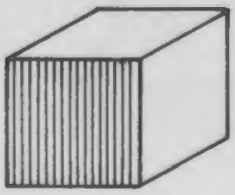

(100)

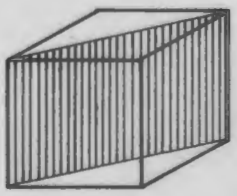

(110)

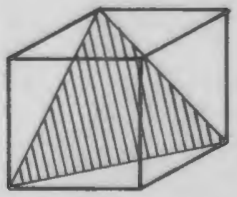

(111)

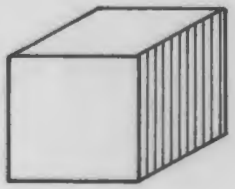

Planes

(010)

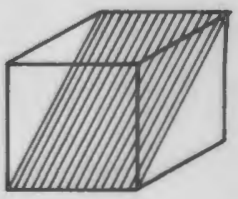

(101)

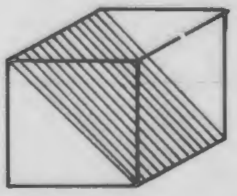

(011)

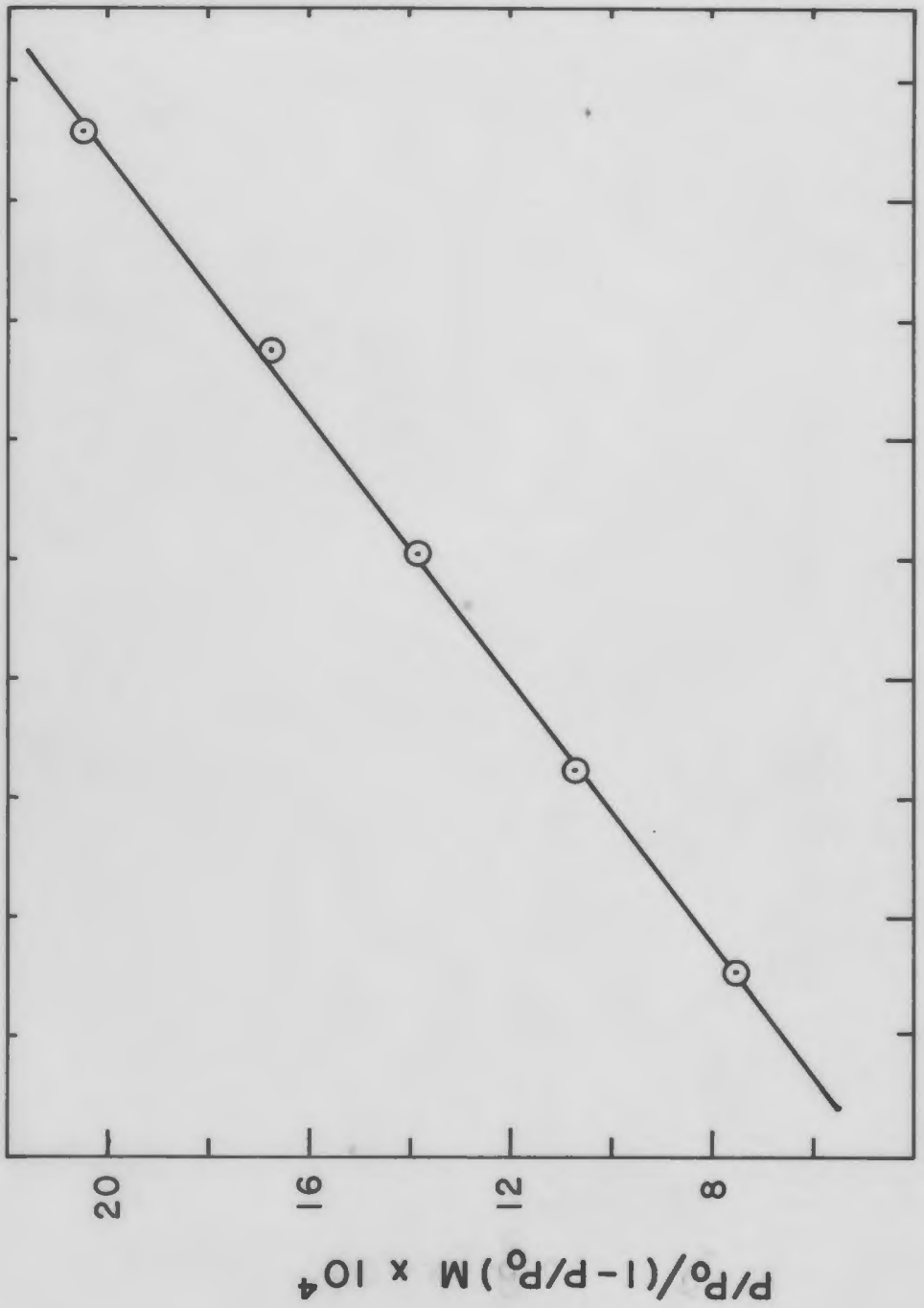

Figure 68. Volumetric BET plot for $CuSO_4$ (200)